EDSC
École Doctorale des
Sciences Chimiques

UNIVERSITÉ DE STRASBOURG

UNIVERSITÉ DE STRASBOURG

THÈSE

Présentée par:

Dang Binh HO

Soutenance le: **25 septembre 2019 à 13h 45**

Pour obtenir le grade de: Docteur de l'université de Strasbourg

Discipline/ specialité: CHIMIE

Iridium(III) silylene complexes: trapping, reactivity and applications

THÈSE dirigée par:

Jean-Pierre DJUKIC   Directeur de recherche, université de Strasbourg

RAPPORTEURS

Jean-Baptiste SORTAIS   Professor, université de Toulouse

Abderrahmane AMGOUNE   Professor, université Claude Bernard, Lyon 1

AUTRES MEMBRES DU JURY:

Michael CHETCUTI   Professor, université de Strasbourg

Acknowledgment

Table of contents

Résumé

1) Introduction

La portée de cette thèse englobe les avancées les plus récentes dans l'étude des liaisons chimiques des complexes iridium-silicium, dans lesquelles un groupe silyle lié à un métal se comporte comme un ligand Z qui maintient une liaison dative avec le centre du métal. Ceci contraste grandement avec le cas où ce groupe se comporte comme un ligand X, c'est-à-dire où ce groupe silyl se lie à Ir par une liaison covalente. Enfin, il est intéressant de noter que les ligands de silylène devraient en principe établir une double liaison avec le centre de l'Ir.

2) Résultats et discussions

Il convient de rappeler la ''méthode de classification par liaison covalente (CBC)'', inventée par Malcolm Green, une méthode ingénieuse pour la classification formelle des composés de coordination. La méthode est basée sur la notion que les atomes d'un ligand directement lié par une liaison primaire au centre métallique sont appelés ''atomes de ligature''. Celles-ci contiennent trois types d'interactions possibles, à savoir la fonction X, la fonction L et la fonction Z.

Pour examiner plus avant le caractère de la liaison Ir-Si, plusieurs iridacycles [(C,N)Cp*Ir(III)-Cl] ({C,N} = benzo[h]quinoline, phenyl pyridine, dibenzo[f,h]quinoline) associées à des anions de type BArF-type ont été synthétisés (schéma 1). Ces complexes d'iridium ont constitué un bon point de départ pour explorer de nouvelles applications catalytiques et pour étudier le comportement de silyl ou de silylium.
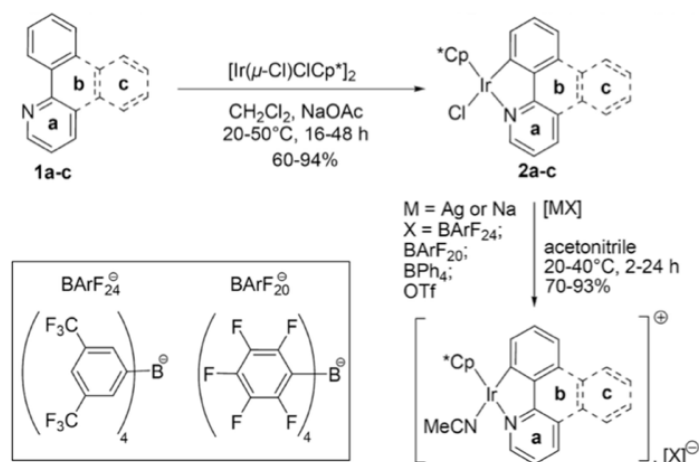
Schéma 1: Synthèse du métallacycle suivie de l'abstraction de chlorure et remplacement par de l'acétonitrile coordiné

Ces complexes cationiques ont démontré une capacité remarquable à catalyser la O-déshydrosilylation des alcools et l'hydrosilylation de composés nitriles par Et_3SiH. Des études mécanistiques ont également montré que l'intermédiaire clé était un hydrido-Ir(III)-silylium hautement réactif, dans lequel le fragment Et_3Si était lié au centre métallique par une liaison dative et se comportait donc comme un ligand de type Z selon le formalisme de Green (schéma 2).
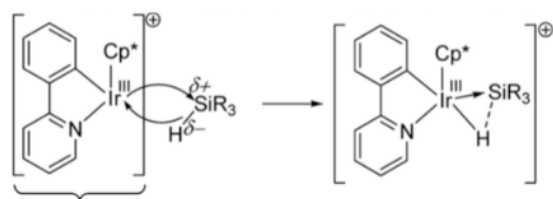
Schéma 2: liaison Si-H activée par Irridacycle

L'idée d'évaluer et d'ajuster le caractère électrophile du fragment silyl et de sa ''silylicité" a été explorée de manière expérimentale et théorique [1].

Pour mener à bien cette étude, une large gamme d'adduits métal – silane et d'autres complexes métal – silyl ont été étudiés par calcul des énergies d'interaction métal – silyl afin de définir la relation de liaison existant entre le centre métallique et une entité SiR_3. En outre, cette recherche a révélé une séparation nette entre les cas dans lesquels le caractère Z du fragment silyl est la meilleure description, et les cas appartenant à des situations "classiques" dans lesquelles le caractère X domine. De plus, nous avons postulé que pour les adduits métal – silane qui possèdent une faible silylicité intrinsèque, une "silylicité" élevée peut être déclenchée par le remplacement du ligand ou par une modification de la charge du complexe.

Tout en travaillant sur ce sujet, nous avons découvert qu'en présence de tétrahydrofurane (THF), les adduits $[(Ir-H) \rightarrow SiRH_2]^+$ se convertissent facilement par élimination de H_2 à une température sub-ambiante en un nouvel au complexe métallacyclique de ''silylene''stabilisé par une molécule de THF (schéma 3).

Ces analogues de silicium de complexes carbèniques ont longtemps attiré l'attention par le passé en tant qu'intermédiaires présumés dans les transformations catalysées par des métaux impliquant des composés organosiliciés. Bien que des complexes métalliques stables de ce type aient été ciblés depuis les années 1960, l'accès à ces espèces reste incertain en raison de leur réactivité élevée.
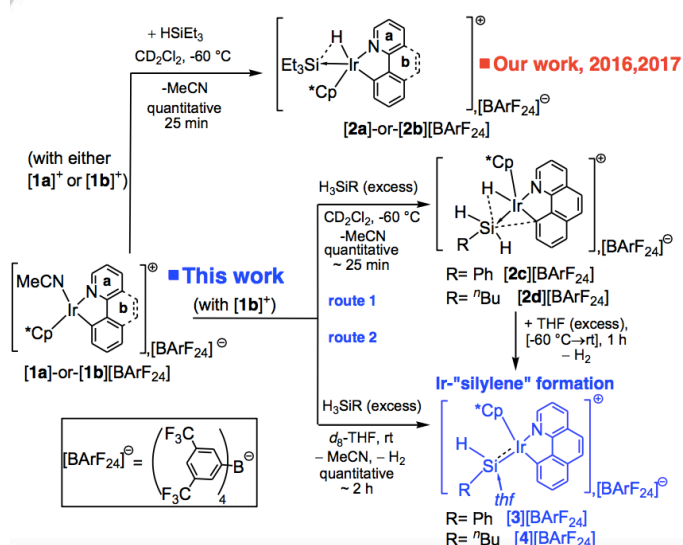
Schéma 3: Résumé de la route vers les complexes de silylène stabilises

L'émergence de complexes silylène-métal via des activations séquentielles de liaison H-Si, suivies de la libération spontanée de H_2 décrite dans cette thèse de doctorat, est unique. En effet, les principales méthodes de préparation des silylènes métalliques

sont basées sur l'abstraction de substituants anioniques, la migration alpha d'hydrogène, la coordination d'un silylène libre ou l'abstraction de substituants sur un ligand de silyl.

L'objectif principal de cette thèse était enfin de caractériser complètement ces complexes a priori insaisissables par des analyses par spectroscopie RMN et par analyse par diffraction des rayons X (schéma 4).

n-Butyl Silylene

Interatomic distance	Length (Å)
Si1 H1	1.40(8)
Si1 Ir1	2.288(1)
O1 Si1	1.825(5)
N1 Ir1	2.084(5)

Phenyl Silylene

Interatomic distance	Length (Å)
Si1 H1	1.3(2)
Si1 Ir1	2.278(3)
O1 Si1	1.88(2)
N1 Ir1	2.09(3)
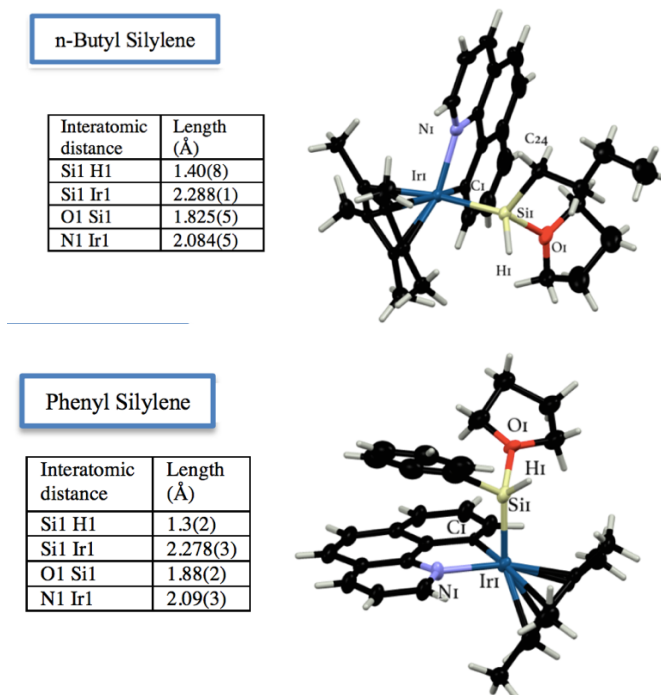
Schéma 4: structure aux rayons X de complexes de silylènes stabilises

Couplé à la chimie des complexes silylène métalliques mentionnés ci-dessus, l'iridacycle cationique **1b** présente une réactivité catalytique intéressante vis-à-vis des nitro-arènes, qui peuvent effectuer la réduction du groupe nitro pour donner des produits dérivés de l'aniline (schéma 5).
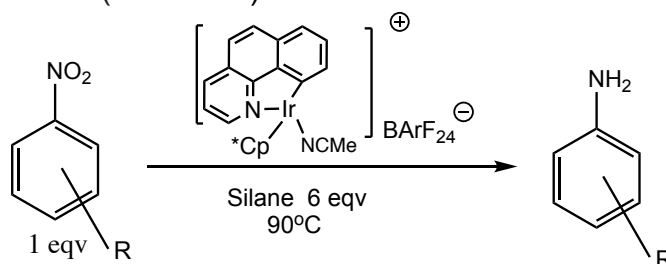
R = Halogen, alryl, nitril, etc

Schéma 5: Iridacycle cationique **1b** effectuer la réduction nitro

Un ensemble d'alkylsilanes a été sondé pour rechercher le plus efficace, tandis que les conditions de réaction catalytique ont été optimisées. Comme on pouvait s'y attendre, les silanes primaires et secondaires capables de former des complexes silylniques d'iridium expriment une réactivité catalytique, contrairement aux silanes tertiaires, qui sont incapables de donner des silylènes. Les résultats suggèrent que

des complexes de silylène hautement électrophiles sont impliqués dans le processus catalytique.

Il est raisonnable de supposer que la réactivité catalytique des espèces cationiques d'hydrido-Ir(III)-silylium, est en corrélation significative avec l'étendue de la polarisation de la molécule. Une telle polarisation qui se produit déjà dans le produit d'addition Ir-silan l'électropositivité du centre Si. En maintenant l'ossature du ligand principal constante, l'introduction d'un substituant fluoré augmente la polarisation de la même molécule et, par voie de conséquence, impacte sa réactivité catalytique (schéma 7).

DECREASE   EXTENT OF MOLECULE POLARIZATION   INCREASE
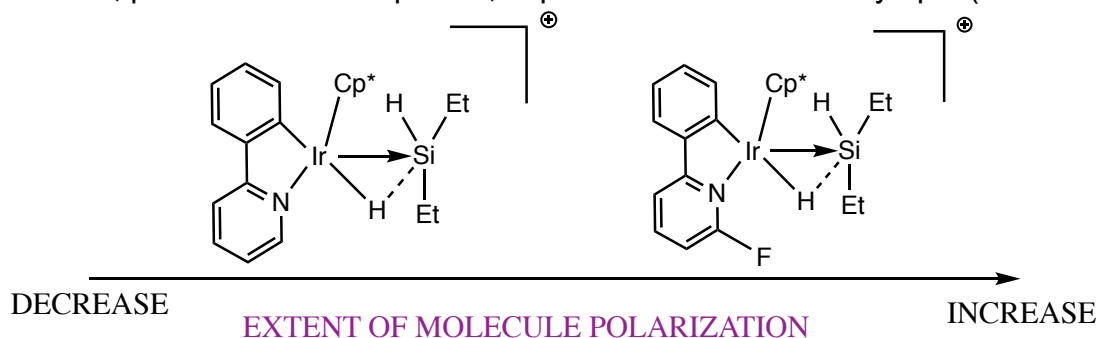
Schéma 6: En ajoutant un groupe attracteur fort, l'intermédiaire clé F-**1a** est plus polarisé que **1a**

On a donc fait réagir AgF$_2$ avec de la 2-phényl-pyridine pour donner lieu à la 2-phényl-pyridine fluorée, qui devait servir de point de départ pour la synthèse de complexes solvato cationiques fluorés **F-1a**. (schéma 7)
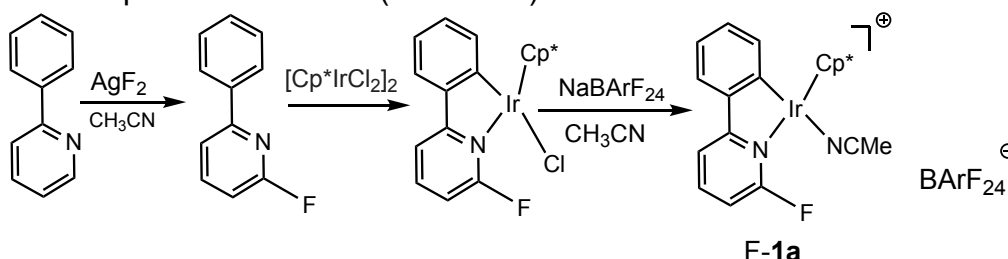
Schéma 7: Synthèse de complexes solvato cationiques fluorés.

Comme on pouvait s'y attendre, F-**1a** présente également une réactivité catalytique remarquable vis-à-vis d'une réaction de test de référence pouvant être suivie par piézométrie, c'est-à-dire la O-déshydrosilylation d'alcools à la température ambiante avec Et$_3$SiH. Un cristal de l'intermédiaire hydrido-Ir(III)-silylium a également été piégé à la suite d'une réaction avec Et$_2$SiH. (schéma 8)
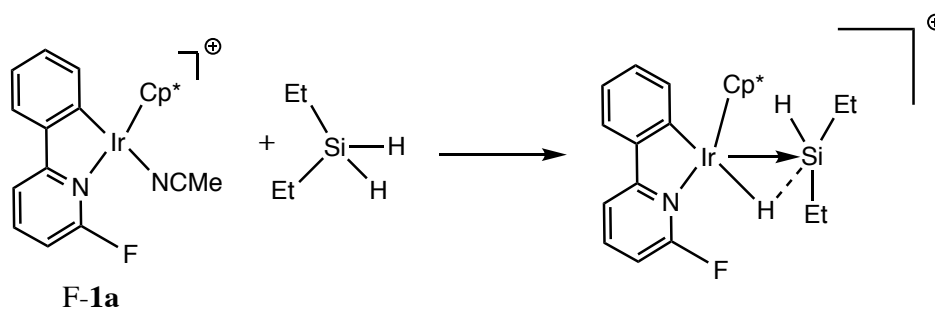
Schéma 8: F-**1a** a réagi avec Et$_2$SiH$_2$ à partir d'un produit d'addition

3) Conclusion générale

En conclusion, s'appuyant sur la découverte d'une nouvelle propriété chimie des intermédiaires hydrido-Ir(III)-silylium, cette thèse a fait progresser les connaissances sur les complexes de coordination de ligands base par la synthèse et la caractérisation structuralle complète de complexes de silylène métalliques extrêmement réactifs. Des méthodes de calcul théorique ont également été utilisées pour éclaircir le mécanisme de conversion des adduits d'Ir-silane en silylènes, dont un grand nombre ont été piégés par cristallisation réactive et ensuite caractérisés par analyse par diffraction des rayons X.

Introduction

1. *The journey to silylene chemistry*

1.1. *First subject: the concept of hemichelation*

Around one hundred years ago, the so-called valence bond theory was proposed by the American chemist Gilbert Lewis[2]. Along with ionic bonding theory, these two theories are of ulmost importance in chemistry. However chemical interactions are much more diverse than that. For instance, hydrogen bonds are the result of electrostatic attraction between hydrogen and other more electronegative atom such as nitrogen, oxygen, or fluorine, etc. Dative bonds (now more generally called donor–acceptor bonds) possess both electrons arising from just one atom.

Unveiling the nature of bonding between atoms or compounds has always earned a widespread interest for chemists because insight into bonding helps us not only interpret the reactivity of given compounds but also predict their behavior in chemistry. The thesis was to aim to fundamentally study the nature of covalent and non-covalent interactions in transition metal complex chemistry as well as to probe complex catalytic systems (multicomponent tandem catalysis reaction, catalysis for the production of small energetic molecules, multicomponent catalysis of C-H, Si-H, B-H, C-F activation).

Our laboratory provided a rational method of synthesis of stable neutral T-shaped 14 electron Pd and Pt complexes[3-5]. The ambiphilic tricarbonyl(η^6-indenyl)chromium anion was used as a hemichelating and heteroditopic ligand, which is capable of chelating a metal center(Pd, Pt) by covalent and noncovalent interaction (scheme 1).
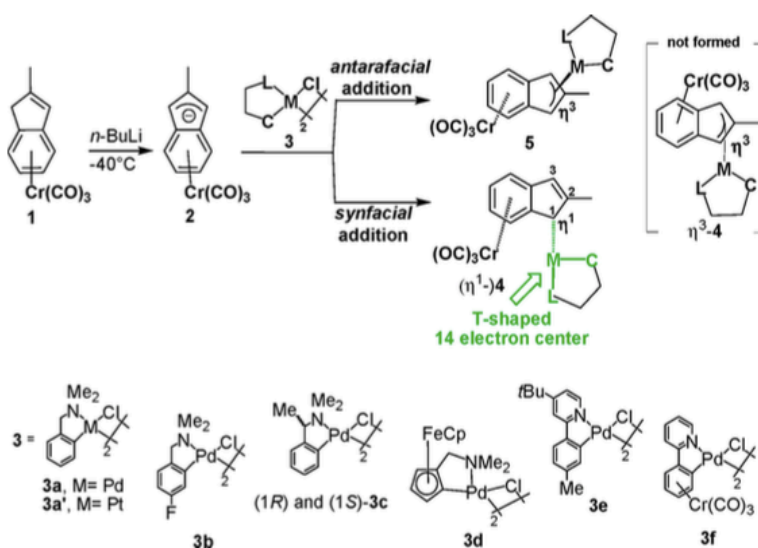
Scheme 1: method of synthesis of stable neutral T-shaped 14 electron Pd and Pt[4]

Chromium anion complexes were reacted with several Pd and Pt metallacycles to afford new air-stable and persistent synfacial heterobimetallic complexes.

Along with this line, numerous other metal complexes served as acceptors were investigated, for example, ClAu(THT) (THT = tetrahydrothiophene), [(NBD)RuCl]₂, [(COD)RuCl]₂ (scheme 2). Those were deprotonated and then treated with tricarbonyl chromium anions as the ambiphilic hemichelating ligand, however, the desired products failed to form.
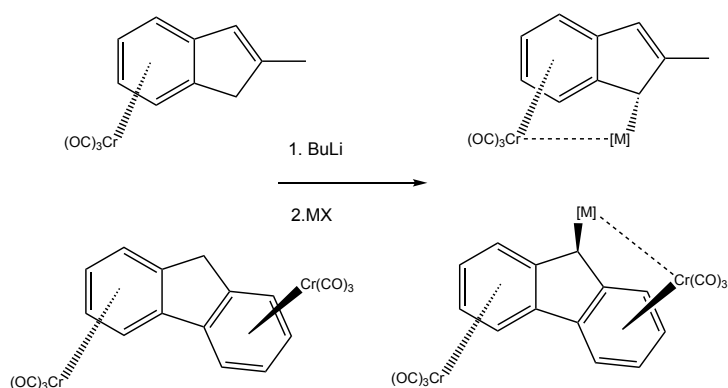
Scheme 2: General method of synthesis hemichelate complexes

Driving the reaction medium to ligand substitution (departure of COD, NBD, Cl, etc…) instead of the redox decomposition is the biggest challenge of those gold complexes. Regrettably, that was unachievable because Cr(0) in chromium complexes is easy to be oxidized by Au(I). Therefore, the reaction often ended up with the formation of black particles as the decomposition of the starting molecular and reactant complexes.

As for Ruthenium complexes, despite their behavior different than gold complexes, which did not lead to the decomposition, their lack of reactivity obstructed any attempt to isolate new binuclear hemichelates.

In the last endeavor, we tried to reproduce the chemistry of Pomeroy[6-13] that evidenced the possibility of forming metal based donor-acceptor complexes using 18-electron complexes as donor ligands such as Cp*Ir(CO)₂ and indenylIr(CO)₂ whose five-coordinate metal centers are expected to expand their coordination numbers to six readily (scheme 3).
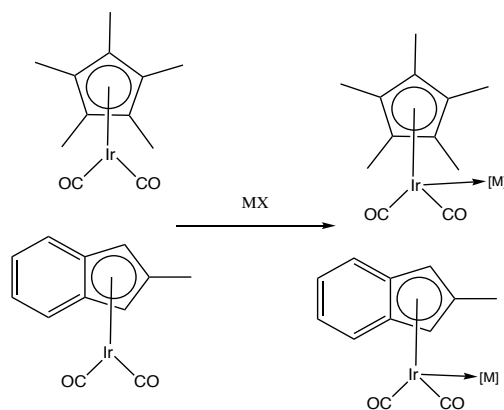
Scheme 3: 18-electron Ir complexes behaving as donor ligands

In addition, third-row neutral transition-metal donors give rise to much stronger dative bonds than their lighter congeners according to Pomeroy *et al*[6, 7, 9, 11, 13]. Nonetheless, these attempts were not successful, owing to the dominance of redox decomposition that ensued almost in all cases and the lack of reactivity of acceptor complexes.

Due to the failure to get promising results on this project, we have refocused our experimental work on the topic "Exploring the reactivity of silyl groups in metal-silane adducts", the aim of which was to understand the nature of the metal-silicon bond in metal-silane adducts.

1.2.   *The second subject: Investigating the reactivity of Silyl groups in metal-silane adducts.*

In this project, we wanted to establish a descriptor of the reactivity of silyl groups in transition metal complexes that would help chemists define the character of the silyl group in new metal-silane adducts. At the same time, the objective was to establish the design of new catalysts and the prediction of their reactivity. This project required the theoretical and experimental investigation of the reactivity of a myriad of known Ir-Si complexes, among which are those synthesized by Maitlis[14, 15] and hold the reputation of being Ir(V) complexes (scheme 4). This study involved the investigation on parameter could contribute to changing the character of Ir-Si bonds, among which the nature of the ligands bound to the metal and the charge were the most interesting.
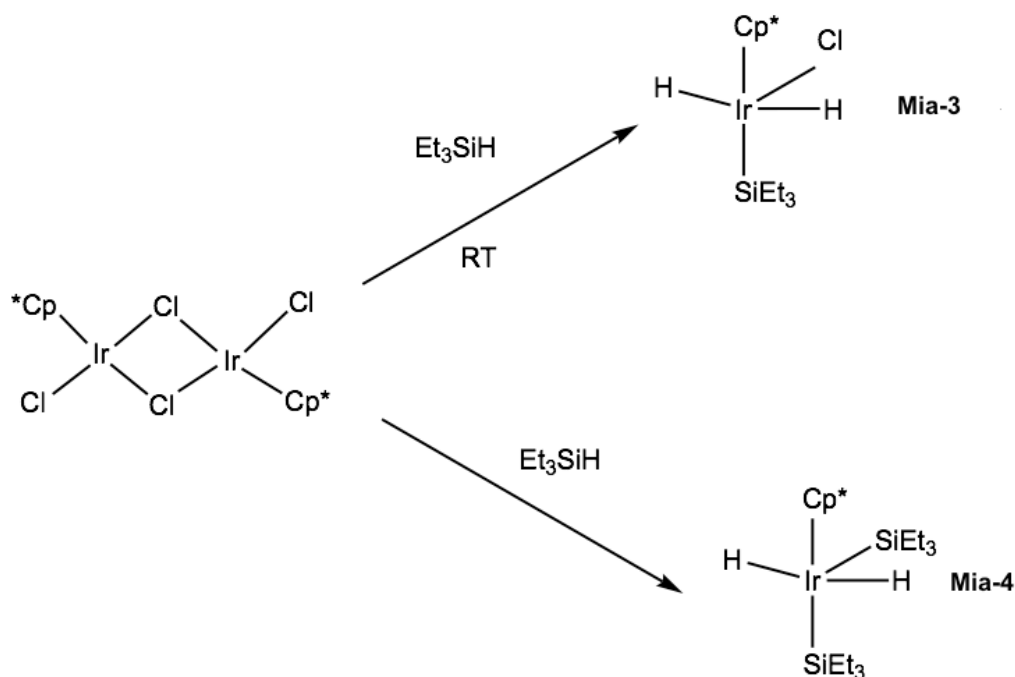
*Scheme 4: Synthesis **Mia-3** and **Mia-4***

Obtained data on this project contributed to our publication in 2017 "Is the R_3Si Moiety in Metal–Silyl Complexes a Z ligand? An Answer from the Interaction Energy"[16].

In this article a broad range of metal–silane adducts and other metal–silyl complexes were investigated by the computation of metal–silyl interaction energies to outline the established tools that rationalize the bonding relationship that exists between the metal center and a SiR_3 moiety. Also, has this research unveiled a net/clear separation between cases in which the Z character of the silyl moiety is the best description, and cases that belong to "classical" situations in which the X character dominates. Moreover, we postulated that for metal–silane adducts that possess a low intrinsic silylicity, the high "silylicity" can be switched on by ligand replacement or a change in the oxidation state of the metal.

To follow up the idea of evaluation and tuning silylicity character as mentioned above, the set of iridacycles [(C,N)Cp*Ir^{III}-Cl] ((C,N)=benzo[h]quinoline, phenyl pyridine, dibenzo[f,h]quinoline) associated with BArF-type anions were synthesized (scheme 5)[17, 18], then serving as a good starting point to explore new catalytic applications and to investigate silyl or silylium behavior in Ir-Si complexes.
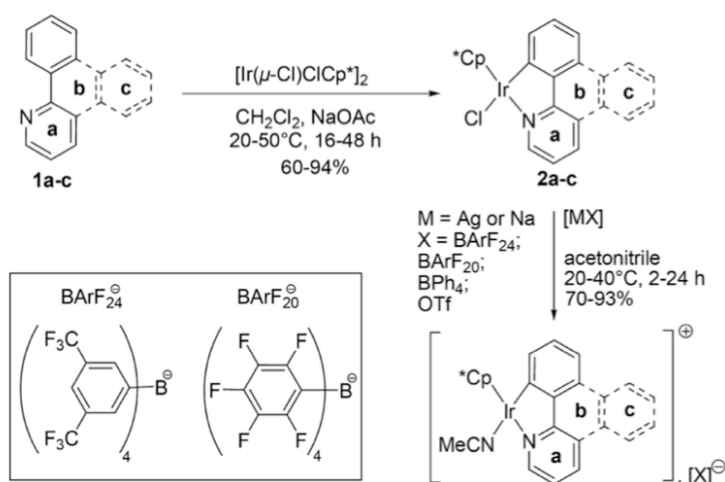
Scheme 5: Synthesis of metallacycle followed by Chloride abstraction and replacement by coordinated acetonitrile[17, 18]

These cationic complexes display a remarkable capability to catalyze the O-dehydrosilylation of alcohols and hydrosilylation of nitrile compounds by Et_3SiH. Mechanistic studies also have shown that the key intermediates are highly reactive hydrido-Ir(III)-silylium species in which the Et_3Si moiety behaves as a Z-type ligand according to Green's formalism (scheme 6)[17].
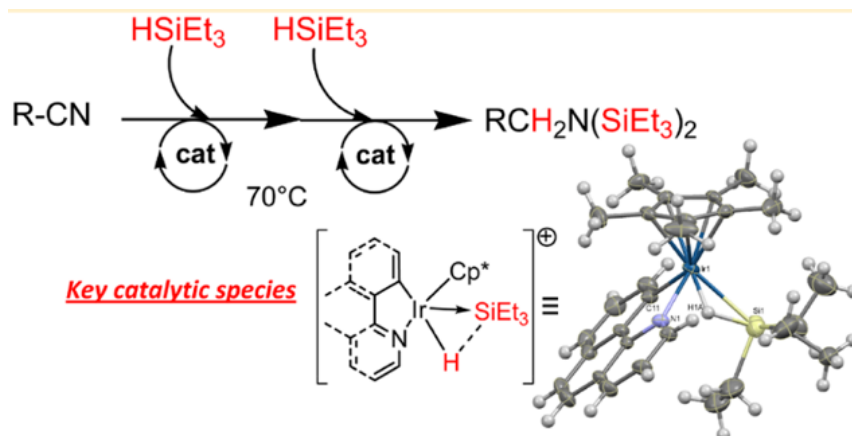
Scheme 6: A catalytic process to yield the N,N-disilylamine in the presence of adducts[17, 18]

Even though adducts could not be preparatively isolated and fully characterized analytically, crystals could be trapped and analyzed by X-ray diffraction analysis.
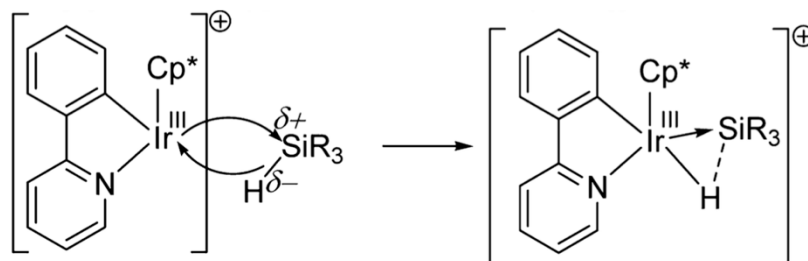
Scheme 7: Si-H bond activated by Irridacycle

1.3. The discovery of Silyene Ir[III] complexes

While working on this topic, we discovered that in the presence of tetrahydrofuran (THF), $[(Ir-H)\rightarrow SiRH_2]^+$ adducts readily convert by H_2 gas elimination at sub-ambient temperature into new THF-stabilized metallacyclic Ir(III)-"silylene". The primary goal of this thesis finally is to fully characterize those complexes by NMR spectroscopic analyses and X-ray diffraction analysis (scheme 8)[19].

Furthermore, DFT calculation and NMR kinetic research were utilized to demonstrate the essential importance of THF, which facilitated H_2 elimination. Catalytic reactivity trials on fluorinated compounds and nitro compounds were also performed.
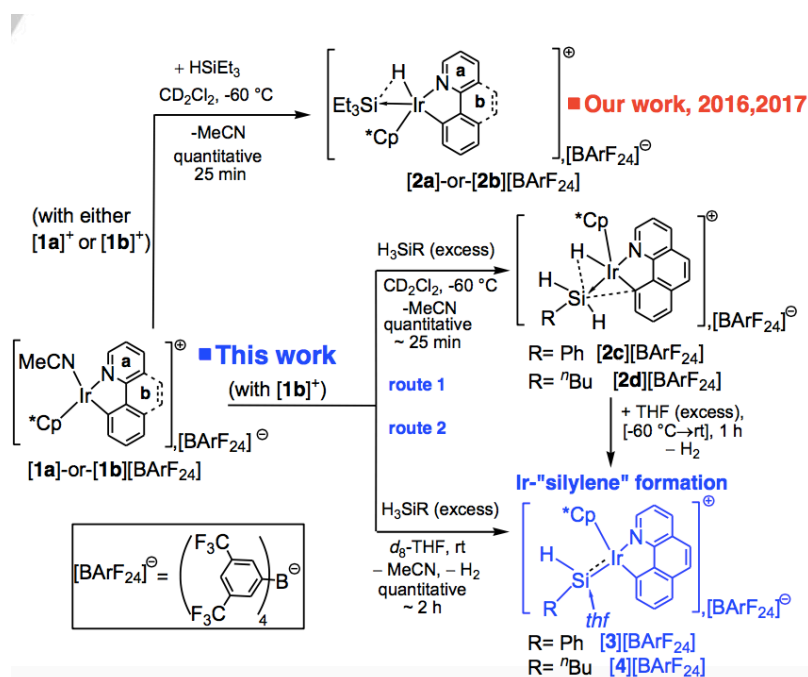
Scheme 8: Summary of our work from 2016 until the discovery of silylene[18]

2. *Problematic.*

Given that silylene metal complexes are of interest as possible intermediates in many transition metal-catalyzed reactions, silylene transfer is one of the most interesting utilizations one can imagine, and also the aspect that requires an ample scrutiny of synthesis and reactivity of those complexes.

The very first effort on silylene tranfers was made in 1962 by Volpin and colleagues[20] to trap bivalent silicon, based on the proposed hypothesis of chemical similarity between carbene and silylene. Those reactive species might be obtained by means of:

(1) The reactions of dimethylchlorosilane and sodium in boiling xylene:
$$(CH_3)_2SiCl_2 + Na \longrightarrow (CH_3)_2Si + 2NaCl$$
(2) The thermolysis of Si-Si bonds in the polymer $[(CH_3)_2Si]_n$ (with n = 55)
$$[(CH_3)_2Si]_n \ (t^o) \longrightarrow n(CH_3)_2Si$$
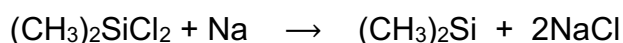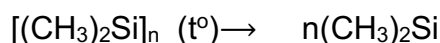
They presumed that in both cases, the presence of diphenylacetylene triggered the addition of the intermediate dimethylsilylene to the triple carbon-carbon bond to give rise to a silacyclopropene (Eq. 1) whose composition, molecular weight, infrared and chemical all lived up to their expectation.
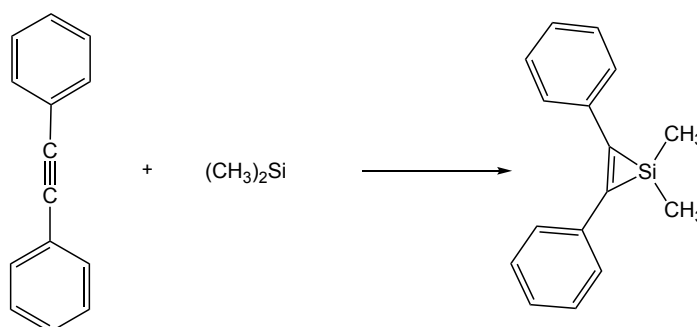
Eq. 1[19]

However, the claim of Volpin and colleagues was soon refuted by the demonstration that the isolated product was not a silacyclopropene but its dimer (Eq. 2)[21, 22].
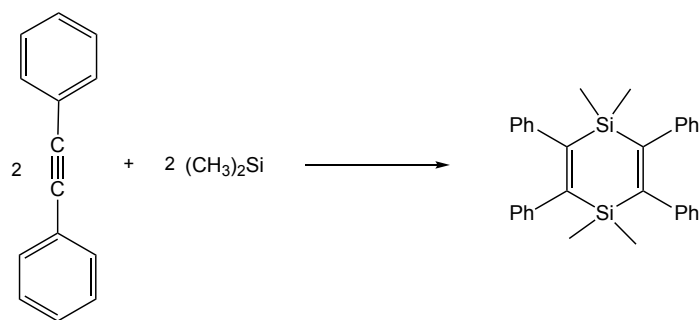
Eq. 2[20] [21]

The success of trapping divalent silylene to produce silacyclopropene was replicated and achieved years later by Conlin and Gaspar who reported that dimethylsilylene was generated by thermolysis of 1,2-dimethoxytetramethyldisilane in the addition of 2-butyne to give tetramethyl- 1-silacyclopropene (Eq. 3)[23].
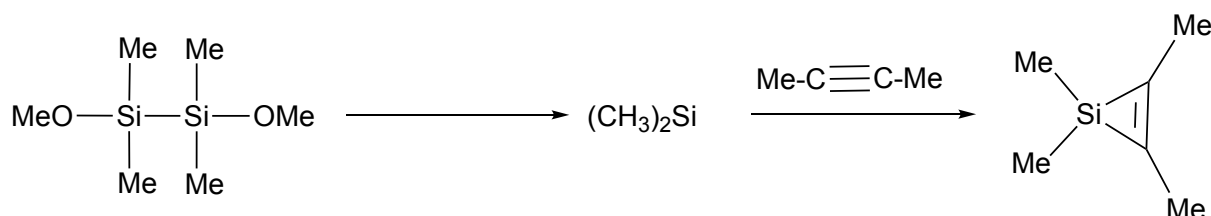
Eq. 3[22]

Those works then have initiated an abundance of research on synthesis of silacyclopropene via silylene transfers. There are three standard methods to trigger the formation of bivalent silicon species: photolysis, thermolysis and metal-catalysis, the latter will be discussed further in this section.

One of the initial works was published by Kumada in 1971 (Eq. 4), in which treatment of pentamethyldisilane with diphenylacetylene catalyzed by a platinum complex gives rise to 1,1,4,4-tetramethyl-1,4- disilacyclohexadiene derivative[24-26].
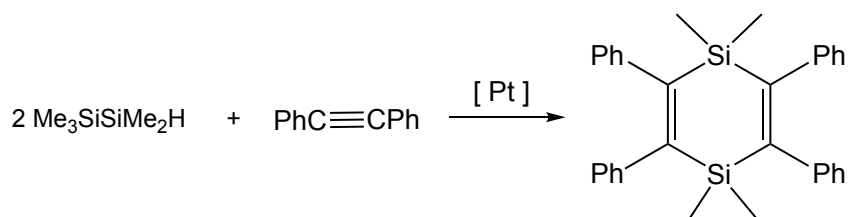
Eq. 4[23-25]

In that account, the authors believed bivalent silicon species was first released by platinum complex after which disilacyclohexadiene was formed via the dimerization of intermediate silacyclopropane that had trapped free "dimethylsilylene" intermediate followed the below mechanism (Eq. 5).
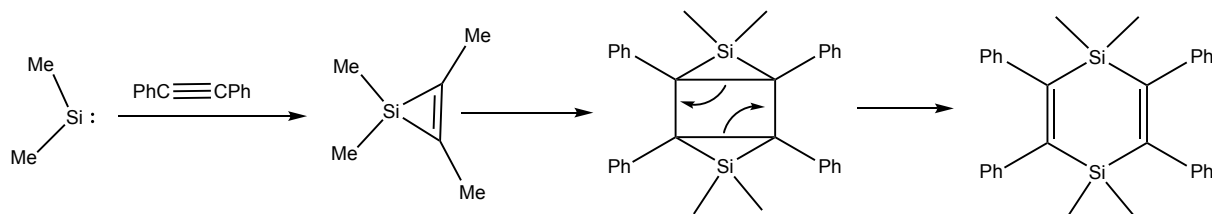
Eq. 5[23-25]

In 1985, Seyferth *et al.* assessed the interaction of silirene 1,1-dimethyl-2,3-bis(trimethylsilyl)silirene with phenylacetylene in the presence of a catalytic amount of bis(triphenylphosphine)palladium dichloride $(Ph_3P)_2PdCl_2$ (Eq. 6)[27].

After 1h, GLC analysis showed that two products had been formed: $Me_3SiC\equiv CSiMe_3$ in 76% yield and a silacyclopentadiene **Sey-6** in 80% yield.
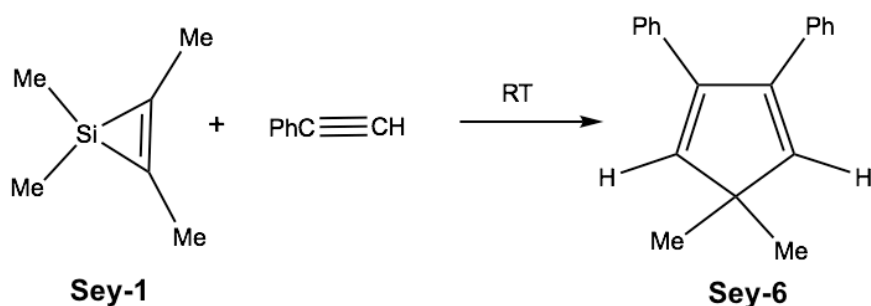
*Eq. 6: **Sey-1** and **Sey-6** [26]*

The proposed mechanism commenced with the formation of the active catalyst $(Ph_3P)_2Pd^0$ resulted from $(Ph_3P)_2PdCl_2$/silirene reactions. Then, an insertion of that low-valent, reactive, coordinatively unsaturated species into the silacyclopropene ring to form **Sey-21** took place. The collapse of Sey-**21** provided $Me_3SiC=CSiMe_3$ and a palladium-silylene complex $(Ph_3P)_2Pd=SiMe_2$ that afterwards reacted with $PhC\equiv CH$ to form a new silacyclopropene **Sey**-**22**. Finally, that three-member ring will interact with $PhC\equiv CH$ to produce Sey-**6**.
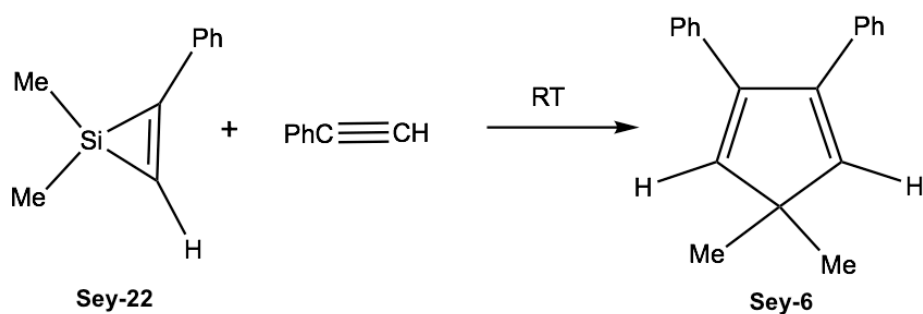
*Eq. 7: **Sey-22** and **Sey-6**[26]*
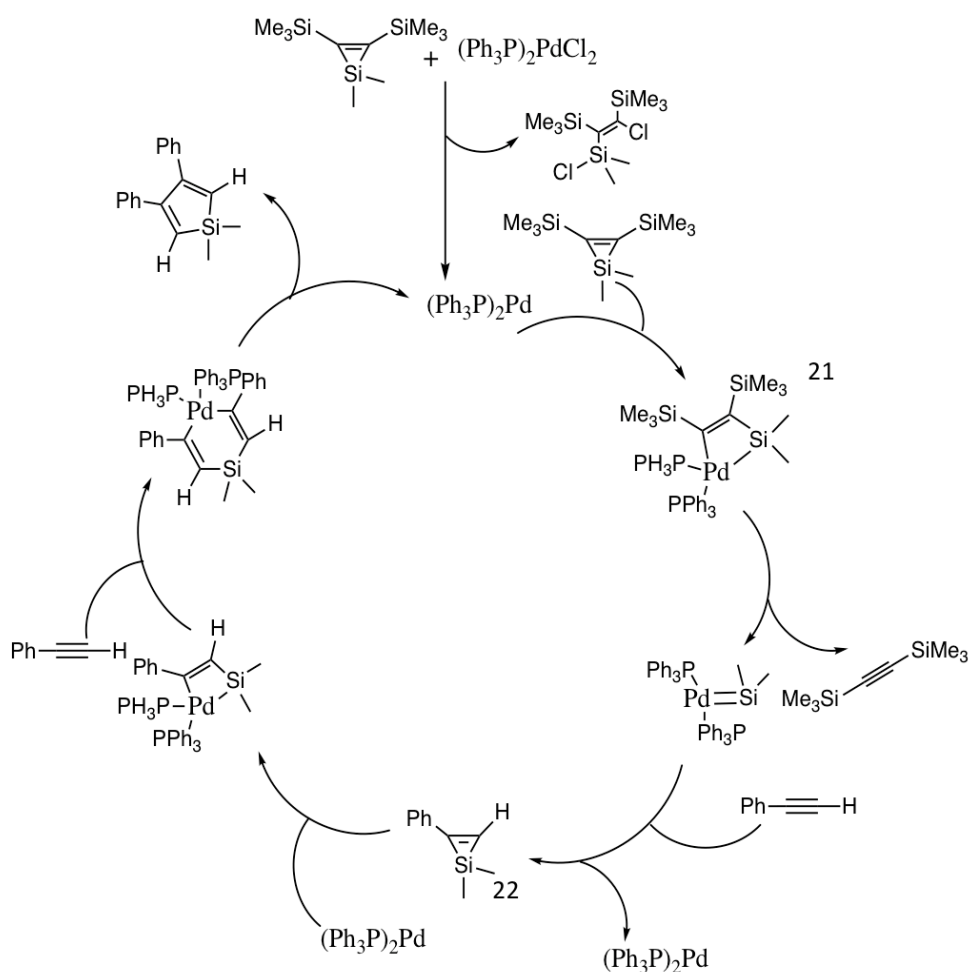
Scheme 9: The proposed mechanism of Seyferth et al.[30]

Yet the presence of silylene palladium intermediate was not evidenced, another mechanism in which the formation of silylene reactive species was cut off was proposed, which turned out to lead to a similar product. (scheme 10)
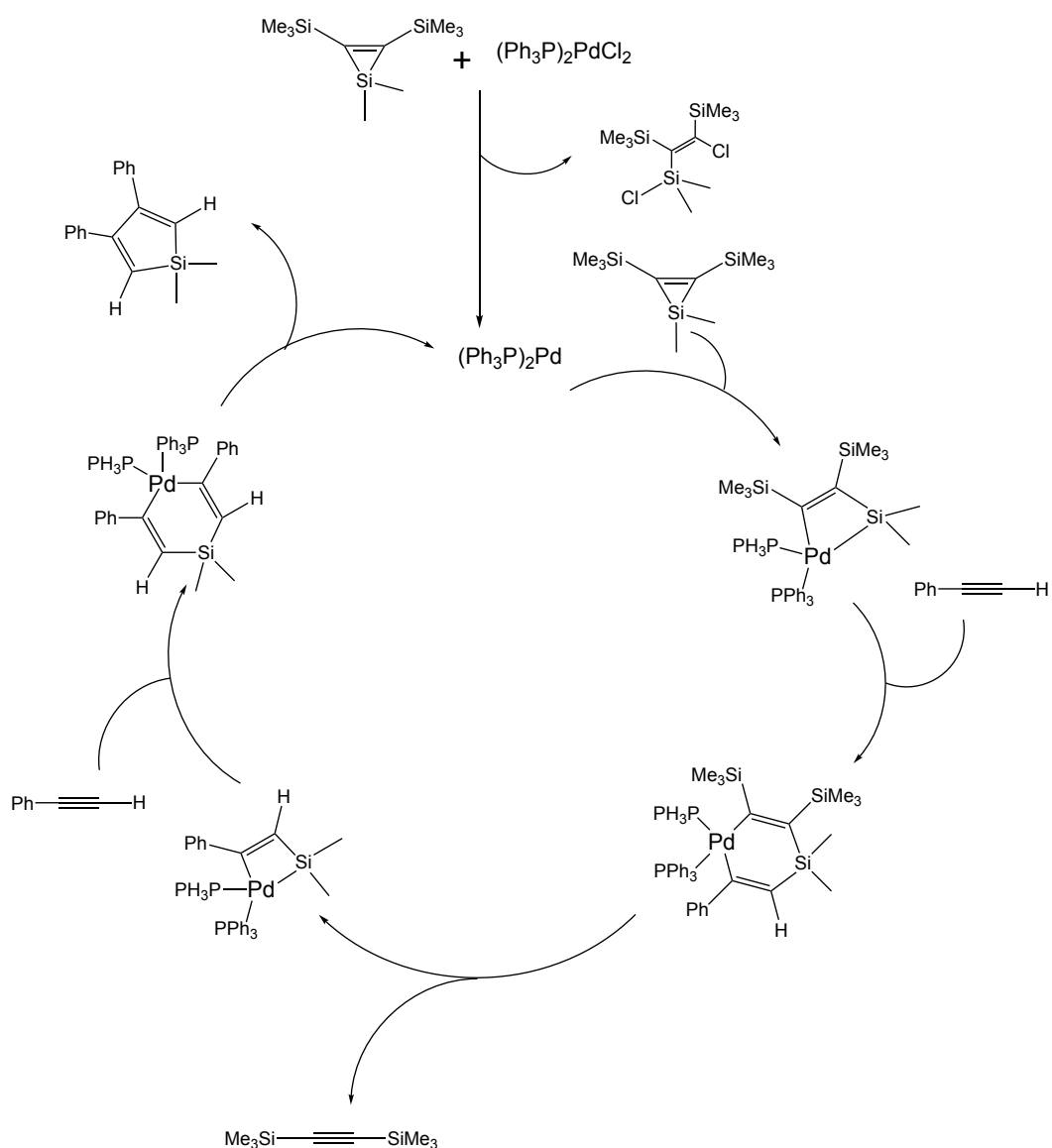
Scheme 10: Our proposed mechanism

The idea of the mentioned-above report was drew on in 1997 by Woerpel, nevertheless the confirmation of silylene's involvement appears to be vague. The siliranes **Woe**-cis-**1** and **Woe**-trans-**1** were treated with a variety of terminal acetylenes in a catalytic amount of $(Ph_3P)_2PdCl_2$ (<3 mol %) to yield siloles **Woe**-**2** (Eq. 8, Table 1)[28].

Entry	Acetylene	Silirane	Isolated yields, %		
			Woe-2	**Woe-Cis-3**	**Woe-Trans-3**
1	Ph	cis-1	55	31	0
2	Ph	trans-1	83	0	1
3	Bu	trans-1	73	0	0
4	CH$_2$OMe	trans-1	67	0	0
5	CO$_2$Et	cis-1	57	14	0

Conditions: 2.0-3.5 equiv of acetylene, 0.2-3.0 mol %

PdCl$_2$(PPh$_3$)$_2$, PhH as solvent (0.1 M), 23 °C.

*Table 1: The siliranes **Woe**-cis-**1** and **Woe**-trans-**1** were treated with a variety of terminal acetylenes in a catalytic amount*
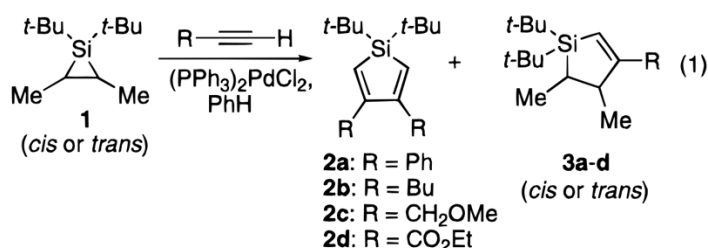
*Eq 8: **Woe-1,2** and **3** [28]*

Woe-trans-**1** was treated with the palladium catalyst without alkyne in C$_6$D$_6$, it slowly rearranged to form the silane **Woe-6** over the course of a few days.
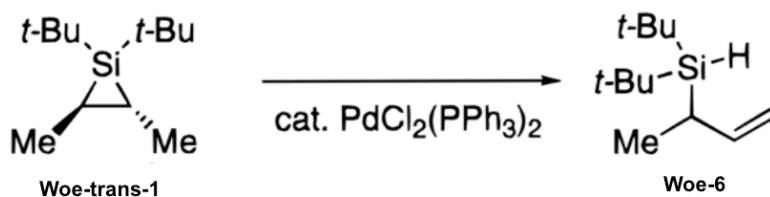
*Eq. 9: **Woe**-trans-**1** and **Woe-6** [28]*

The catalytic cycle shown in Scheme 11 is modified from Seyferth's proposed mechanism (mentioned above). The oxidative addition of in-situ-generated Pd(0)[29] into the C-Si bond of **Woe**-trans-**1** associated with stereospecific retention of configuration at the carbon atom provides palladacyclobutane **Woe**-trans-**7**[30].

In the absence of alkyne, the palladasilacyclobutane intermediate **Woe**-trans-**7** was subjected to beta-hydride elimination and reductive elimination to give rise to allylsilane **Woe**-**6**.

In the presence of an alkyne, association and migratory insertion[31] gives rise to the palladasilacyclohexene **Woe**-trans-**8**[30]. Then **Woe**-trans-**8** would undergo reductive elimination to form the silacyclopentene **Woe**-trans-**3** with retention of configuration at the carbon stereocenter.[32]

Alternatively, **Woe**-trans-**8** may go through migratory deinsertion to release **Woe**-trans-**2**- butene and palladasilacyclobutene **Woe**-**9**. These species would form silole **Woe**-**2** after alkyne association, migratory insertion, and reductive elimination (Eq. 11).[33]
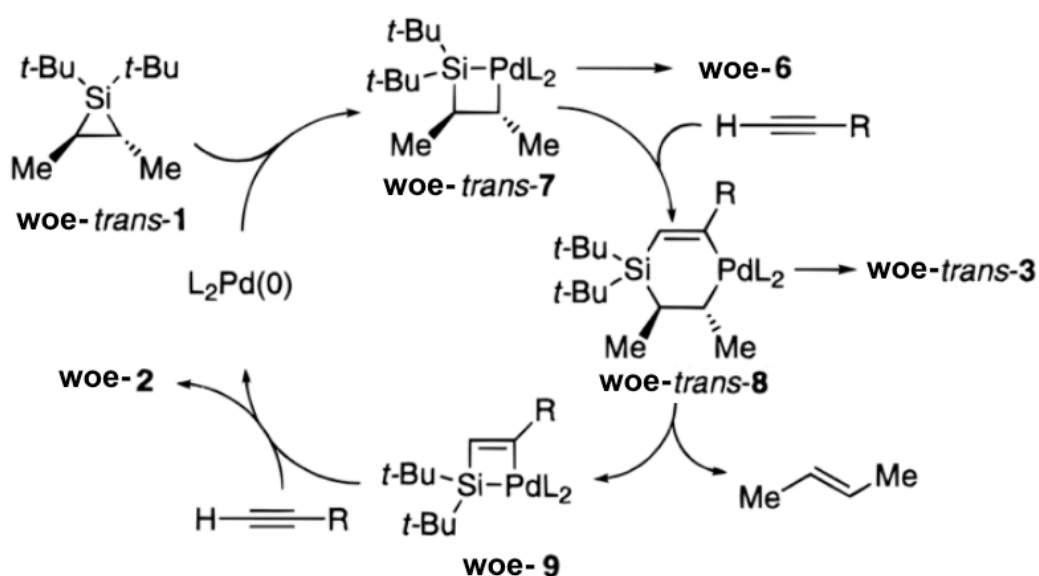
*Scheme 11: Reaction mechanism from **woe-trans-1** to products[28]*

Coupled with reactions towards carbon-carbon unsaturated bond, silylene transfers also can react to other functional groups.

Woerpel *et al*, in 2007, reported[34] a method for the diastereoselective construction of quaternary carbon stereocenters (Eq.10), encompassing silylene transfer into α,β-unsaturated ester to afford silyl ketene acetal which afterward undergoes a stereospecific Ireland-Claisen rearrangement[35, 36] to provide silalactone (Eq. 10).

*Eq 10: **Pel-1*** [34]
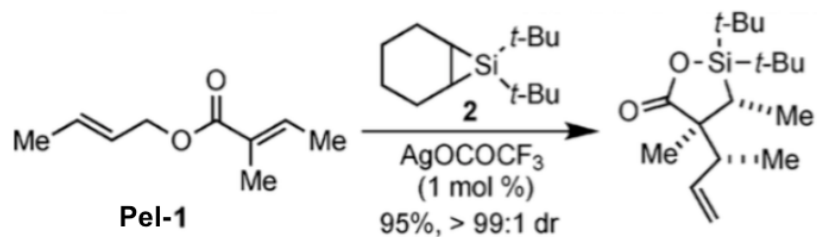
The trapping silylene, catalyzed by AgOCOCF$_3$, by ester **Pel-4** leads to formation of a silacarbonyl ylide **Pel-5** that afterward was 6π electrocyclized to produce oxasilacyclopentene **Pel-6** (Scheme.12). At room temperature, oxasilacyclopentene **Pel-6** underwent an Ireland-Claisen rearrangement via a chairlike transition state (scheme 12) in which the isopropyl substituent adopts an equatorial position[37] to afford silalactone **Pel-7**.

Scheme 12: Controlling Quaternary Carbon Stereochemistry [34]
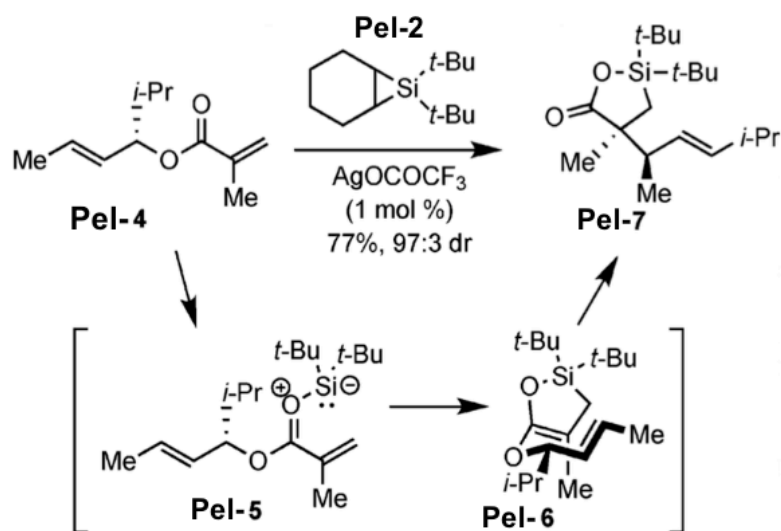
Silylene transfer to alpha-keto esters is also utilized as a strategy for the stereoselective, one-flask synthesis of enantiomerically enriched tertiary alpha-hydroxy acids[38] that are common substructures in natural products and serve as important synthetic intermediates[39, 40].
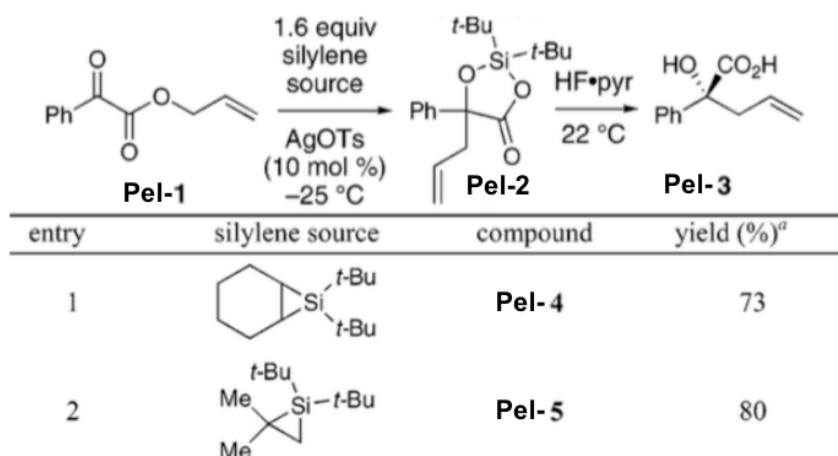
Table 2: Optimization of the Silylene Source[38]

The treatment of ester **Pel**-1 with silacyclopropane **Pel-4** and 10 mol % of AgOTs in toluene resulted in direct formation of silalactones **Pel**-2 in 73% yield as determined by NMR spectroscopy. The product was later purified by HF•Pyridine[41] to afford analytically pure R-hydroxy acid **Pel-3**.

The proposed mechanism for the synthesis of α-hydroxy acids is described in scheme 13. The silver silylenoid species[42] generated by subjecting silacyclopropane **Pel**-4 to AgOTs accompanied by an attack of the ketone carbonyl oxygen gives rise to silacarbonyl ylide **Pel-8**, which can then be 6π-electrocyclized to produce silyl ketene acetal **Pel-9**. Ireland-Claisen rearrangement of silane **Pel-9** then took place via a chair-like transition state to produce silalactone **Pel-10**, which was hydrolyzed eventually to afford alpha-hydroxy acid.
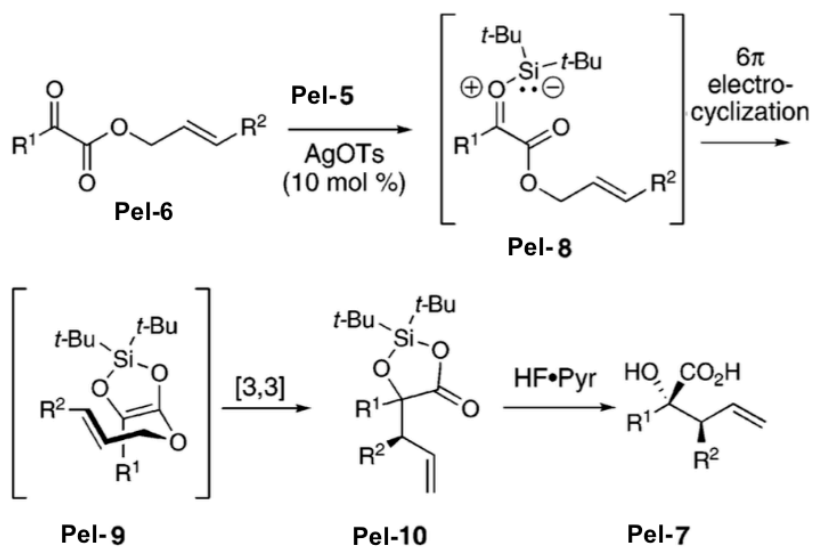
Scheme 13: Proposed mechanism [38]

The authors stated that although divalent silicon species have not been detected, the justification of that mechanism remains compelling thanks to the conversion of ethyl pyruvate to a similar silyl ketene acetal under identical silylene transfer conditions (Eq. 11).[43]
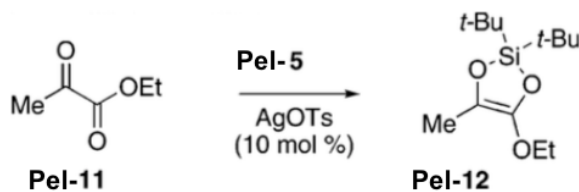
Eq. 11[42]

However, the method is used to generate silylene is totally different in the two publications, Woerpel used AgOTs whereas that of Gehrhus is thermolysis. Notably, no eloquent proof that divalent silicon species substantially appeared.

By pondering those examples above, it's safe to say that although the application of silylene transfer catalyzed by metal in organic chemistry prevails, is well-established, with some attempts made to prove its existence, the generalization of "silylene metal" intermediate remains to be seen.

3. Introduction of silylene metal complexes

3.1. Classification.

Silylene complexes have attracted a great deal of chemists' interest as possible intermediates in numerous stoichiometric and catalytic chemical transformations[44, 45]. Being convergence of transition metal chemistry with main group chemistry, these complexes can be classified into 5 groups according to their distinct structure.

Group	1	2	3	4	5
Structure	$[L_nM] = SiHR_2$	$[L_nM] = SiHR_2$ with D→	$[L_nM] = Si(NR)_2(\ )_n$	$[L_nM]$ Si X $(NR)_2(\ )_n$	$[L_nM] ----- SiRR'$ with H
Example	OC,,, CO ,,,S^{p}Tol OC—Os=Si—Ru CO	[Cp*(Me$_3$P)$_2$Ru=SiPh$_2$]$^+$ with NCMe→	(^{t}Bu N Si=Ni(CO)$_2$ ^{t}Bu)$_2$	^{t}Bu OC,,, V ,,,CO Ph—N Si CO Ph—N Cl ^{t}Bu	Ph B PPh$_2$ Ph$_2$P Ph$_2$P—Ni:Si H

Table 3: Five group of silylene complexes and their examples[44-47].

Group 3: n = 1 or 2; R = bulky aromatic or aliphatic group.
Group 4: n = 1, 2 or 3; X = halogen or H; R = bulky aromatic or aliphatic group
Group 5: R, R' = alkyl group

Type 1 are analogues of carbene complexes ($[L_nM = CR_2]$) without stabilizing-base while type 2 entails a coordinated-base silylene ligand bound to transition metal fragment. Type 3 illustrates NHSi complexes including unsaturated functionalities and/or additional R groups in the ligand skeleton, type 4 are NHSi halide or hydride complexes. Type 5 is silylenes complexes stabilized by the interaction of M−H bonds with the electrophilic silicon center. Type 1 and type 2 will be focused on this thesis.

3.2.   A brief history.

In 1970, Kumada and colleagues presented the monomerization and oligomerization of hydropentamethyldisilane, catalyzed by trans-$PtCl_2(PEt_3)_2$ (Eq. 12), with the possible presence of platinum silylene complexes in their proposed mechanism.

$$Si_2Me_5H \xrightarrow[\text{90 °C, 18 h}]{\text{\textit{trans}-PtCl}_2\text{(PEt}_3\text{)}_2} Si_nMe_{2n+1}H$$

$$n = 1 - 6$$
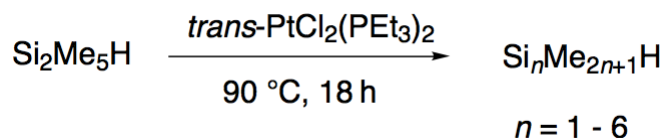
<p align="center">Eq. 12[45, 48]</p>

The reactive species were formed by the oxidative addition of the disilane to the coordinatively unsaturated platinum complex $PtCl_2(PEt_3)$, accompanied by the reductive elimination of the monosilane. These then underwent the addition of disilane or oligosilanes associated with the reductive elimination of $Si_nMe_{2n+1}H$ to regenerate the reactive platinum catalyst[48].
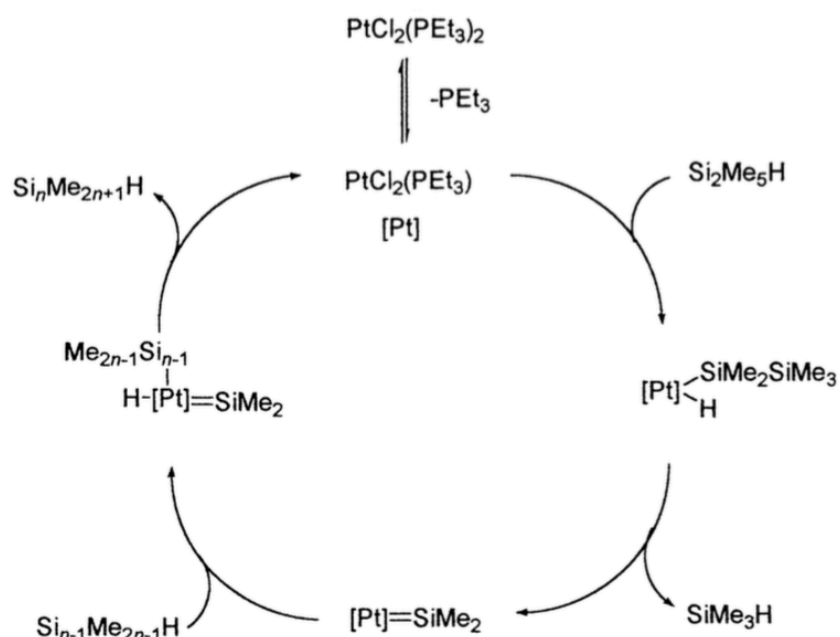
Scheme 14. Possible mechanism of monomerization and oligomerization of hydrodisilane by trans-PtCl$_2$(PEt$_3$).[45, 48]

After that, Ojima *et al.* also reported the formation of the silyl(silylene) complex as a potential intermediate, which plays an essential role in the scrambling substituents and

dehydrogenative silane coupling of dihydrosilane $H_2SiPhMe$ in the presence of Wilkinson's catalyst (Eq. 13)[49].

$$H_2SiPhMe \xrightarrow[\text{70 °C, 1 h}]{RhCl(PPh_3)_3} SiPh_3Me + HSiPh_2Me$$

$$+ \quad \underset{\substack{| \ | \\ Me\,Me}}{H-\overset{\substack{Ph\,Ph \\ | \ |}}{Si}-Si-H} \quad + \quad \underset{\substack{| \ \ | \ \ | \\ Me\,Me\,Me}}{H-\overset{\substack{Ph\,Ph\,Ph \\ | \ \ | \ \ |}}{Si}-Si-Si-H}$$
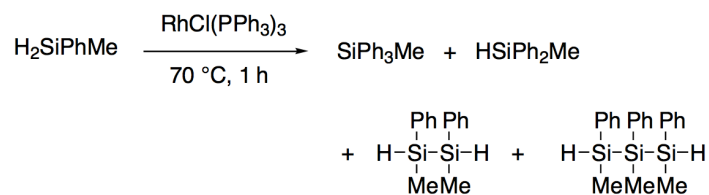
Eq. 13

The mechanism presented in scheme 15 shows that the oxidative addition reactions of two molecules of the dihydrosilane to the coordinatively unsaturated complex [Rh] producing a silyl(silylene) complex are crucial. Afterwards, the intermediate could undergo either a 1,3-R-shift in the complex followed by the reductive elimination of a monosilane to form a scrambling of the substituents or 1,2-silyl shift in the complex followed by further reductive elimination to yield the dehydrogenative coupling product (scheme. 15).
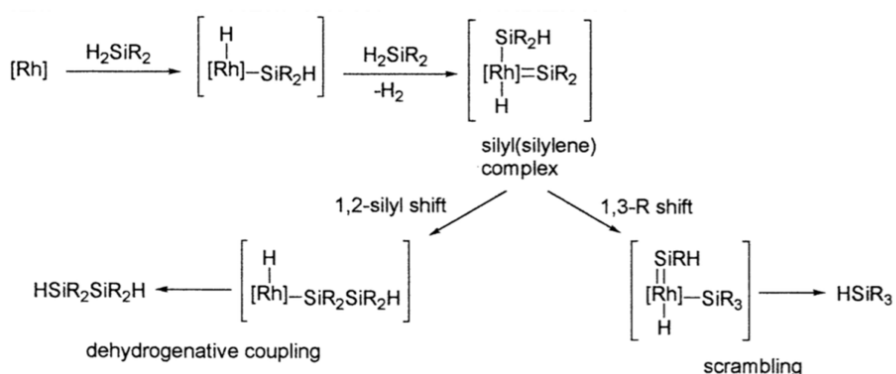
Scheme 15[45, 48]: Proposed mechanism of reaction Eq.13

Around ten years later, the first synthesis of silylene metal complex has first come to light by Schmid and Welz[50] (Eq. 14). The photolysis of $Fe(CO)_5$, in the presence of $HSiMe_2(NEt_2)$, generated a base stabilized-silylene complex **Wel-2** $(OC)_4Fe(=SiMe_2\bullet NHEt_2)$.
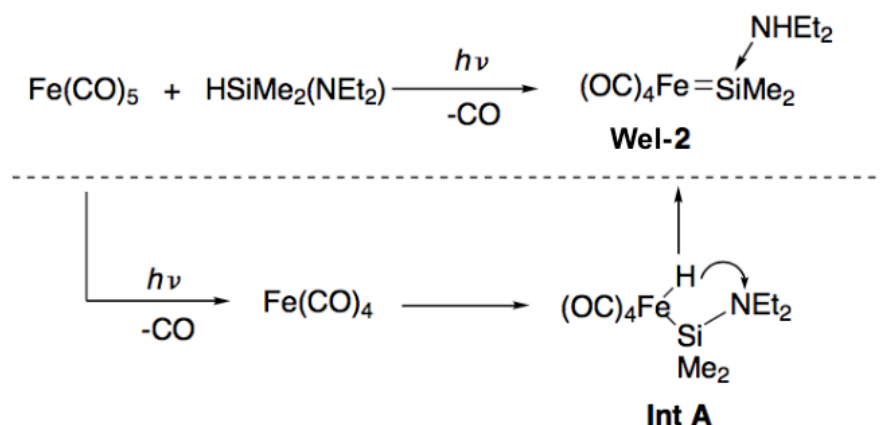
*Eq 14: **Wel-2** [50]*

The irradiation of $Fe(CO)_5$ produced the 16-electron complex $Fe(CO)_4$ that later reacted with $HSiMe_2(NEt_2)$ to give rise to the oxidative addition product Intermediate A. Finally, the basicity of diethylamino being stronger than the iron counterpart drove the proton migration from the iron center to the diethylamino group in Intermediate A to provide the final product. However, this complex is too unstable to be structurally characterized by X-ray.

The ground-breaking result arose in 1987 when Zybill and colleagues proposed a synthesis route to silyleneiron complexes $(OC)_4Fe=Si(O^tBu)_2 \cdot base$ by utilizing a salt elimination method and their X-ray crystallographic structures [45, 51].
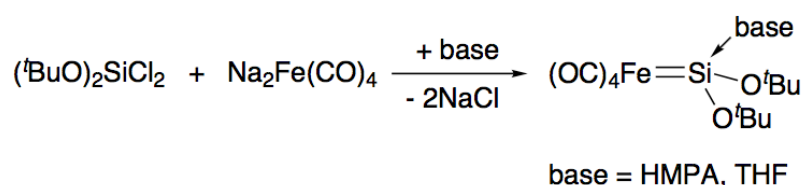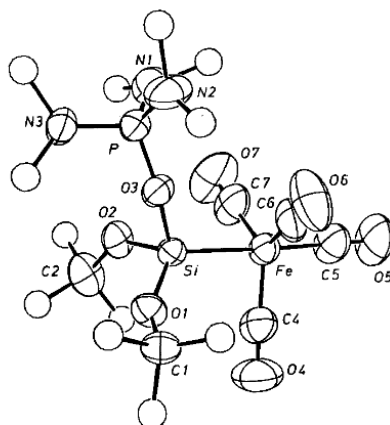
base = HMPA, THF

Eq. 15 [44, 50]

33

Figure 1: X-ray structure of iron silylene complex published by Zybill et al[51].

Braunstein and colleagues successfully used almost the same routine to synthesize an analogue of Schmid and Welz's Iron silylene complexes $(OC)_4Fe=Si(NMe_2)_2$ •$NHMe_2$ that also could be structurally determined by X-ray crystallographic (Eq. 16)[45, 52].

$$Fe(CO)_5 + HSi(NMe_2)_3 \xrightarrow[-CO]{h\nu} (OC)_4Fe=Si \begin{smallmatrix} NHMe_2 \\ NMe_2 \\ NMe_2 \end{smallmatrix}$$
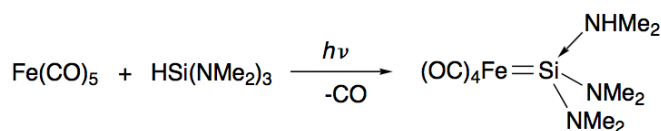
Eq. 16

3.3.   Synthesis of metal silylene complexes

Because of the close positional relationship in the periodic table, the chemical reactivity of carbon and silicon was expected to be similar, so the preliminary research on silicon was carried out with the preconception that the chemical properties of these two elements would resemble each other[53]. The enigma whether silylene complex, heavier analogues of the notorious carbenes complex, exists as stable entities could be raised by theoreticians around in the 1980s. The energy of the M=Si bond for the hypothetical complex $[(OC)_5Cr=Si(OH)H]$ was calculated to be only 29.6 kcal/mol while that of the corresponding hypothetical complex $[(OC)_5Cr=C(OH)H]$ is 44.4 kcal/mol[54, 55]. Therefore, the attainment of stable silylene complexes was deemed achievable.

Although the perusal on silylene complex chemistry shed light on major discoveries, for instance the establishment of the high reactivity of simple hydrosilanes or finding polysilanes with sigma-conjugated backbone and silicone polymer[56, 57], those effort appeared not to be of success due to the inherent instability of silicon compounds. Although the M=Si double bond in the silylene complexes partly possesses σ-donation/ π-back donation related to carbene complexes, the back donation from the $d\pi$ orbital of the metal center to the vacant p orbital of the silylene silicon atom is weaker than in the carbene one. (Figure. 2)
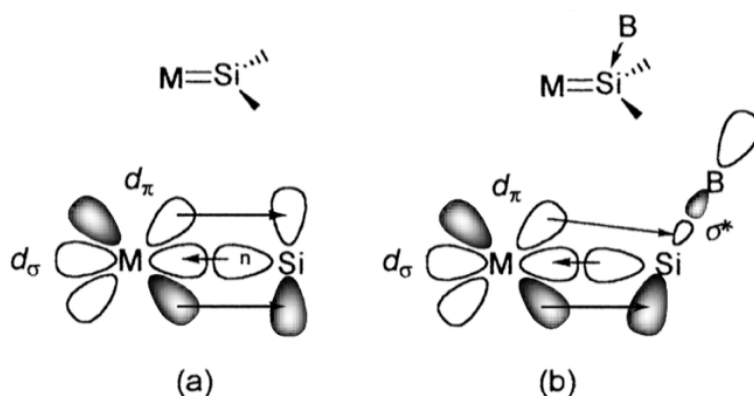
Figure 2: Schematic diagram of the M=Si bonds of silylene complex (a) and base-stabilized silylene complex (b). B denotes a base[45, 54].

That also explains why the M=Si double bond is strongly polarized toward $M^{(-)}$=$Si^{(+)}$ resulting in high electron-deficiency on the silicon atom. Therefore, theoretically speaking, in the presence of a base, the base-coordinating constituted from the donation from dπ metal orbital to the σ* orbital of the silicon-based bond will stabilize the silylene system[50, 55, 58-61].

To date, the development of a variety of preparative methods have facilitated the synthesis of transition-metal silylene complexes; this account will describe several of those findings.

3.3.1. Ligation *of Free Silylene to Metal Complexes*

The most straightforward method to synthesize silylene complexes was acheived by using coordinative unsaturated metal fragment [M] and a free silylene[45, 62]. (Eq.17)

$$[M] \; + \; :SiR_2 \longrightarrow [M]{=}SiR_2$$
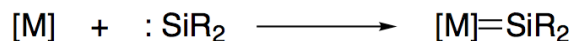
<p align="center">*Eq 17[45, 62]*</p>

Tilley *et al.* reported the capturing a thermally unstable silylene by way of irradiation of $(Me_3Si)_2SiMes_2$ (Mes = mesityl of 2,4,6- $Me_3C_6H_2$) in the presence of low-valent platinum species L_2Pt (L = iPr$_3$P and Cy$_3$P) to form a terminal three-coordinate Pt–silylene complexes $L_2Pt{=}SiMes_2$ (scheme 16) [63, 64].

$$(Me_3Si)_2SiMes_2 \xrightarrow[-Si_2Me_6]{h\nu} \left[Mes_2Si: \right] \xrightarrow{(R_3P)_2Pt} \underset{R_3P}{\overset{R_3P}{>}}Pt{=}Si\underset{Mes}{\overset{Mes}{<}}$$
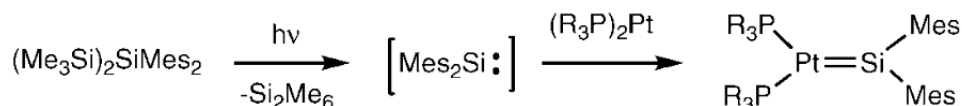
<p align="center">*Scheme 16: Coordination of a free silylene[65]*</p>

Denk *et al.* reported the first silylene complex of nickel as well as the first bis-silylene complex without Lewis base stabilization synthesized from a stable silylene and metal carbonyls $Ni(CO)_4$. It is acutely air- and moisture-sensitive yet quite thermally stable (mp 160 °C, decomp.). Although changing the reaction conditions (inverse addition of **Den-1** to an excessive excess of $Ni(CO)_4$ at -80°C) or on the effort comproportionation of **Den-3** with $Ni(CO)_4$, monosubstitution product **Den-2** was not detected (Eq. 18) [66, 67].

Den-1   **Den-2**   **Den-3**
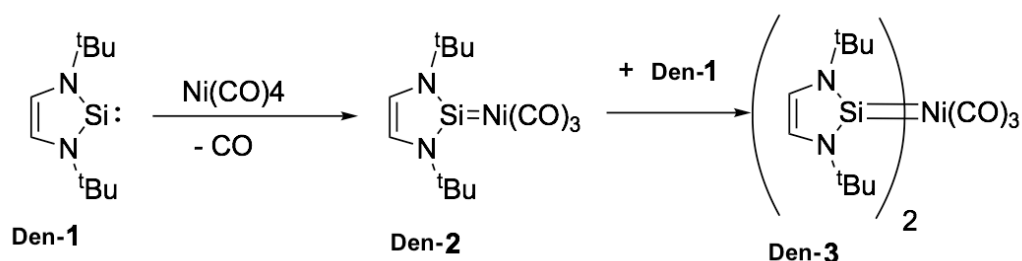
<p align="center">*Eq. 18[66,67]*</p>

Woo described first donor-stabilized silylene complexes of metalloporphyrin osmium $(TTP)Os{=}SiMe_2{\cdot}THF$ (TPP = meso-tetra-p-tolylporphyrin). The successful outcome was accomplished by employing the reaction of $[Os(TTP)]_2$ with hexamethylsilacyclopropan serving as a useful reagent for generating transient dimethylsilylene under mild condition[68, 69]. This idea was founded on the ground that bulky substituents on silicon would increase kinetic stability and an electron-rich, late transition metal would stabilize adjacent electron-deficient silicon atom.[70] (Eq.19)

$$\text{Os(TPP)}_2 \quad + \quad \underset{\underset{\text{Me}_2\text{C}-\text{CMe}_2}{\underset{|}{\text{Si}}}{\overset{\text{Me}_2}{\triangle}} \quad \xrightarrow[\text{-Me}_2\text{C}=\text{CMe}_2]{\Delta,\ \text{THF}} \quad (\text{TPP})\text{Os}=\overset{\uparrow\ \text{THF}}{\text{SiMe}_2}$$

Eq. 19[70]
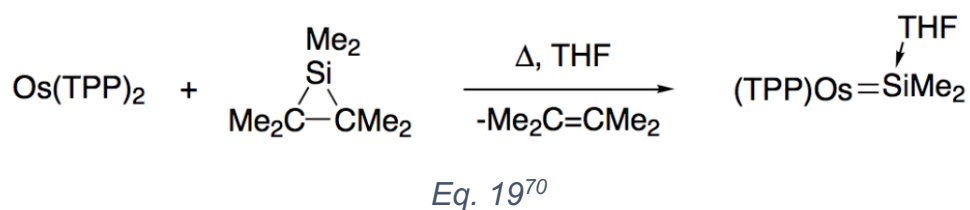
3.3.2. *Metal-Mediated dihydrogen elimination from dihydrosilanes*

Corriu et al have established the method using the photolysis of hydrosilanes with metal carbonyl accompanied with the external or internal Lewis base stabilization (Eq. 20) [71-73].

$$\text{Ph}_2\text{SiH}_2 \quad + \quad \text{Fe(CO)}_5 \quad \xrightarrow[\substack{+\ \text{HMPA}\\ \text{-CO, -H}_2}]{h\nu} \quad (\text{OC})_4\text{Fe}=\overset{\uparrow\ \text{HMPA}}{\text{SiPh}_2}$$
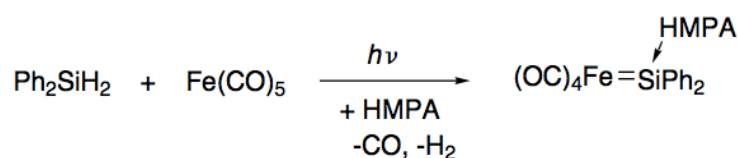
(HMPA = hexamethylphosphoric triamide)

Eq. 20[73]

This method has been extended on an array of transition metal carbonyl complexes as Fe(CO)_5, Cr(CO)_6, CpCo(CO)_2, and RCpMn(CO)_3 (R = H, CH_3) that could generate 16e metal species by releasing one CO compound under photolytic conditions. For example iron pentacarbonyl.

internal Lewis base stabilization
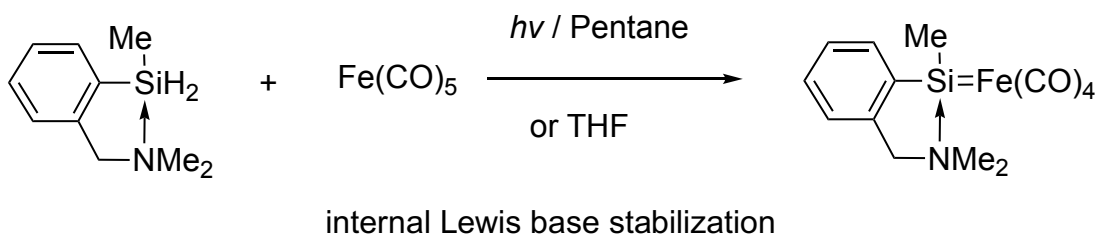
Eq 21[71-73]

3.3.3. Alpha hydrogen migration.

Tilley *et al.* have contributed to the work on silylene complexes via silyl ligand whose substituent is prone to migrate to a vacant coordination site on metal, especially hydrogen which could trigger 1,2-H shift from silyl ligand to the central metal[65]. The first application of that method is shown in the equation below.

α-Hydrogen migration
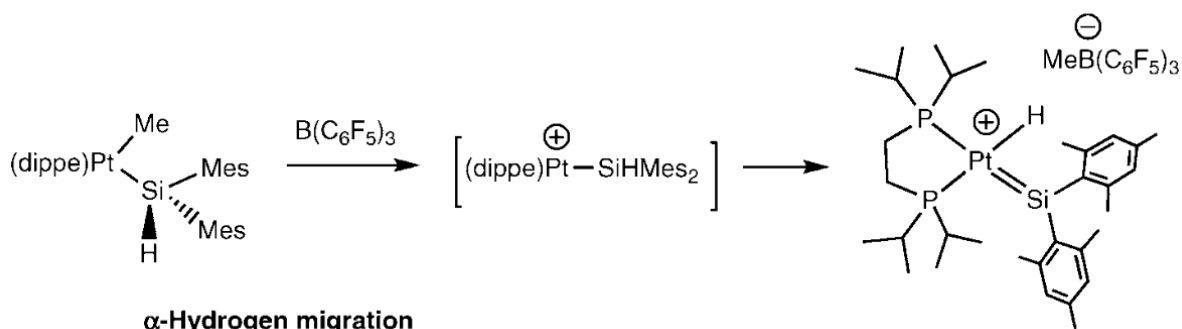
dippe = 1,2-bis(diisopropyl- 2 phosphino)ethane

Eq. 22[65]

$B(C_6F_5)_3$ abstracted a methide ion (CH_3^-) on platinum complex (dippe)PtMe(Si-HMes$_2$) to form the three-coordinate cation platinum silyl intermediate [(dippe)Pt(Si-HMes$_2$)]$^+$. By possessing a vacant coordination site on metal center, the reactive species afterward underwent presumptively the 1,2-hydrogen migration from Si to metal center to result in platinum silylene complex (Eq.22).

This method demonstrated its reproducibility by an application on fac-IrH(Me)(SiHMes$_2$)(PMe$_3$)$_3$ to provide the cationic silylene complex [fac-(Me$_3$P)$_3$H$_2$Ir=SiMes$_2$][MeB(C$_6$F$_5$)$_3$][74]. (Eq. 23)
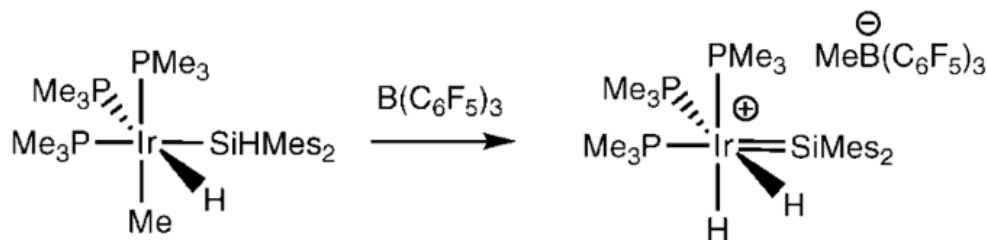
Eq 23[72]

Another example is the treatment of Cp*(Me$_3$P)(Br)(H)Os(SiHRR′) (R = H, aryl, or silyl; R′ = R or aryl) with the anion metathesis reagent LiB(C$_6$F$_5$)$_4$•3Et$_2$O which is able to abstract bromide anion in CD$_2$Cl$_2$ to afford a cationic osmium complex with terminal silylene ligands[75](eq. 24)
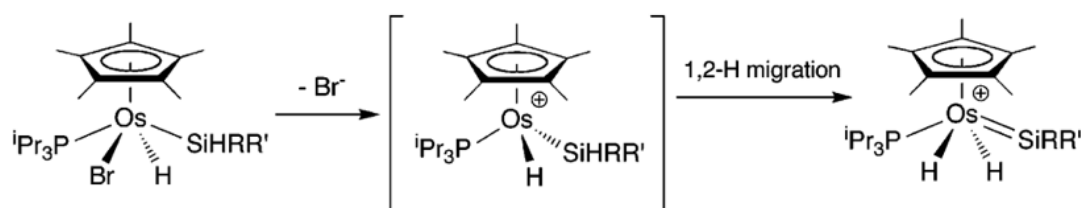
Eq 24[73]

1,2 hydrogen migration from silicon to the metal center also is triggered by a combination of sequence processes including silane Si–H oxidative addition, reductive elimination to expose a coordinative position (figure 3).
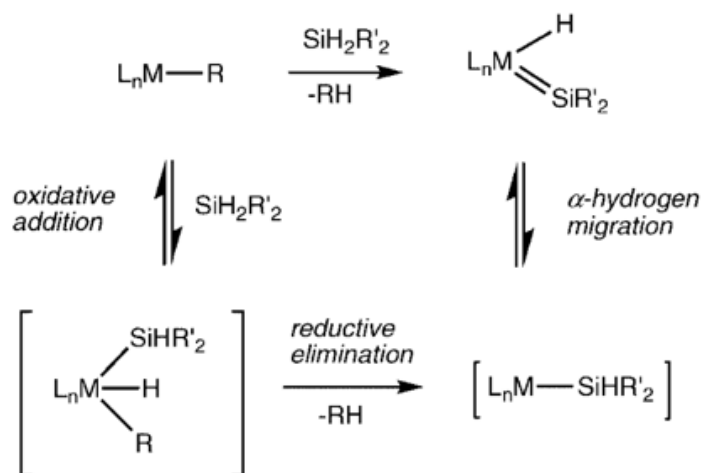
Figure 3: three sequence processes including silane Si–H oxidative addition, reductive elimination, and 1,2 hydrogen migration[65].

The reaction between $[PhBP_3]IrH(\eta^3-C_8H_{13})$ ($PhBP_3=PhB(CH_2PPh_2)_3^-$) and dimethyl silane accompanied by the departure of cyclooctene to produce $[PhBP_3]H_2Ir=SiMes_2$[74, 76] follows the above-mentioned mechanism.

Eq 25[72]
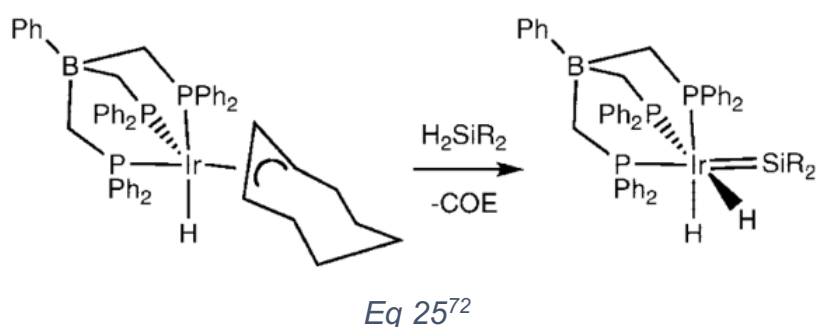
3.3.4. Abstraction substituent on silicon ligand

This method is based on anion metathesis, in which a labile substituent on silicon (halide, triflate, or thiolate) is replaced by a non-coordinating anion to yield cationic silylene complexes. Furthermore, this method can be applied to a variety of silicon substituents of metal complexes from group 8, 9, 10[77].

$$[M]-\overset{\overset{\displaystyle X}{|}}{SiR_2} \xrightarrow{-X} [M]\overset{\oplus}{=}SiR_2$$

X = halide, thiolate, triflate
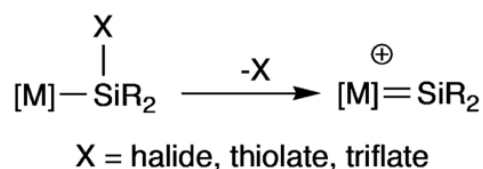
Scheme 17: Silicon bound substitute abstraction[76]

Those complexes, synthesized by Tilley et al[65, 75, 78-80], shown below are the first examples of isolated base-free silylene species resulted from an abstraction of a triflate group from $Cp^*(Me_3P)_2RuSi(SR)_2OTf$ (R = p-tol or Et).
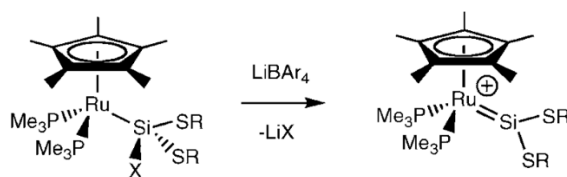
Eq 26[76].

Another successful application of this method is hydride abstraction resulted from a hydrosilylation complex in the presence of HMPA (Hexamethylphosphoramide), which produced an excellent yield of a cationic silyleneiron complex stabilized by HMPA[45, 81].
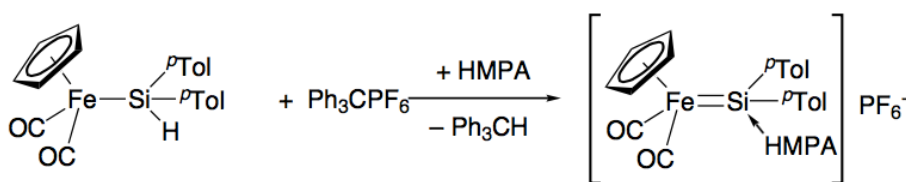
Eq 27[44, 80]

3.3.5. Synthesis of silylene group 5

This documented section is dedicated to the synthesis of group 5 silylenes resulting from interaction between M−H bonds and silicon center.

J. C. Peters et al in 2006 reported that the $[(PhBP^{iPr}_3)Fe^{II}(H)(\eta^3-H_2SiR_2)]$ species formed by the reaction between $[(PhBP^{iPr}_3)FeMe]$ **Pet-1** and $PhSiH_3$ (eq. 28) leads to the quantitative formation of a single diamagnetic red product **Pet-2,** which is the first thoroughly characterized examples of ''arrested'' silane adducts of iron that exhibit an η^3 binding mode (i.e., $Fe(\eta^3-H_2SiR_2))$[82]
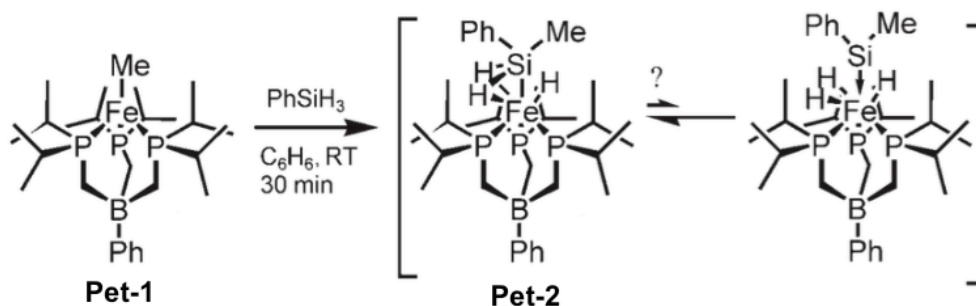
*Eq 28: Reaction of **Pet-1** with phenylsilane[82]*

Due to inevitable uncertainty in accurately locating the positions of hydrogen atoms being adjacent to much heavier atoms by X-ray crystallography, a related complex was produced to facilitate structural assignment. Complex **Pet-1** reacts with one equivalent of mesitylsilane (H_3SiMes) to generate product **Pet-3**, analogues of reaction shown in Eq. 28, in quantitative yield.

As in the case of **Pet-2**, two of the three hydrides are located within bonding distance of the silicon atom in each molecule (Si...H5: 1.56 and 1.62 Å; Si...H6: 1.67 and 1.74 Å), while the third hydride seems to be outside the bonding radius of the Si atom (Si⋯H4: 2.14 and 1.97 Å). The Fe⋯Si distances in both molecules for Pet-**3** (2.131 (Å) and **Pet-1** 2.141 Å) are substantially identical to **Pet-2** (2.1280(7) Å). Despite the inevitable uncertainty in the specific Fe⋯H and Si⋯H distances, the remarkable similarity between the structures of **Pet-2** and **Pet-3** justifies the presence of two 3-centered Fe-H-Si interactions in the solid state and one Fe-H(hydride) interaction.
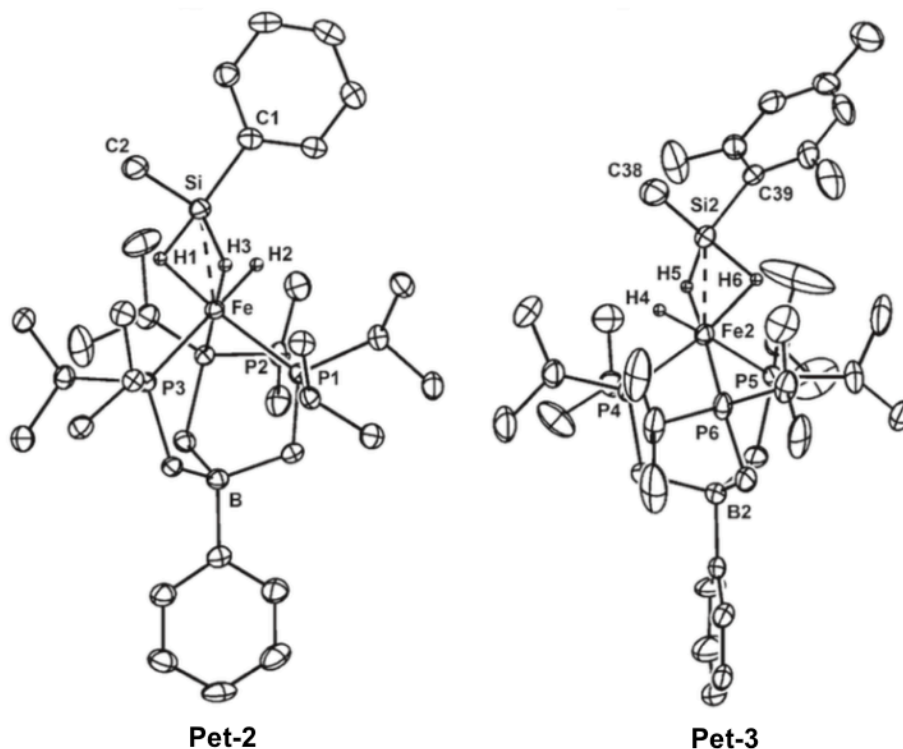
*Figure 4: Solid-state molecular structure of [(PhBP$^{iPr}_3$)Fe^{II}(H)(H$_2$SiPhMe)] **Pet-2** and[(PhBP$^{iPr}_3$)Fe^{II}(H)(H$_2$SiMesMe)] **Pet-3** showing 50 % displacement ellipsoids [82]*

Given the tendency for the [PhBP$^{iPr}_3$]Fe backbone to be subject to two-electron redox processes, mechanism is bound to undergo an oxidative addition/reductive elimination as shown in the path a. In this route, silane first coordinates to the Fe^{II} center, and then an oxidative addition takes place. Reductive 1,2-methyl migration from iron to silicon finally yields an isomer of **Pet-2** (or **Pet-3**)[83-85].
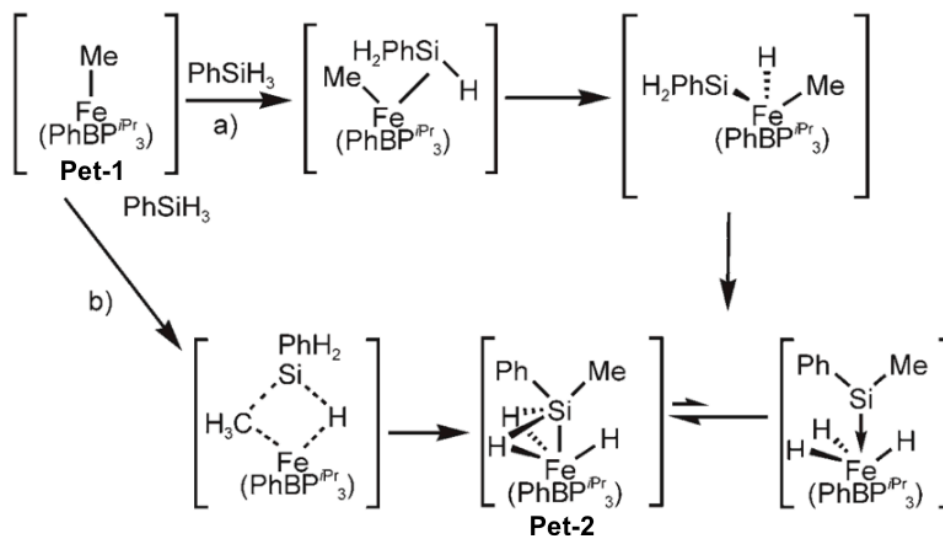
*Scheme 18: Two possible mechanisms for the formation of **Pet-2** [82]*

Another scenario (pathway b) is that the methyl group is likely to migrate through a sigma-bond metathesis, furnishing a plausible and potentially low energy pathway.

In 2010, G. L. Hillhouse and co-worker reported a Ni(II) complex, ensuing from partial 1,2-H migration from silicon to metal central, possessing unusual 3-center Ni, Si, H interactions[86].
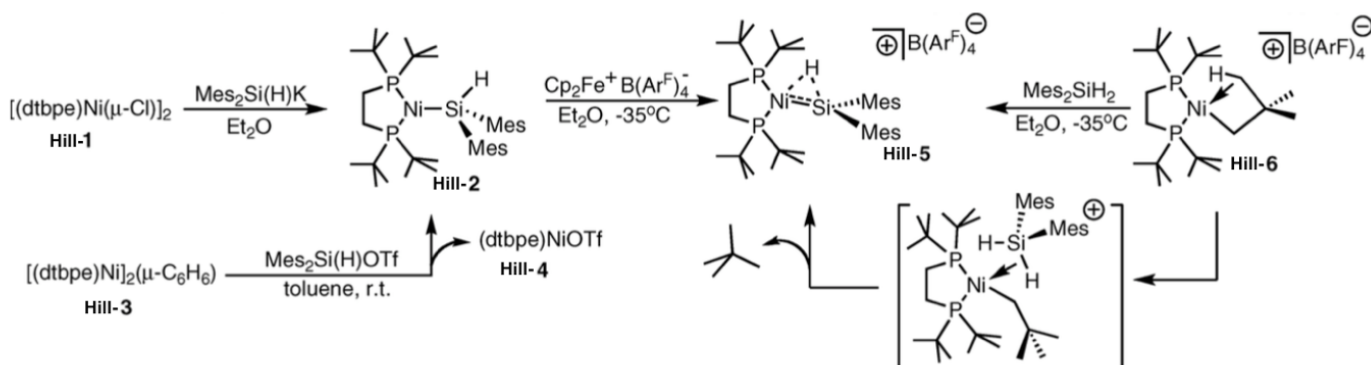
Scheme 19: Synthesis routines to Hil-5[86]

A Ni(I) silyl complex **Hil-2** holding an H bound silyl substituents was oxidized by ferrocenium [Cp$_2$Fe][B(Ar^F)$_4$] (Scheme 19 , ArF = 3,5 - (CF$_3$)$_2$C$_6$H$_3$) to afford the diamagnetic [(dtbpe)Ni(μ- H)SiMes$_2$][BArF$_4$] Hil-**5** in 85% yield.

Another pathway used a metathesis route in which the sigma donor silane coordination from Mes$_2$SiH$_2$ replaces a weak C-H agostic interaction[87], to produce an intermediate that afterward undergoes intramolecular H-abstraction followed by neopentane elimination to give rise to **Hil-5**.

X-ray crystallography supports hydrogen bridging nickel and silicon (Ni-H) 1.70(7) Å, Si-H) 1.64(7) Å), prompting distorted square-planar coordination geometry at nickel. The Ni-Si distance (2.147(2) Å) is 9% shorter than that in **Hil-2** and is close in value reported for Ni silylene complexes (~2.14 Å)[88].

Tilley *et al.* presented molybdenum silylene complexes provided by the reaction of the benzyl precursor Cp*(dmpe)Mo(η^3-CH$_2$Ph) with silanes using the alpha hydrogen migration mentioned above[78, 89].
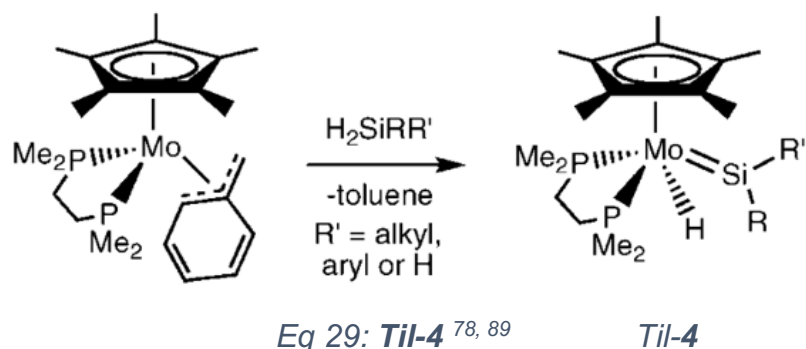
X-ray analysis showed that the H-Mo and H-Si bond lengths of 1.85(Å) and 1.39(Å), respectively, although X-ray diffraction cannot locate exactly hydride positions in the vicinity of a heavy metal, the refined position for the hydride ligand of **Til-4** might suggest that in the solid state some H•••Si interaction exists (Figure 5).
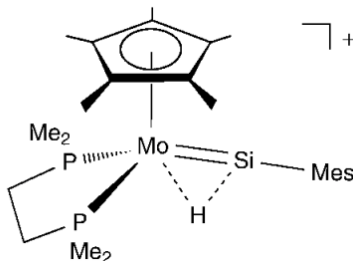
Figure 5: proposed H•••Si interaction

4.   *Metallacycles*

Cyclometalation was discovered in the early 1960s[90, 91], which later became one of the most popular organometallic reactions, providing a straightforward entry to organometallic compounds featuring a metal-carbon σ bond.

Alongside with the development of cyclometalation as a whole, interest in cycloiridated complexes has been greatly attracted by the findings of exceptional activities of iridacycles in catalysis and for photophysical applications[92].

Recently our lab has reported on the capability of readily accessible Cp*Ir-based iridacycles to promote the double hydrosilylation of a series of nitrile groups containing organic substrates following a so-called autotandem[93][17, 94] catalyzed process. We have developed the use of such iridacycles as potential catalysts of "one-pot"

autotandem[95, 96] reactions applied to the fast room-temperature O-dehydrosilylation of alcohols including benzylic or aliphatic.

The intermediates $(R_3Si)(H)Ir$ arising from the reaction of the 18-electron irridacycle cationic with a silane can reasonably be considered as the key catalytic species of aforementioned reactions; this species was trapped and structurally characterized, and its electronic structure was investigated by state-of-the-art DFT methods.
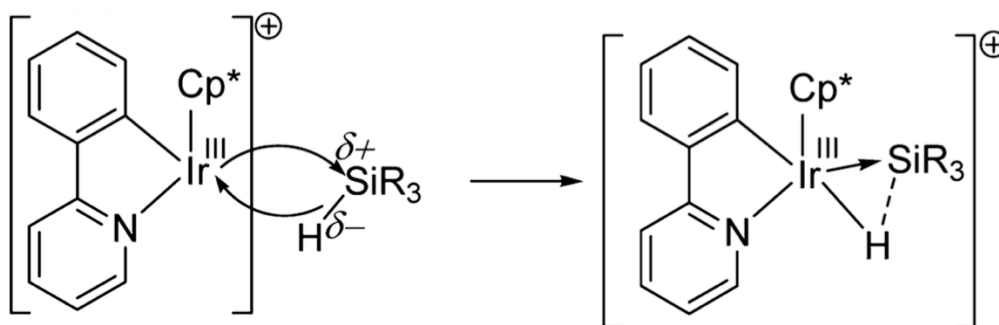
Scheme 7: Si-H bond activated by Irridacycle[17, 18]

This thesis is based on a strong background of interaction between Ir and ailicon that has established for years in our laboratory.

Result and

discussion

1. *Is the R₃Si Moiety in Metal-Silyl Complexes a Z ligand?*

The hydrosilation reactions have riveted chemists' longstanding interest in understanding their mechanical insight due to their efficiency, selectivity, and wide-range application from industrial processes to laboratory scale syntheses. Among a variety of catalysts and catalytic cycles available for these reactions, the conventional Chalk- Harrod mechanism[97, 98] is well-known, which was utilized first time to interpret platinum catalyst olefin hydrosilation reactions in the 1960's[97, 99-101] and then to apply for rhodium-catalyzed ketone hydrosilations by Ojima in 1975[102, 103].

This historical Chalk-Harrod mechanism includes oxidative addition processes in which initial reaction of a silane of general formula R_3SiH (R = aryl, alkyl, halido and hydrogen) interacts with a metal center, resulting in the formal oxidation of the metal center and the formation of two new M-H and $M-SiR_3$ bonds. The silyl ligand in this case is usually considered as the X-type according to the covalent bond classification formalism (abbr. CBC)[104-107]. However, classifying definitively the H and SiR_3 ligands as X-type may be oversimplified owing to the fact that H and Si can be mutually interacting, and the H-Si bonding interaction is unlikely entirely fragmented[105, 108-111].

Moreover, the inherent polarization of the Si-H bond may engender another scenario[17] wherein a formal hydride would transfer to the metal, initiating a concerted or non-concerted transfer of a formal silylium either to the metal[17, 112], to a neighboring group or to the organic substrate (termed ionic activation by Tilley et al.). (scheme 20)
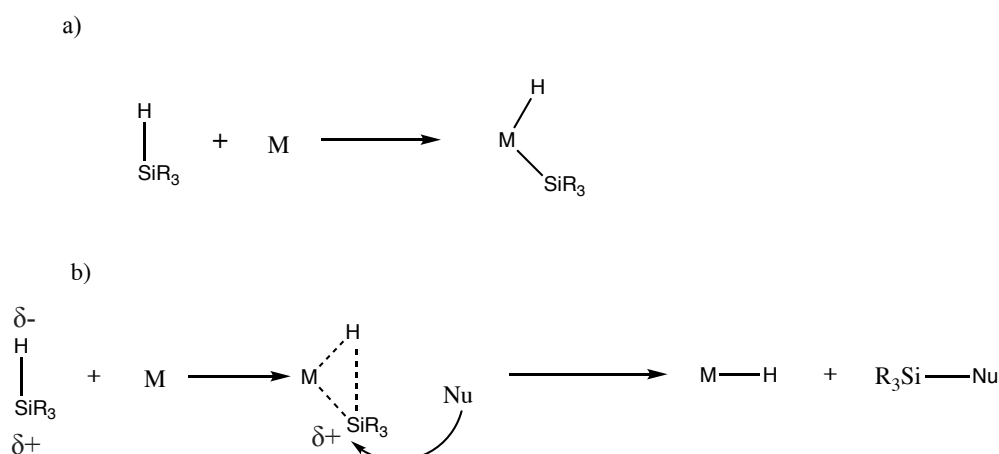
Scheme 20: The two main modes of activation of silanes : a) oxidative addition; b) heterolytic polar "electrophilic" activation of the Si-H bond.

Therefore, reckoning metal-bound silyl as a Z ligand[113] (a Lewis type acceptor, namely here [SiR$_3$]$^+$), as a X ligand or in some cases, even as L ligand[108, 114] predicated on the degree of the interaction between silicon fragment and metal center becomes the fundamental issue. More interestingly, based on that, one can logically deduce a possibility of catalytic reactivity of given catalysis or the electronic structure of the M(H)(SiR$_3$) motif.

In fact, not all metal-silyl compounds are catalytically active or even possess a tendency to release easily the SiR$_3$ moiety by a chemical reaction, nor are the chemical properties and the reactivity of known cases of M-SiR$_3$ complexes comprehensively documented. In addition, reports provide a solid ground that reactive M-H-SiR$_3$ intermediates -or silane-metal adducts- that manifest a crucial role in catalytic events or study reactivity of M(H)(SiR$_3$) motif are scarce because of the baffling issues of isolating[17, 115] and using them as reactants in stoichiometric reactions. As a result, a lack of experimental information on the actual reactivity of a considered metal-silyl fragment will prevent identifying whether the silyl group holds an X, a L or Z character.

It is of necessity that establishing reliable descriptor of bonding could differentiate electrophilic silyl ligands -or "silyliums"- Z ligands (Figure 6) from other situations and suggest rationally the properties of a given catalyst.
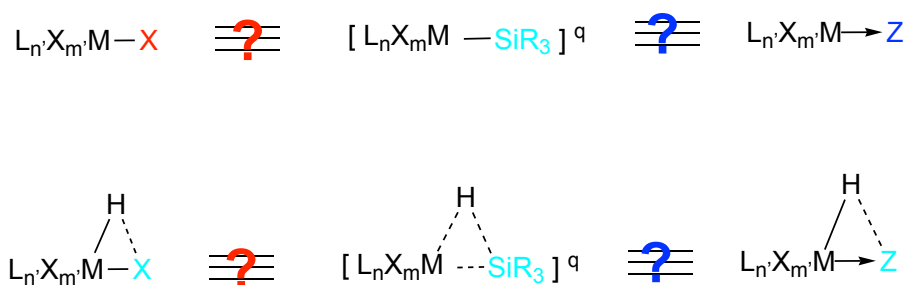
Figure 6. How to best formulate a metal-silyl/silane complex ?

Our main goal was to suggest a simple approach, based on the usefulness of some established tools of the density functional theory in order to assess the "relative intrinsic silylicity" of a metal-silyl complex to provide a formal Lewis acidic silylium[116-118] [SiR$_3$]$^+$ fragment. By doing that, it could facilitate not only rationalizing Lewis formulations, but also clarifying the mechanisms that metal-silyl complex involved, as well as the

dubious concepts lying behind hydrosilylation reactions in which electrophilic silyls are engaged.

In this study, we made use of interaction energies acquired from the energy decomposition analysis EDA [119] by using the protocol implemented in the SCM-Amsterdam Density Functional suite of its 2016 version[120]. The EDA, according to Ziegler and Rauk[119], produces a dichotomy of the inter-fragment interaction energy partitioned into Pauli repulsion, electrostatic attractive, orbital attractive and, with dispersion corrected functionals, dispersion attractive interaction energy terms. This dichotomy into repulsive and attractive energetic contributions is a very powerful tool for the analysis of the nature of chemical bonds[121-124] (Eq. 30).

$$\Delta E_{int} = \Delta E_p + \Delta E_c + \Delta_d + \Delta E_o$$

ΔE_p: Pauli repulsion; ΔE_c: attractive electrostatic; ΔE_d: attractive dispersion; ΔE_o: attractive orbital

Eq 30

The EDA requires the formal fragmentation of a molecule into two fragments, the geometries of which are kept identical to those in the molecule under scrutiny: for convenience, those geometries of the fragments are termed "prepared" as they are geometrically prepared to give rise to the final molecule in its relaxed geometry without deformation.

The considered fragmentation scheme entails the disruption of a formal "silylium" fragment and the charged or neutral organometallic counterpart in their unrelaxed geometries (Eq. 31), this notwithstanding the "chemical realisticness" of the fragmentation scheme (Eq. 31)
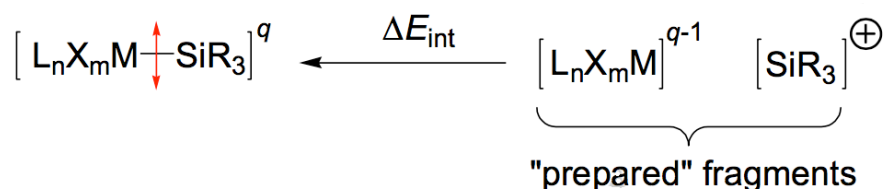
Eq 31[16]

We previously showed that although the triflate ion is one of the weakest Lewis bases and one of the best nucleofuges[125, 126], it had the ability to capture the Et_3Si group of

UVAWIZ[17, 18] (Figure 7), implying that the interaction between the silicon atom and the iridium center was not quite considerable. Silyl group of UVAWIZ clearly behaving like a Z ligand[17] can be utilized as a standard to compare to other metal-silyl complexes for the sake of distinguishing situations similar to UVAWIZ.
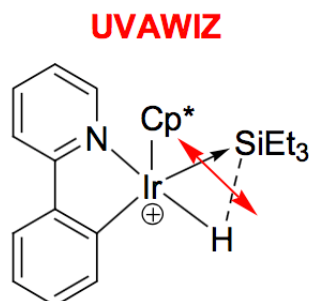
Figure 7

We define the "relative intrinsic silylicity" Π (the greek letter Π was chosen because it is the initial of the Greek word Π that means "elemental silicon") as the ratio of the inter- fragment interaction energy of the triflate with the "silylium" of TfO-SiR$_3$ and the interaction energy of the metal fragment with the same formal "silylium" in a metal-SiR$_3$ compound (Eq. 30)

$$\Pi = [\ \Delta E_{int}\ (R_3Si\text{-}OTf)]\ /\ [\Delta E_{int}(R_3Si\text{-}M)]$$

Eq. 32

The relative intrinsic silylicity Π is a descriptor of the Lewis acidic (electrophilic) character of a given SiR$_3$ moiety, where values <1 characterize low "silylium" releasing ability and values >1 high releasing ability.

To carry out mentioned idea, theoretical and experimental investigation were exerted on the reactivity of known Ir-Si complexes **2**, **3**, and **4** which hold the reputation of being Ir(V) complexes.

Theoretical work shows that the Π of considered complexes **2**, **3**, **4** are 0.55, 0.74, and 0.67, respectively, which also means their "silylium" releasing ability is low since it is less than 1. This conclusion then was cemented by a myriad of experimental work.

We considered reactions of **3** with a number of Lewis bases such as DMAP, [^{n}Bu$_4$N]OTf, CH$_3$CN in different solvent, even in the presence of CO atmosphere for evaluation the possible "silylium" nature of the silyl groups bound. However, the data clearly showed that the Ir-Si bond is much too strong to be cleaved, meaning that the SiR$_3$ group, in this case, is a typical X-ligand.
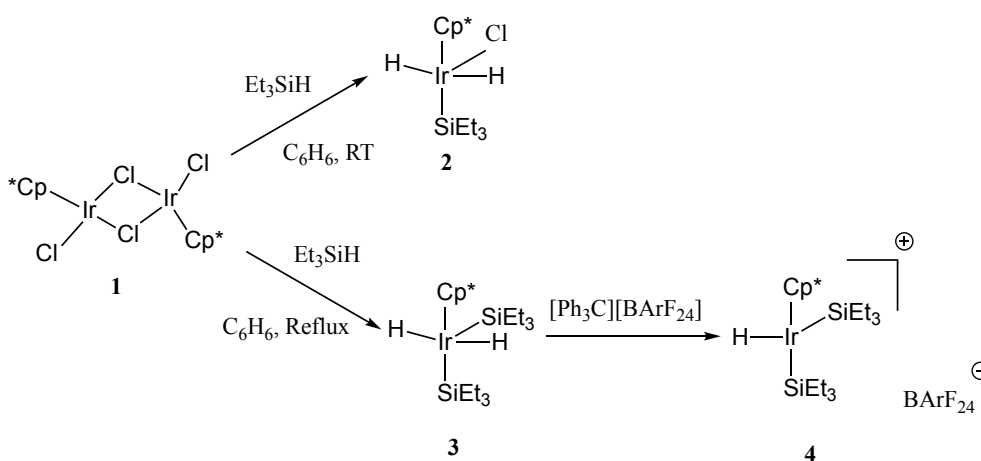
*Scheme 21: Synthesis of **2, 3, 4***

Compound **2**, of which chlorido ligand can be modified by using substitution reactions was alternatively investigated to probe the relationship between structure and reactivity. Grignard reagents CH$_3$MgCl, C$_6$H$_5$MgCl were used to substitute chlorido ligand. However, all attempts to isolate any new substitution product failed.

Following the same idea with the previous reaction, AgOTf was combined with Grignard reagents for the purpose of precipitating AgCl which played as the driving force for replacement Cl by Me or Ph. However, issues mentioned above remain unsolved.

The other approach for modulating the structure of the Ir-Si complexes was using that using trityl tetrakis(pentafluophenyl)borate as a hydride abstraction reagent which could afford a cationic complex after reacting to hydrido-metal-sily compounds. Several tests with **7** in various solvents were carried out. Although the desired product and side product were detected by NMR, the new isolation product failed because of its high reactivity.

2. *Cultivating Iridium silane adduct chemistry*

2.1. *Introduction*

Transition metal silylenes whose high reactivity ensues from the extremely electrophilic character of the Si center serve as putative pivotal intermediates in a myriad of essential reactions as hydrosilylation, synthesis of chlorosilanes[79, 127, 128]. Those complexes also provide attractive stoichiometric reactivity toward small molecules such as chlorinated hydrocarbons[75, 129], epoxides[130], nitriles[131], isocyanates[132, 133], and carbonyl compounds[132-134]. Although having absorbing chemists' interest for decades, establishing a routine method to synthesize transition metal silylenes remains elusive and problematic.

As mentioned in introduction part, there are several methods[65] for preparing metal silylenes for instance anionic-substituent abstraction[79, 80] from a metal hydrosilyl precursor, sequential H-Si activations[71, 135, 136] in the reaction of an RM precursor (e.g., R= alkyl, aryl) with a hydrosilane[137], coordination of free silylene[71] or Si-H activation combining with α -hydrogen migration[65]. Among those paths, applications of directly forming metal silylenes by double H-Si bond activation[89, 138][74, 139] are prevail, however, a spontaneous elimination of H_2 followed by double Si-H bond activation are relatively scarce[140][71][135][73, 141, 142]. There are reports were taken into consideration as references for this research.

Recently, Tilley et al. reported that silylene [L_3(H)Ru=SiRR'] can be acquired by reversible H_2 elimination from a [L_3(H)Ru(η^3-H_2SiRR')] intermediate, which then showed catalytic turnover in ketone hydrosilylation[143].
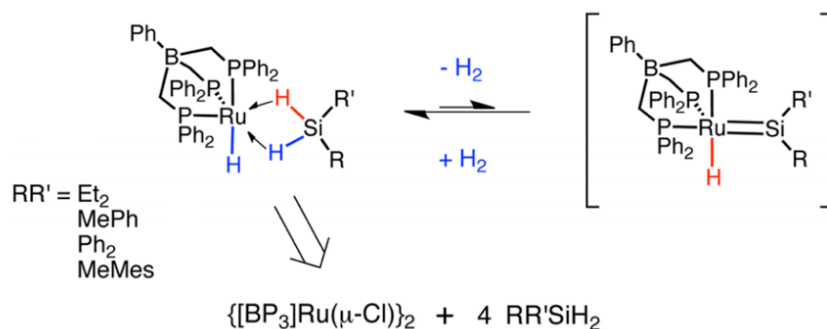
Scheme 22: [L₃(H)Ru=SiRR'] can be acquired by reversible H₂ elimination from a [L₃(H)Ru(η³-H₂SiRR')] intermediate[142]

Corriu et al. indicated that iron silylene complexes can be obtained by reaction of Fe(CO)₅ with a hydrosilane[71] [72] [73] under photolytic conditions associated with the presence of a Lewis base as an exogenous donor ligands bonding to the Si center, which allegedly promotes an increase in the "basicity of the H-Si bond" and thus facilitates H_2 elimination.
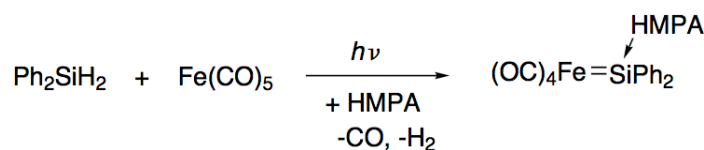
Eq 33: reaction of Fe(CO)₅ with a hydrosilane in the presence of a lewis base [70-72]

It was proposed by Tilley et al.[65] that conversion of hydrosilanes to silylene complexes by Si-H activation and α-hydrogen migration could be an excellent basis for new catalytic applications. (Eq. 34)
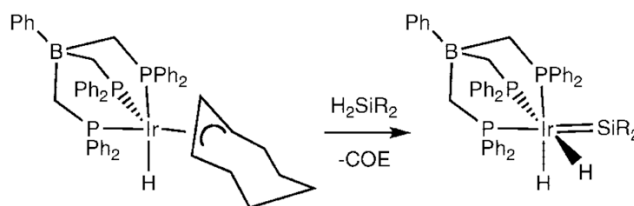
Eq 34: Conversion of hydrosilanes to silylene complexes by Si-H activation and α-hydrogen migration [64]

Based on those observations, we investigated the reactivity of hydrosilanes towards iridacycles [**1a,b**] [BArF₂₄] (Scheme 23-24).
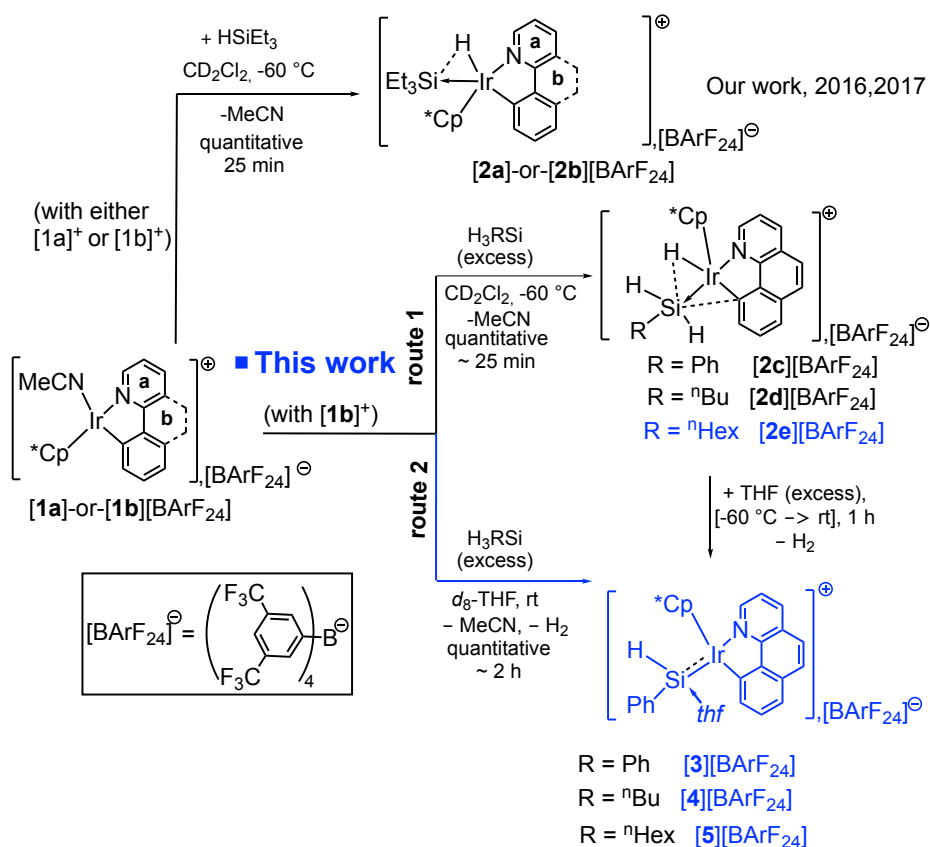
Scheme 23: Reactions of [1a,b]+ with triethylsilane, phenylsilane and n-butylsilane. Cp*: η^5-C$_5$Me$_5$.
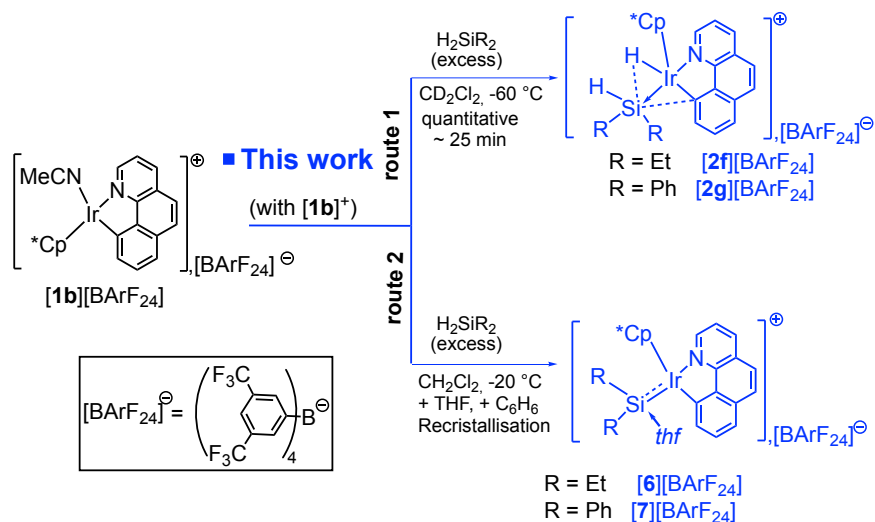
Scheme 24: Reactions of [1b]+ with dialkyl silanes as diethylsilane, diphenylsilane. Cp*: η^5-C$_5$Me$_5$.

Complexes [1a,b][BArF$_{24}$] are efficient precatalysts for the alcoholysis of silanes[17] and the hydrosilylation of carbonyls and nitriles[18]. Interestingly, the products of the reaction of [1a,b][BArF$_{24}$] with HSiEt$_3$, [2a,b][BArF$_{24}$] are neither so-called σ complexes[144][108],

54

[109, 114, 115, 145] nor the products of the oxidative addition of the Si-H bond to the Ir center[144 114 108 105] or any of its arrested states[146-148], but [(IrH)→SiEt$_3$]$^+$.

The donor–acceptor complexes (Scheme 7) resulted from concerted transfer of hydride from the silane to the electrophilic Ir^{III} center and captured a labile silylium moiety[17 18] .
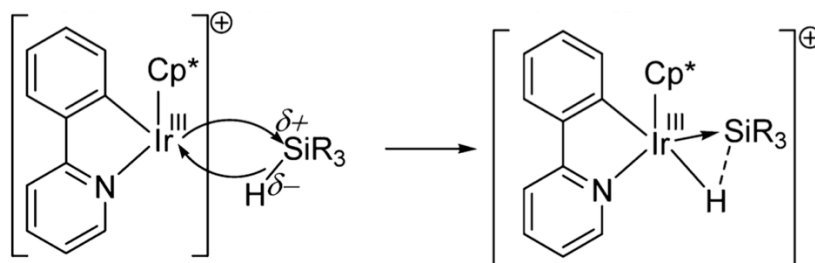
Scheme 7[17, 18]: Si-H bond activated by Irridacycle [1a]$^+$

This study would investigate a wide range of the reaction of [**1b**][BArF$_{24}$] with primary alkyl silane (phenylsilane, n-butylsilane, n-hexylsilane) and secondary alkyl silane (diethyl and diphenyl silanes).

The result revealed that reaction of [**1b**][BArF$_{24}$] with primary alkyl silanes in CD$_2$Cl$_2$ gave rise to [(IrH)→SiRH$_2$]$^+$ adducts. Afterward, by adding THF, those complexes transformed into highly unstable cationic Ir^{III} silylenes, of which all their crystals were successfully trapped by reactive crystallization.

In addition, reaction of reaction of [**1b**][BArF$_{24}$] with secondary alkyl silanes (dietyl and diphenyl silane) also produced [(IrH)→SiR$_2$H]$^+$ adducts whose structures then were X-ray characterized. Although the transformation from these adducts to silylene failed to be clearly observed by NMR, a minute amount of the latter crystal was successfully isolated for crystallographic characterization.

For the sake of legibility, we will discuss sparely reaction of [**1b**][BArF$_{24}$] with primary alkyl silanes and secondary alkyl silanes.

2.2. *Reactions of [1a,b]+ with triethylsilane, phenylsilane and n-butylsilane*

The reaction of a solution of [**1b**][BArF_24] (1 equiv) in CD_2Cl_2 with $HSiR_3$ (4 equiv) was monitored by NMR spectroscopy at -60°C and produced quantitatively and selectively products [**2c**], [**2d**], [**2e**][BArF_24].

R = Ph   [**2c**][BArF_24]

R = nBu   [**2d**][BArF_24]

R = nHex   [**2e**][BArF_24]
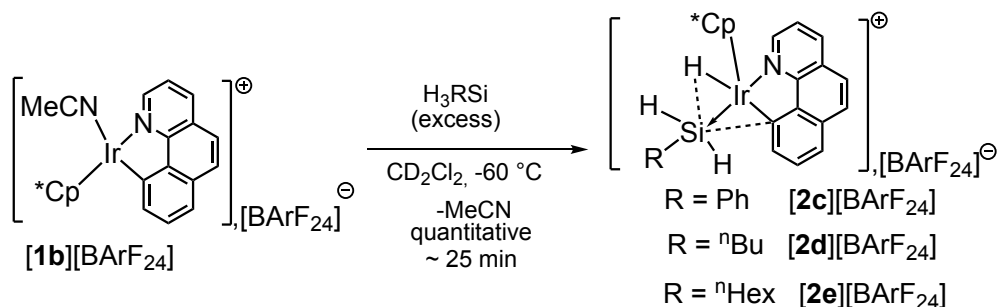
Scheme 25: The reaction of a solution of [1b][BArF_24] with HSiR_3 generating products [2c], [2d], [2e][BArF_24].
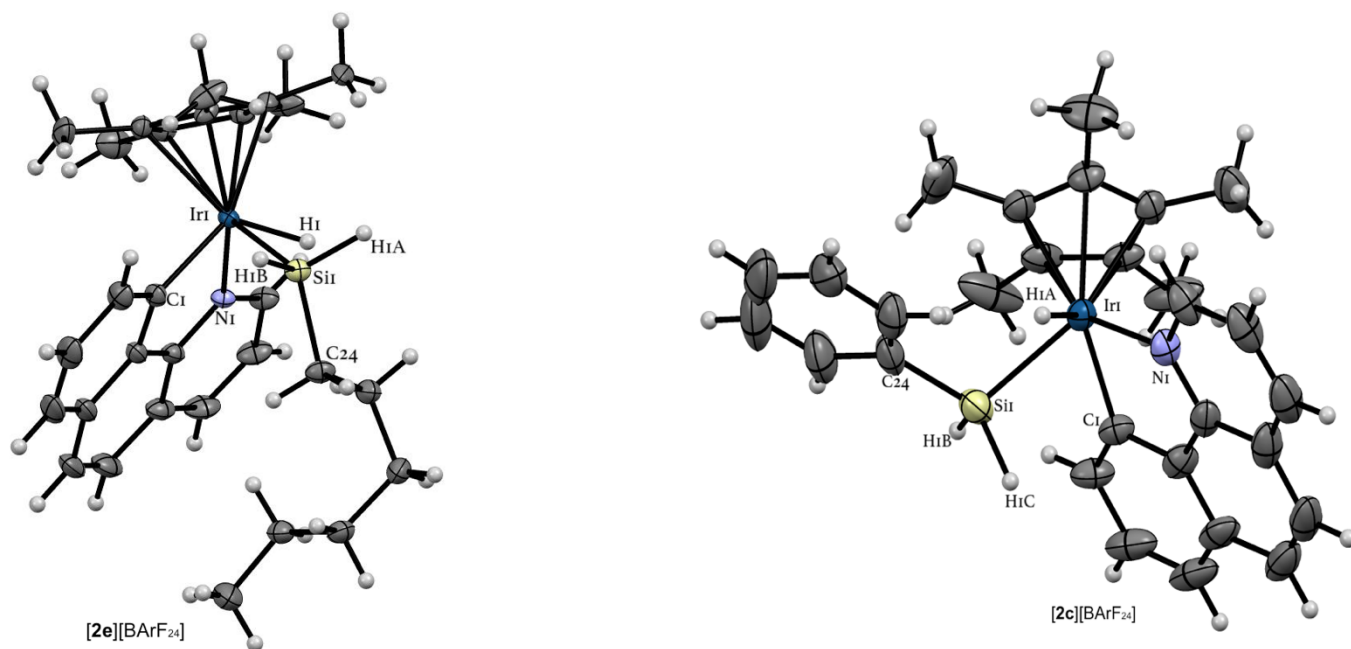
[**2e**][BArF_24]

[**2c**][BArF_24]

Figure 8: ORTEP at 50% probability of the structure of [2c]+ determined by XRD analysis. The [BArF_24]- anion and atoms corresponding to occupational disorder are omitted for the sake of clarity. Selected interatomic distances [Å] and angles [°] for [2c][BArF_24]: Si1-Ir1 2.407(2), Si1-Hi1B 1.17(8), N1-Ir1 2.086(5), Ir1-H1A 1.81(9), Si1-H(Ir1) 2.239(8), Si1-Ir1-H1A 62(3), N1-Ir1-Si1 105.2(1), N1-Ir1-H1A 70(3).

ORTEP at 50% probability of the structure of [2e]+ determined by XRD analysis. The [BArF_24]- anion and atoms corresponding to occupational disorder are omitted for the sake of clarity. Selected interatomic distances [Å] and angles [°] for [2e][BArF_24]: Si1-Ir1 2.4220(7), Si1-Hi1B 1.39(3), N1-Ir1 2.092(2), Ir1-H1A 1.48(3), Si1-H(Ir1) 1.986(7) ,Si1-Ir1-H1A 55(1), N1-Ir1-Si1 108.07(4), N1-Ir1-H1A 80(1).

All three complex [**2c-e**][BArF2$_4$] were characterized by a typical ^{1}H-NMR Ir-*H* resonance at δ = -11.5 ppm. It is noteworthy that no sign of hydrosilylation[17, 18] of the released CH$_3$CN (singlet at δ = 1.98 ppm) was evidenced with [**2c-d**][BArF$_{24}$]

R= Ph [**2c**][BArF$_{24}$]

R= nBu [**2d**][BArF$_{24}$]

R= nHex [**2e**][BArF$_{24}$]
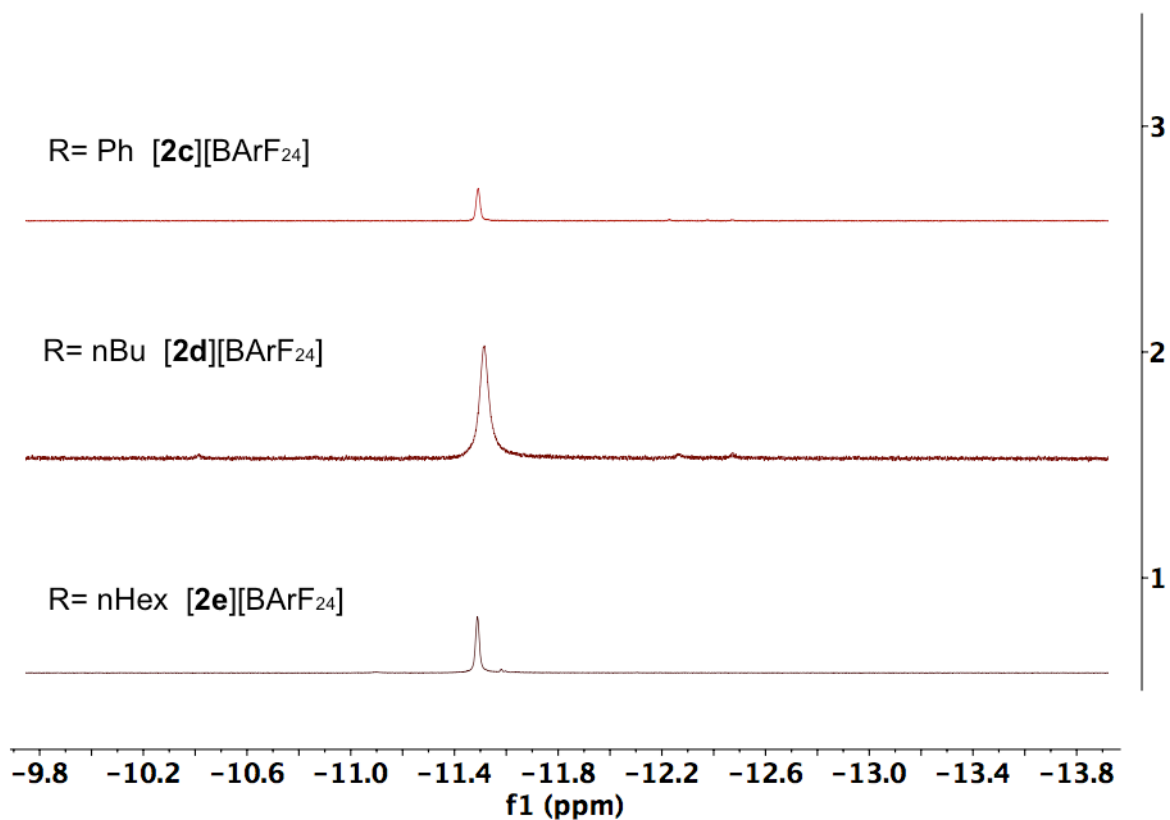
*Figure 9: typical Ir-H of [**2a-c**][BArF$_{24}$]*
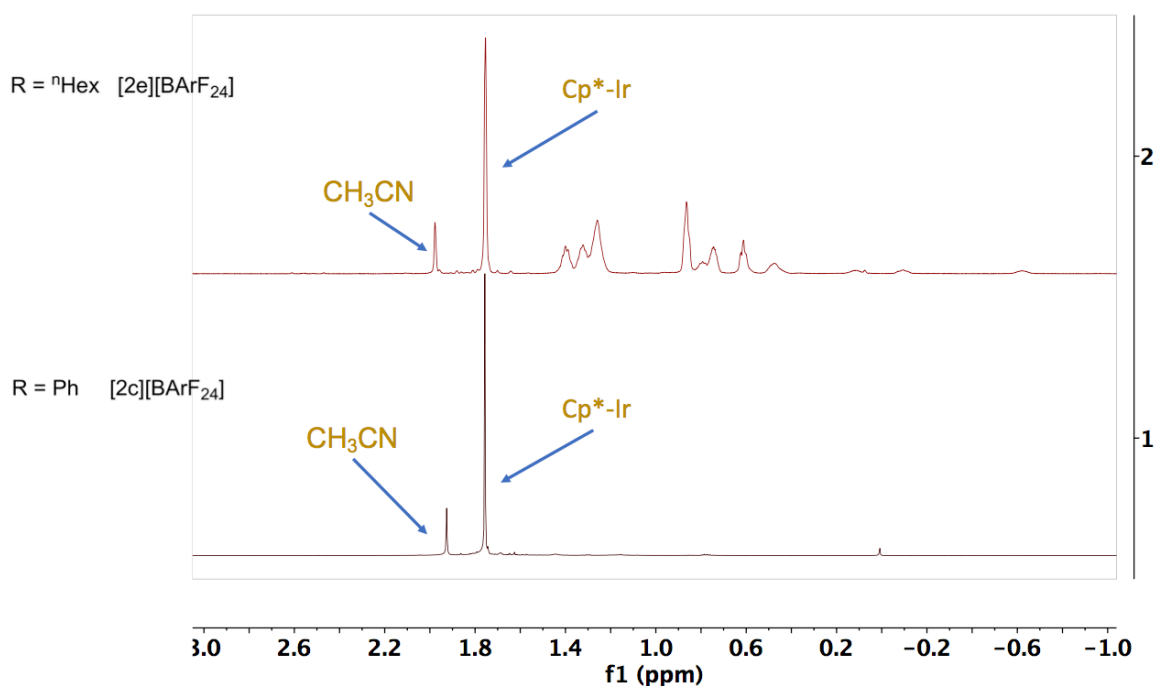
Figure 10: Free CH_3CN and Ir-Cp of [2c], [2e][BArF24].*

Complex [2c][BArF24] possessed a typical ^{1}H NMR Ir-H resonance at δ = -11.5 ppm, for which the ^{1}H,^{29}Si HMQC NMR spectrum shows a weak cross-peak correlation with a ^{29}Si resonance at δ = -35.6 ppm being about 21 ppm downfield from the value found for "free" H_3SiPh δ = -56.7 ppm).
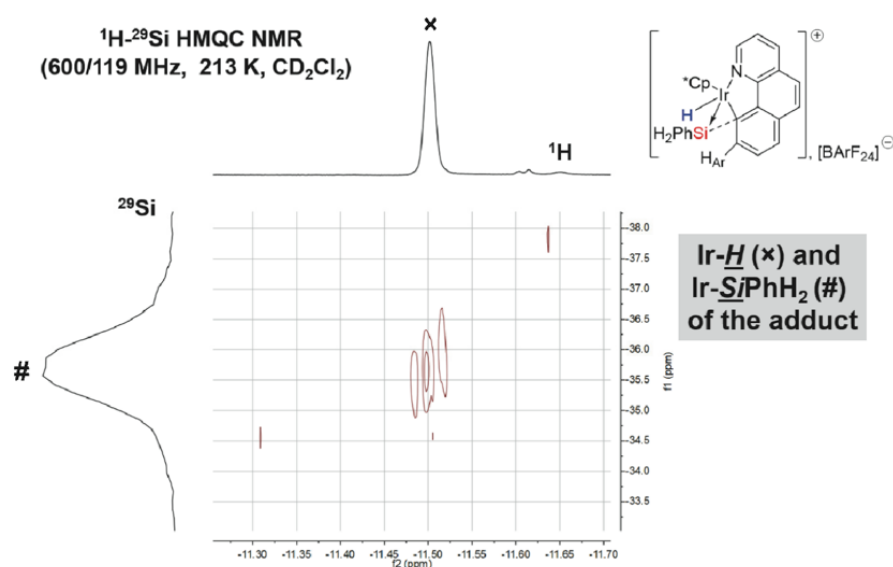
Figure 11: cross-peak correlation with a ^{29}Si of Ir-H of [2c][BArF24]

The ^{1}H,^{29}Si HMQC NMR spectrum of [2c]$^+$ (Figure 12) also shows that the ^{29}Si resonance at δ = -35.6 ppm correlates with several other ^{1}H resonances of the Ir-bound

Cp* ligand (s, δ = 1.79 ppm) and PhSi(H$_\alpha$)(H$_\alpha$') (H$_\alpha$': δ = 3.84 ppm, 1JH-Si =197 Hz; Ha: δ =4.40 ppm, ^{1}JH-Si =224 Hz; Ph: δ = 6.19, 6.46, 6.65 ppm). The Ha and H$_\alpha$' signals appear as doublet of doublets because of the two distinct H$_\alpha$-Si-H$_\alpha$' (1JH,H = 12 Hz) and H$_\alpha$/H$_\alpha$'-Si-IrH [^{3}J(Ha'-H) = 3.6 ; ^{3}J(H$_\alpha$- H) = 2.6 Hz] couplings.
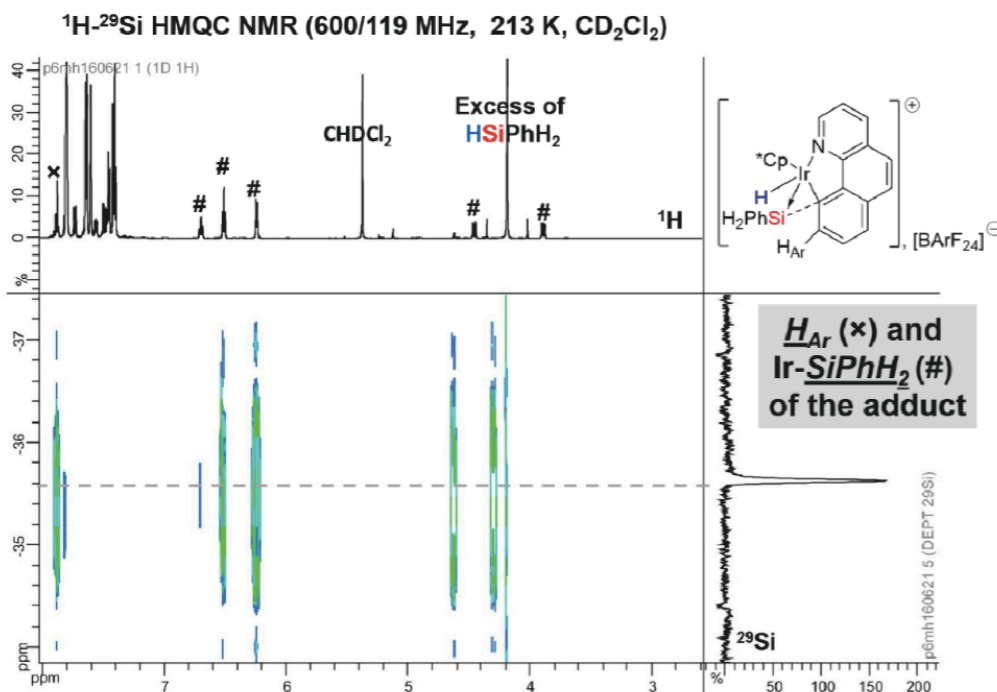
Figure 12: cross-peak correlation with a ^{29}Si of Ir-SiH$_2$Ph of [2c][BArF$_{24}$]

^{1}H,^{29}Si HMQC NMR spectrum of **[2d]$^+$** and **[2e]$^+$** also shows that the ^{29}Si resonance correlates with 1H resonances of the alkylSi(H$_\alpha$)(H$_\alpha$') like in **[2c]$^+$** case. (Figure 13, 14)
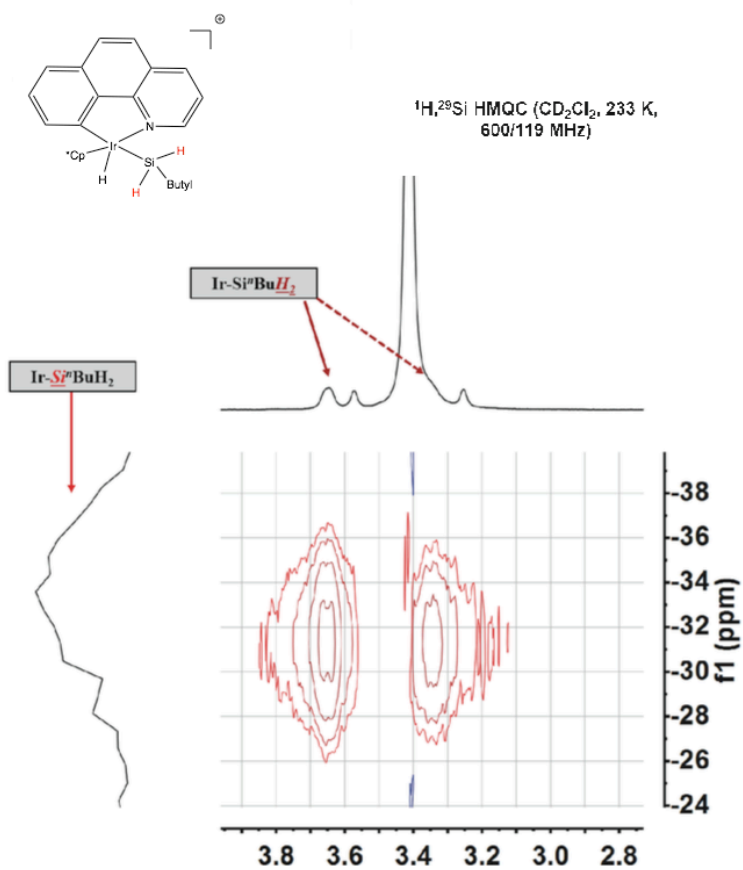
*Figure 13: cross-peak correlation with a ^{29}Si δ = -31.00 ppm of Ir-SiH_2Bu of [**2d**][BArF$_{24}$]*

HMQC ¹H-²⁹Si
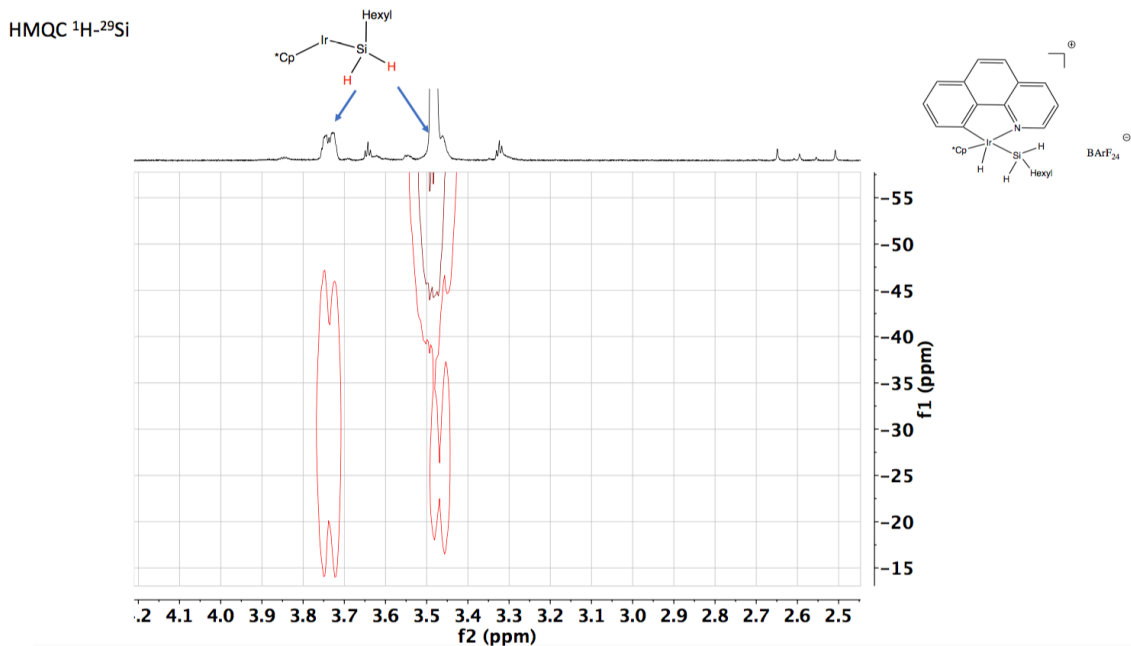
*Figure 14: cross-peak correlation with a ^{29}Si δ = -30.00 ppmof Ir-SiH_2Hex of [**2e**][BArF₂₄*

2.3. Reactions of [1,b]⁺ with diethylsilane and diphenylsilane

Treating a solution of [**1b**][BArF₂₄] (1 equiv) in CD_2Cl_2 with dialkyl silanes H_2SiR_2 (4 equiv) at -60°C formed quantitatively and selectively products [**2f**], [**2g**][BArF₂₄].
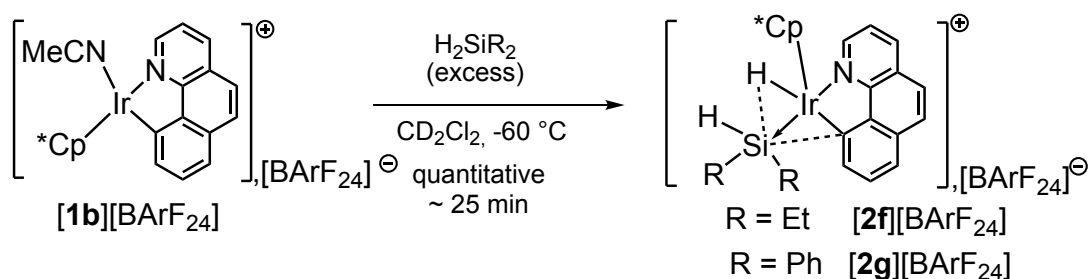
*Scheme 26: Treating a solution of [**1b**][BArF₂₄] with dialkyl silanes H_2SiR_2 (4 equiv) produced products [**2f**], [**2g**][BArF₂₄].*

Both complexes [**2f**], [**2g**][BArF₂₄] show a typical peak of Ir-*H* at around δ = -11ppm. (figure 15). However only Ir-*H* of [**2g**][BArF₂₄] presented a correlation with ^{29}Si in HMQC at δ = 0.00 ppm (figure 16).

61
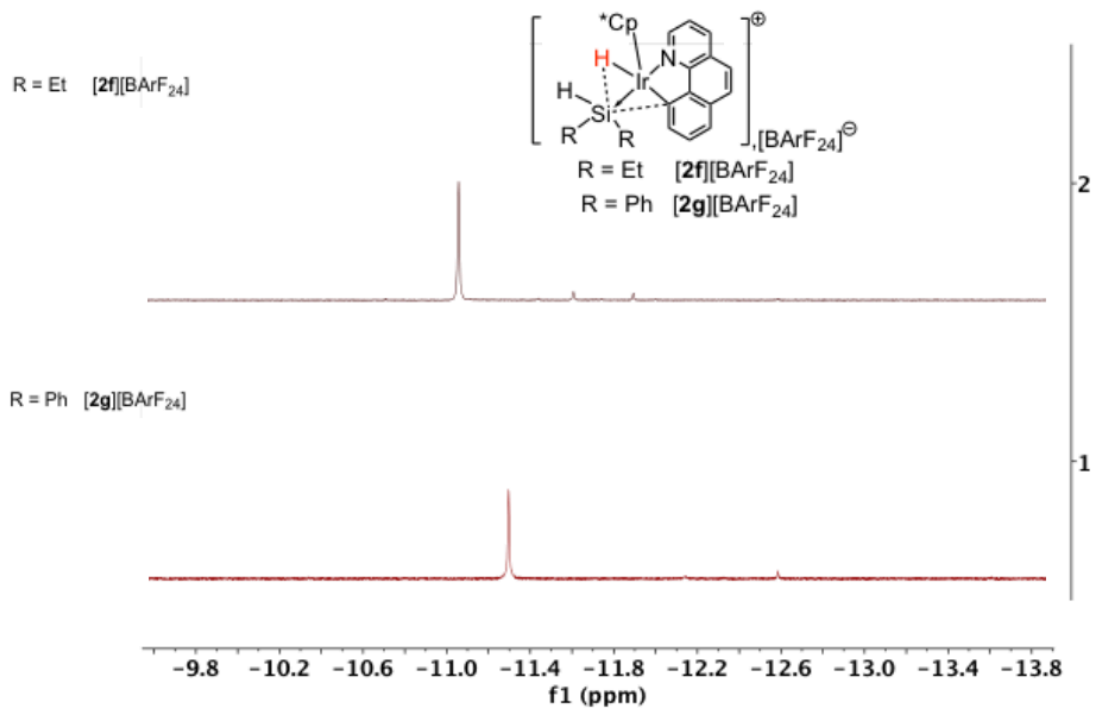
Figure 15: typical Ir-H of [2f] and [2g] [BArF24]
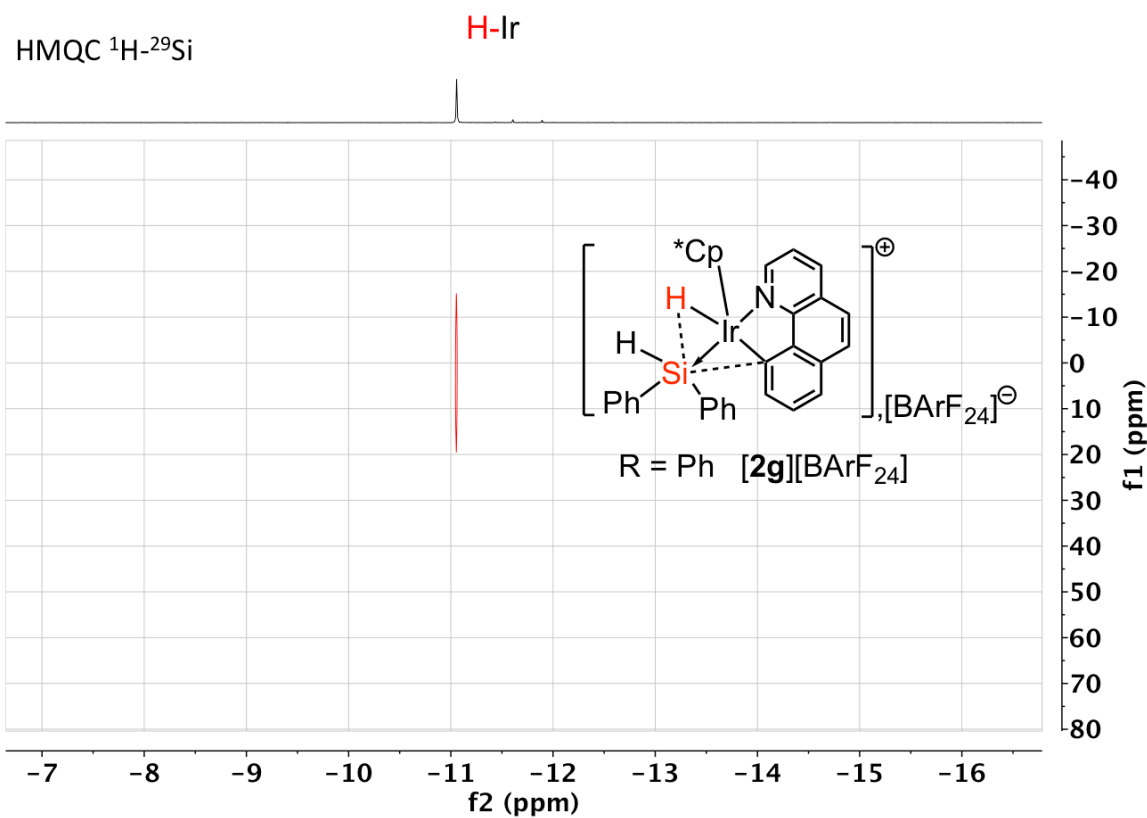
Figure 16: cross-peak correlation with a ^{29}Si δ = 0.00 of Ir-H of [2g][BArF$_{24}$]

The ^{1}H-^{29}Si HMQC NMR spectra of both [**2f**] and [**2g**][BArF$_{24}$] show that there are resonance correlations between ^{29}Si and Ir-bound Cp*, alkyl group on Ir-R$_2$SiH$_2$ and one of the "aromatic" hydrogen atoms of the C,N ligand. (Figure 17, 18)
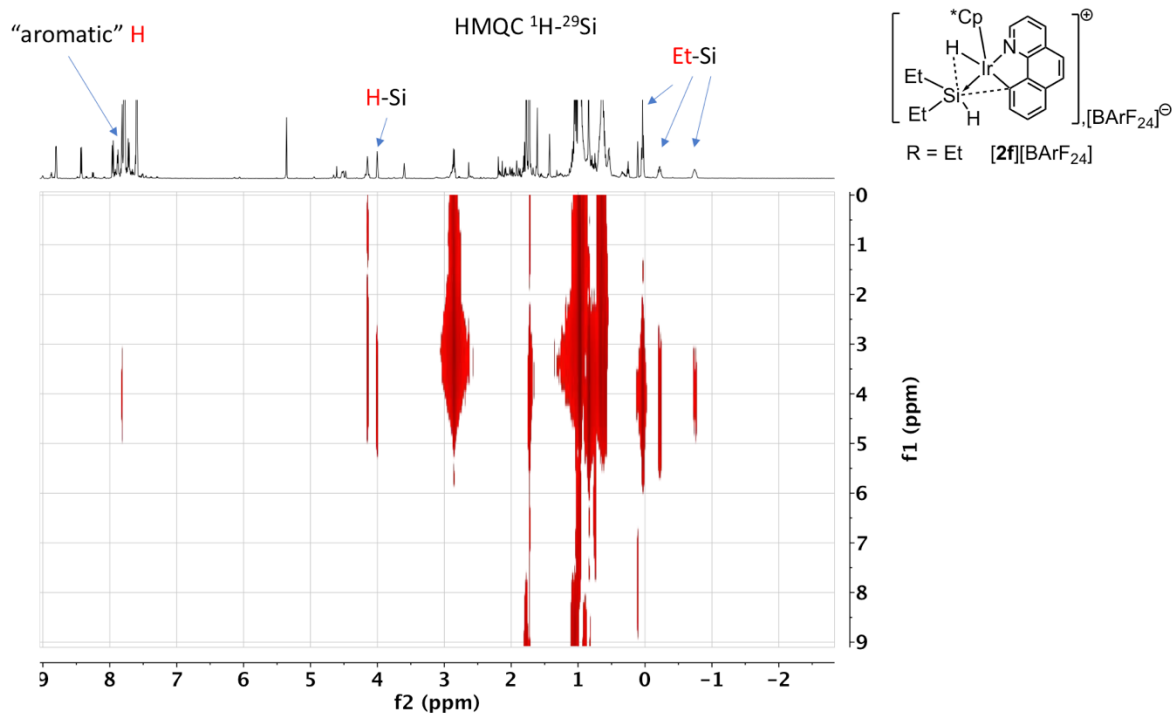
Figure 17: Correlation of ^{29}Si δ = -4.00 with Ir-bound Cp*, alkyl group on Ir-R$_2$SiH and one of the "aromatic" hydrogen atoms of the C,N ligand in [**2f**][BArF$_{24}$]
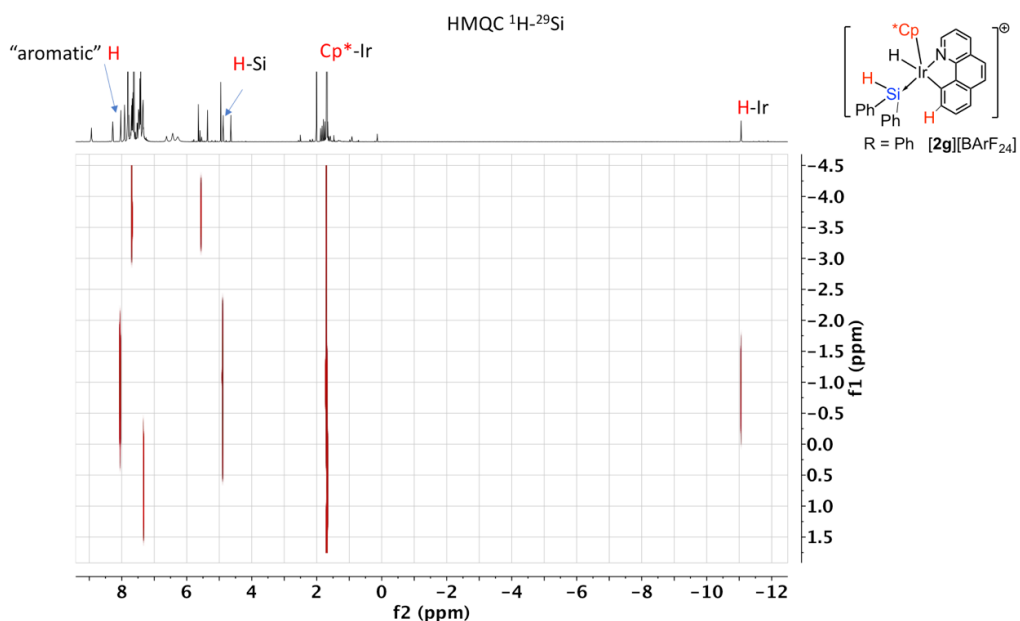
Figure 18: correlation of ^{29}Si δ = -1.00 with Ir-bound Cp*, alkyl group on Ir-R$_2$SiH and one of the "aromatic" hydrogen atoms of the C,N ligand in [**2g**][BArF$_{24}$]
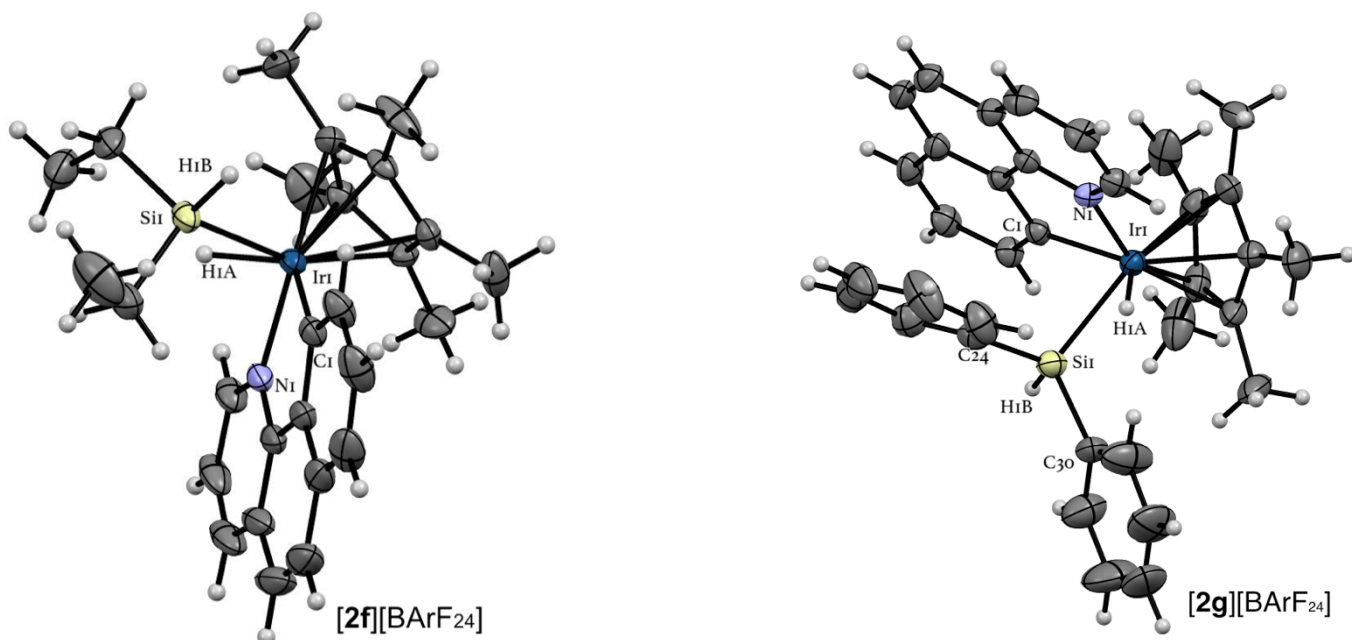
Figure 19: ORTEP at 50% probability of the structure of [2f]⁺ determined by XRD analysis. The [BArF₂₄]⁻ anion and atoms corresponding to occupational disorder are omitted for the sake of clarity. Selected interatomic distances [Å] and angles [°] for [2f][BArF₂₄]: Si1-Ir1 2.455(2), Si1-Hi1B 1.39(7), N1-Ir1 2.092(4), Ir1-H1A 1.52(6), Si1-H(Ir1) 2.066(6), Si1-Ir1-H1A 57(3), N1-Ir1-Si1 107.0(1), N1-Ir1-H1A 75(3).

ORTEP at 50% probability of the structure of [2g]⁺ determined by XRD analysis. The [BArF₂₄]⁻ anion and atoms corresponding to occupational disorder are omitted for the sake of clarity. Selected interatomic distances [Å] and angles [°] for [2g][BArF₂₄]: Si1-Ir1 2.435(1), Si1-Hi1B 1.52(7), N1-Ir1 2.083(4), Ir1-H1A 1.449(7), Si1-Ir1-H1A 55.65(9), N1-Ir1-Si1 99.19(9), N1-Ir1-H1A 75.27(9).

Product	Interatomic distances (Å)		
	Ir-H	Ir-Si	Si-H(Ir)
[2c][BArF₂₄]	1.81(9)	2.407(2)	2.239(8)
[2e][BArF₂₄]	1.48(3)	2.4220(7)	1.986(7)
[2f][BArF₂₄]	1.52(6)	2.455(2)	2.066(6)
[2g][BArF₂₄]	1.449(7)	2.435(1)	1.523(7)
[2h][BArF₂₄][17]	1.47	2.5008(8)	2.10
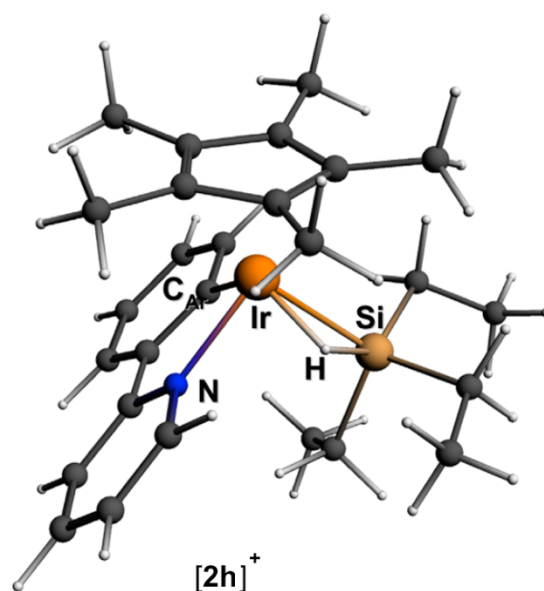
Table 4: Interatomic distances of adducts and X-ray structure of [2h][BArF₂₄] [17]

Interatomic distances fluctuate evidently, among which Ir-H and Si-H(Ir) interatomic distances of [**2c**][BArF$_{24}$][17] are longest (1.81(9) Å and 2.239(8) Å respectively) while those of other complexes only approximate averagely 1.499 Å (Ir-H) and 1.861 Å (Si-H). Ir-Si Interatomic distance of [**2c**][BArF$_{24}$] (2.107 Å) is shortest compared to average (≈ 2.402 Å) and that of [**2h**][BArF$_{24}$] is longest (2.5008(8)).

These atomic distances (table 4) cement our statement on the formal oxidation state of Ir center in previous research[17, 18]. In such complexes, Si atom carries a great charge density depletion and binds to Ir center via a dative bond Ir→Si (figure 20). Hence, the silylium [$R_1R_2R_3Si$]$^+$ is actually isoelectronic to neutral boranes BR_3 that are prototypical Z-type ligand according to Green's formalism[104-107]. As a result, a [ML_3X_3Z] formation in which formal oxidation state of iridium is III is more reasonable than [ML_3X_4]$^+$ Ir(V).
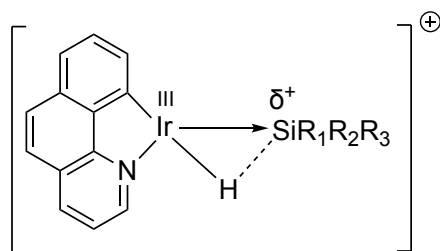
Figure 20: Si atom binds to Ir center via a dative bond Ir→Si

2.4. *Conformational analysis of [2c]$^+$*

The ^{29}Si -^{1}H cross-peak at δ =- 35.60 ppm correlates with proton H_{Ar} (labeled as H_{Ar} in figure 21, δ = 7.82 ppm), and this is also a scalar coupling from the Si atom through the Ir atom and the carbanionic C_{ipso} atom of the benzo[*h*]quinolinyl ligand.
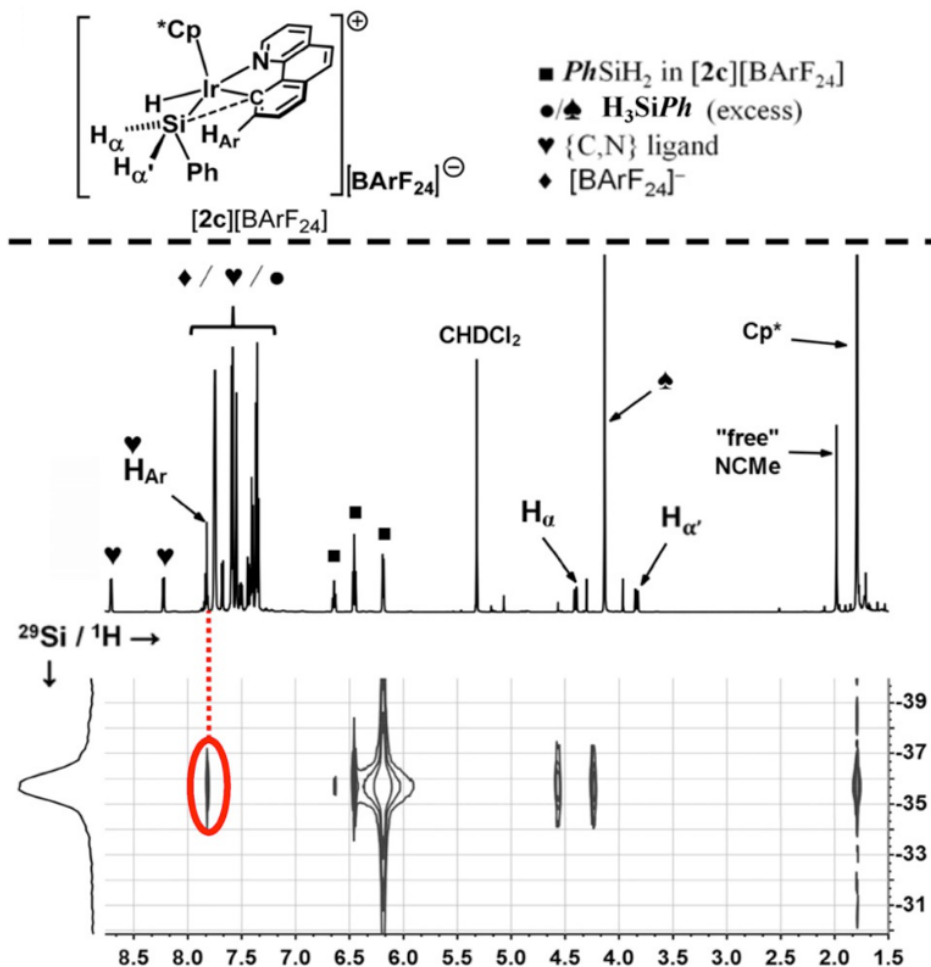
*Figure 21: Excerpt of the ^1H,^{29}Si HMQC NMR spectrum of [**2c**][BArF$_{24}$] (CD$_2$Cl$_2$, 213K) optimized for medium-to-low values of J(^1H,^{29}Si); the circled cross-peak correlation corresponds to scalar-coupled Si and H$_{Ar}$ nuclei.*

Theory suggests that the Si center links to the hydridoiridacycle in **[2c]⁺** (Figure 22) through secondary interactions comprising the neighboring hydrido ligand (Ir-H) and the aromatic chelating ligand. DFT investigations revealed the two low-lying conformational isomers of Ir-H silylium complex **[2c]⁺** are [**2c-r1**]⁺ and [**2c-r2**]⁺ (Figure 22), the former is the lowest-lying and has the largest computed absolute value of the scalar coupling constant J(Si-H$_{Ar}$). Interestingly, **[2c-r2]⁺,** the conformational isomer with the shortest H$_{Ir}$-Si distance, has the highest energy and the smallest computed[149] J(Si-H$_{Ar}$) coupling constant.

Notwithstanding a rather short C$_{ipso}$-Si distance of 2.819 Å (comparing to 3.019 Å in **[2 c-r2]⁺**) Bader QTAIM analysis of the structure of **[2c-r1]⁺** did not reveal any Si-C$_{Ar}$ bonding interaction. The small Wiberg[150] index for the C$_{ipso}$-Si interaction of 0.12 (0.09

in **[2c-r2]⁺**) apparently excludes the hypothesis that the H_{Ar}-Si coupling described in Figure 21 might ensue from a ^3J scalar coupling of a weak covalent interaction between the Ir-bound C_{ipso} atom and the Si center rather from a ^4J coupling.

	[2c-r1]⁺	[2c-r2]⁺
ΔE_{ZPE} (kcal mol^{-1})	0	+6.3
N_i/N (298.15 K)	1	0
Ir-Si (Å)	2.443	2.471
H_{Ir}-Si (Å)	2.119	2.054
$J(Si-H_{Ir})$ (Hz)	-0.6	-0.9
$J(Si-H_{Ar})$ (Hz)	-2.1	-0.4
$J(H_{\alpha}-H_{\alpha'})$ (Hz)	13	8.4
$J(Si-H_{\alpha})$ (Hz)	-152	-182
$J(Si-H_{\alpha'})$ (Hz)	-175	-153

[2b]⁺
$J(Si-H_{Ir})$: -5.8 Hz
$J(Si-H_{Ar})$: +0.0 Hz
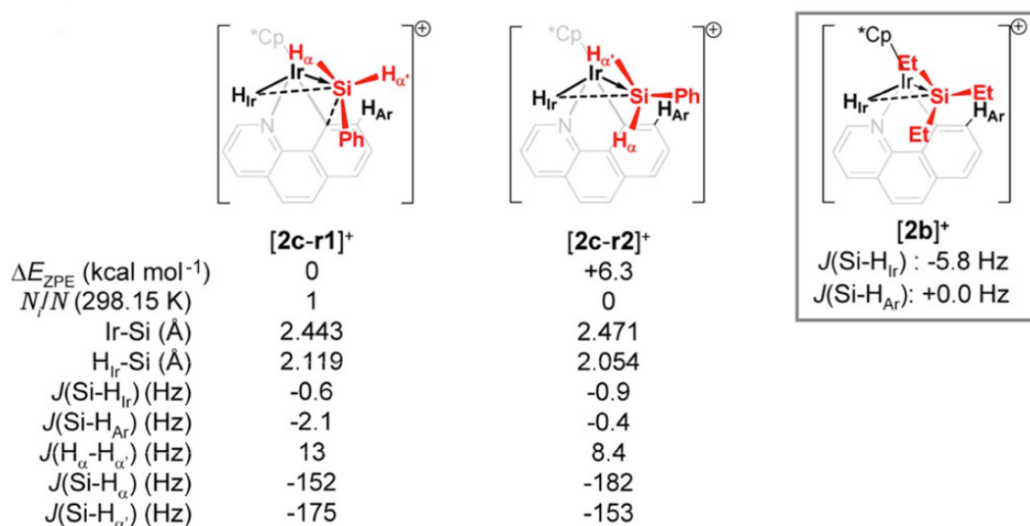
*Figure 22: Computed low-lying rotamers of **[2c]⁺** and relevant NMR coupling constants compared to **[2b]⁺** ;[18] Δ_{ZPE} is the relative energy including zero-point energy contribution; N_i/N is the Boltzmann weight; scalar coupling constants were computed by the DFT-based CPL[149] method. The J(Si-HCp*) coupling constants for the 15 ^1H nuclei of the Cp* ligand in the static DFT model of **[2c-r1]⁺** were estimated to span -0.5 Hz and 0 Hz ; the significant coupling of the Cp* protons in figure.... is consistent with a time-averaged ^4J scalar coupling.*

This "secondary interaction" becomes pertinent if considering the extended transition state natural orbital for chemical valence[151, 152] (ETS-NOCV) analysis of the interaction of cation [H₂SiPh]⁺ with the neutral hydrido iridium residue in **[2c-r1]⁺** (Figure 23).
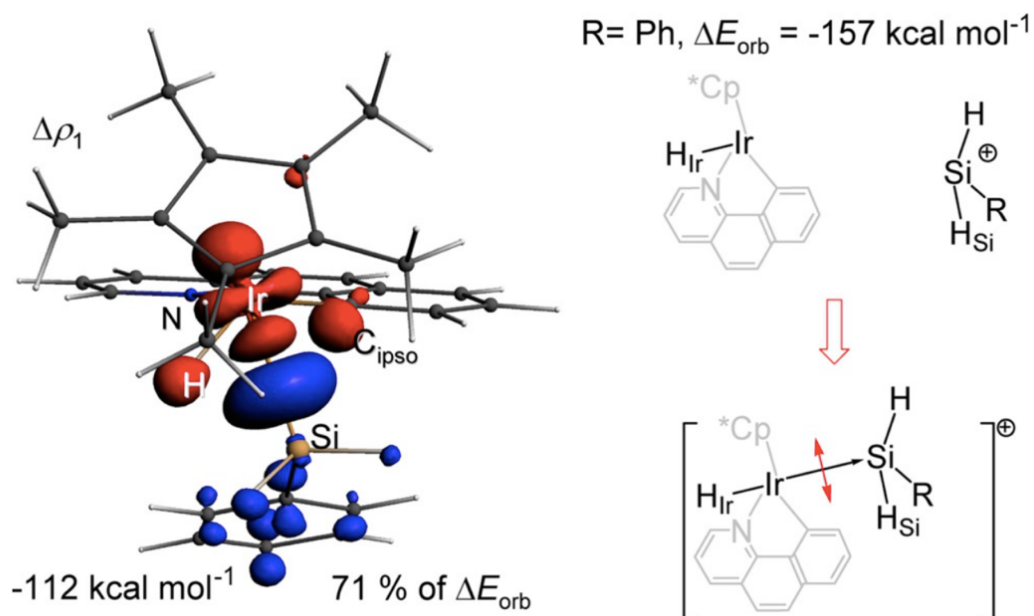
Figure 23: ETS-NOCV analysis of the interaction of silylium cation [SiH₂Ph]⁺ with the hydrido iridium group of [2c–r1]⁺. The deformation density isosurface (0.007 e bohr⁻³) Δρ₁ shows that donation of electron density takes place mainly from a delocalized interaction of the Si center with the Ir, hydridic H, and carbanionic C_ipso centers to enhance a quite diffuse four-center interaction in which the Ir-Si component dominates. Red and blue lobes are associated with donating and accepting orbital components, respectively.

Large electron density channeled into the quite diffuse Ir-Si bond stems from three donor orbital contributors located at the Ir atom, the Ir-H$_{Ir}$ bond, and the C$_{ipso}$ atom; the Ir-Si interaction is ostensibly the strongest with a Wiberg[150] bond index of 0.44 (w(H$_{Ir}$-Si) = 0.18). The sum of Wiberg indices for Si-C$_{ipso}$, Si-H$_{Ir}$, and Si-Ir interactions ($\sum w$ = 0.74) indicates that secondary interactions of H$_{Ir}$ and C$_{ipso}$ with the Si center contribute to the cohesion of [2c-r1]⁺.

3. Entrapment of THF-Stabilized Iridacyclic Ir^{III} Silylenes and theoretical study of their structure.

3.1. Discovery of THF-Stabilized Iridacyclic Ir^{III} Silylenes

While attempting to grow crystals of **[2c-h]**[BArF$_{24}$], we realized that addition of limited amounts of THF induced the formation of new yellow crystals, XRD analysis of which revealed the structures of THF-bound silylene complexes **[3]**[BArF$_{24}$], **[4]**[BArF$_{24}$] and **[5]**[BArF$_{24}$] (Scheme 27).

Due to their high reactivity, all attempts to isolate pure **[3, 4, 5]**[BArF2$_{4}$] on a preparative scale failed. After workup, the reaction medium gave starting complex **[1b]**[BArF$_{24}$] or a μ-hydrido iridacyclic dimer already reported previously[18].

^{1}H NMR monitoring revealed that, the reaction of [**1b**][BArF$_{24}$] with H$_3$SiR (R = Ph, nBu, nHex) in CD$_2$Cl$_2$ generated the concomitant production of H$_2$ and [**3**][BArF$_{24}$] (Scheme 27) by adding an excess of THF and warming to room temperature.

R = Ph	**[2c]**[BArF$_{24}$]	
R = ^{n}Bu	**[2d]**[BArF$_{24}$]	
R = ^{n}Hex	**[2e]**[BArF$_{24}$]	

R = Ph	**[3]**[BArF$_{24}$]	
R = ^{n}Bu	**[4]**[BArF$_{24}$]	
R = ^{n}Hex	**[5]**[BArF$_{24}$]	
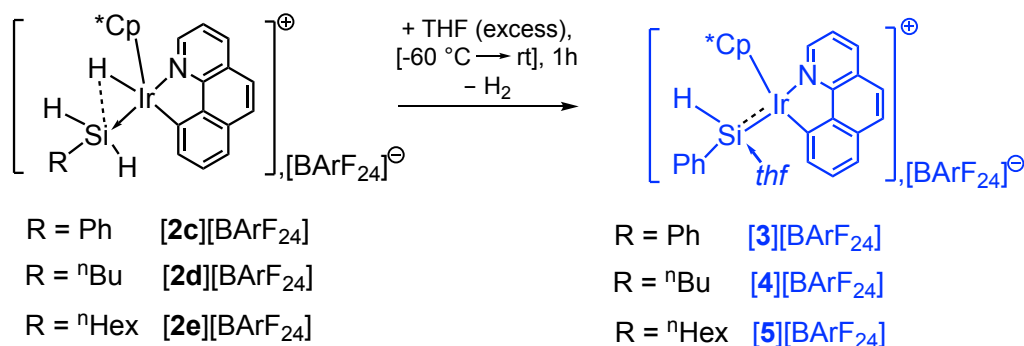
Scheme 27: complexes [3,4,5][BArF$_{24}$] can be obtained sequentially from [1b]$^+$ by treatment of [2c,d,e][BArF$_{24}$] respectively with THF

It was furthermore found in details that complexes **[3,4,5]**[BArF$_{24}$] can be obtained sequentially from [**1b**]$^+$ by treatment of **[2c,d,e]**[BArF$_{24}$] with THF (Scheme 27) or directly treating [**1b**][BArF$_{24}$] with H$_3$SiR (R = Ph, nBu, nHex) in pure [D$_8$]THF (Scheme 28). Although an endeavor of synthesis of diethyl and diphenyl silylene Ir complexes using the same manner failed to replicate, their X-ray structures were isolated and characterized.
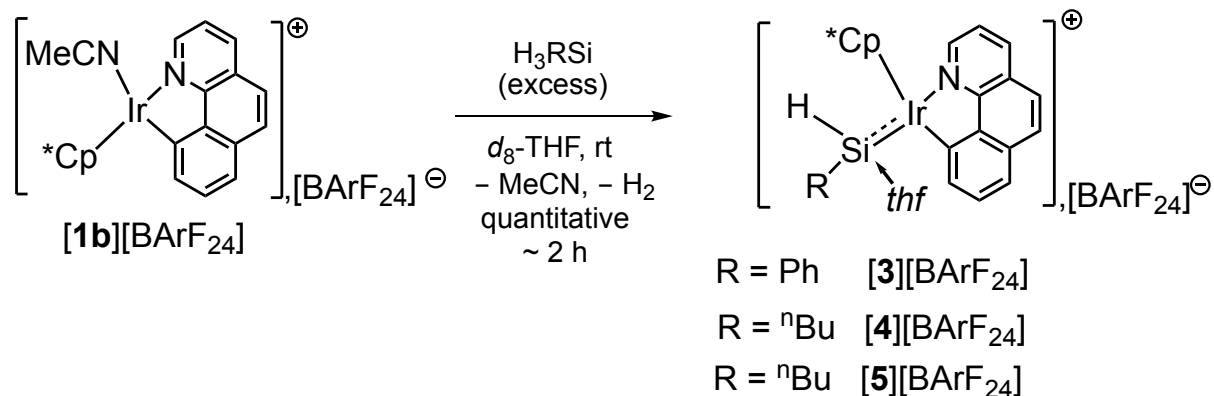
Scheme 28: complexes *[3,4,5][BArF_{24}]* can be obtained directly by treating *[1b][BArF_{24}]* with H_3SiR (R = Ph, nBu, nHex) in pure [D_8]THF

^{1}H NMR analysis (25 °C, CD_2Cl_2) of **[3][BArF_{24}]** disclosed a singlet at δ = 5.73 ppm with [1]J_{H-Si} = 99 Hz assigned to the Si-bound H atom, as well as the typical signals of Ir-bound Cp* (δ = 1.74 ppm) and the C,N ligand (δ = 7.88–9.02 ppm). (figure 24)
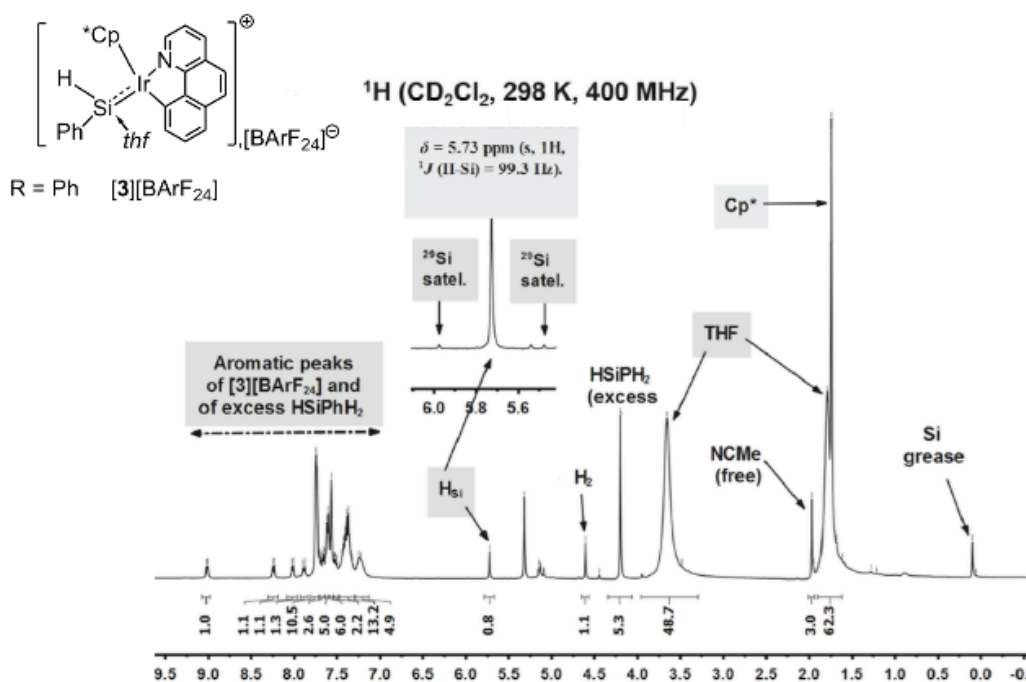
Figure 24: ^{1}H NMR analysis (25°C, CD_2Cl_2) of **[3][BArF_{24}]**

^{1}H-^{29}Si HMQC NMR spectra recorded at -60°C (CD_2Cl_2) showed a cross-peak correlation between the [29]Si satellites of the broad ^{1}H resonance of the Si-H bond at δ = 5.59ppm and the [29]Si resonance at δ = 72.8ppm. Although ^{1}H signals of free THF overlapped with those of the Si-bound THF at room temperature, at -60°C the latter signals sharpened into four broad peaks integrating for about 2H each at δ=0.65, 0.85,

2.05, and 2.30 ppm (see more in experimental section) as a consequence of coordination of THF to the stereogenic Si center. The $\Delta\delta$ (^{29}Si) shift of about +108 ppm on going from [**2c**][BArF$_{24}$] to [**3**][BArF$_{24}$] is consistent with substantial depletion of electron density at the Si center[72]. (figure 25)
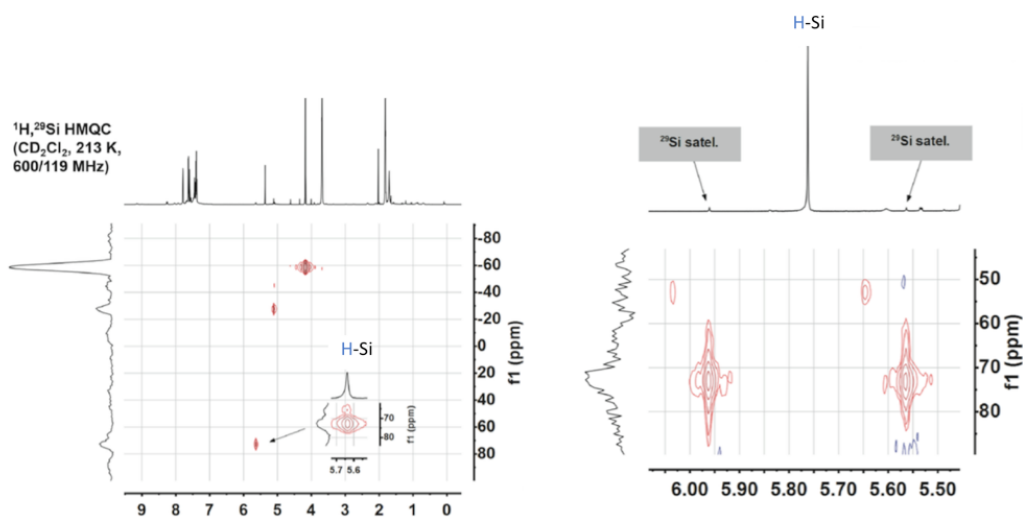
Figure 25: ^{1}H-^{29}Si HMQC NMR spectra of [**3**][BArF$_{24}$]

^{1}H NMR analysis (-40 °C, [D$_8$]THF) of [**4**][BArF$_{24}$] disclosed a triplet at δ = 4.78 ppm with ^{1}JH,Si = 95Hz for the Si-bound H atom, as well as the typical signals of Si-coordinated THF (four broad peaks at d = 0.65, 0.83, 2.07, 2.31 ppm). A ^{1}H,^{29}Si HMQC NMR experiment (-40 °C, [D$_8$]THF) showed the presence of a cross-peak correlation between the 1H resonance of the Si-H bond at δ = 4.78 ppm and the ^{29}Si resonance at δ =71.3ppm. (figure 26)
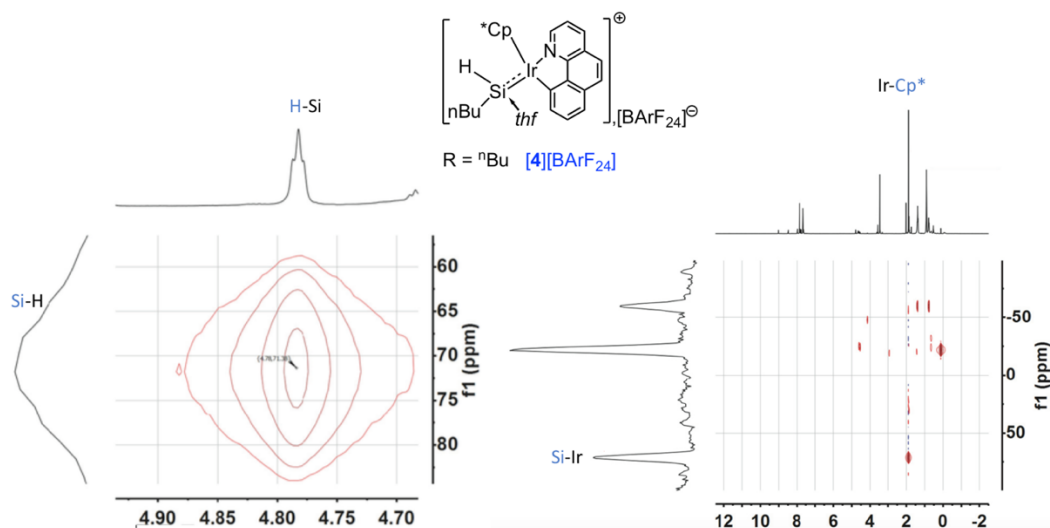
*Figure 26: ^1H-^{29}Si HMQC NMR spectra of [**4**][BArF$_{24}$]*

^1H-^{29}Si HMQC NMR of [**5**][BArF$_{24}$] spectra recorded at -40°C (CD$_2$Cl$_2$) represented a cross-peak correlation between Si-H bond at δ = 5.02 ppm and the ^{29}Si resonance at δ = 80.1 ppm, NOESY shows the typical signals of Si-coordinated THF (four broad peaks at δ =1.81, 3.72 ppm) with H-Si δ = 5.02 ppm. (figure 27)
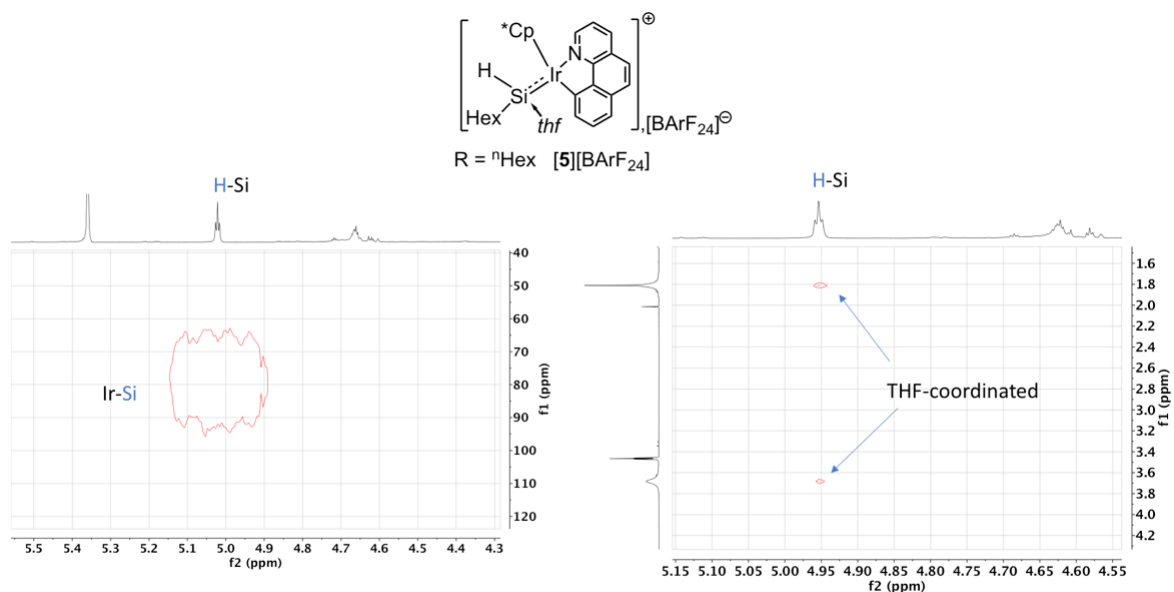
*Figure 27: ^1H-^{29}Si HMQC and ^1H NOESY NMR spectra of [**5**][BArF$_{24}$]*

3.2. *Following the formation of sillylenes from adduct by ^{1}H-NMR.*

Tracking ^{1}H NMR of the reaction of [**2c**][BArF$_{24}$] (formed in situ by reaction of an 85 m$_M$ CD$_2$Cl$_2$ solution of [**1b**][BArF$_{24}$] with 5 equiv of H$_3$SiPh at -60 ^{o}C) with about 5 equiv of THF at 25 ^{o}C in a J. Young sealed tube showed rapid release of H$_2$ gas in solution and full conversion to [**3**][BArF$_{24}$] within about 20 min (Figure 28).
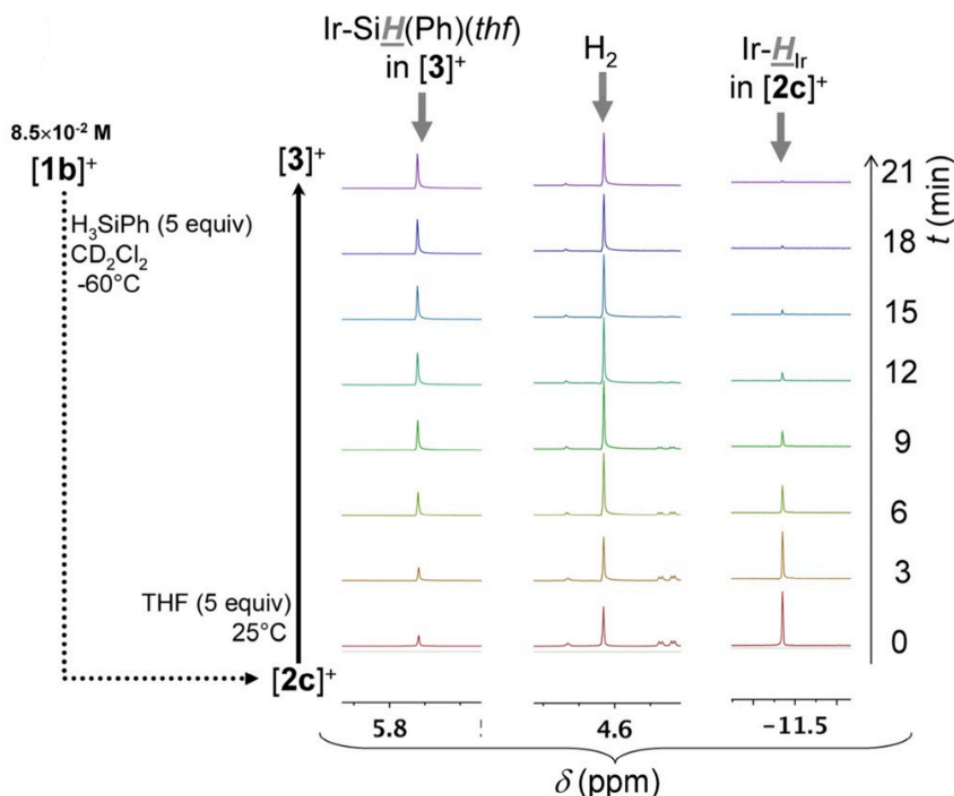
Figure 28: Focused view on typical signals of the 1H NMR spectrum monitoring as a function of time the conversion of a freshly prepared solution of [2c]$^+$ (made from [1b]$^+$, see dotted arrow) to [3]$^+$ upon addition of THF in CD$_2$Cl$_2$ solution at 25°C; spectra were acquired at 3 min time intervals, and t = 0 corresponds to the first spectrum, which was recorded about 3–4 min after introduction of the sealed J. Young NMR sample tube containing the mixture into the spectrometer.

By using electrospray mass spectroscopy (heater temperature: 200°C) in positive-ion mode to characterize adducts [**2c,d**]$^+$, analysis of the total ion current represented, in both cases, a main peak corresponding to the [(benzo[h]quinolinyl- $\kappa^{C,N}$)IrCp*]$^+$ cation at m/z = 506 Da. Nevertheless, minor signals could also be detected and assigned to a new ion resulting from [**2c,d**]$^+$ having gained one oxygen atom. The most illustrative example is that obtained from a fresh CH$_2$Cl$_2$ solution of [**2d**]$^+$ injected directly in the

ionization chamber without any preliminary treatment, which showed a reasonable signal-to-noise ratio (Figure 28). The hypothesis is this ion might be an iridium silylene complex having captured or reacted with a molecule of water.
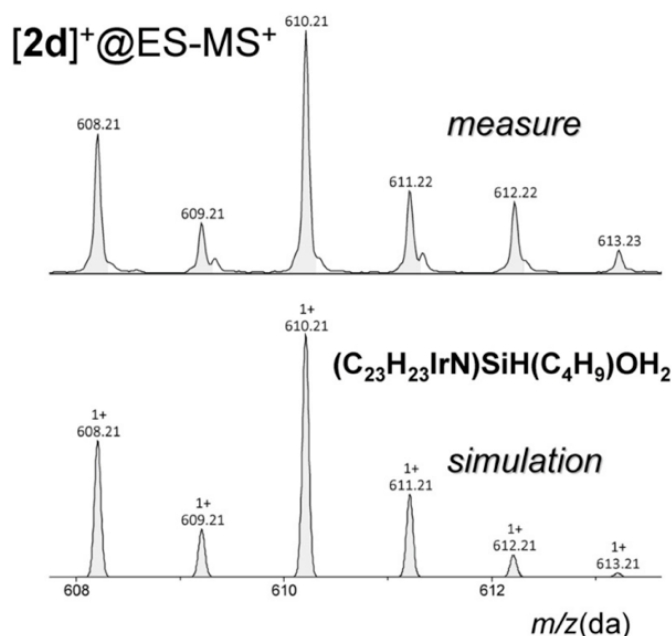
Figure 29: Isotopic signature of one of the minor products of fragmentation of [2d][BArF_{24}], injected as a solution in CH_2Cl_2 in the ionization chamber of an ESI (positive-ion mode) spectrometer.

3.3. *Recrystallisation silylene metal complexes.*

Reactive crystallization was utilized to obtain a variety of Ir silylene complexes, including Ir dialkyl silylenes (diethyl and diphenyl), which could not be observed in ^{1}H NMR. This growing crystals method grounds on a diffusion of a heptane solution of silanes into a solution of [1b]+ in CH_2Cl_2/THF through a buffer layer of dry benzene proved to be the only way to trap crystals of the key Ir silylene complexes.

The structures (Figure 30) reveal that Si-Ir interatomic distances remain somewhat in the range of those reported for exogenous-donor-devoid Ir[III] silylene complexes[74, 127] [76] (Ir-Si ≈ 2.25 Å), of the triflate-bonded Ir silylene of Klei, Tilley, and Bergman[153](Ir-Si ≈ 2.30 Å), and other known neutral donor-bound metal silylene complexes[77, 154-157] (M-

Si(donor)RR ≈ 2.26–2.32 Å). The Ir-Si distances of silylene are consistently shorter by about 0.2 Å than in their adduct precursor, including [2a,b]+ .[17, 18]
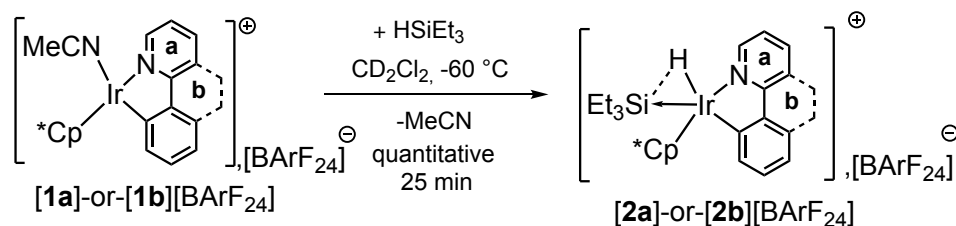
Scheme 29: the synthesis of [2a]+ and [2b]+
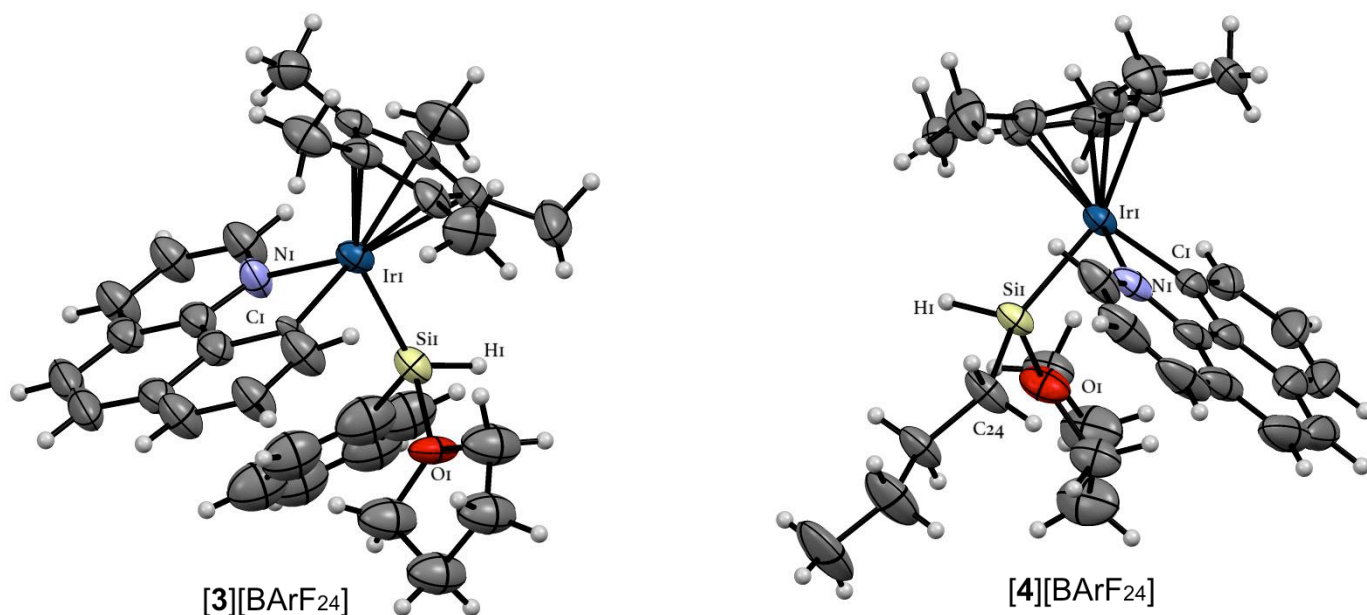
[3][BArF24]

[4][BArF24]

Figure 30: ORTEP at 50% probability of the structure of [3]+ determined by XRD analysis. The [BArF24]- anion and atoms corresponding to occupational disorder are omitted for the sake of clarity. Selected interatomic distances [Å] and angles [º] for [3][BArF24]: Si1-Ir1 2.278(3), Si1-H1 1.3(2), O1-Si1 1.88(2),N1-Ir1 2.09(3), O1-Si1-Ir1 115.7(5), O1-Si1-H1 100(9), N1-Ir1-Si1 88.7(8), Ir1-Si1-H1 126(9).

ORTEP at 50% probability of the structure of [4]+ determined by XRD analysis. The [BArF24]- anion and atoms corresponding to occupational disorder are omitted for the sake of clarity. Selected interatomic distances [Å] and angles [º] for [4][BArF24]: Si1-Ir1 2.288(1), Si1-H1 1.40(8), O1-Si1 1.825(5), N1-Ir1 2.084(5), O1-Si1-Ir1 115.8(2), O1-Si1-H1 90(3), N1-Ir1-Si1 87.3(1), Ir1-Si1-H1 119(3).
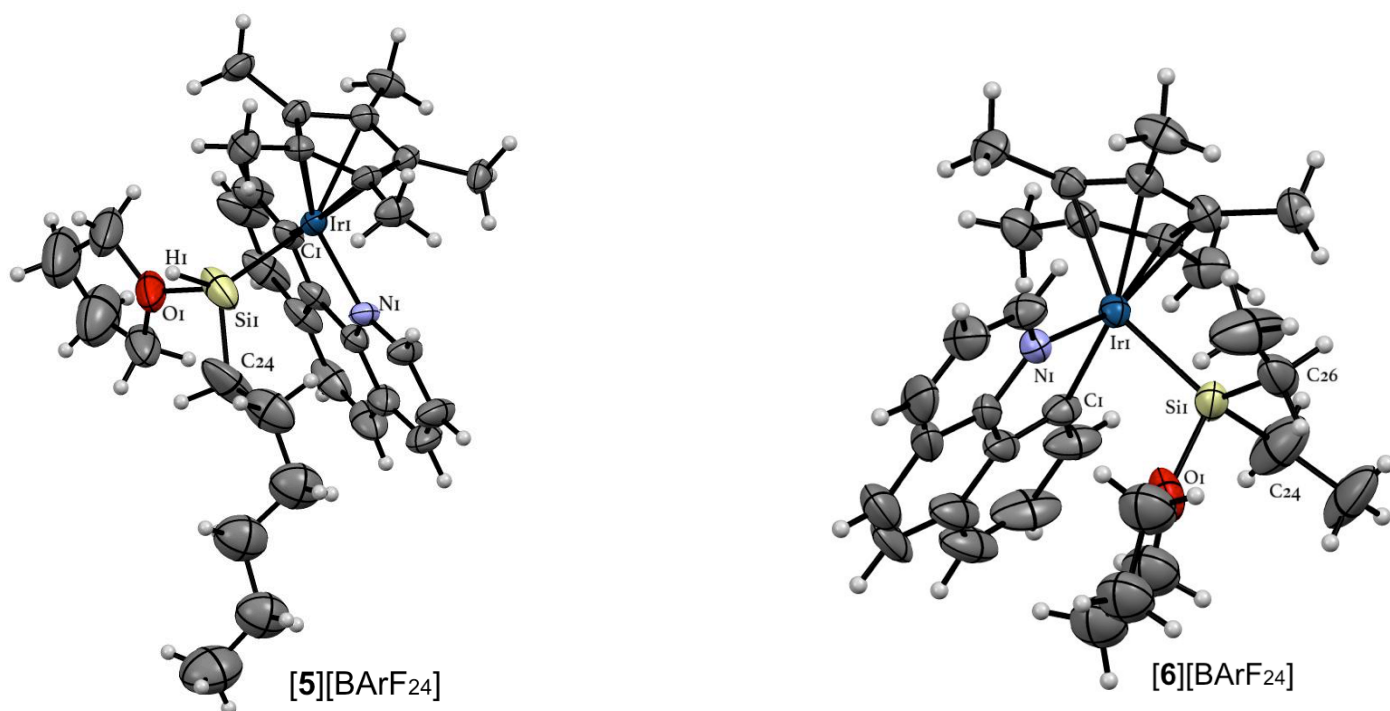
[5][BArF24]

[6][BArF24]

Figure 31: ORTEP at 50% probability of the structure of [5]$^+$ determined by XRD analysis. The [BArF$_{24}$]$^-$ anion and atoms corresponding to occupational disorder are omitted for the sake of clarity. Selected interatomic distances [Å] and angles [º] for [5][BArF$_{24}$]: Si1-Ir1 2.290(3), Si1-H1 1.45(9), O1-Si1 1.860(8), N1-Ir1 2.073(4), O1-Si1-Ir1 115.2(2), O1-Si1-H1 95(5), N1-Ir1-Si1 87.5(1), Ir1-Si1-H1 124(5).

ORTEP at 50% probability of the structure of [6]$^+$ determined by XRD analysis. The [BArF$_{24}$]$^-$ anion and atoms corresponding to occupational disorder are omitted for the sake of clarity. Selected interatomic distances [Å] and angles [º] for [6][BArF$_{24}$]: Si1-Ir1 2.317(2), O1-Si1 1.838(6), N1-Ir1 2.082(4), O1-Si1-Ir1 112.1(2), N1-Ir1-Si1 91.5(1), C24-Si1-C26 106.1 (4), C24-Si1-Ir1 116.1(4).
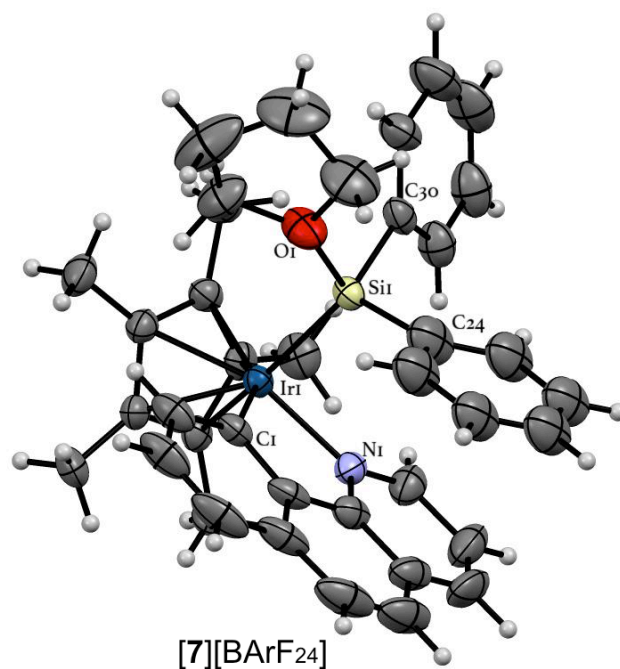
[7][BArF24]

Figure 32 : ORTEP at 50% probability of the structure of [7]+ determined by XRD analysis. The [BArF24]−
anion and atoms corresponding to occupational disorder are omitted for the sake of clarity. Selected
interatomic distances [Å] and angles [°] for [7][BArF24]: Si1-Ir1 2.323(1), O1-Si1 1.849(3), N1-Ir1 2.085(3),
O1-Si1-Ir1 115.3(2), N1-Ir1-Si1 86.1(1), C24-Si1-C30 106.8(4), C24-Si1-Ir1 116.9(2)

	Interatomic distances (Å)		
	Ir-Si	O-Si	N-Ir
[3][BArF24]	2.278(3)	1.88(2)	2.09(3)
[4][BArF24]	2.288(1)	1.825(5)	2.084(5)
[5][BArF24]	2.290(3)	1.860(8)	2.073(4)
[6][BArF24]	2.317(2)	1.838(6)	2.082(4)
[7][BArF24]	2.323(1)	1.849(3)	2.085(3)

Table 5: Comparing selected Interatomic distances (Å) of all silylene complexes

Among those complexes differences of Interatomic distances are not considerable, [**7**][BArF$_{24}$] possessed the longest Ir-Si bond 2.323(1) Å while distance from coordinated-THF to Si center of [**3**][BArF$_{24}$] is furthest 1.88(2) Å.

		Interatomic distances (Å)	
		Adduct	Silylene
Adduct	Silyene	Ir-Si	Ir-Si
[**2c**][BArF$_{24}$]	[**3**][BArF$_{24}$]	2.407(2)	2.278(3)
No crystal	[**4**][BArF$_{24}$]	x	2.288(1)
[**2e**][BArF$_{24}$]	[**5**][BArF$_{24}$]	2.4220(7)	2.290(3)
[**2f**][BArF$_{24}$]	[**6**][BArF$_{24}$]	2.455(2)	2.317(2)
[**2g**][BArF$_{24}$]	[**7**][BArF$_{24}$]	2.435(1)	2.323(1)

Table 6 : Comparing Interatomic distances of Ir-Si bond in crystal of silylene with their precursor adducts

Ir-Si bond is approximately 0.15 (Å) shorter in silylenes compared to their precursor adducts, the widest difference 0.138 (Å) belongs to the tranformation from [**2f**]$^+$ to [**6**]$^+$ while the tranformation from [**2g**] into [**7**] possessing the slightest change 0.112 (Å).

3.4. *Theoretical investigations of Ir-Si bonding*

Probing bond structure in transition metal silylene complexes have been of great attraction to chemists for years[55, 58, 158-160]. Especially, Investigating on the σ-donor/ π-acceptor character of silylenes and its tuning by a change of substituents are one of the most interesting aspects there are[161]. Accompanied with that, the effects of the nature of the metal on the dominant electronic configuration and its related effect on the π-accepting properties also have been addressed[58, 159, 160]. To deal with those issues, ab initio[58, 60, 160] and DFT studies[59, 162] are often employed, which also showed that metal silylenes of late transition metals generally had a significantly less π-

accepting character than the parent (Fischer) carbene ligands. Ziegler et al published a prominent work in this field[59, 162], in which they harnessed extensively an energy decomposition analysis (EDA)-derived approach to weight the σ-donating versus π-accepting contributions.

In this thesis, both EDA and a fragment-based method ETS-NOCV[151, 152] analysis, were leveraged to estimate symmetry-wise decomposition of inter-fragment orbital interactions, their energetic contribution to the overall orbital interaction energy, and to project an intuitive visualization of how electron density is redistributed in the wide variety of molecular natural orbitals and bonds of the product.

Presuming the bonding of a neutral **:**SiRH(THF) moiety (Figure 33) to the cationic iridacyclic residue, molecular-fragment-based ETS-NOCV analysis[151] manifested that, deformation densities $\Delta\rho_1$ in figure 33a and b clearly represent the electron-density transfers taking place on buildup of the Si-to-Ir σ bond in accordance with the chosen interaction scheme. The ETS-NOCV[151] analysis of the THF-devoid analogue of [**3**]$^+$ (Figure 33a) confirms the π-accepting property of the **:**SiPh(H) moiety and consolidation of the Ir–Si bond [wbi(Ir-Si)=0.83], which is represented by deformation density $\Delta\rho_2$. In this case, the metal–Si π-backdonation orbital interaction (Figure 33a) represents about 20% of the interfragment orbital interaction energy.
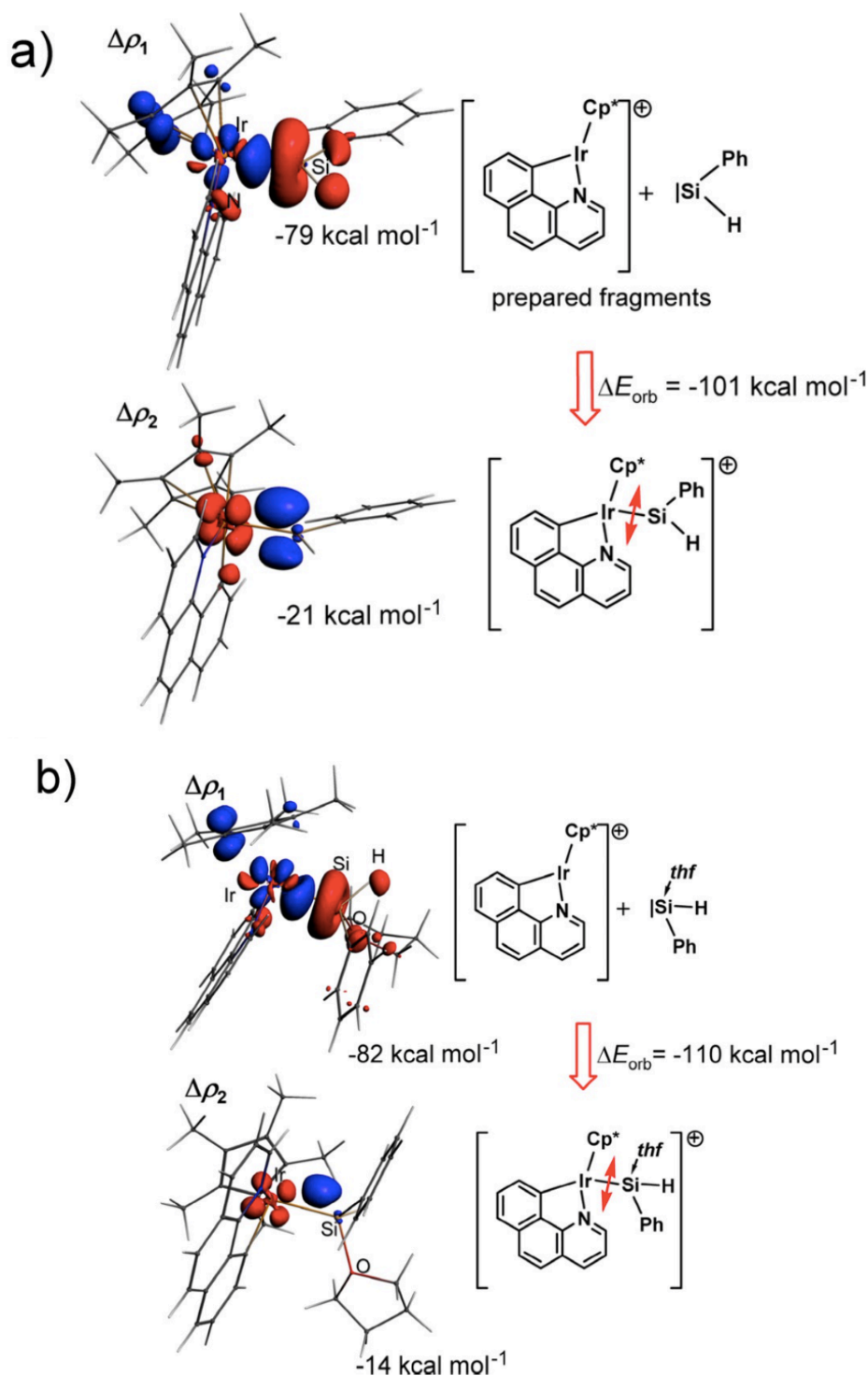
Figure 33. a) Main deformation density isosurface plots (0.005 e bohr⁻3) resulting from the ETS-NOCV analysis of the interaction of a neutral prepared Si(H)Ph silylene fragment with the cationic iridacyclic group in THF-devoid [3]⁺.

b) Main deformation density isosurface plots (0.005 ebohr⁻3) resulting from the ETS-NOCV analysis of the interaction of a neutral prepared THF-bound Si(H)Ph(THF) silylene fragment with the cationic iridacyclic group in [3]⁺.The double arrows show which bond is virtually disrupted in the fragmentation.Red and blue isosurfaces correspond to donating and accepting orbitals, respectively. Orbital interaction energies ΔE_k associated with a deformation density isosurface are given underneath each isosurface plot. Selected distances [Å] for the computed

In spite of the THF–Si interaction, a considerable π-accepting character ($\Delta\rho_2$ in Figure 33b) resides at the Si center in [3]⁺ (Wiberg[150] Ir–Si bond index wbi = 0.68) and [4]⁺ (wbi = 0.67). This residual π-accepting character is characterized by the metal-to-Si p-backdonation deformation density plot $\Delta\rho_2$ (Figure 33b), which accounts for about 10% of the total interfragment orbital interaction energy.

Calimano and Tilley[127] reported a pertinent relevant reference in which a cationic Ir^III silylene complex with a "bare" Si center was synthesized. ETS-NOCV analysis was replicated accompanied with the assumption of an interaction between a neutral :SiPh₂ silylene and a cationic Ir-centered residue. The result shows that Ir-to-Si π-back-donation accounts for only 14% of the total interfragment orbital interaction energy, which is less than for the fictitious THF- devoid [3]⁺ and likely an outcome of the weaker donating properties of the ligand set in the PNP complex (Figure 34).
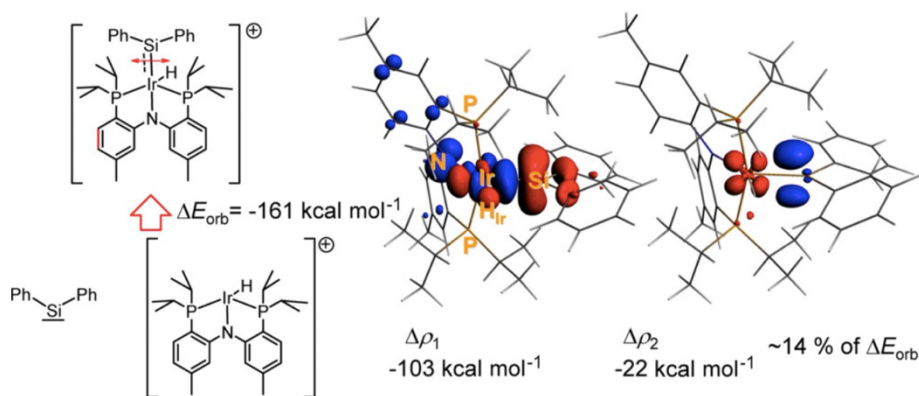
Figure 34. Main deformation density isosurface plots (0.005 e bohr⁻3) resulting from the ETS-NOCV analysis of the interaction of a neutral prepared silylene fragment SiPh₂ with the cationic Ir^III group of an Ir silylene complex reported by Calimano and Tilley[127] .The double red arrow suggests which bond is cleaved in the fragmentation mode. Δρ1 corresponds to the establishment of the Si–Ir σ bond. $\Delta\rho_2$ corresponds to Ir-to-Si π backbonding, the associated interaction energy ΔE_k of which represents about 14 % of the total interfragment orbital interaction energy. Red and blue isosurfaces correspond to donating and accepting orbitals, respectively. The Wiberg bond index for the Ir–Si interaction is 0.81.

3.5. _Gibbs energy profile of formation of the THF-bound IrSi(H$_2$)Ph silylene complex_

THF played a pivotal role in the H$_2$ elimination step in the line with the computed reaction-energy profile. The formation of [**2c**]$^+$ is exoergonic at 298 K (Figure 35a). In the absence of THF, the concerted coupling of the hydridic Si-bound H$_{Si}$ atom with the Ir-bound H$_{Ir}$ atom demands a prohibitive activation energy $\Delta G^{o\#}$ of about +30 kcal mol$^-$1 (via transition state TS-I, Figure 35a), overall process resulting in the THF- free silylene complex is endoergonic ($\Delta G^o \approx$ + 11 kcal mol^{-1}). On the contrary, in the presence of one molecule of THF (perfect-gas conditions in vacuum), the formation of van der Waals complex [vdW-**2c**]$^+$ requires about +17 kcalmol^{-1}.

However, that barrier, evidenced experimentally, is completely overcome by leveraging THF in large excess or as solvent of the reaction, which leading plausibly to intermediate [vdW-**2c**]$^+$. The conversion of [vdW-**2c**]$^+$ to THF-stabilized silylene complex [**3**]$^+$ has an activation barrier of about +14 kcalmol^{-1} through **TS-I-thf** with an exoergonicity ΔG^o ([**2c**] + THF $\rightarrow$ [**3**]$^+$) of –4 kcalmol^{-1} , which confirms that in pure THF [**3**]$^+$ was formed spontaneously[127].

In view of utilizing natural atomic charges analysis, the coordination of THF not only served as the driving force of this reaction but also triggered variable character of the Ir-bound hydrido ligand, which is capable of behaving as H$^-$ in key hydrosilylation steps or as H$^+$, as shown here.

Bonding of THF to the Si center actually give rise to[71] a net increase of the formal natural[163] negative charge of the Si-bound H atoms and a 50% increase of the natural charge difference Δq between the H$_{Si1}$ and H$_{Ir}$ atoms in **TS-I-_thf_** compared to **TS-I** ($\Delta q(H_{Ir}–H_{Si})$**TS-I-_thf_** = 0.26, $\Delta q(H_{Ir}–H_{Si})$**TS-I** = 0.17; Figure 35b). Coulombic interactions between H$_{Si1}$ and H$_{Ir}$ essentially assist the formation of H$_2$. Put differently, the relative "acidity" of the latter Ir-bound hydrido ligand H$_{Ir}$ and the hydridic character of H$_{Si1}$ intensified by the interaction with THF to facilitate H$_2$ release. Corriu and coworkers[71] observed the same phenomenon on Fe complexes.
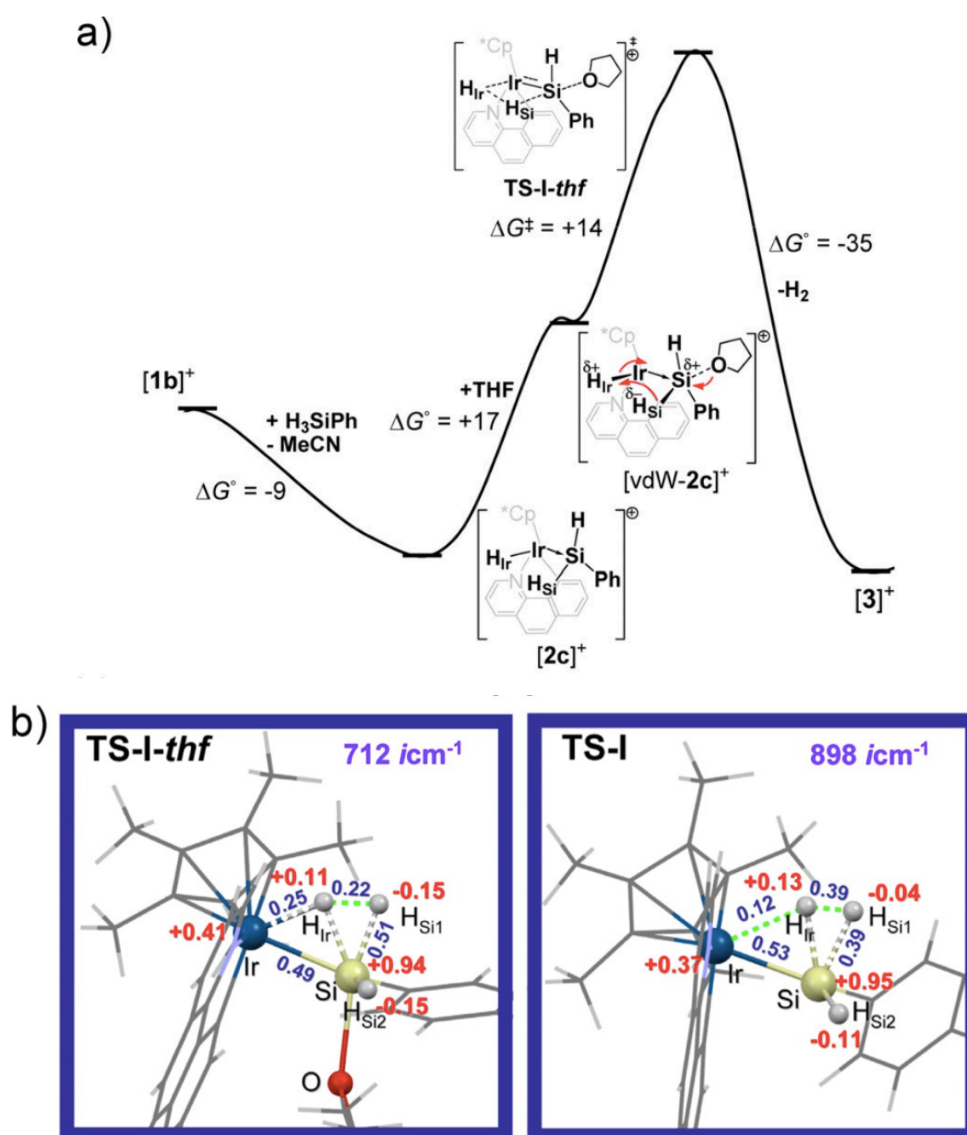
*Figure 35: a) Proposed Gibbs energy profile for the THF-assisted formation of [3]+, as computed by DFT (Gibbs enthalpies in kcal mol⁻1) assuming Coulomb-interaction-supported interaction of H atoms in **TS-I**-thf; the Gibbs enthalpy (298.15 K, 1 atm) for the [1b]+→[3]+ reaction is about −13 kcal mol⁻1.*

*b) Detailed description of the Wiberg bond indices (in blue font) and (NPA) natural charges (in red font) at the core motif undergoing bond cleavage in transition states **TS-I**-thf and TS-I.*

H$_2$ Elimination mechanism was also probed by ETS-NOCV analysis was conducted by mean of fragmenting **TS-I-*thf*** into two fragments comprising H$_2$ and [**3**]+ in their static prepared geometry to provide insights into the transformation of [**2c**]+ into [**3**]+. This assessment shed light on major change in the Ir-Si interaction and the electron-density redistribution resulting from the departure of H$_2$ as well. The fragmentation enables discernible visualization of the density transfers that take place especially toward the Ir-H$_{Ir}$-H$_{Si}$-Si motif. On account of the microreversibility principle, one can state from

deformation density $\Delta\rho_1$ (Figure 36) that the departure of H_2 involves: 1) electron-density donation to the Ir center and the Ir-Si σ bond from the σ Ir-H$_{Ir}$ and Si-H(Si) bonds.

2) minor donation from the Si-bound THF oxygen atom.

3) crucial transfer of density to H_{Ir}, which rebalances the charge density between this hydrogen atom and H_{Si} in the process of H_2 formation.
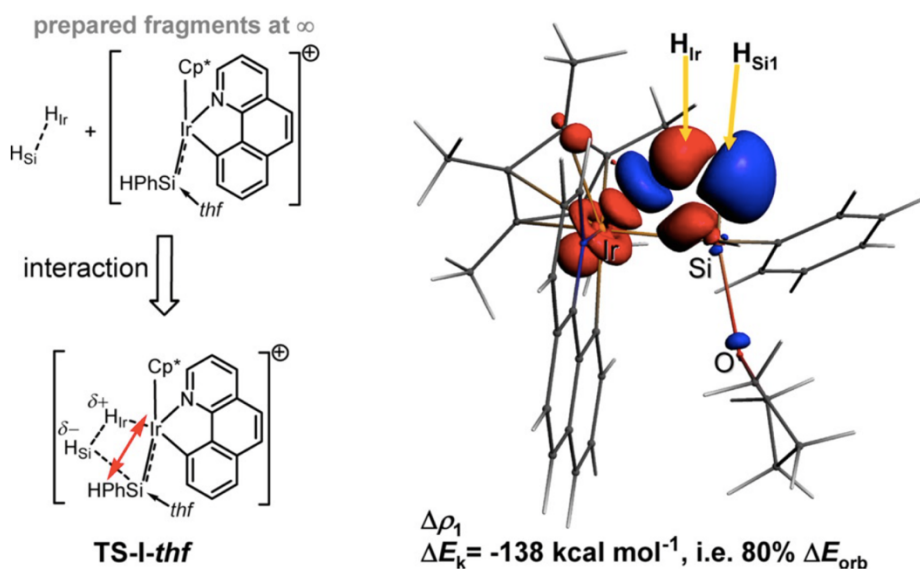
Figure 36. Plot of deformation density Δρ₁ (0.005 e/bohr ⁻3) emerging from the ETS-NOCV analysis of the fictitious interactions of the prepared fragments of H₂ and THF-bound Ir-silylene cation conducting to transition state TS-I-thf (the double red arrow indicates which bonds are cleaved in the fragmentation scheme). The red and blue isosurfaces (0.005 e bohr ⁻3) are associated with orbitals donating and accepting electron density, respectively. The interaction of H₂ with prepared [3]⁺ suggests strong polarization of the H-H bond and donation to the Ir-H$_{Ir}$ and H$_{Si1}$-Si σ bonds from H$_{Ir}$ and Ir centers along with the Si-Ir σ bond. In the reverse transformation, that is H₂ release and its dissociation from [3]⁺, orbitals depleted in electron density are now those colored in blue and the accepting orbitals are colored in red.

Figure 37 represents the electron-density redistribution (red arrows) in the H_2-release process based on the ETS-NOCV analysis, which consists of, transformation from a donor–acceptor Ir→Si interaction[17, 18] (wbi ≈ 0.44, silylicity, Π [16] related to the [SiPhH$_2$]⁺ moiety ≈ 1.3) in [2c]⁺ to a reversed dative Ir ←Si or a coordinative Ir-Si bond carrying some Ir→Si π character in [3]⁺. Related conclusions can be rendered for [2d]⁺ and [4]⁺ (silylicity related to [SinBuH$_2$] Π ≈ 1.3).
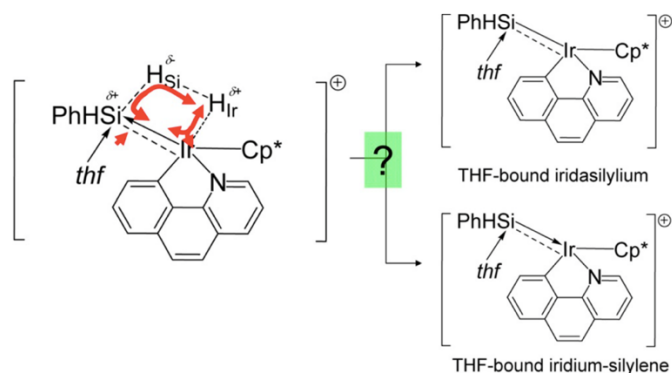
*Figure 37. Extrusion of H₂ from **TS-I**-**thf** (left-hand side) via redistribution electron density (red arrows) fortifies the Ir-Si bond and leads to [**3**]⁺ (right-hand side) in such way that the exact nature of the Si-centered ligand remains vague regardless of its significant residual p-acidic character (dashed bond).*

4. _Reduction of nitroarenes_

Since the nature of (metalla)silylium's catalytic reactivity was ascertained, there have been endeavors making use of that property on O-dehydrosilylation of alcohols[17], reduction of nitriles through N-silylation[18] or the most recent and appealing dehydrofluorination[19]. To continue to cultivate that fruitful chemistry, nitroarenes reduction via hydrosilyltion was delved into subsequently.

The synthesis of amine arenes via the reduction of nitroarenes laid in the center of organic chemistry which is frequently utilized in the synthesis of pharmaceuticals, agrochemicals, dye intermediates, and pigments, etc.[164] Conventional methods used for that transformation are Béchamp[165, 166] (Fe/HCl) or sulfide[165] (H₂S) reduction are fraught with pitfalls as using grossly excessive of iron powder[167], disposing of a large amount of waste of toxic substances[167, 168] and formation of the mephitic sulfur-containing side-products[165]. Generally, the industrial-scale reductions of nitro compound are currently conducted by utilizing the heterogeneous catalyst. Nevertheless, there is a limited number of commercially available catalysts, and rest are altered for the specific substrates. Therefore, leveraging hydrosilylation of nitroarenes that provides a cheaper, safer alternative and carried out under mild condition is of utmost importance.

Since Lipowitz *et al.* reported initial work of nitroarene reduction under hydrosilylation condition using PMHS as a hydride source catalyzed by bis(dibutylacetoxytin) oxide

(DBATO) in 1973[165, 169], there has been a series of metals were tested catalytic reactivity for instance: Pd[169-172], Pt[173], Re[174], Sn[175]. Along with this line, Iridacycle **1b** has been investigated and represented catalytic reactivity. A set of silanes was perused in the same condition (90°C, C_6H_{14} solvent) with 4-Nitrotoluene as a model substrate to indicate the most effective one. $HexSiH_3$ was determined to be the best in terms of yields of desired anilines. (Eq. 35, Table 7)
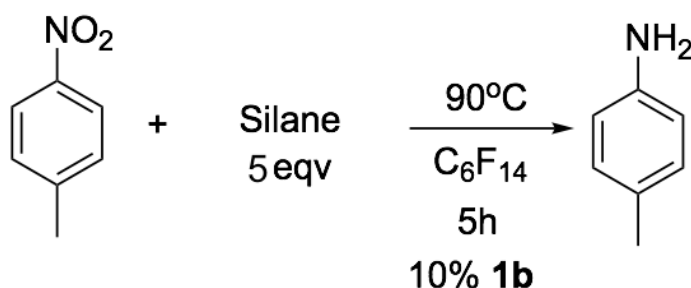
Eq. 35

Silanes	Conversion (%)	Yield (%)
triethylsilane	no conversion	
di-tert-butylsilane	no conversion	
diethylsilane	100	10
phenylsilane	no conversion	
butylsilane	no conversion	
hexylsilane	100	40

Table 7: A set of silanes was perused in the same condition (90°C, C_6F_{14} solvent) with 4-Nitrotoluene as a model substrate to indicate the most effective one

More interestingly, mono and dialky silanes (diethyl and hexylsilane) were reactive whereas tertiary alkyl silane (triethyl silane) was not, that is supposedly on account of the tertiary one lacking a possibility of H_2 elimination in accord with our aforementioned mechanism. This phenomenon provided a reliable indication that iridium silylene species presumably involving in nitro reduction process. (Eq. 36, table 8)
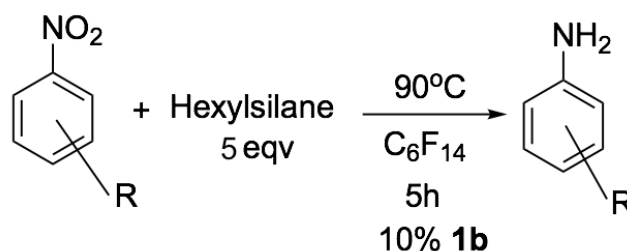
Eq. 36

Substrate	Conversion (%)	Yield (%)
4-nitrotoluene	100	40
4-nitroanisole	100	40
1-terbutyl-4-nitrobenzene	100	47,6
1-nitronaphthalene	100	?
1,4-dinitrobenzene	30	12
3-nitroaniline	72	25
4-nitroaniline	35	13

Table 8: 1b catalyzed reduction of nitroarenes to amines

A set of nitroaromatics were tested with hexylsilane as reductive agent under optimized condition 90°C, 5h, 10% **1b** catalyst. Results were show in a table below. Generally, hexylsilane showed a promising reactivity with 4 substrates were converted 100%. However, the yield is quite low and defining a conversion is unachievable in some cases due to a lingering issue that formation of toxic hydroxyl- amine intermediate and side products such as azo and azoxy, which leads to the color impurities in the reaction products (scheme 30)[165] albeit product mixture treated by dilute acid acetic and extracted in organic phase.
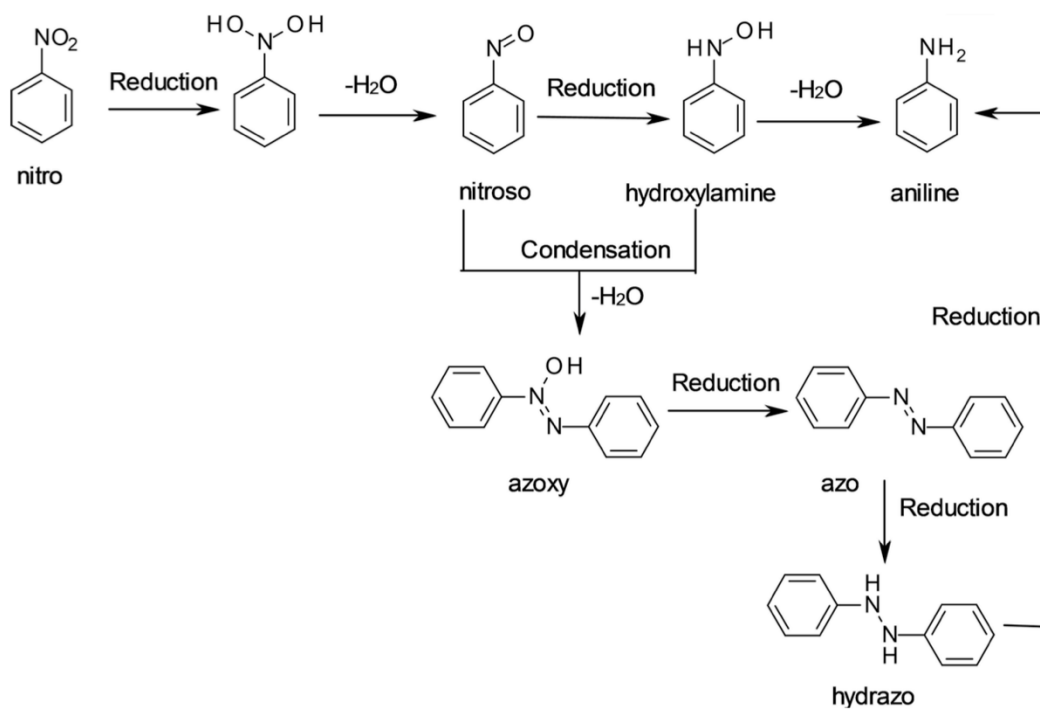
Scheme 30: General pathway for nitroarene reduction and intermediates[165].

5. *Enhancement catalytic reactivity of adduct by utilizing fluorinated ligand.*

5.1. *Synthesis*

Continuing with previous section, it is safe to hypothesize that cationic hydrido-Ir(III)-silylium species, whose catalytic reactivity is of significant correlation with the extend of polarization of the molecule[16-18] therefore enhance the polarization in the key intermediates molecule is also means increase its catalytic reactivity. The polarization occurs already in the Ir-silane adduct stemming from the electropositivity of Si centre will be aggravated by adding an electron withdrawing group in N,C ligand. (figure 38)
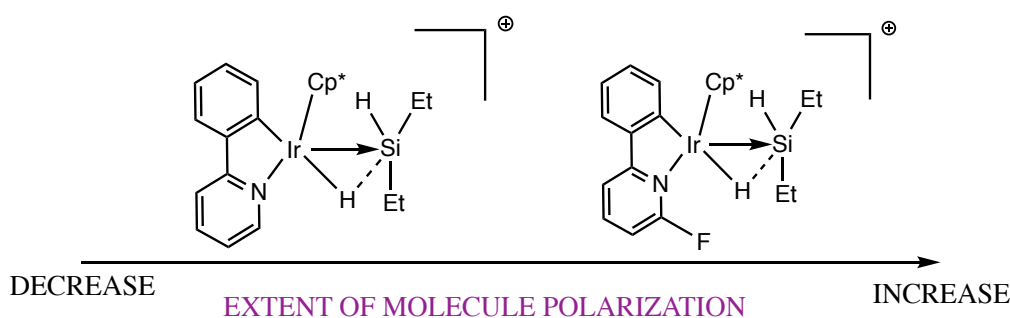
*Figure 38: By adding a strong electron-withdrawing group, the key intermediate F-**1a** is more polarized than **1a***

Based on that foundation, AgF_2 was utilized reacted with 2-phenyl-pyridine to give rise to fluorinated 2-phenylpyridine[176-178], that then underwent the cyclometallation with $[Cp*IrCl_2]_2$ dimer and finally produced fluorinated cationic solvento complexes F-**1a**. Experimentally, F-phenylpyridine was cyclometalated in far longer time (5 days at room temperature) than normal phenylpyridine ligand, which could mean Electron-withdrawing group impede a C-H activation or nitrogen coordination of $[Cp*IrCl_2]_2$. However, a subsequent formation of solvato complex took places rapidly as observed in **1a** case. (scheme 31)
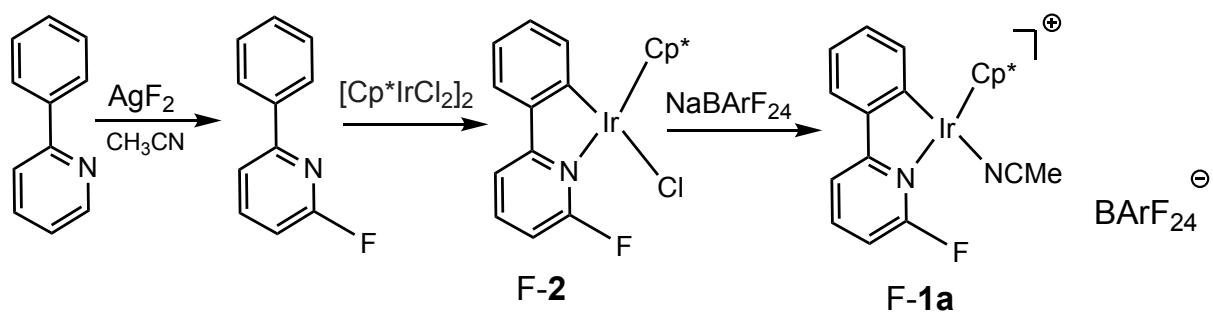
Scheme 31: Synthesis of fluorinated cationic solvento complexes.
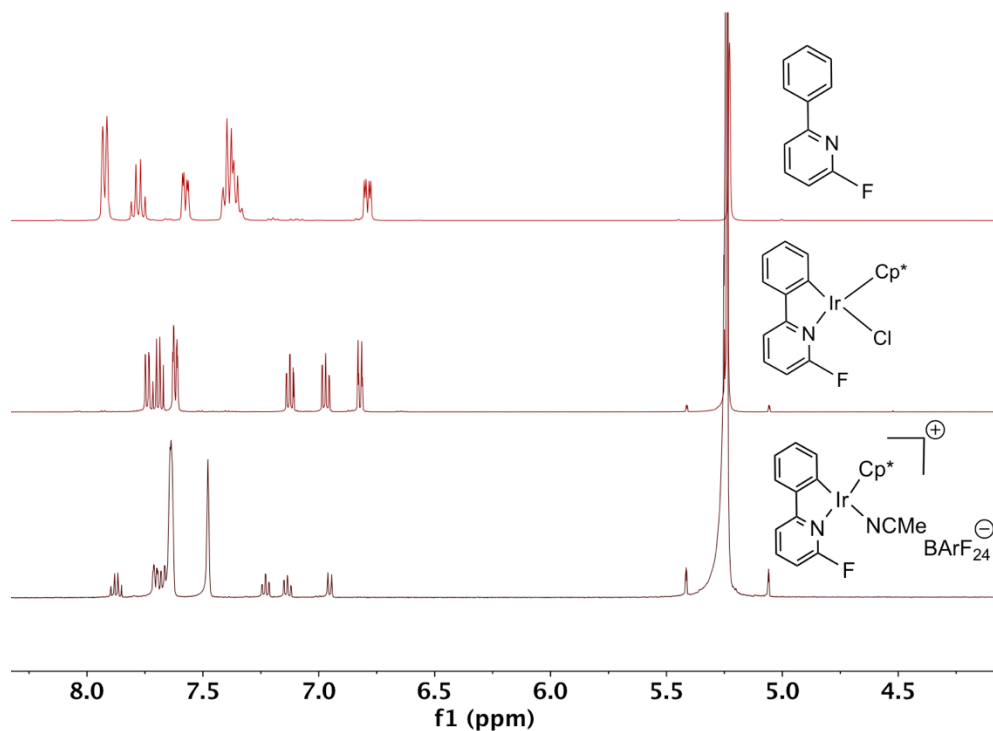
Figure 39: 1H-NMR of F- Phenylpyridine, F- Phenylpyridine Iridacycle, and sovato complexe

^{19}F-^{1}H NMR of F-**2** and F-**1a** shows that ^{19}F S($\delta \approx$ -58 ppm) corelates with not only adjacent protons but also distant ones. (figure 40, 41)
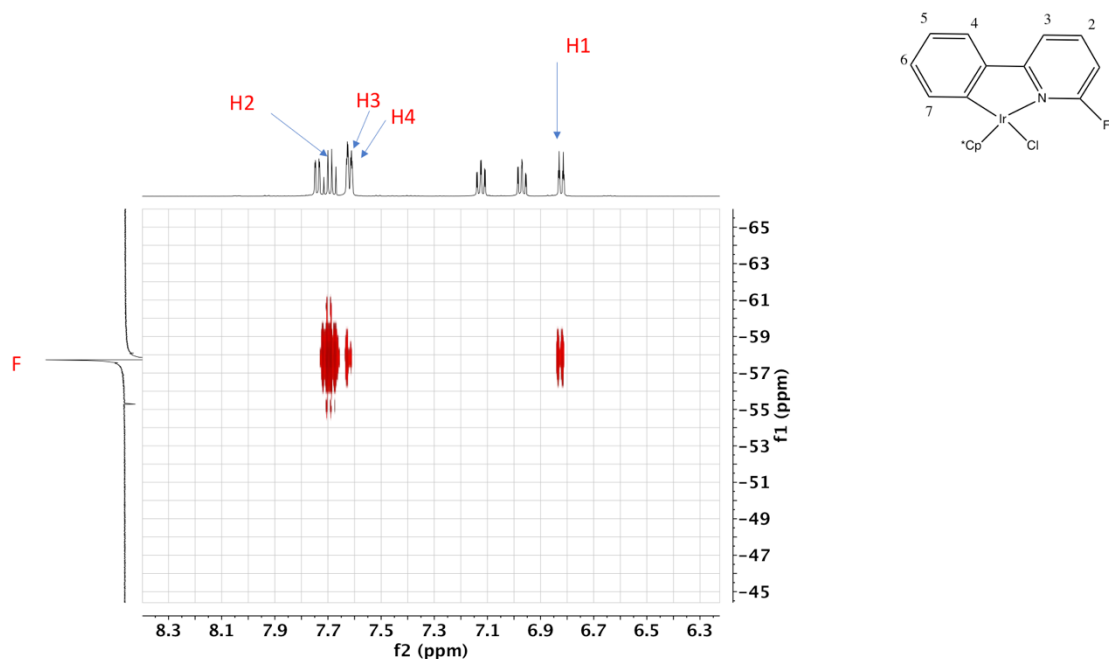
*Figure 40: ^{19}F-^{1}H NMR of F-**2***

COSY ^{1}H-^{19}F
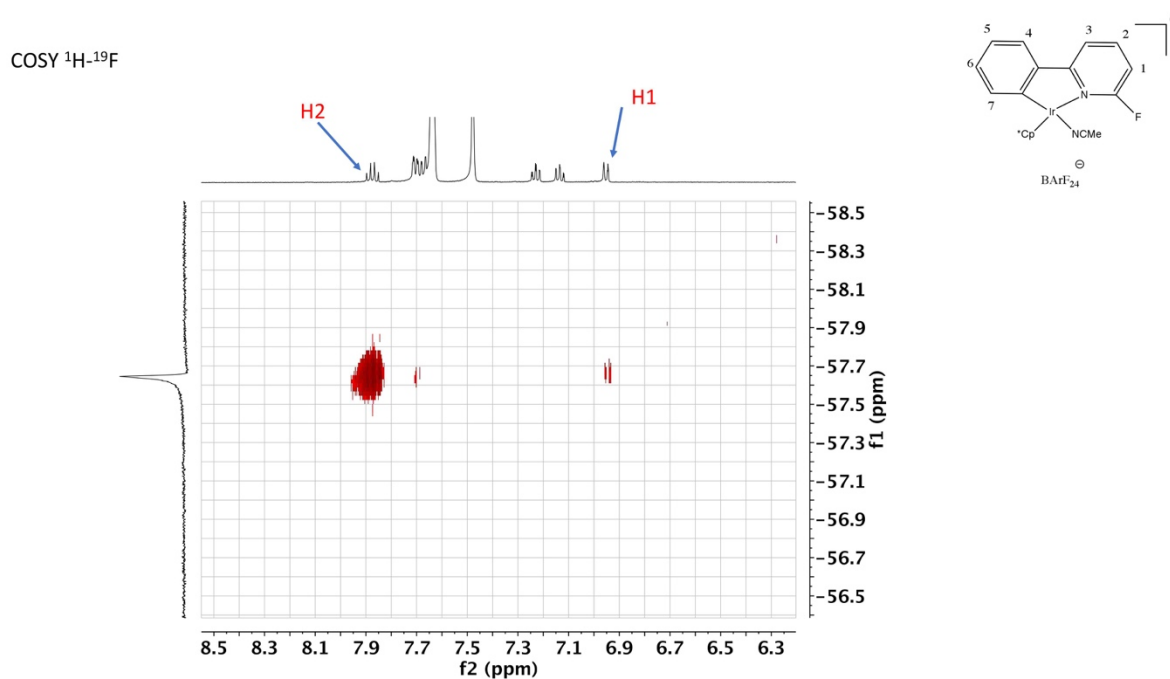
*Figure 41: ^{19}F-^{1}H NMR of F-**1a***

As expected, F-**1a** also displays remarkable catalytic reactivity toward a benchmark test reaction that can be followed by piezometry, i.e. the O-dehydrosilylation of alcohols at room temperature with Et_3SiH. A hydrido-Ir(III)-silylium intermediate crystal was trapped as well following on a reaction with Et_2SiH.
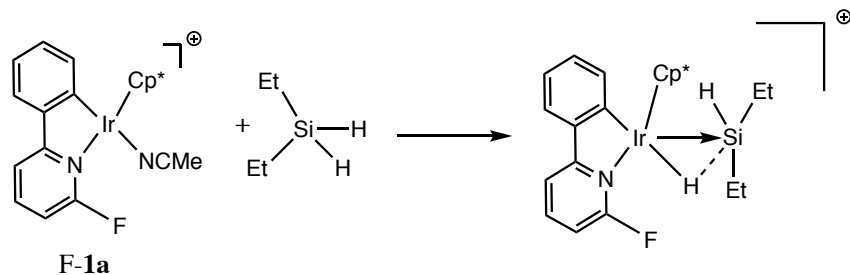
*Eq 37: F-**1a** reacted with Et$_2$SiH$_2$ to from an adduct*

F-1a

F-5a
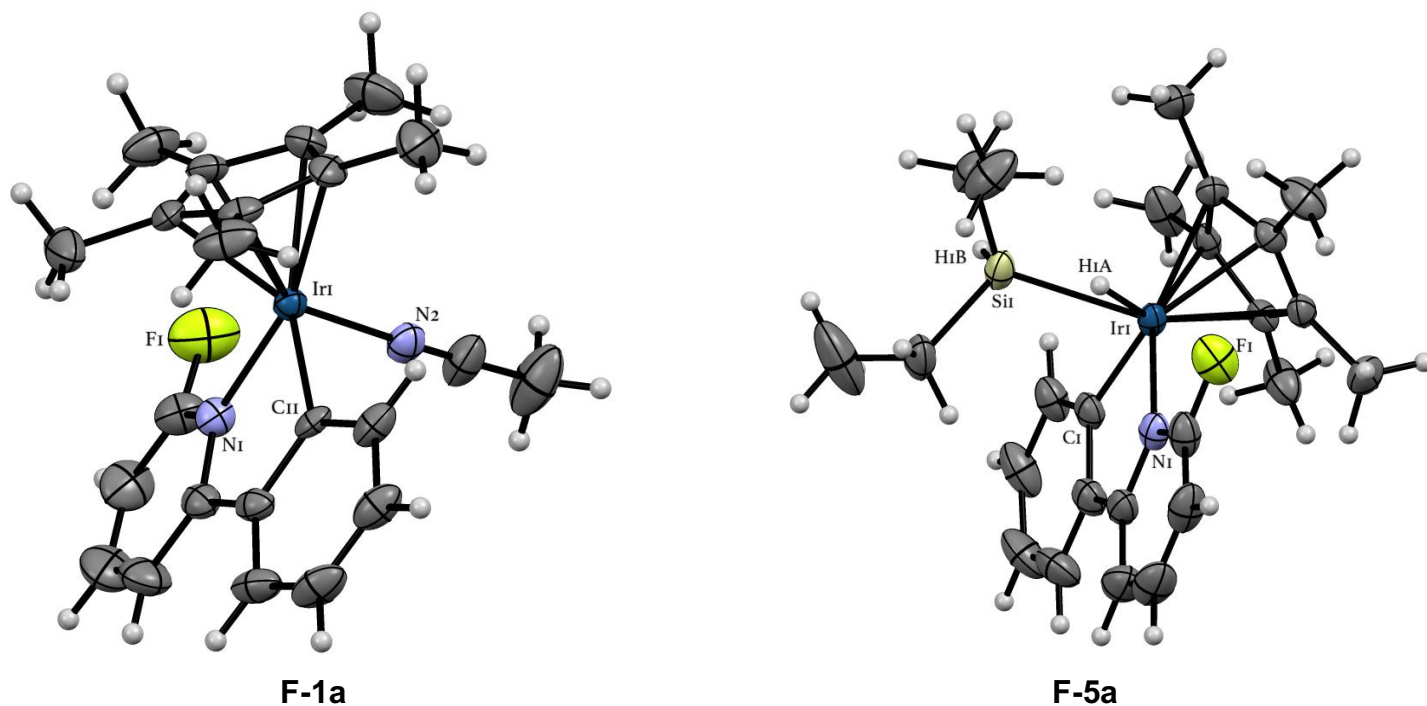
*Figure 42: ORTEP at 50% probability of the structure of **F-1a** determined by XRD analysis. The [BArF$_{24}$]⁻ anion and atoms corresponding to occupational disorder are omitted for the sake of clarity. Selected interatomic distances [Å] and angles [°] for [**F-1a**][BArF$_{24}$]: N2-Ir1 2.052(5), N1-Ir1 2.115(6), C11-Ir1 2.051(5), N1-C1-F1 115.2(6), N1-Ir1-N2 84.7(2), C11-Ir1-N1 77.4(2) ORTEP at 50% probability of the structure of **F-2a** adduct determined by XRD analysis. The [BArF$_{24}$]⁻ anion and atoms corresponding to occupational disorder are omitted for the sake of clarity. Selected interatomic distances [Å] and angles [°] for the product: Si1-Ir1 2.464(1), Si1-H1B 1.49(5), N1-Ir1 2.107(4), Ir1-H1A 1.52(4), Si1-Ir1-H1A 52(2), N1-C11-F1 115.6(4), N1-Ir1-Si1 105.2(1), N1-Ir1-H1A 80(2)*

Product	Interatomic distances (Å)		
	Ir-H	Ir-Si	Si-H(Ir)
[2c][BArF$_{24}$]	1.81(9)	2.407(2)	2.239(8)
[2e][BArF$_{24}$]	1.48(3)	2.4220(7)	1.986(7)
[2f][BArF$_{24}$]	1.52(6)	2.455(2)	2.066(6)
[2g][BArF$_{24}$]	1.449(7)	2.435(1)	1.523(7)
[2h][BArF$_{24}$][17]	1.47	2.5008(8)	2.10
[F-5a] [BArF$_{24}$]	1.52(4)	2.464(1)	1.950(5)

*Table 9: Interatomic distances (Å) of all **1b**-adduct, **1a**-triethylsilane [**2h**][BArF$_{24}$] adduct and [**F-5a**]$^+$ adduct*

Distinctions in term of interatomic distances of Ir-H, Ir-Si and Si-H(Ir) among [**F-5a**]$^+$ [**2h**]$^+$ and [**2f**]$^+$ are not substantial especially with Ir-Si bond while Ir-H bond of [**2f**]$^+$ and [**F-5a**]$^+$ are of the same length. Hence, it appears that the fluorination did not affect that much on Ir-H, Ir-Si and Si-H(Ir) bonds of those complexes. Although changes in such mentioned bonds are not visible, it will be inattentive if concluding that the fluorination was deviated from the original idea that it will ameliorate catalytic reactivity of intermediates. Because in this case only molecules possessing similar structures with [**F-5a**] were examined, characters of other of adducts of F-**1a** remain unknown, no mention this is a simple bond length comparison without regarding the participation of fluorine substitute in catalytic reaction mechanism.

5. 2. *Comparative piezometric study of hydrosilylation catalysts*

5.2.1. Introduction

In continuation with work initiated in 2016-2017[17, 18], this research consists of the evaluation of various catalytic reactivity and potential hydrosilylation catalysts based on their ability to promote a dehydro-O-silylation reaction of alcohols by a silane (Eq 38.). This reaction is capable of producing gaseous dihydrogen which, once the saturation has reached in the liquid phase, will be released into the gas phase. This property is pivotal to profile the indirect kinetic data by measuring the quantities of unleashed gas and to determine the initial speed of the reaction, which is considered as a characteristic of the catalysts. These measurements applied on a variety of catalysts are justified and comparable if a mechanism of the reaction and the release of H_2 took place under a constant condition.

$$R\!-\!OH + HSiR_3 \xrightarrow{\text{Cat}} R\!-\!OSiR_3 + H_{2(g)}$$
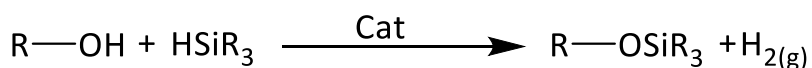
Eq. 38: Reaction of deshydro-O-silylation of catalytic alcohol

5.2.2. From metrology to catalysis

In this account, the aim was to exploit a direct method to determine the kinetics of the dehydro-O-silylation reaction of alcohols by silanes (Eq 38). Due to the insoluble gas H_2 released, there are two options to collect data: either using an operator to record volume variations counted on the isobaric and isothermal volumetric determination of the quantity of hydrogen liberated as a function of time[179] or employing isochoric and isothermal piezometric based on the measurement of pressure variation inside a closed chamber in which the reaction occurs[17]. The latter choice was justified here by the fact that, unlike volumetry, this is a technique that allows a total automation of the capture of pressure variations through a piezoelectric pressure probe of which there are relatively accurate models to translate pressure variations into potential differences that are linearly related to the measured pressure. Connected to an Analog-Logic converter, a piezoelectric pressure probe allows the measurement of relative pressure variations conducted in a few ms time resolution. However, limitations of most probe inherently stem from employed technology; the sensitivity to pressure variation at low ΔP, and the electronic latency time causing the delay between the physical variation of pressure and its effective detection by the probe. To avoid these limits, all the experiments were carried out so that the maximum pressure variation reaching

between t = 0 and t = end is lower than the upper limit of the probe (relative Pmax = 6.90 bar for a Mykrolis probe P / N A332984-007, voltage = 0.05 <P <5.05 Vcontinuous) and higher than 4 bar to reduce the error on the measurement at low pressures. According to the manufacturer specifications, the measurement error is indeed crucial at very low pressures, however, it is less than 2% of the voltage measured at 1.37 bar and less than 0.5% at 5.52 bar. The deviation of the measurement of the pressure as a function of the temperature is $\pm0.02\%$ of the voltage compared to a standard measurement at 20.0°C due to an integrated compensation device covering the temperature range of -20 °C to +60°C.

5.2.3. Catalytic hydrosilylation

The hydrosilylation of unsaturated organic compounds is essentially a reduction reaction carried out by the metallo-promoted addition of the polarized $Si(\delta^+)$-$H(\delta^-)$ bond of a hydrosilane towards a multiple bond[180]. This reaction has emerged with growing prominence as an alternative to hydrogenation and reduction reactions catalyzed by aluminum and borohydride, which pose many safety concerns in industrial facilities[181] . Although thermochemically "spontaneous", the uncatalyzed hydrosilylation reaction is kinetically discernibly slow, which requires a catalyst to lower its activation barrier[182]. Calas *et al.* have described the first hydrosilylation catalyst based on $ZnCl_2$[183]. Due to a great interest in this chemical reaction[184] [185], great efforts have been made to develop more efficient and selective catalysts. For instance, cobalt complexes for the hydrosilylation of nitrile[186], ruthenium for the hydrosilylation of carbonyl[187], gold for the hydrosilylation of urea[188], iron and nickel for the hydrosilylation of the alkene[182], and iridium-based complexes for double hydrosilylation of nitriles to amines were implemented. Alongside that path, metallacycles in figure 43 (**A1**, **A2**, **A3**) or (**1a**, **F-1a**, **1b** would be subjects for this report. The hydrosilylation reaction can be carried out under two different mechanisms in the initiation phase leading to a formation of the key catalytic species: the first type[16] is an oxidation mechanism which comprises an oxidative addition of the Si-H bond onto a metal, then followed by a conventional migration of silyl group and hydro ligands to an organic substrate; the second type[16] involves the electrophilic activation of the hydrosilane by a hydride transfer to a metal center ensuing a formation of a silylium which then can be either captured by the complex to form a donor-acceptor adduct, or by the substrate to generate a hydrosilylated product. A dehydro-O-silylation reaction studied in this work was

characteristic of electrophilic catalysts that was subjected to the second type of activation mechanism[189] as shown in scheme below.
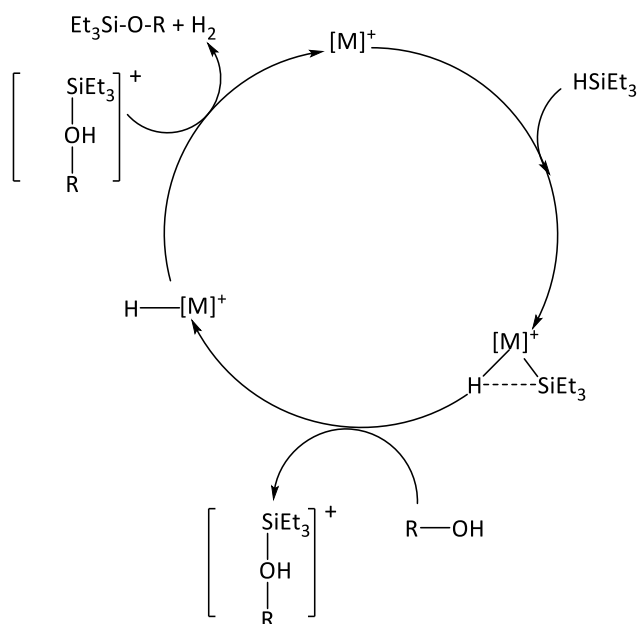
Scheme 32: proposed mechanism for the reaction of alcohol dehydro-O-silylation[17, 18].

Catalysts used in this study are composed of a cationic organometallic complex of iridium, and a counter anion which can play the least likely role on the reactivity and on the binding affinity of the complexes[190]. Accordingly, chosen counter anions must be non-coordinating and modestly reactive to avoid any potential interactions with other ions or molecules in a medium. Based on these criteria, BArF was the most favored; other non-coordinating anions like (BF_4^-, PF_6^-, ClO_4^-) have demonstrated a high effect in the targeted reactions[191, 192].

In this work, a dehydro-O-silylation reaction of benzyl alcohol, propan-2-ol and hexafluoropropan-2-ol (Figure 44) were studied in the presence of 3 iridium catalysts synthesized in the laboratory (Figure 43).

1a   **F-1a**   **1b**
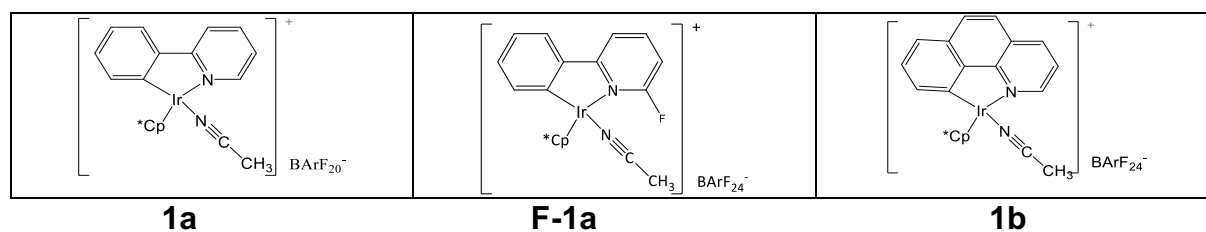
Figure 43: Structure of catalysts synthesized in our laboratory based on iridium
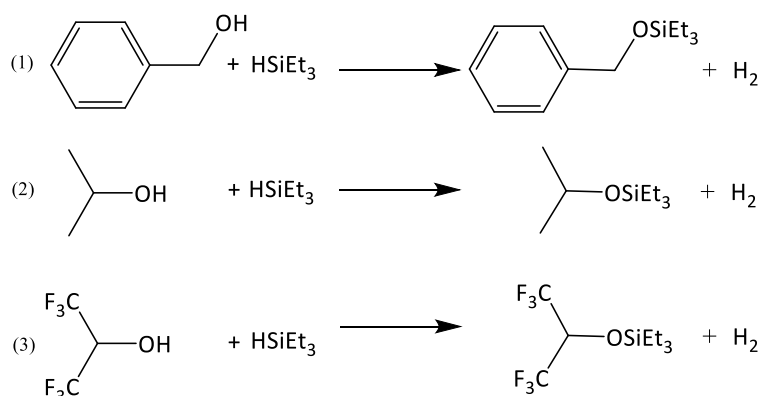
Figure 44: Reaction of alcohol dehydro-O-silylation: (1) benzyl alcohol + triethylsilane; (2) isopropanol + triethylsilane; (3) hexafluoroisopropanol + triethylsilane

A kinetic method allows a determination of not only rate constant but also other significant parameters of a reaction[193], especially, thermodynamic activation energies (enthalpies activation, activation entropy) by mean of the Eyring-Polanyi equation under standardized conditions.

Since the polarity of the reaction medium would change from a very polar medium to a non-polar medium, it is illogical to determine an absolute rate constant of a reaction. Hence, kinetic parameters were measured in the time limit as within the first 10% conversion during the reaction time. In case the initiation phase of a given catalysis is particularly long, it is necessary to readjust the calculation of the rate constants and initial rate constants.

5.2.3.1 Curves

Triethylsilane concentration was used in the kinetic equations to determine the initial rate of catalysis as well as the initial rate constant.
The pressure released by the dehydro-O-silylation enables a measure of a number of moles of the eliminated hydrogen grounded on the equation of the perfect gas PV =

nRT (P: pressure in atm; V: volume in L = 30.7×10^{-3} - volume of the solution, n: number of moles in mol, R: constant of the perfect gas = 0.008206 L.atm.mol^{-1}.K^{-1}, T: temperature in K).

From the number of moles of dihydrogen, the concentration of triethylsilane as a function of time would be established (number of moles of triethylsilane at a time t = number of initial moles - number of moles of dihydrogen released).

5.2.4. Thermodynamic calculation

The Eyring-Polanyi equation was applied to calculate the thermodynamic activation parameters of the catalysts (enthalpy, entropy and free enthalpy): **Ln(k/T) = -ΔH‡/RT + Ln(k$_B$/h) + ΔS‡/R** (with k: absolute catalyst rate constant, T: thermodynamic temperature, ΔH‡ = activation enthalpy, R = universal ideal gas constant = 1,987 cal.mol^{-1}.K^{-1}, k$_B$ = constant of Boltzmann = $1.38064852 \times 10^{-23}$J.K^{-1}; h = Planck constant = $6.62607015 \times 10^{-34}$ Js; ΔS‡ = entropy of activation) by plotting the line of ln(k / T) as a function of 1 / T the enthalpy and entropy can be deduced.

5.2.5. Comparison catalysts

The purpose of this step was to extract information about catalytic reactivity of given catalysts on dehydro-O-silylation reactions carried out under identical conditions in order to compare results.

| $A_1 = 1a$ | $A_2 = F\text{-}1a$ | $A_3 = 1b$ |
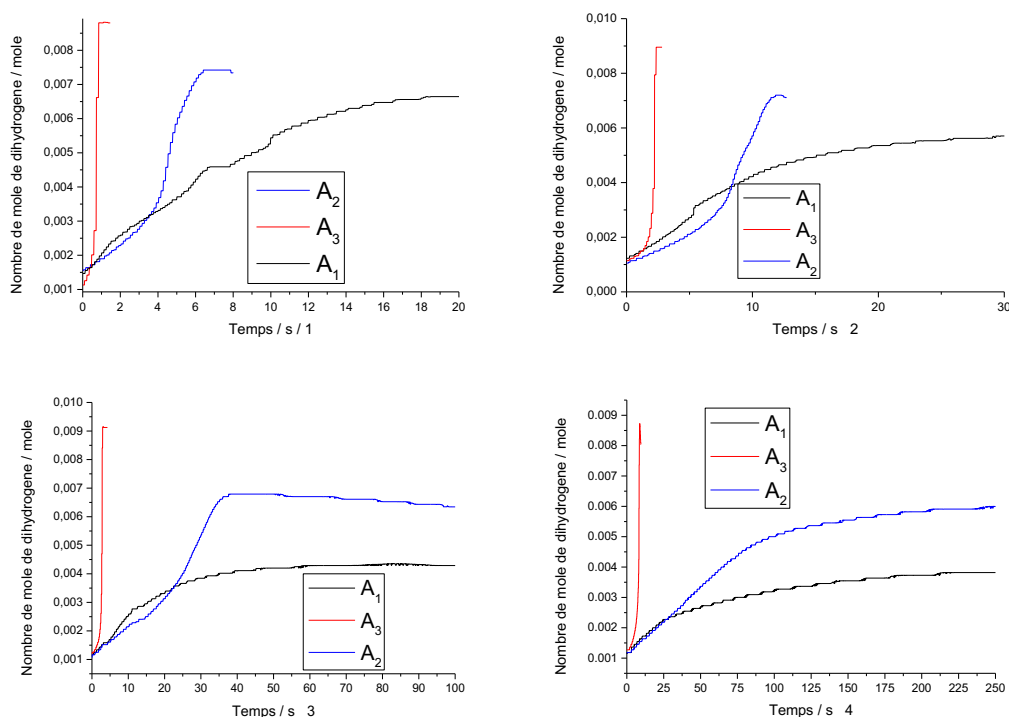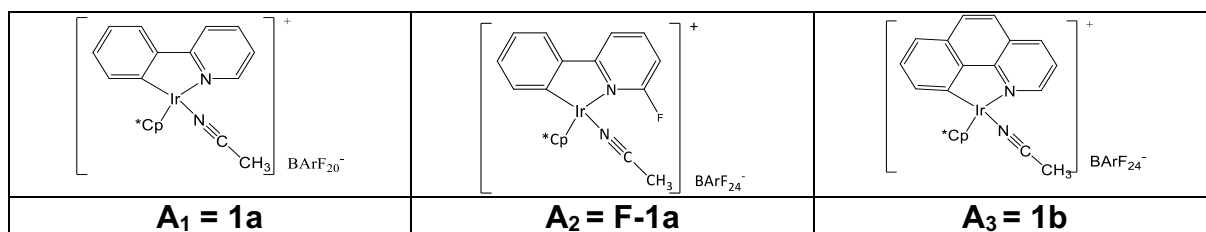
Figure 45: Curves of moles of dihydrogen as a function of time in different types of catalysts at different temperatures: (1) T = 293 K; (2) T = 288 K; (3) T = 283 K; (4) T = 278 K, [Catalyst] 0 = 2.77 × 10^{-3} mol / L.

According to figure 45, the absolute rate of the catalyst of the dehydro-O-silylation reaction (reaction of benzyl alcohol with triethylsilane) is highest in the presence of the catalyst A3.

The catalyst **1a** seems to be the least efficient catalyst. For catalyst F-**1a**, it was found that the amount of liberated dihydrogen increased slowly from the beginning, then an inflection showing an H_2 production almost as fast as with **1b**. This phenomenon suggested that the catalyst F-**1a** has an initiation step longer than the other two catalysts at room temperature.

Generally, the rate equation of a chemistry reaction is in the form of a differential equation containing the time and the concentrations of the different species presenting

in the reaction medium and the initial rate constant k[194]. Due to the aforementioned issue (changes of polarity), the constant of initial rate was calculated in the first 10% of conversion as described here:

$$v_i = k_i[A]^n[B]^m[cat]^w$$

v_i: initial rate of the reaction

k_i: initial rate constant

[A], [B], [cat]: concentrations of the compounds A, B and the catalyst

n, m and w: partial orders in A, B and the catalyst

Our work on these catalysts helped guide the research in which the equation $v_i = k'[cat]^w$ was utilized to determine the order of the reaction relative to the catalyst with v_i: initial rate of the reaction; k': apparent initial rate constant at which A and B concentration were constant; [cat]: catalyst concentration in (mol / L); w: partial order of the catalyst.

To calculate the order of the reaction, several experiments were carried out under [A], [B] as constant, and [cat] variables. After that, one can draw the line of Ln(v) plotted against Ln([Cat]) of which a slope designates an order of the reaction relative to the catalyst Ln(v) = Ln(k') + w.Ln([Cat]).

5.2.5.1. catalyst 1a:

A mixture of benzyl alcohol (0.5 mL, 5 mmol) and triethylsilane (0.8 mL, 5 mmol) was produced in a double-neck Schlenk type reactor. Catalyst **1a** was used in different concentrations at different temperatures. The absolute rate of the initial catalyst of the reaction was determined from the slope of the straight-line tangent to t_0.

Concentration (M) **T=293 K**	Time (s)	Yield (%)	Initiale rate (mol.L^{-1}.s^{-1}×10^{-4})	TON	TOF$_i$ (h^{-1})
2.77×10^{-3}	8	100	5.66	1000	4000000
1.85×10^{-3}	117	92	2.27	1439	2726526
1.38×10^{-3}	200	100	1.81	2000	2880000
2.77×10^{-4}	450	46	0.0587	4600	301090

Concentration (M) T=288 K	Time (s)	Yield (%)	Initial rate $(mol.L^{-1}.s^{-1}\times10^{-4})$	TON	TOF_i (h^{-1})
2.77×10^{-3}	15	100	2.49	1000	1800000
1.85×10^{-3}	135	82	1.08	1242	1039813
1.38×10^{-3}	153	56	0.513	1120	560000
2.77×10^{-4}	225	34	0.0245	3400	311450

Concentration (M) T=283 K	Time (s)	Yield (%)	Initial rate $(mol.L^{-1}.s^{-1}\times10^{-4})$	TON	TOF_i (h^{-1})
2.77×10^{-3}	60	84	1.28	840	1042758
1.85×10^{-3}	120	72	0.63	1090	726666
1.38×10^{-3}	220	72	0.47	1440	730140
2.77×10^{-4}	327	34	0.022	3400	298536

Concentration (M) T=278 K	Time (s)	Yield (%)	Initial rate $(mol.L^{-1}.s^{-1}\times10^{-4})$	TON	TOF_i (h^{-1})
2.77×10^{-3}	220	76	0.42	760	325714
1.85×10^{-3}	160	60	0.36	909	355695
1.38×10^{-3}	280	49	0.19	980	336000
2.77×10^{-4}	360	44	0.045	4000	431137

*Table 10: Catalytic performance of **1a** on the dehydro-O-silylation of alcohols at different temperatures.TON: number of cycles (turnover number), amount of substrate converted by the amount of catalyst used = mole of product formed / mole of catalyst.TOF$_i$: number of cycles per unit time, at a reaction time corresponding to 10% conversion.*

The number of TOF cycles represents the maximum number of molecule conversion per catalytic site, and the number of TOF cycles per unit of time, therefore the higher TOF is, the more active the catalysts are[195, 196]. In the case of catalyst **1a**, it was found that the TOF decreases following a decline of catalyst concentration.

The slope of the line of $\ln(v) = \ln(k') + w.\ln([Cat])$ is:

T(K)	293	288	283	278
Slope	1.9	1.6	1.8	1

Table 11: different slope values of the line of Ln (vi) versus ln [cat] at different temperatures.

According to table 12, the alcohol dehydro-O-silylation reaction is pseudo-second-order.

5.2.5.2. Catalyst F-1a:

A mixture of benzyl alcohol (0.5 ml, 5 mmol) and triethylsilane (0.8 ml, 5 mmol) is added in a double-neck Schlenk type reactor. Catalyst F-**1a** was injected on different concentrations at different temperatures. In this situation, an initiation step was observed in the presence of this catalyst, thus it would be kinetically studied separately from the catalysis step.

It was no longer possible to distinguish the initiation phase due to a decrease in the temperature and / or the concentration of the catalyst causing a deactivation of the catalysis

5.2.5.2.1. Calculations in the initiation stage

Concentration (M) **T=293 K**	Time (s)	Yield (%)	Initiale rate $(mol.L^{-1}.s^{-1} \times 10^{-4})$	TON	TOF_i (h^{-1})
2.77×10^{-3}	7,5	40	2.8	400	1800000
2.08×10^{-3}	10,9	32	1.974	426	639000
1.38×10^{-3}	16,6	20	0.83	400	436363
2.77×10^{-4}	225	62	0.144	6200	1395000

Concentration (M) **T=288 K**	Time (s)	Yield (%)	Initial rate (mol.L^{-1}.s^{-1}×10^{-4})	TON	TOF$_i$ (h^{-1})
2.77×10^{-3}	8	30	1.9	310	1528767
2.08×10^{-3}	22.2	32	0.68	413	874588
1.38×10^{-3}	30.6	20	0.53	760	1347783
2.77×10^{-4}	225	60	0.14	6000	900000

Concentration (M) **T=283 K**	Time (s)	Yield (%)	Initial rate (mol.L^{-1}.s^{-1}×10^{-4})	TON	TOF$_i$ (h^{-1})
2.77×10^{-3}	34.2	100	1.2	1000	1493775
2.08×10^{-3}	36.4	74	1.03	986	686576
1.38×10^{-3}	139.3	76	0.43	1520	692658
2.77×10^{-4}	370.5	37	0.076	3700	774418

Concentration (M) **T=278 K**	Time (s)	Yield (%)	Initial rate (mol.L^{-1}.s^{-1}×10^{-4})	TON	TOF$_i$ (h^{-1})
2.77×10^{-3}	109.9	100	0.42	1000	330548
2.08×10^{-3}	145.2	80	0.35	1066	423342
1.38×10^{-3}	212	62	0.17	1240	235940
2.77×10^{-4}	418.8	22	0.026	2200	414442

*Table 12: Catalytic performance of F-**1a** on the dehydro-O-silylation of alcohols at different temperatures.*

The slope of the line of $\ln(v) = \ln(k') + w.\ln([Cat])$ is:

Température (K)	293	288	283	278
Slope	1.22	1.2	1.16	1.17

Table 13: Different slope value of the line of ln v according to ln [cat] at different temperatures

5.2.5.2.2. Calculations in the catalysis step after the rate of inflection point

Concentration (M) **T=293 K**	Time (s)	Yield (%)	Initial rate $(mol.L^{-1}.s^{-1} \times 10^{-4})$	TON	TOF_i (h^{-1})
2.77×10^{-3}	3.1	60	16	600	7200000
2.08×10^{-3}	7.1	68	8.88	906	2174400
1.38×10^{-3}	14	80	2.85	1600	1152000

Concentration (M) **T=288 K**	Time (s)	Yield (%)	Initial rate $(mol.L^{-1}.s^{-1} \times 10^{-4})$	TON	TOF_i (h^{-1})
2.77×10^{-3}	5.3	70	8.1	690	4968000
2.08×10^{-3}	29.5	68	0.91	920	2365714
1.38×10^{-3}	38.8	80	0.73	1240	2029090

*Table 14: Catalytic performance of F-**1a** in the dehydro-O-silylation of alcohols at different temperatures.*

The slope of the line of $\ln(v) = \ln(k') + w.\ln([Cat])$ is:

T(K)	293	288
slope	2.5	3.2

Table 15: Different slope value of the line of ln v according to ln[cat] at different temperatures

The slope values obtained in these cases were rather different presumably since the catalytic system did not follow the same mechanism involving **1a** or F-**1a**, order of catalyst was considered approximately about 2.

5.2.5.3 Catalyst 1b:

A mixture of benzyl alcohol (0.5 ml, 5 mmol) and triethylsilane (0.8 ml, 5 mmol) is added in a double-neck Schlenk type reactor. Catalyst **1b** is injected on different concentrations at different temperatures.

Concentration (M) **T=293 K**	Time (s)	Yield (%)	Initiale rate $(mol.L^{-1}.s^{-1} \times 10^{-4})$	TON	TOF_i (h^{-1})
2.77×10^{-3}	0.74	100	16.7	1000	11612903
2.08×10^{-3}	0.77	100	20.6	1333	15480000
1.38×10^{-3}	1.4	100	6.86	2000	8000000
2.77×10^{-4}	115	74	0.425	7400	2858369

Concentration (M) **T=288 K**	Time (s)	Yield (%)	Initial rate $(mol.L^{-1}.s^{-1} \times 10^{-4})$	TON	TOF_i (h^{-1})
2.77×10^{-3}	2.4	100	7.73	1000	2278481
2.08×10^{-3}	1.6	100	127	1333	3427714
1.38×10^{-3}	1.8	100	10.4	2000	7578947
2.77×10^{-4}	250	72	0.244	7200	1620000

Concentration (M) **T=283 K**	Time (s)	Yield (%)	Initial rate $(mol.L^{-1}.s^{-1} \times 10^{-4})$	TON	TOF_i (h^{-1})
2.77×10^{-3}	2.4	100	8.81	1000	1241379
2.08×10^{-3}	1.6	100	7.01	1333	1548000
1.38×10^{-3}	1.8	100	3.42	2000	1714285
2.77×10^{-4}	250	53	0.279	5300	1526400

Concentration (M) **T=278 K**	Time (s)	Yield (%)	Initial rate $(mol.L^{-1}.s^{-1} \times 10^{-4})$	TON	TOF_i (h^{-1})
2.77×10^{-3}	2.4	100	1.38	1000	923076
2.08×10^{-3}	1.6	100	1.51	1333	1499625
1.38×10^{-3}	1.8	100	1.21	2000	1565217
2.77×10^{-4}	250	51	0.12	5100	1092857

*Table 16: Catalytic performance of **1b** in the dehydro-O-silylation of alcohols at different temperatures.*

The slope of the line of $\ln(v) = \ln(k') + w.\ln([Cat])$ is:

T(K)	293	288	283	278
Slope	1.6	2	1.5	1.1

Table 17: different slope value of the line of ln v depending on ln[cat] at different temperatures

Arcording to Table 18, the reaction of dehydro-O-silylation is of pseudo-second order. The TOFs in the presence of the catalyst **1b** were higher than in the presence of the catalysts F-**1a** and **1a**. This shows that catalyst **1b** is more effective than catalyst F-**1a** and more effective than catalyst **1a** under the same conditions.

From Tables 12 and 16 the slope of the equation ln v = ln k'+ n.ln[Cat] was close to 1 at 278 K which was clearly different from those of other temperatures. Hence, the limitation of this method was evident at this instance.

Because of time limitation, the reaction order of triethylsilane could not be determined, for which one could apply the kinetic equation of first order ln [A] = - k't + ln [A] 0 and second order 1/ [A] = 1/[A_0] + kt to determine the rate constant where [A] is the concentration of the reagent at a time t; [A_0] is the concentration of the initial reagent; k': is the apparent speed constant; t is the time.

5.2.5.4. **Determination of the rate constant of a reaction (1):**

The rate constant is indispensable to understand a chemical reaction. To calculate that, the kinetic equation corresponding to the order must be exercised.

5.2.5.4.1 Catalyst **1a**:

Temperature (K) Ordre 1	[Catalyst] (mmol/L)	2.77	1.851	1.388	0.277
293 K	$k\ (s^{-1})$	0.1909	0.0657	0.0447	0.0046
288 K	$k\ (s^{-1})$	0.0783	0.0293	0.0166	0.0075
283 K	$k\ (s^{-1})$	0.0353	0.0192	0.0173	0.0021
278 K	$k\ (s^{-1})$	0.0176	0.0095	0.0062	0.0024
273 K	$k\ (s^{-1})$	0.0082	0.0055	0.0119	0.0012

*Table 18 : Rate constants (1) of catalyst **1a** at different concentration and different temperatures.*

Temperature (K) Ordre 2	[Catalyst] (mmol/L)	2.77	1.851	1.388	0.277
293 K	$k\ (L.mol^{-1}.s^{-1})$	0.1012	0.0332	0.0225	0.0022
288 K	$k\ (L.mol^{-1}.s^{-1})$	0.0417	0.0145	0.0082	0.0036
283 K	$k\ (L.mol^{-1}.s^{-1})$	0.0173	0.0097	0.0084	0.0013
278 K	$k\ (L.mol^{-1}.s^{-1})$	0.0087	0.0046	0.0031	0.0011

*Table 19: Table of reaction rate constants (1) of **1a** at different temperatures.*

5.2.5.4.2. Catalyst F-1a

Temperature (K) Ordre 1	[Catalyst] (mmol/L)	2.77	2.083	1.388	0.277
293 K	k (s^{-1})	0.33	0.08	0.063	0.00414
288 K	k (s^{-1})	0.08	0.034	0.052	0.00424
283 K	k (s^{-1})	0.07	0.03	0.024	0.00292
278 K	k (s^{-1})	0.016	0.013	0.007	0.00064

Table 20: Table of reaction rate constants (1) of catalyst A2 at different concentration and different temperatures.

Temperature (K) Ordre 2	[Catalyst] (mmol/L)	2.77	2.083	1.388	0.277
293 K	k (L.mol $^{-1}$.s^{-1})	0.1884	0.1766	0.1649	0.0024
288 K	k (L.mol $^{-1}$.s^{-1})	0.1755	0.0542	0.0685	0.0026
283 K	k (L.mol $^{-1}$.s^{-1})	0.1086	0.0538	0.0324	0.0011
278 K	k (L.mol $^{-1}$.s^{-1})	0.0255	0.0166	0.0072	0.0004

Table 21: Table of reaction rate constants (1) of F-1a at different temperatures.

5.2.5.4.3. Catalyst 1b

Temperature (K) Ordre 1	[Catalyst] (mmol/L)	2.77	2.083	1.388	2.773
293 K	k (s^{-1})	0.5032	0.1126	1.13063	0.0132
288 K	k (s^{-1})	0.0811	0.0362	0.3915	0.0087
283 K	k (s^{-1})	0.0644	0.0735	0.0415	0.0071
278 K	k (s^{-1})	0.0447	0.0554	0.0313	0.0053

Table 22: Table of reaction rate constants (1) of catalyst 1b at different concentration and different temperatures.

Temperature (K) Ordre 2	[Catalyst] (mmol/L)	2,77	2,083	1,388	0,277
293 K	k (L.mol $^{-1}$.s^{-1})	0.2661	0.0536	0.7262	0.0065
288 K	k (L.mol $^{-1}$.s^{-1})	0.0376	0.019	0.2404	0.0043
283 K	k (L.mol $^{-1}$.s^{-1})	0.0284	0.0374	0.0207	0.0034
278 K	k (L.mol $^{-1}$.s^{-1})	0.0236	0.0283	0.0161	0.0026

Table 23: Table of reaction rate constants (1) of 1b at different temperatures.

According to Tables 19, 20 and 21, the values of the rate constants, at different temperatures, for the catalyst **1a** are smaller than that of catalyst F-**1a**, and even smaller than that of the catalyst **1b**. These values ratify our hypothesis that the catalyst A3 is more efficient than the catalyst F-**1a** and more effective than the catalyst **1a**.

5.2.5.5. Determination of the thermodynamic activation parameters of the reaction (1)

The thermodynamic activation energies (enthalpy and entropy) are specific and characteristic for every chemical system. Based on this information, a determination of a free enthalpy of a reaction can be carried out, which represents needed energy to overcome the highest activation barrier in the kinetically limiting step. As a result, an efficiency of different catalysts can be compared according to free enthalpy. Values of the rate constant were leveraged to specify a thermodynamic activation parameter extracted from the Eyring-Polanyi equation:

$$\textbf{(Ln(k/T) = -\Delta H^{\ddagger}/RT + Ln(k_B/h) + \Delta S^{\ddagger}/R).}$$

5.2.5.5.1 Catalyst 1a

$[Catalyst]_0$ (mol/L)	2.77×10^{-3}	1.851×10^{-3}	1.388×10^{-3}	2.77×10^{-4}
$\Delta H^{\ddagger}$ (kcal.mol^{-1})	24.3 ± 0,8	18.7 ± 1.0	10.8 ± 5.0	11.6 ± 4.3
$\Delta S^{\ddagger}$ (cal.mol^{-1}.K^{-1})	20.8 ± 2,8	-0.23 ± 3.6	-28.3 ± 17.8	-29.0 ± 15.3
$\Delta G^{\ddagger}$ (kcal.mol^{-1})	18.2 ± 0,02	18.8 ± 0.6	19.0 ± 0.21	20.1 ± 0.2

Table 24: Different values of the thermodynamic constants as a function of the concentration of the catalyst 1a according to the order of kinetic equation is 1

$[Catalyst]_0$ (mol/L)	2.77×10^{-3}	1.85×10^{-3}	1.39×10^{-3}	$2,77 \times 10^{-4}$
$\Delta H^{\ddagger}$ (kcal.mol^{-1})	26.5 ± 0.8	20.3 ± 1.8	15.2 ± 15	10.5 ± 7.6
$\Delta S^{\ddagger}$ (cal.mol^{-1}.K^{-1})	27.5 ± 2.9	3.9 ± 6.3	-20.1 ± 52.8	-34.1 ± 40.9
$\Delta G^{\ddagger}$ (kcal.mol^{-1})	18.4 ± 0.05	19.1 ± 0.05	21.1 ± 0.4	20.5 ± 4.4

*Table 25 : Different values of the thermodynamic constants as a function of the concentration of the catalyst **1a** according to the order of kinetic equation is 2*

5.2.5.5.2 Catalyst F-1a

[Catalyst]$_0$ (mol/L)	2.77×10^{-3}	2.083×10^{-3}	1.388×10^{-3}	2.77×10^{-4}
$\Delta H^{\ddagger}$ (kcal.mol^{-1})	23.4 ± 1.2	14.8 ± 3.4	15.9 ± 2.6	19.1 ± 7.2
$\Delta S^{\ddagger}$ (cal.mol^{-1}.K^{-1})	17.6 ± 4.2	-14.2 ± 12.1	-11.2 ± 9.1	-3.6 ± 5.5
$\Delta G^{\ddagger}$ (kcal.mol^{-1})	18.2 ± 0.07	18.9 ± 0.2	19.2 ± 0.06	20.1 ± 5.5

Table 26: Different values of the thermodynamic constants as a function of the concentration of the catalyst F-1a according to the order of kinetic equation is 1

[Catalyst]$_0$ (mol/L)	2.77×10^{-3}	2.083×10^{-3}	1.388×10^{-3}	2.77×10^{-4}
$\Delta H^{\ddagger}$ (kcal.mol^{-1})	20.8 ± 7.3	22.9 ± 5.4	33 ± 3.8	20 ± 6.0
$\Delta S^{\ddagger}$ (cal.mol^{-1}.K^{-1})	9.99 ± 15.7	16 ± 19.1	50.7 ± 13.5	-1.4 ± 21
$\Delta G^{\ddagger}$ (kcal.mol^{-1})	17.8 ± 2.7	18.2 ± 0.2	18.1 ± 0.1	20.4 ± 7.9

Table 27: Different values of the thermodynamic constants as a function of the concentration of the catalyst F-1a according to the order of kinetic equation is 2

5.2.5.5.3 Catalyst 1b:

[Catalyst]$_0$ (mol/L)	2.77×10^{-3}	2.083×10^{-3}	1.388×10^{-3}	2.77×10^{-4}
$\Delta H^{\ddagger}$ (kcal.mol^{-1})	23.5 ± 8.7	3.9 ± 7.8	41.5 ± 8.4	8.9 ± 1.0
$\Delta S^{\ddagger}$ (cal.mol^{-1}.K^{-1})	19.45 ± 30.4	-50.1 ± 27.5	83.3 ± 29.5	-36.7 ± 3.5
$\Delta G^{\ddagger}$ (Kcal.mol^{-1})	17.8 ± 0.2	18.6 ± 0.2	17.09 ± 0.2	19.6 ± 0.02

Table 28: Different values of the thermodynamic constants as a function of the concentration of the catalyst 1b according to the order of kinetic equation is 1

[Catalyst]$_0$ (mol/L)	2.77×10^{-3}	2.083×10^{-3}	1.388×10^{-3}	2.77×10^{-4}
$\Delta H^{\ddagger}$ (kcal.mol^{-1})	24.4 ± 9.9	1.7 ± 0.5	45.3 ± 9.4	9.3 ± 0,9
$\Delta S^{\ddagger}$ (cal.mol^{-1}.K^{-1})	21.1 ± 34.9	-58.6 ± 2.1	95.5 ± 33	-36.9 ± 3.2
$\Delta G^{\ddagger}$ (kcal.mol^{-1})	18.2 ± 0.3	18.9 ± 0.05	17.3 ± 0.2	20.1 ± 0.04

*Table 29: Different values of the thermodynamic constants as a function of the concentration of the catalyst **1b** according to the order of kinetic equation is 2*

The values of free enthalpy showed that by applying the second order kinetic equation, a presence of the catalyst **1a** caused reactions needing more energy to form products, which validates our hypothesis that **1a** is the least efficient. As for catalysts F-**1a** and **1b**, these free enthalpy values are overlapping. Activation entropy values were compromised by grave errors attributable to an extremely limited temperature range and an insufficient number of measurements. The same type of error on the entropy of activation can be committed as well if kinetic measurements are carried out by NMR within a severely limited range of temperatures. Inadequately spaced measurements also contributed to systematic errors resulted from a limited estimation of the pressure sensor, which is less precise at very low dynamic pressure variations.

5.2.5.6. Determination of the rate constant and the thermodynamic activation energy of the (2) dehydro-O-silylation reaction of isopropanol

A mixture of isopropanol (0.4 ml, 5 mmol) and triethylsilane (0.8 ml, 5 mmol) is added in a double-walled Schlenk type reactor. The catalyst is injected at different temperatures.

5.2.5.6.1. Catalyst 1a:

T (K)	Time (s)	Yield (%)	Initial rate $(mol.L^{-1}.s^{-1}\times10^{-6})$	TON	TOFi (h^{-1})	k Ordre 1 $(L.mol^{-1}.s^{-1})$	k Ordre 2 $(L.mol^{-1}.s^{-1})$
293	928	41	9.5	410	79783	0.0031	0.0014
288	929	29	6.07	290	65950	0.0014	0.0007
283	853	23	1.96	230	26095	0.0005	0.0003
278	723	12	0.61	120	15542	0.0001	0.0001

Table 30: Catalytic performance of **1a** in the dehydro-O-silylation of Isopropanol at different temperatures $[Catalyst]_0$ = 2.77 × 10^{-3} mol / L.

$[Catalyst]_0$ (mol/L)	$\Delta H^{\ddagger}$ $(kcal.mol^{-1})$	$\Delta S^{\ddagger}$ $(cal.mol^{-1}.K^{-1})$	$\Delta G^{\ddagger}$ $(kcal.mol^{-1})$
2.77×10^{-3}(Ordre 1)	36.9±4.3	56.3±15.1	20.4±0.1
2.77×10^{-3}(Ordre 2)	27.7±1.7	23.2 ± 6.2	20.1 ± 0.1

Table 31: Values of thermodynamic Constants in the presence of catalyst **1a** $[Catalyst]_0$ = 2.77 × 10^{-3} mol / L.

5.2.5.6.2. Catalyst 1b

T (K)	Time (s)	Yield (%)	Initial rate $(mol.L^{-1}.s^{-1}\times10^{-5})$	TON	TOFi (h^{-1})	k Ordre 1 $(L.mol^{-1}.s^{-1})$	k Ordre 2 $(L.mol^{-1}.s^{-1})$
298	390	80	2.25	800	128000	0.0059	0.0029
293	689	63	1.03	630	100800	0.0034	0.0016
288	745	31	0.512	310	65516	0.0016	0.0008
283	831	26	0.478	260	39945	0.0011	0.0005

Table 32: Catalytic performance of **1b** in the dehydro-O-silylation of Isopropanol at different temperatures $[Catalyst]_0$ = 2.77 × 10^{-3} mol / L.

$[Catalyst]_0$ (mol/L)	$\Delta H^{\ddagger}$ $(kcal.mol^{-1})$	$\Delta S^{\ddagger}$ $(cal.mol^{-1}.K^{-1})$	$\Delta G^{\ddagger}$ $(kcal.mol^{-1})$
2.77×10^{-3}(Ordre 1)	18.6±1.6	-6.4±5.5	20.5±0,01
2.77×10^{-3}(Ordre 2)	19.3±1.1	-5.2 ± 3.8	20.8± 0,01

Table 33: Values of thermodynamic constants in the presence of Catalyst **1b** $[Catalyst]_0$ = 2.77 × 10^{-3} mol / L.

T (K)	Time (s)	Yield (%)	Initial rate $(mol.L^{-1}.s^{-1} \times 10^{-4})$	TON	TOFi (h^{-1})	k Ordre 1 $(L.mol^{-1}.s^{-1})$	k Ordre 2 $(L.mol^{-1}.s^{-1})$
298	19	100	1.18	285	256500	0.0369	0.0195
293	101	94	0.828	268	178666	0.0204	0.0105
288	332	61	0.533	173	47907	0.0082	0.0041
283	379	52	0.189	148	21307	0.0063	0.0029

*Table 34: Catalytic performance of **1b** in the dehydro-O-silylation of isopropanol at different temperatures [Catalyst]$_0$ = 9.69 × 10^{-3} mol / L.*

[Catalyst]$_0$ (mol/L)	$\Delta H^{\ddagger}$ (kcal.mol^{-1})	$\Delta S^{\ddagger}$ (cal.mol^{-1}.K^{-1})	$\Delta G^{\ddagger}$ (kcal.mol^{-1})
9,69×10^{-3}(Ordre 1)	20.7±2.7	4.3±0.9	19.4±2.4
9,69×10^{-3}(Ordre 2)	21.7±2.9	6.3 ± 9.9	19.8

*Table 35: Values of thermodynamic constants in the presence of Catalyst **1b** [Catalyst]$_0$ = 9.69 × 10^{-3} mol / L.*

Comparing values of rate constants and thermodynamic energies stemming from the dehydro-O-silylation of isopropanol and benzyl alcohol with triethylsilane shows that the aromatic ring resonance effect was in favor of reaction (1), which also played a part in in stabilizing intermediate compounds and gave rise to a higher Bronsted acidity of benzyl alcohol (pKa = 15.4) than isopropanol (pKa = 16.5).

5.2.5.7. Determination of the rate constant and the thermodynamic coefficients of the reaction (3)

A mixture of hexafluoroisopropanol (0.6 ml, 5 mmol) and triethylsilane (0.8 ml, 5 mmol) were added in a double-neck Schlenk type reactor and the same amount of the catalyst A3 was injected at different temperatures.

Temperature (K)	Time (s)	Yield (%)	Initial rate $(mol.L^{-1}.s^{-1} \times 10^{-6})$	TON	TOFi (h^{-1})	k Ordre 1 $(L.mol^{-1}.s^{-1})$	k Ordre 2 $(L.mol^{-1}.s^{-1})$
298	902	26	1.85	74	20227	0.0005	0.0002
293	885	16	0.536	45.6	8710	0.0002	0.00013
288	722	11	0.099	31	5145	0.0003	0.00018
283	724	10	0.82	28.5	4104	0.0005	0.00026

*Table 36: Catalytic performance of **1b** in the dehydro-O-silylation of Hexafluoroisopropanol at different temperatures [Catalyst]$_0$ = 9.69 × 10^{-3} mol / L.*

Kinetic measurements showed, in this case, H_2 production, rate constants, TON, TOFi are relatively lower than those of isopropanol. Consequently, the plot Eyring's equation was liberally scattered and not linearly correlated as expected because values would have been tainted by errors.

This result is particularly interesting because it indicates that although pKa of hexafluorinated alcohol is 9.2[197], thermodynamically stronger than both isopropanol and benzyl alcohol, nevertheless, it seemed to possess a lower kinetic acidity under the conditions in which one of the key steps is the deprotonation of the intermediate $[RF-O(H)-SiEt_3]^+$ by a hydro-iridium [species]phpyCp*Ir-H acting as an iridium hydride[(III).]

5.2.5.8. Conclusion

By studying a wide range of known compounds as well as recently synthesized compounds in our laboratory, it was proven that the piezometric method developed during this research allows a determination of characteristics of a catalytic reaction such as TON, TOFi, and more broadly certain extent of activation energies. This also foster establishing of a silanes electrophilic activation mechanism and optimizing catalytic quality.

This study demonstrated that the catalyst **1a** has a similar catalytic activity to **1b**. Nevertheless, the induction period was longer, indicating its activation triggered by the departure of acetonitrile was kinetic lock which did not exist in the **1a** and **1b** cases.

In addition, the dehydro-O-silylation of isopropanol, hexafluoroisopropanol, and benzyl alcohol, is less dependent on the thermodynamic acidity than on its kinetic acidity of alcohol during the key step of deprotonating an intermediate $[RF-O(H)-SiEt_3]^+$ by a hydro-iridium species [phpy] Cp*Ir-H serving as an iridium hydride (III).

PERSPECTIVES

Although a wide range of iridacyclic silylene complexes were isolated and fully characterized, preparative synthesis of those compounds is still a lingering hurdle due to their inherently high reactivity. Using silanes with bulky aromatic substituents affecting considerably on Ir-Si bond and stability of a whole system through conjugation system on the silicon atom could provide a solution.

Transfer divalent silicon species and further utilize those in organic synthesis are worthy being exerted more effort especially applications of silylene transfer in organic chemistry remain sparse.

The scope of this research can be expanded to other transition metals for example, Cobalt, Ruthenium, Rhodium associated with diversifying ligands.

Preliminary result on fluorinated Iridacycle complexes is very promising in term of both synthesis and catalyst. Further attempt will be made to replicate a fruitful result of **1b** and hopefully facile isolation and preparative synthesis will be achievable in this case. Relied on this result, more fluorinated ligand should be made and leveraged not only with Iridium but also Cobalt, Ruthenium, Rhodium.

Bringing variety to stabilizing silicon ligand and trapping free silylene species will be also targeted.

References

1.   Binh, D. H.; Milovanović, M.; Puertes-Mico, J.; Hamdaoui, M.; Zarić, S. D.; Djukic, J.-P., Is the R3Si Moiety in Metal–Silyl Complexes a Z ligand? An Answer from the Interaction Energy. *Chem.: Eur. J* **2017,** *23* (67), 17058-17069.

2.   Lewis, G. N., THE ATOM AND THE MOLECULE. *J. Am. Chem. Soc.* **1916,** *38* (4), 762-785.

3.   Werlé, C.; Hamdaoui, M.; Bailly, C.; Le Goff, X.-F.; Brelot, L.; Djukic, J.-P., Electron-Deficient η1-Indenyl,η3-allylpalladium(II) Complexes Stabilized by Fluxional Non-covalent Interactions. *J. Am. Chem. Soc.* **2013,** *135* (5), 1715-1718.

4.   Werlé, C.; Karmazin, L.; Bailly, C.; Ricard, L.; Djukic, J.-P., Stabilization of an Electron-Unsaturated Pd(I)–Pd(I) Unit by Double Hemichelation. *Organometallics* **2015,** *34* (12), 3055-3064.

5.   Werlé, C.; Bailly, C.; Karmazin-Brelot, L.; Le Goff, X.-F.; Pfeffer, M.; Djukic, J.-P., First Stabilization of 14-Electron Rhodium(I) Complexes by Hemichelation. *Angew. Chem. Int. Ed.* **2014,** *53* (37), 9827-9831.

6.   Jiang, F.; Biradha, K.; Leong, W. K.; Pomeroy, R. K.; Zaworotko, M. J., Dicarbonylcyclopentadienyliridium, (η-C5H5)Ir(CO)2, as a ligand. *Can. J. Chem.* **1999,** *77* (8), 1327-1335.

7.   Einstein, F. W. B.; Pomeroy, R. K.; Rushman, P.; Willis, A. C., Preparation and crystal structure of (OC)5OsOs(CO)3(GeCl3)(Cl): a compound with an unsupported, donor–acceptor metal–metal bond. *J. Chem. Soc., Chem. Commun.* **1983,** (15), 854-855.

8.   Fleming, M. M.; Pomeroy, R. K.; Rushman, P., Dissociation and isomerization of (OC)5OsRu(CO)3(SiCl3)(Br), a compound with an osmium—ruthenium donor—acceptor bond. *J. Organomet. Chem.* **1984,** *273* (2), C33-C38.

9.   Einstein, F. W. B.; Pomeroy, R. K.; Rushman, P.; Willis, A. C., Synthesis, structure and fluxional properties of (.eta.5-C5Me5)(OC)2IrW(CO)5. A compound with an iridium-tungsten dative bond. *Organometallics* **1985,** *4* (2), 250-255.

10.   Einstein, F. W. B.; Martin, L. R.; Pomeroy, R. K.; Rushman, P., A cluster compound with an unsupported, dative metal–metal bond: structure and unusual nonrigidity of (Me3P)(OC)4OsOs3(CO)11. *J. Chem. Soc., Chem. Commun.* **1985,** (6), 345-346.

11.   Einstein, F. W. B.; Jennings, M. C.; Krentz, R.; Pomeroy, R. K.; Rushman, P.; Willis, A. C., Comparison of dative and covalent metal-metal bonds: structures of the isomers (Me3P)(OC)4OsRe(CO)4(Br) and (Br)(Me3P)(OC)3OsRe(CO)5. *Inorg. Chem.* **1987,** *26* (8), 1341-1344.

12.   Johnston, V. J.; Einstein, F. W. B.; Pomeroy, R. K., Structures of the new binary metal carbonyl Os4(CO)15 and (.eta.5-C5Me5)(OC)IrOs3(CO)11. Clusters with three-center-two-electron metal-metal bonds? *J. Am. Chem. Soc.* **1987,** *109* (23), 7220-7222.

13.   Davis, H. B.; Einstein, F. W. B.; Glavina, P. G.; Jones, T.; Pomeroy, R. K.; Rushman, P., Complexes with unbridged dative bonds between osmium and a Group 6 element. Structures of (Me3P)(OC)4OsM(CO)5 (M = chromium, tungsten). *Organometallics* **1989,** *8* (4), 1030-1039.

14.   Fernandez, M. J.; Bailey, P. M.; Bentz, P. O.; Ricci, J. S.; Koetzle, T. F.; Maitlis, P. M., Synthesis, x-ray, and low-temperature neutron-diffraction study of a rhodium(V) complex: dihydridobis(triethylsilyl)(pentamethylcyclopentadienyl)rhodium. *J. Am. Chem. Soc.* **1984,** *106* (19), 5458-5463.

15.   Ricc, J. S.; Koetzle, T. F.; Fernandez, M.-J.; Maitlis, P. M.; Green, J. C., Dihydridobis(triethylsilyl)pentamethylcyclopentadienyliridium(V):Neutron diffraction and photoelectron spectroscopic studies. *J. Organomet. Chem.* **1986,** *299* (3), 383-389.

16.   Binh, D. H.; Milovanović, M.; Puertes-Mico, J.; Hamdaoui, M.; Zarić, S. D.; Djukic, J.-P., Is the R3Si Moiety in Metal–Silyl Complexes a Z ligand? An Answer from the Interaction Energy. *Chem.: Eur. J* **2017,** *23* (67), 17058-17069.

17.   Hamdaoui, M.; Ney, M.; Sarda, V.; Karmazin, L.; Bailly, C.; Sieffert, N.; Dohm, S.; Hansen, A.; Grimme, S.; Djukic, J.-P., Evidence of a Donor–Acceptor (Ir–H)→SiR3 Interaction in a Trapped Ir(III) Silane Catalytic Intermediate. *Organometallics* **2016,** *35* (13), 2207-2223.

18.   Hamdaoui, M.; Desrousseaux, C.; Habbita, H.; Djukic, J.-P., Iridacycles as Catalysts for the Autotandem Conversion of Nitriles into Amines by Hydrosilylation: Experimental Investigation and Scope. *Organometallics* **2017,** *36* (24), 4864-4882.

19.   Binh, D. H.; Hamdaoui, M.; Fischer-Krauser, D.; Karmazin, L.; Bailly, C.; Djukic, J.-P., Entrapment of THF-Stabilized Iridacyclic IrIII Silylenes from Double H–Si Bond Activation and H2 Elimination. *Chem.: Eur. J* **2018,** *24* (66), 17577-17589.

20.   Volpin, M. E.; Koreshkov, Y. D.; Dulova, V. G.; Kursanov, D. N., Three-membered heteroaromatic compounds—I. *Tetrahedron* **1962,** *18* (1), 107-122.

21.   West, R.; Bailey, R. E., The Nature of "Silirene" Compounds. *J. Am. Chem. Soc.* **1963,** *85* (18), 2871-2872.

22.   Johnson, F.; Gohlke, R. S.; Nasutavicus, W. A., The structure of "siliriness" and "germireness". *J. Organomet. Chem.* **1965,** *3* (3), 233-244.

23.   Conlin, R. T.; Gaspar, P. P., Tetramethylsilacyclopropene. *J. Am. Chem. Soc.* **1976,** *98* (12), 3715-3716.

24.   Yamamoto, K.; Okinoshima, H.; Kumada, M., Evidence for "silylenoid" species in disproportionation of pentamethyldisilane catalyzed by trans-[PtCl2 (Et3P)2]. *J. Organomet. Chem.* **1971,** *27* (2), C31-C32.

25.   Atwell, W. H.; Weyenberg, D. R., Divalent Silicon Intermediates. *Angew. Chem. Int. Ed.* **1969,** *8* (7), 469-477.

26.   Atwell, W. H.; Weyenberg, D. R., Silylene chemistry. I. The thermolysis of methoxypolysilanes. *J. Am. Chem. Soc.* **1968,** *90* (13), 3438-3443.

27.   Seyferth, D.; Shannon, M. L.; Vick, S. C.; Lim, T. F. O., Silacyclopropenes. 3. Palladium-catalyzed insertion reactions. *Organometallics* **1985,** *4* (1), 57-62.

28.   Palmer, W. S.; Woerpel, K. A., Stereospecific Palladium-Catalyzed Reactions of Siliranes with Alkynes. *Organometallics* **1997,** *16* (6), 1097-1099.

29.   Yamashita, H.; Tanaka, M.; Honda, K., Oxidative Addition of the Si-C Bonds of Silacyclobutanes to Pt(PEt3)3 and Highly Selective Platinum(0)-Catalyzed Di- or Polymerization of 1,1-Dimethyl-1-silacyclobutane. *J. Am. Chem. Soc.* **1995,** *117* (34), 8873-8874.

30.   Krause, J.; Haack, K.-J.; Pörschke, K.-R.; Gabor, B.; Goddard, R.; Pluta, C.; Seevogel, K., A Palladium-Catalyzed Stannole Synthesis. *J. Am. Chem. Soc.* **1996,** *118* (4), 804-821.

31.   Tilley, T. D., *In The Silicon-Heteroatom Bond*. Wiley: New York, 1991.

32.   Milstein, D.; Stille, J. K., Mechanism of reductive elimination. Reaction of alkylpalladium(II) complexes with tetraorganotin, organolithium, and Grignard reagents. Evidence for palladium(IV) intermediacy. *J. Am. Chem. Soc.* **1979,** *101* (17), 4981-4991.

33.   Ishikawa, M.; Ohshita, J.; Ito, Y.; Iyoda, J., Silicon-carbon unsaturated compounds. 22. The formation and reactions of a nickelasilacyclobutene. *J. Am. Chem. Soc.* **1986,** *108* (23), 7417-7419.

34. Calad, S. A.; Woerpel, K. A., Formation of Chiral Quaternary Carbon Stereocenters Using Silylene Transfer Reactions: Enantioselective Synthesis of (+)-5-epi-Acetomycin. *Org. Lett.* **2007,** *9* (6), 1037-1040.

35. Ireland, R. E.; Wipf, P.; Armstrong, J. D., Stereochemical control in the ester enolate Claisen rearrangement. 1. Stereoselectivity in silyl ketene acetal formation. *J. Org. Chem.* **1991,** *56* (2), 650-657.

36. Chai, Y.; Hong, S.-p.; Lindsay, H. A.; McFarland, C.; McIntosh, M. C., New aspects of the Ireland and related Claisen rearrangements. *Tetrahedron* **2002,** *58* (15), 2905-2928.

37. Faulkner, D. J.; Petersen, M. R., A synthesis of trans-trisubstituted olefins using the claisen rearrangement. *Tetrahedron Lett.* **1969,** *10* (38), 3243-3246.

38. Howard, B. E.; Woerpel, K. A., Synthesis of Tertiary α-Hydroxy Acids by Silylene Transfer to α-Keto Esters. *Org. Lett.* **2007,** *9* (22), 4651-4653.

39. Bunte, J. O.; Cuzzupe, A. N.; Daly, A. M.; Rizzacasa, M. A., Formal Total Synthesis of (+)-Zaragozic Acid C through an Ireland–Claisen Rearrangement. *Angew. Chem. Int. Ed.* **2006,** *45* (38), 6376-6380.

40. Garry M. Coppola; Schuster, H. F., *α-Hydroxy Acids in Enantioselective Syntheses*. Wiley-VCH: Weinheim, 1997.

41. Trost, B. M.; Caldwell, C. G., The di-t-butylsilylene protecting group for diols. *Tetrahedron Lett.* **1981,** *22* (50), 4999-5002.

42. Driver, T. G.; Woerpel, K. A., Mechanism of Silver-Mediated Di-tert-butylsilylene Transfer from a Silacyclopropane to an Alkene. *J. Am. Chem. Soc.* **2004,** *126* (32), 9993-10002.

43. Heinicke, J.; Gehrhus, B., Zur chemie der silylene: Cycloadditionen von methoxymethylsilylen mit heterodienen. *J. Organomet. Chem.* **1992,** *423* (1), 13-21.

44. Blom, B.; Stoelzel, M.; Driess, M., New Vistas in N-Heterocyclic Silylene (NHSi) Transition-Metal Coordination Chemistry: Syntheses, Structures and Reactivity towards Activation of Small Molecules. *Chem.: Eur. J* **2013,** *19* (1), 40-62.

45. Ogino, H., Synthesis of Silylene and Silyl(silylene)metal Complexes. **2002,** *2* (5), 291-306.

46. Fukuda, T.; Yoshimoto, T.; Hashimoto, H.; Tobita, H., Synthesis of a Tungsten–Silylyne Complex via Stepwise Proton and Hydride Abstraction from a Hydrido Hydrosilylene Complex. *Organometallics* **2016,** *35* (7), 921-924.

47. Sakaba, H.; Oike, H.; Arai, Y.; Kwon, E., Reactions of Tungsten Acetylide–Silylene Complexes with Pyridines: Direct Observation of Silylene/Silyl Migration in Tungsten Acetylide and Carbyne/Vinylidene Frameworks. *Organometallics* **2012,** *31* (23), 8172-8177.

48. Yamamoto, K.; Okinoshima, H.; Kumada, M., Disproportionation of pentamethyldisilane and sym-tetramethyldisilane catalysed by platinum complexes. *J. Organomet. Chem.* **1970,** *23* (1), C7-C8.

49. Ojima, I.; Inaba, S.-I.; Kogure, T.; Nagai, Y., The action of tris(triphenylphosphine)chlororhodium on polyhydromonosilanes. *J. Organomet. Chem.* **1973,** *55* (1), C7-C8.

50. Schmid, G.; Welz, E., Base-Stabilized Silyleneiron Complexes. **1977,** *16* (11), 785-786.

51. Zybill, C.; Müller, G., Synthesis and Structure of [(OC)4Fe Si(OtBu)2·HMPT], a Donor-Stabilized Silanediyl ("Silylene") Complex. **1987,** *26* (7), 669-670.

52. Bodensieck, U.; Braunstein, P.; Faure, T.; Knorr, M.; Stern, C.; Deck, W., Platinum–Iron Silylene Complexes and Metal-Promoted Substituent Exchange between Si(NMe2)3 and P(OEt)3 Ligands. **1995,** *33* (23-24), 2440-2442.

53.   Kipping, F. S., Organic Derivatives of Silicon. *Proc.R.Soc.London, Ser. A* **1937,** *159*, 139-148.

54.   Braunstein, P.; Knorr, M.; Stern, C., Bimetallic silicon chemistry: New opportunities in coordination and organometallic chemistry. *Coord. Chem. Rev.* **1998,** *178-180*, 903-965.

55.   Nakatsuji, H.; Ushio, J.; Yonezawa, T., Does a silylene☐metal complex exist? *J. Organomet. Chem.* **1983,** *258* (1), C1-C4.

56.   Miller, R. D.; Michl, J., Polysilane high polymers. *Chem. Rev.* **1989,** *89* (6), 1359-1410.

57.   West, R., The polysilane high polymers. *J. Organomet. Chem.* **1986,** *300* (1), 327-346.

58.   Cundari, T. R.; Gordon, M. S., Nature of the transition metal-silicon double bond. *The Journal of Physical Chemistry* **1992,** *96* (2), 631-636.

59.   Jacobsen, H.; Ziegler, T., Trends in Structure and Bonding of Fischer Type Chromium Carbenes and Silylenes. A Density Functional Study. *Organometallics* **1995,** *14* (1), 224-230.

60.   Marquez, A.; Fernandez Sanz, J., Electronic structure of the transition-metal-carbene-like complexes (CO)5Mo-M'H2 (M' = carbon, silicon, germanium and tin). A theoretical study based on ab initio CASSCF calculations. *J. Am. Chem. Soc.* **1992,** *114* (8), 2903-2909.

61.   Ueno, K.; Tobita, H.; Ogino, H., Silicon-silicon interaction in bis(silylene)iron, disilanyliron, and bis(silyl)iron complexes. *J. Organomet. Chem.* **1992,** *430* (1), 93-104.

62.   Okazaki, M.; Tobita, H.; Ogino, H., Reactivity of silylene complexes. *Dalton Transactions* **2003,** (4), 493-506.

63.   Feldman, J. D.; Mitchell, G. P.; Nolte, J.-O.; Tilley, T. D., Isolation and Characterization of Neutral Platinum Silylene Complexes of the Type (R3P)2PtSiMes2 (Mes = 2,4,6-Trimethylphenyl). *J. Am. Chem. Soc.* **1998,** *120* (43), 11184-11185.

64.   Feldman, J. D.; Mitchell, G. P.; Nolte, J.-O.; Tilley, T. D., Synthesis and study of platinum silylene complexes of the type (R3P)2Pt=SiMes2 (Mes = 2,4,6-trimethylphenyl). *Can. J. Chem.* **2003,** *81* (11), 1127-1136.

65.   Waterman, R.; Hayes, P. G.; Tilley, T. D., Synthetic Development and Chemical Reactivity of Transition-Metal Silylene Complexes. *Acc. Chem. Res.* **2007,** *40* (8), 712-719.

66.   Denk, M.; Hayashi, R. K.; West, R., Silylene complexes from a stable silylene and metal carbonyls: synthesis and structure of [Ni{(ButN–CH☐CH–NBut)Si}2(CO)2], a donor-free bis-silylene complex. *J. Chem. Soc., Chem. Commun.* **1994,** (1), 33-34.

67.   Gehrhus, B.; Hitchcock, P. B.; Lappert, M. F.; Maciejewski, H., Silylenenickel(0) or Silyl(silylene)platinum(II) Complexes by Reaction of Si[(NCH2But)2C6H4-1,2] with [NiCl2(PPh3)2], [Ni(cod)2], or [PtCl2(PPh3)2]. *Organometallics* **1998,** *17* (26), 5599-5601.

68.   Seyferth, D.; Annarelli, D. C.; Duncan, D. P., Hexamethylsilirane. 3. Dimethylsilylene-transfer chemistry. *Organometallics* **1982,** *1* (10), 1288-1294.

69.   Berry, D. H.; Jiang, Q., Dimethylsilylene insertion into tantalum-hydride bonds. *J. Am. Chem. Soc.* **1987,** *109* (20), 6210-6212.

70.   Woo, L. K.; Smith, D. A.; Young, V. G., Synthesis, reactivity, and characterization of the first donor-stabilized silylene complexes of osmium meso-tetra-p-tolylporphyrin (TTP)Os:SiR2.cntdot.THF (R = Me, Et, iso-Pr) and the molecular structure of (TTP)Os:SiEt2.cntdot.2THF. *Organometallics* **1991,** *10* (12), 3977-3982.

71.   Chauhan, B. P. S.; Corriu, R. J. P.; Lanneau, G. F.; Priou, C.; Auner, N.; Handwerker, H.; Herdtweck, E., Lewis Base-Stabilized Transition Metal Complexes of Divalent Silicon Species. *Organometallics* **1995,** *14* (4), 1657-1666.

72.   Corriu, R. J. P.; Chauhan, B. P. S.; Lanneau, G. F., Base Stabilization of Functionalized Silylene Transition Metal Complexes. *Organometallics* **1995,** *14* (4), 1646-1656.

73.   Corriu, R. J. P.; Lanneau, G. F.; Chauhan, B. P. S., Photochemical reaction of 16-e metal species generated from Fe(CO)5, Cr(CO)6, or RCpMn(CO)3 (R = H, Me), with primary and secondary arylsilanes in the presence of internal or external electron donors: formation of functionally stabilized hydrosilanediyl-transition metal complexes. *Organometallics* **1993,** *12* (6), 2001-2003.

74.   Feldman, J. D.; Peters, J. C.; Tilley, T. D., Activations of Silanes with [PhB(CH2PPh2)3]Ir(H)(η3-C8H13). Formation of Iridium Silylene Complexes via the Extrusion of Silylenes from Secondary Silanes R2SiH2. *Organometallics* **2002,** *21* (20), 4065-4075.

75.   Glaser, P. B.; Tilley, T. D., Synthesis and Reactivity of Silyl and Silylene Ligands in the Coordination Sphere of the 14-Electron Fragment Cp*(iPr3P)Os+. *Organometallics* **2004,** *23* (24), 5799-5812.

76.   Peters, J. C.; Feldman, J. D.; Tilley, T. D., Silylene Extrusion from a Silane: Direct Conversion of Mes2SiH2 to an Iridium Silylene Dihydride. *J. Am. Chem. Soc.* **1999,** *121* (42), 9871-9872.

77.   Straus, D. A.; Tilley, T. D.; Rheingold, A. L.; Geib, S. J., Preparation, characterization, and x-ray crystal structure of an acetonitrile-complexed ruthenium silylene. *J. Am. Chem. Soc.* **1987,** *109* (19), 5872-5873.

78.   Mork, B. V.; Tilley, T. D., Multiple Bonding Between Silicon and Molybdenum: A Transition-Metal Complex with Considerable Silylyne Character. **2003,** *42* (3), 357-360.

79.   Fasulo, M. E.; Lipke, M. C.; Tilley, T. D., Structural and mechanistic investigation of a cationic hydrogen-substituted ruthenium silylene catalyst for alkene hydrosilation. *Chemical Science* **2013,** *4* (10), 3882-3887.

80.   Lipke, M. C.; Liberman-Martin, A. L.; Tilley, T. D., Electrophilic Activation of Silicon–Hydrogen Bonds in Catalytic Hydrosilations. **2017,** *56* (9), 2260-2294.

81.   Kobayashi, H.; Ueno, K.; Ogino, H., Synthesis and Structure of the Cationic External Donor-Stabilized Silyleneiron Complex [Cp(OC)2Fe=Si(p-Tol)2·HMPA]PF6 by Hydride Abstraction from a (Hydrosilyl)iron Complex. *Chem. Lett.* **1999,** *28* (3), 239-340.

82.   Thomas, C. M.; Peters, J. C., An η3-H2SiR2 Adduct of [{PhB(CH2PiPr2)3}FeIIH]. *Angew. Chem. Int. Ed.* **2006,** *45* (5), 776-780.

83.   Betley, T. A.; Peters, J. C., A Tetrahedrally Coordinated L3Fe−Nx Platform that Accommodates Terminal Nitride (FeIV≡N) and Dinitrogen (FeI−N2−FeI) Ligands. *J. Am. Chem. Soc.* **2004,** *126* (20), 6252-6254.

84.   Betley, T. A.; Peters, J. C., Dinitrogen Chemistry from Trigonally Coordinated Iron and Cobalt Platforms. *J. Am. Chem. Soc.* **2003,** *125* (36), 10782-10783.

85.   Daida, E. J.; Peters, J. C., Considering FeII/IV Redox Processes as Mechanistically Relevant to the Catalytic Hydrogenation of Olefins by [PhBPiPr3]Fe−Hx Species. *Inorg. Chem.* **2004,** *43* (23), 7474-7485.

86.   Iluc, V. M.; Hillhouse, G. L., Arrested 1,2-Hydrogen Migration from Silicon to Nickel upon Oxidation of a Three-Coordinate Ni(I) Silyl Complex. *J. Am. Chem. Soc.* **2010,** *132* (34), 11890-11892.

87.   Kitiachvili, K. D.; Mindiola, D. J.; Hillhouse, G. L., Preparation of Stable Alkyl Complexes of Ni(I) and Their One-Electron Oxidation to Ni(II) Complex Cations. *J. Am. Chem. Soc.* **2004,** *126* (34), 10554-10555.

88.   Schmedake, T. A.; Haaf, M.; Paradise, B. J.; Powell, D.; West, R., Two Trigonal Ni(silylene)3 Complexes. *Organometallics* **2000,** *19* (17), 3263-3265.

89.   Mork, B. V.; Tilley, T. D.; Schultz, A. J.; Cowan, J. A., Silylene Hydride Complexes of Molybdenum with Silicon–Hydrogen Interactions: Neutron Structure of (η5-C5Me5)(Me2PCH2CH2PMe2)Mo(H)(SiEt2). *J. Am. Chem. Soc.* **2004,** *126* (33), 10428-10440.

90.   Kleiman, J. P.; Dubeck, M., The Preparation of Cyclopentadienyl [o-(Phenylazo)Phenyl]Nickel. *J. Am. Chem. Soc.* **1963,** *85* (10), 1544-1545.

91.   Cope, A. C.; Siekman, R. W., Formation of Covalent Bonds from Platinum or Palladium to Carbon by Direct Substitution. *J. Am. Chem. Soc.* **1965,** *87* (14), 3272-3273.

92.   Albrecht, M., Cyclometalation Using d-Block Transition Metals: Fundamental Aspects and Recent Trends. *Chem. Rev.* **2010,** *110* (2), 576-623.

93.   Ito, M.; Itazaki, M.; Nakazawa, H., Selective Double Hydrosilylation of Nitriles Catalyzed by an Iron Complex Containing Indium Trihalide. *ChemCatChem* **2016,** *8* (21), 3323-3325.

94.   Iali, W.; Paglia, F. L.; Goff, X.-F. L.; Sredojević, D.; Pfeffer, M.; Djukic, J.-P., Room temperature tandem hydroamination and hydrosilation/protodesilation catalysis by a tricarbonylchromium-bound iridacycle. *Chem. Commun.* **2012,** *48* (83), 10310-10312.

95.   Fogg, D. E.; dos Santos, E. N., Tandem catalysis: a taxonomy and illustrative review. *Coord. Chem. Rev.* **2004,** *248* (21), 2365-2379.

96.   Shindoh, N.; Takemoto, Y.; Takasu, K., Auto-Tandem Catalysis: A Single Catalyst Activating Mechanistically Distinct Reactions in a Single Reactor. *Eur. J. Org. Chem.* **2009,** *15* (45), 12168-12179.

97.   Chalk, A. J.; Harrod, J. F., Homogeneous Catalysis. II. The Mechanism of the Hydrosilation of Olefins Catalyzed by Group VIII Metal Complexes1. *J. Am. Chem. Soc.* **1965,** *87* (1), 16-21.

98.   Troegel, D.; Stohrer, J., Recent advances and actual challenges in late transition metal catalyzed hydrosilylation of olefins from an industrial point of view. *Coord. Chem. Rev.* **2011,** *255* (13), 1440-1459.

99.   Randolph, C. L.; Wrighton, M. S., Photochemical reactions of (.eta.5-pentamethylcyclopentadienyl)dicarbonyliron alkyl and silyl complexes: reversible ethylene insertion into an iron-silicon bond and implications for the mechanism of transition-metal-catalyzed hydrosilation of alkenes. *J. Am. Chem. Soc.* **1986,** *108* (12), 3366-3374.

100.   Seitz, F.; Wrighton, M. S., Photochemical Reaction of [(CO)4Co(SiEt3)] with Ethylene: Implications for Cobaltcarbonyl-Catalyzed Hydrosilation of Alkenes. *Angew. Chem. Int. Ed.* **1988,** *27* (2), 289-291.

101.   Duckett, S. B.; Perutz, R. N., Mechanism of homogeneous hydrosilation of alkenes by (.eta.5-cyclopentadienyl)rhodium. *Organometallics* **1992,** *11* (1), 90-98.

102.   Ojima, I.; Nihonyanagi, M.; Kogure, T.; Kumagai, M.; Horiuchi, S.; Nakatsugawa, K.; Nagai, Y., Reduction of carbonyl compounds via hydrosilylation: I. Hydrosilylation of carbonyl compounds catalyzed by tris(triphenylphosphine)chlororhodium. *J. Organomet. Chem.* **1975,** *94* (3), 449-461.

103.   Ojima, I.; Kogure, T.; Kumagai, M.; Horiuchi, S.; Sato, T., Reduction of carbonyl compounds via hydrosilylation: II. Asymmetric reduction of ketones via hydrosilylation catalyzed by a rhodium(I) complex with chiral phosphine ligands. *J. Organomet. Chem.* **1976,** *122* (1), 83-97.

104.   Green, M. L. H., A new approach to the formal classification of covalent compounds of the elements. *J. Organomet. Chem.* **1995,** *500* (1), 127-148.

105.   Green, J. C.; Green, M. L. H.; Parkin, G., The occurrence and representation of three-centre two-electron bonds in covalent inorganic compounds. *Chem. Commun.* **2012,** *48* (94), 11481-11503.

106.   Green, M. L. H.; Parkin, G., Application of the Covalent Bond Classification Method for the Teaching of Inorganic Chemistry. *J. Chem. Educ.* **2014,** *91* (6), 807-816.

107.   Green, M. L. H.; Parkin, G., The classification and representation of main group element compounds that feature three-center four-electron interactions. *Dalton Transactions* **2016,** *45* (47), 18784-18795.

108.   Corey, J. Y., Reactions of Hydrosilanes with Transition Metal Complexes and Characterization of the Products. *Chem. Rev.* **2011,** *111* (2), 863-1071.

109.   Perutz, R. N.; Sabo-Etienne, S., The σ-CAM Mechanism: σ Complexes as the Basis of σ-Bond Metathesis at Late-Transition-Metal Centers. *Angew. Chem. Int. Ed.* **2007,** *46* (15), 2578-2592.

110.   McGrady, G. S.; Sirsch, P.; Chatterton, N. P.; Ostermann, A.; Gatti, C.; Altmannshofer, S.; Herz, V.; Eickerling, G.; Scherer, W., Nature of the Bonding in Metal-Silane σ-Complexes. *Inorg. Chem.* **2009,** *48* (4), 1588-1598.

111.   Pirnot, M. T.; Wang, Y.-M.; Buchwald, S. L., Copper Hydride Catalyzed Hydroamination of Alkenes and Alkynes. *Angew. Chem. Int. Ed.* **2016,** *55* (1), 48-57.

112.   Wang, W.; Wang, J.; Huang, L.; Wei, H., Mechanistic insights into hydrogen generation for catalytic hydrolysis and alcoholysis of silanes with high-valent oxorhenium(v) complexes. *Catal. Sci. Technol* **2015,** *5* (4), 2157-2166.

113.   Jones, J. S.; Wade, C. R.; Gabbaï, F. P., Redox and Anion Exchange Chemistry of a Stibine–Nickel Complex: Writing the L, X, Z Ligand Alphabet with a Single Element. **2014,** *53* (34), 8876-8879.

114.   Corey, J. Y.; Braddock-Wilking, J., Reactions of Hydrosilanes with Transition-Metal Complexes: Formation of Stable Transition-Metal Silyl Compounds. *Chem. Rev.* **1999,** *99* (1), 175-292.

115.   Yang, J.; White, P. S.; Brookhart, M., Scope and Mechanism of the Iridium-Catalyzed Cleavage of Alkyl Ethers with Triethylsilane. *J. Am. Chem. Soc.* **2008,** *130* (51), 17509-17518.

116.   Nödling, A. R.; Müther, K.; Rohde, V. H. G.; Hilt, G.; Oestreich, M., Ferrocene-Stabilized Silicon Cations as Catalysts for Diels–Alder Reactions: Attempted Experimental Quantification of Lewis Acidity and ReactIR Kinetic Analysis. *Organometallics* **2014,** *33* (1), 302-308.

117.   Großekappenberg, H.; Reißmann, M.; Schmidtmann, M.; Müller, T., Correction to Quantitative Assessment of the Lewis Acidity of Silylium Ions. *Organometallics* **2015,** *34* (22), 5496-5496.

118.   Großekappenberg, H.; Reißmann, M.; Schmidtmann, M.; Müller, T., Quantitative Assessment of the Lewis Acidity of Silylium Ions. *Organometallics* **2015,** *34* (20), 4952-4958.

119.   Ziegler, T.; Rauk, A., Carbon monoxide, carbon monosulfide, molecular nitrogen, phosphorus trifluoride, and methyl isocyanide as .sigma. donors and .pi. acceptors. A theoretical study by the Hartree-Fock-Slater transition-state method. *Inorg. Chem.* **1979,** *18* (7), 1755-1759.

120.   te Velde, G.; Bickelhaupt, F. M.; Baerends, E. J.; Fonseca Guerra, C.; van Gisbergen, S. J. A.; Snijders, J. G.; Ziegler, T., Chemistry with ADF. *J. Comput. Chem.* **2001,** *22* (9), 931-967.

121.   Diefenbach, A.; Bickelhaupt, F. M.; Frenking, G., The Nature of the Transition Metal–Carbonyl Bond and the Question about the Valence Orbitals of Transition Metals. A

Bond-Energy Decomposition Analysis of TM(CO)6q (TMq = Hf2-, Ta-, W, Re+, Os2+, Ir3+). *J. Am. Chem. Soc.* **2000,** *122* (27), 6449-6458.

122.   Bayat, M.; Salehzadeh, S.; Frenking, G., Energy decomposition analysis of the metal-imine bond in [(CO)4M–SB] (M = Cr, Mo, W; SB: RHCN–CH2CH2–NCHR). *J. Organomet. Chem.* **2012,** *697* (1), 74-79.

123.   Gonthier, J. F.; Steinmann, S. N.; Wodrich, M. D.; Corminboeuf, C., Quantification of "fuzzy" chemical concepts: a computational perspective. *Chem. Soc. Rev.* **2012,** *41* (13), 4671-4687.

124.   Hopffgarten, M. v.; Frenking, G., Energy decomposition analysis. **2012,** *2* (1), 43-62.

125.   Stang, P. J.; Anderson, A. G., Hammett and Taft substituent constants for the mesylate, tosylate, and triflate groups. *J. Org. Chem.* **1976,** *41* (5), 781-785.

126.   Howells, R. D.; Mc Cown, J. D., Trifluoromethanesulfonic acid and derivatives. *Chem. Rev.* **1977,** *77* (1), 69-92.

127.   Calimano, E.; Tilley, T. D., Synthesis and Structure of PNP-Supported Iridium Silyl and Silylene Complexes: Catalytic Hydrosilation of Alkenes. *J. Am. Chem. Soc.* **2009,** *131* (31), 11161-11173.

128.   Smith, P. W.; Tilley, T. D., Silane–Allyl Coupling Reactions of Cp*(iPr2MeP)Fe(η3-C3H5) and Synthetic Access to the Hydrido–Dinitrogen Complex Cp*(iPr2MeP)FeH(N2). *Organometallics* **2015,** *34* (11), 2134-2138.

129.   Wanandi, P. W.; Glaser, P. B.; Tilley, T. D., Reactivity of an Osmium Silylene Complex toward Chlorocarbons: Promotion of Metal Redox Chemistry by a Silylene Ligand and Relevance to the Mechanism of the Direct Process. *J. Am. Chem. Soc.* **2000,** *122* (5), 972-973.

130.   Hashimoto, H.; Ochiai, M.; Tobita, H., Reactions of a hydrido(hydrosilylene)tungsten complex with oxiranes. *J. Organomet. Chem.* **2007,** *692* (1), 36-43.

131.   Watanabe, T.; Hashimoto, H.; Tobita, H., Stoichiometric Hydrosilylation of Nitriles with Hydrido(hydrosilylene)tungsten Complexes: Formation of W−Si−N Three-Membered Ring Complexes and Their Unique Thermal Behaviors. *J. Am. Chem. Soc.* **2006,** *128* (7), 2176-2177.

132.   Watanabe, T.; Hashimoto, H.; Tobita, H., Reactions of Hydrido(hydrosilylene)tungsten Complexes with α,β-Unsaturated Carbonyl Compounds: Selective Formation of (η3-Siloxyallyl)tungsten Complexes. *J. Am. Chem. Soc.* **2007,** *129* (37), 11338-11339.

133.   Ochiai, M.; Hashimoto, H.; Tobita, H., Reactions of a hydrido(hydrosilylene)ruthenium complex with carbonyl compounds. *Dalton Transactions* **2009,** (10), 1812-1814.

134.   Watanabe, T.; Hashimoto, H.; Tobita, H., Hydrido(hydrosilylene)tungsten Complexes with Strong Interactions between the Silylene and Hydrido Ligands. **2004,** *43* (2), 218-221.

135.   Lipke, M. C.; Tilley, T. D., Hypercoordinate Ketone Adducts of Electrophilic η3-H2SiRR′ Ligands on Ruthenium as Key Intermediates for Efficient and Robust Catalytic Hydrosilation. *J. Am. Chem. Soc.* **2014,** *136* (46), 16387-16398.

136.   Gusev, D. G.; Fontaine, F.-G.; Lough, A. J.; Zargarian, D., Polyhydrido(silylene)osmium and Silyl(dinitrogen)ruthenium Products Through Redistribution of Phenylsilane with Osmium and Ruthenium Pincer Complexes. *Angew. Chem. Int. Ed.* **2003,** *42* (2), 216-219.

137.   Handford, R. C.; Smith, P. W.; Tilley, T. D., Silylene Complexes of Late 3d Transition Metals Supported by tris-Phosphinoborate Ligands. *Organometallics* **2018,** *37* (21), 4077-4085.

138.   Rankin, M. A.; MacLean, D. F.; Schatte, G.; McDonald, R.; Stradiotto, M., Silylene Extrusion from Organosilanes via Double Geminal Si–H Bond Activation by a Cp*Ru(κ2-P,N)+ Complex: Observation of a Key Stoichiometric Step in the Glaser–Tilley Alkene Hydrosilylation Mechanism. *J. Am. Chem. Soc.* **2007,** *129* (51), 15855-15864.

139.   Fasulo, M. E.; Glaser, P. B.; Tilley, T. D., Cp*(PiPr3)RuOTf: A Reagent for Access to Ruthenium Silylene Complexes. *Organometallics* **2011,** *30* (20), 5524-5531.

140.   Handwerker, H.; Leis, C.; Probst, R.; Bissinger, P.; Grohmann, A.; Kiprof, P.; Herdtweck, E.; Bluemel, J.; Auner, N.; Zybill, C., Reversible intramolecular base-stabilization in silylene (silanediyl) complexes: surprising reactivity for silylene coordination compounds with a dynamic N…Si…N bond. *Organometallics* **1993,** *12* (6), 2162-2176.

141.   Price, J. S.; Emslie, D. J. H.; Britten, J. F., Manganese Silylene Hydride Complexes: Synthesis and Reactivity with Ethylene to Afford Silene Hydride Complexes. *Angew. Chem. Int. Ed.* **2017,** *56* (22), 6223-6227.

142.   Dannappel, K.; Nienhaus, R.; Schürmann, M.; Costisella, B.; Jurkschat, K., The UV-Light Initiated Reaction of Organosilanes with Tungsten Hexacarbonyl: Formation of an Organosilylene Complex and Organosilylium Salts *Z. Anorg. Allg. Chem.* **2009,** *635* (13-14), 2126-2134.

143.   Lipke, M. C.; Neumeyer, F.; Tilley, T. D., Interconversion of η3-H2SiRR′ σ-Complexes and 16-Electron Silylene Complexes via Reversible H–H or C–H Elimination. *J. Am. Chem. Soc.* **2014,** *136* (16), 6092-6102.

144.   Corey, J. Y., Reactions of Hydrosilanes with Transition Metal Complexes. *Chem. Rev.* **2016,** *116* (19), 11291-11435.

145.   Yang, J.; White, P. S.; Schauer, C. K.; Brookhart, M., Structural and Spectroscopic Characterization of an Unprecedented Cationic Transition-Metal η1-Silane Complex. *Angew. Chem. Int. Ed.* **2008,** *47* (22), 4141-4143.

146.   Nikonov, G. I., *Advances in Organometallic Chemistry*. 2005; Vol. 53.

147.   Scherer, W.; Meixner, P.; Barquera-Lozada, J. E.; Hauf, C.; Obenhuber, A.; Brück, A.; Wolstenholme, D. J.; Ruhland, K.; Leusser, D.; Stalke, D., A Unifying Bonding Concept for Metal Hydrosilane Complexes. *Angew. Chem. Int. Ed.* **2013,** *52* (23), 6092-6096.

148.   Hauf, C.; Barquera-Lozada, J. E.; Meixner, P.; Eickerling, G.; Altmannshofer, S.; Stalke, D.; Zell, T.; Schmidt, D.; Radius, U.; Scherer, W., Remanent Si–H Interactions in Late Transition Metal Silane Complexes. *Z. Anorg. Allg. Chem.* **2013,** *639* (11), 1996-2004.

149.   Autschbach, J.; Ziegler, T., Nuclear spin–spin coupling constants from regular approximate relativistic density functional calculations. I. Formalism and scalar relativistic results for heavy metal compounds. *J. Chem. Phys.* **2000,** *113* (3), 936-947.

150.   Wiberg, K. B., Application of the pople-santry-segal CNDO method to the cyclopropylcarbinyl and cyclobutyl cation and to bicyclobutane. *Tetrahedron* **1968,** *24* (3), 1083-1096.

151.   Mitoraj, M. P.; Michalak, A.; Ziegler, T., A Combined Charge and Energy Decomposition Scheme for Bond Analysis. *J. Chem. Theory Comput.* **2009,** *5* (4), 962-975.

152.   Mitoraj, M. P.; Michalak, A.; Ziegler, T., On the Nature of the Agostic Bond between Metal Centers and β-Hydrogen Atoms in Alkyl Complexes. An Analysis Based on the Extended Transition State Method and the Natural Orbitals for Chemical Valence Scheme (ETS-NOCV). *Organometallics* **2009,** *28* (13), 3727-3733.

153.   Bergman, S. R. K. D. T. G., Reactions of Cp*(PMe3)Ir(Me)OTf with Silanes: Role of Base-Free Silylene Complexes in Rearrangements of the Resulting Silicon-Based Ligands . *Organometallics* **2002,** *21* (16), 3376-3387.

154.   Ueno, K.; Sakai, M.; Ogino, H., Synthesis, Structure, and Fluxional Behavior of Base-Stabilized Silyl(silylene)tungsten Complexes. *Organometallics* **1998,** *17* (11), 2138-2140.

155.   Calimano, E.; Tilley, T. D., Alkene Hydrosilation by a Cationic Hydrogen-Substituted Iridium Silylene Complex. *J. Am. Chem. Soc.* **2008,** *130* (29), 9226-9227.

156.   Sakaba, H.; Hirata, T.; Kabuto, C.; Kabuto, K., Synthesis, Structure, and Dynamic Behavior of Tungsten Dihydride Silyl Complexes Cp*(CO)2W(H)2(SiHPhR) (R = Ph, H, Cl). *Organometallics* **2006,** *25* (21), 5145-5150.

157.   Sakaba, H.; Hirata, T.; Kabuto, C.; Kabuto, K., Synthesis and structure of a tungsten dichlorosilyl dihydride complex. *J. Organomet. Chem.* **2007,** *692* (1), 402-407.

158.   Abronin, I. A.; Avdyuhina, N. A.; Morozova, L. V.; Magomedov, G. K. I., MNDO calculations of carbene and its analogue complexes with chromium pentacarbonyl. *J. Mol. Struct. THEOCHEM* **1991,** *228*, 19-25.

159.   Grumbine, S. D.; Tilley, T. D.; Arnold, F. P.; Rheingold, A. L., A Fischer-type silylene complex of platinum: [trans-(Cy3P)2(H)Pt:Si(SEt)2]BPh4. *J. Am. Chem. Soc.* **1993,** *115* (17), 7884-7885.

160.   Cundari, T. R.; Gordon, M. S., Strategies for designing a high-valent transition-metal silylidene complex. *Organometallics* **1992,** *11* (9), 3122-3129.

161.   Arnold, F. P., Theoretical Studies of the Bonding in Cationic Ruthenium Silylenes. *Organometallics* **1999,** *18* (23), 4800-4809.

162.   Jacobsen, H.; Ziegler, T., Transition Metal Fischer-Type Complexes. Density Functional Analysis of the Systems (CO)5CrEH2 (E = C, Si, Ge, Sn) and (CO)5MCH2 (M = Mo, W, Mn+). *Inorg. Chem.* **1996,** *35* (3), 775-783.

163.   E. D. Glendening, J., K. Badenhoop, A. E. Reed, J. E. Carpenter, J. A. Bohmann, C. M. Morales, P. Karafiloglou, C. R. Landis, F. Weinhold, Theoretical Chemistry Institute, University of Wisconsin, Madison: 2013.

164.   Orlandi, M.; Brenna, D.; Harms, R.; Jost, S.; Benaglia, M., Recent Developments in the Reduction of Aromatic and Aliphatic Nitro Compounds to Amines. *Org. Process Res. Dev.* **2018,** *22* (4), 430-445.

165.   Shaikh, N. S., Sustainable Amine Synthesis: Iron Catalyzed Reactions of Hydrosilanes with Imines, Amides, Nitroarenes and Nitriles. *ChemistrySelect* **2019,** *4* (22), 6753-6777.

166.   Béchamp, A., *Ann. Chim. Phys.* **1854,** *42*, 186-196.

167.   Junge, K.; Wendt, B.; Shaikh, N.; Beller, M., Iron-catalyzed selective reduction of nitroarenes to anilines using organosilanes. *Chem. Commun.* **2010,** *46* (10), 1769-1771.

168.   Roger Arthur Sheldon, H. v. B., *Fine Chemicals through Heterogeneous Catalysis*. WILEY-VCH Verlag GmbH: 2000.

169.   Lipowitz, J.; Bowman, S. A., Use of polymethylhydrosiloxane as a selective, neutral reducing agent for aldehydes, ketones, olefins, and aromatic nitro compounds. *J. Org. Chem.* **1973,** *38* (1), 162-165.

170.   Iovel, I.; Golomba, L.; Fleisher, M.; Popelis, J.; Grinberga, S.; Lukevics, E., Hydrosilylation Of (Hetero)aromatic Aldimines in the Presence of a Pd(I) Complex. *Chemistry of Heterocyclic Compounds* **2004,** *40* (6), 701-714.

171.   Rahaim, R. J.; Maleczka, R. E., Pd-Catalyzed Silicon Hydride Reductions of Aromatic and Aliphatic Nitro Groups. *Org. Lett.* **2005,** *7* (22), 5087-5090.

172.   Srinivasan, B.; Huang, X., Functionalization of magnetic nanoparticles with organic molecules: Loading level determination and evaluation of linker length effect on immobilization. *Chirality* **2008,** *20* (3-4), 265-277.

173.   K. A. Andrianov, V. I. S. a. M. I. F., *Zh. Obshch. Khim.* **1977,** *47*, 485.

174.   de Noronha, R. G.; Romão, C. C.; Fernandes, A. C., Highly Chemo- and Regioselective Reduction of Aromatic Nitro Compounds Using the System Silane/Oxo-Rhenium Complexes. *J. Org. Chem.* **2009,** *74* (18), 6960-6964.

175.   Tormo, J.; Hays, D. S.; Fu, G. C., Bu3SnH-Catalyzed Reduction of Nitroalkanes to Alkanes. *J. Org. Chem.* **1998,** *63* (16), 5296-5297.

176.   Fier, P. S.; Hartwig, J. F., Selective C-H Fluorination of Pyridines and Diazines Inspired by a Classic Amination Reaction. *Science* **2013,** *342* (6161), 956.

177.   Fier, P. S.; Hartwig, J. F., Synthesis and Late-Stage Functionalization of Complex Molecules through C–H Fluorination and Nucleophilic Aromatic Substitution. *J. Am. Chem. Soc.* **2014,** *136* (28), 10139-10147.

178.   Patrick S. Fier, J. F. H., *Org. Synth* **2017,** (94), 46-53.

179.   Au - Brack, P.; Au - Dann, S.; Au - Wijayantha, K. G. U.; Au - Adcock, P.; Au - Foster, S., A Simple, Low-cost, and Robust System to Measure the Volume of Hydrogen Evolved by Chemical Reactions with Aqueous Solutions. *JoVE* **2016,** (114), e54383.

180.   Sun, J.; Deng, L., Cobalt Complex-Catalyzed Hydrosilylation of Alkenes and Alkynes. *ACS Catal.* **2016,** *6* (1), 290-300.

181.   Marciniec, B., *Comprehensive Handbook on Hydrosilylation*. elsevier.: Pergamon, 1992; Vol. 1.

182.   Du, X.; Huang, Z., Advances in Base-Metal-Catalyzed Alkene Hydrosilylation. *ACS Catal.* **2017,** *7* (2), 1227-1243.

183.   Calas, R. F., E.; Bazouin, A. C.R. , *Acad. Sci* **1961,** *252*, 420–422.

184.   Bottini, M.; Magrini, A.; Rosato, N.; Bergamaschi, A.; Mustelin, T., Dispersion of Pristine Single-walled Carbon Nanotubes in Water by a Thiolated Organosilane: Application in Supramolecular Nanoassemblies. *J. Phys. Chem. B* **2006,** *110* (28), 13685-13688.

185.   Klaehn, J. R.; Luther, T. A.; Orme, C. J.; Jones, M. G.; Wertsching, A. K.; Peterson, E. S., Soluble N-Substituted Organosilane Polybenzimidazoles. *Macromolecules* **2007,** *40* (21), 7487-7492.

186.   Murai, T.; Sakane, T.; Kato, S., Cobalt carbonyl catalyzed reduction of aromatic nitriles with a hydrosilane leading to N,N-disilylamines. *Tetrahedron Lett.* **1985,** *26* (42), 5145-5148.

187.   Nolin, K. A.; Krumper, J. R.; Pluth, M. D.; Bergman, R. G.; Toste, F. D., Analysis of an Unprecedented Mechanism for the Catalytic Hydrosilylation of Carbonyl Compounds. *J. Am. Chem. Soc.* **2007,** *129* (47), 14684-14696.

188.   Taniguchi, K.; Itagaki, S.; Yamaguchi, K.; Mizuno, N., Heterogeneous-Gold-Catalyzed Acceptorless Cross-Dehydrogenative Coupling of Hydrosilanes and Isocyanic Acid Generated in situ from Urea. *Angew. Chem. Int. Ed.* **2013,** *52* (32), 8420-8423.

189.   Moitra, N.; Ichii, S.; Kamei, T.; Kanamori, K.; Zhu, Y.; Takeda, K.; Nakanishi, K.; Shimada, T., Surface Functionalization of Silica by Si‑H Activation of Hydrosilanes. *J. Am. Chem. Soc.* **2014,** *136* (33), 11570-11573.

190.   Doxsee, K. M., Counter anion effects on complexation of cations. *J. Org. Chem.* **1989,** *54* (19), 4712-4715.

191.   Yakelis, N. A.; Bergman, R. G., Safe Preparation and Purification of Sodium Tetrakis[(3,5-trifluoromethyl)phenyl]borate (NaBArF24): Reliable and Sensitive Analysis of Water in Solutions of Fluorinated Tetraarylborates. *Organometallics* **2005,** *24* (14), 3579-3581.

192.   Brookhart, M.; Grant, B.; Volpe, A. F., [(3,5-(CF3)2C6H3)4B]-[H(OEt2)2]+: a convenient reagent for generation and stabilization of cationic, highly electrophilic organometallic complexes. *Organometallics* **1992,** *11* (11), 3920-3922.

193.   Hoke, S. H.; Yang, S. S.; Cooks, R. G.; Hrovat, D. A.; Borden, W. T., Proton Affinities of Free Radicals Measured by the Kinetic Method. *J. Am. Chem. Soc.* **1994,** *116* (11), 4888-4892.

194.   Ginell, R.; Simha, R., On the Kinetics of Polymerization Reactions. I. First Order Initiation Reaction1. *J. Am. Chem. Soc.* **1943,** *65* (4), 706-715.

195.   Wodrich, M. D.; Sawatlon, B.; Solel, E.; Kozuch, S.; Corminboeuf, C., Activity-Based Screening of Homogeneous Catalysts through the Rapid Assessment of Theoretically Derived Turnover Frequencies. *ACS Catal.* **2019,** *9* (6), 5716-5725.

196.   Boudart, M., Turnover Rates in Heterogeneous Catalysis. *Chem. Rev.* **1995,** *95* (3), 661-666.

197.   Kida, T.; Sato, S.-i.; Yoshida, H.; Teragaki, A.; Akashi, M., 1,1,1,3,3,3-Hexafluoro-2-propanol (HFIP) as a novel and effective solvent to facilely prepare cyclodextrin-assembled materials. *Chem. Commun.* **2014,** *50* (91), 14245-14248.

198.   Weinhold, F., Natural Bond Orbital Methods. In *Encyclopedia of Computational Chemistry*, von Ragué-Schleyer, P.; Allinger, N. L.; Clark, T.; Gasteiger, J.; Kollman, P. A.; Schaefer, H. F.; Schreiner, P. R., Eds. John Wiley & Sons, Chichester, UK: 1998; Vol. 3, pp 1792-1811.

199.   Glendening, E. D.; Badenhoop, J. K.; Reed, A. E.; Carpenter, J. E.; Bohmann, J. A.; Morales, C. M.; Landis, C. R.; Weinhold, F. *NBO 6.0.*, Theoretical Chemistry Institute, University of Wisconsin, Madison, 2013.

200.   Wiberg, K. B., *Tetrahedron* **1968,** *24*, 1083-1096.

201.   Mitoraj, M. P.; Michalak, A.; Ziegler, T., *J. Chem. Theory Comput.* **2009,** *5*, 962-975.

202.   Mitoraj, M. P.; Michalak, A.; Ziegler, T., *Organometallics* **2009,** *28*, 3727-3733.

Experimental Section

General Methods and Technical Details

Experimental techniques and materials

All experiments were conducted under a dry argon atmosphere using standard Schlenk and glovebox techniques (unless otherwise indicated). All glassware was oven-dried prior to use. All solvents were distilled over sodium or CaH_2 under argon before use. Deuterated solvents (including PhF) were dried over sodium or CaH_2, filtered over activated neutral alumina, and stored under argon before use. The following compounds were purchased from the indicated companies and used as such (unless otherwise stated): $HSiEt_3$ (Aldrich, 100 mL, 97%), $HSiPhH_2$ [(Alfa-Aesar, 25 g, 97%), (purified by bulb-to-bulb distillation over CaH_2 and stored under argon over MS-3Å)], PMHS (Alfa-Aesar, 100 g), 1-fluoroheptane (**1-FH**) (Aldrich, 1 g, 98%), fluorocyclohexane (**F-Cy**) (TCI-Chemicals, 5 g, > 98%). Ligand name abbreviations: Cp*, (1,2,3,4,5-pentamethyl-η^5-cyclopentadienyl); PhPy, 2-(2-pyridyl)phenyl, B[*h*]Q, benzo[*h*]quinolinyl. [**1a,b**][BArF$_{24}$] were prepared following published procedures.[1,2] ^{1}H (300, 400, 500, and 600 MHz), ^{13}C (75 and 126 MHz), ^{19}F (282 MHz), and ^{29}Si (119 MHz) NMR spectra were measured on Bruker DPX 300 and 400, Avance I 500, and Avance III 600 spectrometers. All chemical shifts (δ) are expressed in parts per million (ppm). For ^{1}H and ^{13}C NMR, values of δ are reported relative to Me_4Si as an external reference standard and referenced against peaks of solvents (only partially deuterated solvent is visible in ^{1}H) as secondary reference standards. For other nuclei, the reported values of δ are referenced to external reference standards ($CF_3C_6H_5$ in $CDCl_3$ for ^{19}F, Me_4Si in $CDCl_3$ for ^{29}Si).

X ray diffraction analysis of [**3**][BArF$_{24}$] CCDC 1826970

X-Ray diffraction data collection was carried out on a Bruker APEX II DUO Kappa-CCD diffractometer equipped with an Oxford Cryosystem liquid N$_2$ device, using Cu-Kα radiation (λ = 1.54178 Å). The crystal-detector distance was 40mm. The cell parameters were determined (APEX2 software)[3] from reflections taken from tree sets of 20 frames, each at 10s exposure. The structure was solved by Direct methods using the program SHELXS-2014.[4] The refinement and all further calculations were carried out using SHELXL-2014.[5] The H-atom H1 bound to Si1 was added in calculated position and then refined without the "AFIX" instruction. The other H-atoms were included in calculated positions and treated as riding atoms using SHELXL default parameters. The non-H atoms were refined anisotropically, using weighted full-matrix least-squares on F^2. A semi-empirical absorption correction was applied using SADABS in APEX2[3]; transmission factors: T$_{min}$/T$_{max}$ = 0.5294/0.7528. The benzoquinolinyl ligand is disordered over two positions, the THF molecule and the phenyl group linked to Si1 are disordered over two positions (all in all), the fluorine atoms F4, F5, F6, F14, F15, F19, F20, F21, F22, F23 and F24 from the counter-anion are disordered over two positions.

Note : Table S4 and S5 gather acquisition and refinement data for [**3**][BArf$_{24}$] and [**4**][BArF$_{24}$] (CCDC 1843843)

Computational methods and technical details

Computations were performed with the methods of density functional theory using the SCM-ADF2016.01 package[6–8] considering the molecules in the gas phase. The PBE functional[9] implemented in the Amsterdam Density Functional package[7] (ADF2016 version) and augmented with Grimme's DFT-D3(BJ) implementation of dispersion with a Becke−Johnson (BJ) damping function was used in all geometry optimizations.[10,11] Geometry optimizations by energy gradient minimization were carried out in all cases with integration grid accuracy comprised between 4.5 and 6.5, an energy gradient convergence criterion of 10^{-3} au, and a tight to very tight SCF convergence criterion. Counterpoise correction for basis set superposition error (BSSE) was neglected throughout this study. Within the PBE scheme, electron correlation was treated within the local density approximation (LDA) in the PW92[12] parametrization. With ADF2016.01, unless otherwise stated, all computations were carried out using scalar relativistic corrections within the zeroth order regular approximation for relativistic effects[13–15] with ad hoc all-electron (abbreviated ae) single polarization function triple-ζ Slater type basis sets (TZP). Vibrational modes were analytically computed to verify that the optimized geometries were related to energy minima or to transition states. The geometries of [**2c**], [**2d**], [**3**]$^+$, [**4**]$^+$ and all other intermediates, transition states and reactants were computed at the ZORA-PBE-D3(BJ)/ae-TZP level and its minimum energy nature confirmed by the absence of any imaginary mode above 50 $i$cm^{-1} in its computed vibrational spectrum. Intrinsic interaction energies, ETS-NOCV analyses, Natural population analyses (NPA) as well as Wiberg index determinations were performed with the gas-phase geometry relaxed at the (ZORA) PBE-D3(BJ) level using all-electron TZP basis sets with the GENNBO[16] 6.0 module of ADF. NMR coupling constants were computed with the ADF CPL module at the ZORA-SAOP/all-electron TZP basis sets. Drawings of molecular structures and isosurfaces were produced with ADFview2013.

Formation of [2c][BArF$_{24}$] by Reaction of [1b][BArF$_{24}$] with HSiPhH$_2$: Procedure, NMR Data, and Spectra

Typical procedure for NMR analysis

In a glovebox, HSiPhH$_2$ (10.0 μL, 81.1 μmol) was added to a solution of [1b][BArF$_{24}$] (29 mg, 20.6 μmol) in CD$_2$Cl$_2$ (0.65 mL). The resulting solution was shaken and transferred into a J. Young NMR sample tube which was subsequently tightly sealed for analysis. After 25 minutes of reaction, the NMR tube was frozen at < -60 °C. Multinuclear NMR analysis (at -60 °C) of the reaction revealed the total and exclusive conversion of [1b][BArF$_{24}$] to [2c][BArF$_{24}$], along with the released CH$_3$CN (from [1b][BArF$_{24}$]) and excess of HSiPhH$_2$ in a ratio of ~1:1:3 (see NMR spectra below).
NMR data

Data for [2c][BArF$_{24}$] are as follows: ^{1}H NMR (600 MHz, 213 K, CD$_2$Cl$_2$): δ = 8.71 (d, 1H, H$_{Ar}$ B[*h*]Q, *J* = 5.4 Hz), 8.22 (d, 1H, H$_{Ar}$ B[*h*]Q, *J* = 7.9 Hz), 7.81-7.85 (m, 2H, H$_{Ar}$ B[*h*]Q), 7.75 (m, 8H, H$_{ortho}$ BArF$_{24}$), 7.68 (d, 1H, H$_{Ar}$ B[*h*]Q, *J* = 8.8 Hz), 7.55 (m, 4H, H$_{para}$ BArF$_{24}$), 7.51 (d, 1H, H$_{Ar}$ B[*h*]Q, *J* = 8.0 Hz), 7.50 (d, 1H, H$_{Ar}$ B[*h*]Q, *J* = 8.0 Hz), 7.44 (d, 1H, H$_{Ar}$ B[*h*]Q, *J* = 8.7 Hz), 6.65 (t, 1H, [Ir-H]-[SiH$_2$*Ph*], *J* = 7.5 Hz), 6.46 (t, 2H, [Ir-H]-[SiH$_2$*Ph*], *J* = 7.5 Hz), 6.19 (d, 2H, [Ir-H]-[SiH$_2$*Ph*], *J* = 7.5 Hz), 4.40 (dd, 1H, [Ir-H]-[Si*H*$_2$Ph], *J*$^1_{H-H}$ = 11.8 Hz, $^1J_{H-Si}$ = 197.0 Hz; *J*$^2_{H-H}$ = 2.6 Hz), 3.84 (dd, 1H, [Ir-H] →[Si*H*$_2$Ph], *J*$^1_{H-H}$ = 11.8 Hz, $^1J_{H-Si}$ = 224.0 Hz; *J*$^2_{H-H}$ = 3.6 Hz), 1.79 (s, 15H, Cp-*Me$_5$*), −11.50 (bs, 1H, [Ir-*H*]-[SiH$_2$Ph]). The reaction described above was repeated (-40 °C) for recording ^{13}C and 2D related NMR spectra. ^{13}C (151 MHz, 233 K, CD$_2$Cl$_2$): δ = 161.8 (1:1:1:1 quartet, $^1J_{C-B}$ = 49.5 Hz, *C*-B in BArF$_{24}$), 155.8 (B[*h*]Q), 152.0 (H-*C*=N, B[*h*]Q), 144.6 (B[*h*]Q), 141.5 (B[*h*]Q), 138.7 (*C*-H, B[*h*]Q), 138.1 (B[*h*]Q), 136.5 (*C*-H, B[*h*]Q), 135.2 (B[*h*]Q), 134.2 (*C*-H, IrSi*Ph*H$_2$), 134.7 (m, *C*-H$_{ortho}$ in BArF$_{24}$), 133.0 (*C*-H, H$_{Ar}$^{ortho} in IrSi*Ph*H$_2$), 130.8 (*C*-H, B[*h*]Q), 130.3 (B[*h*]Q), 128.8 (qq, $^2J_{C-F}$ = 32.8 Hz, $^3J_{C-F}$ = 2.9 Hz, *C*$_{Ar}$-CF$_3$ in BArF$_{24}$), 128.8 (*C*-H, H$_{Ar}$^{para} in IrSi*Ph*H$_2$ [this ^{13}C signal could not be directly detected as it overlapped with one quadruplet signal assigned to the BArF$_{24}$ anion [^{13}C-^{19}F coupling]; its presence was inferred from 2D ^{1}H,^{13}C HSQC/HMBC NMR), 126.8 (*C*-H, H$_{Ar}$^{meta} in IrSi*Ph*H$_2$), 128.3 (*C*-Si, IrSi*Ph*H$_2$), 125.5 (q, $^1J_{C-F}$ = 272.2 Hz, CF$_3$ in BArF$_{24}$), 124.5 (*C*-H, B[*h*]Q), 124.1 (*C*-H, B[*h*]Q), 123 (*C*-H, B[*h*]Q), 123.7 (q, $^1J_{C-F}$ = 272.8 Hz, *C*F$_3$ in BArF$_{24}$), 117.6 (m, C-H^{para} in

BArF$_{24}$), 103.1 (*Cp*-Me$_5$), 8.69 (Cp-*Me$_5$*). ^{29}Si-DEPT NMR (119 MHz, 213 K, CD$_2$Cl$_2$): δ = -35.64 (s, [Ir-H]-[*Si*H$_2$Ph]). Data for "free" HSiPhH$_2$ are as follows: ^{1}H NMR (600 MHz, 213 K, CD$_2$Cl$_2$): δ = 7.58-7.59 (m, 1H, *Ph*SiH$_3$), 7.44 (m, 2H, *Ph*SiH$_3$), 7.35-7.37 (m, 2H, *Ph*SiH$_3$), 4.13 (s, 3H, *Ph*SiH$_3$, $^1J_{\text{H-Si}}$ = 200.1 Hz. ^{29}Si-DEPT NMR (119 MHz, 213 K, CD$_2$Cl$_2$): δ = -58.75 (s, Ph*Si*H$_3$). Data for "free" CH$_3$CN are as follows: ^{1}H NMR (600 MHz, 213 K, CD$_2$Cl$_2$): δ = 1.98 (s, 3H, C*H$_3$*CN); ^{13}C (151 MHz, 233 K, CD$_2$Cl$_2$): δ = 117.7 (N*C*Me), 2.33 (NC*Me*).

NMR spectra

^{1}H NMR
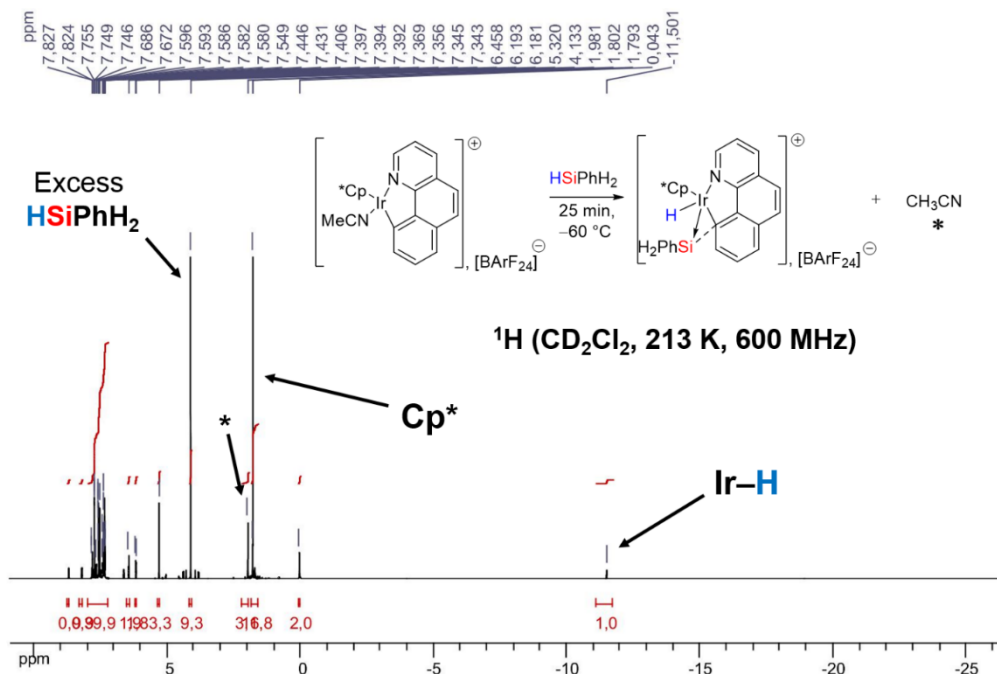
Figure S- 1

^1H NMR (continued)

^1H (CD_2Cl_2, 213 K, 600 MHz)   Hydride region

Ir–H

Figure S- 2

Figure S- 3

Figure S- 4

¹H NMR (continued)

¹H (CD₂Cl₂, 213 K, 600 MHz)

Ir-SiPh_H_2

4.4 (dd, J= 11.8Hz, 2.6Hz)

3.84 (dd, J= 11.8Hz, 3.6Hz)

0.9   0.9

ppm 4.46   4.44   4.42   4.4   4.38   4.36   ppm 3.88   3.86   3.84   3.82   3.8   3.78

Figure S- 5

ppm
4.414
4.410
4.395
4.390

4.133

3.848
3.843
3.829
3.823

¹H (CD₂Cl₂, 213 K, 600 MHz)

Ir-SiPh_H_2 (#)

\#   \#

Excess of
HSiPhH₂

0.9   0.9

ppm 4.5   4.45   4.4   4.35   4.3   4.25   4.2   4.15   4.1   4.05   4   3.95   3.9   3.85   3.8

Figure S- 6

139

Figure S- 7

Figure S- 8

^{1}H-^{1}H COSY NMR (600 MHz, 213 K, CD$_2$Cl$_2$)
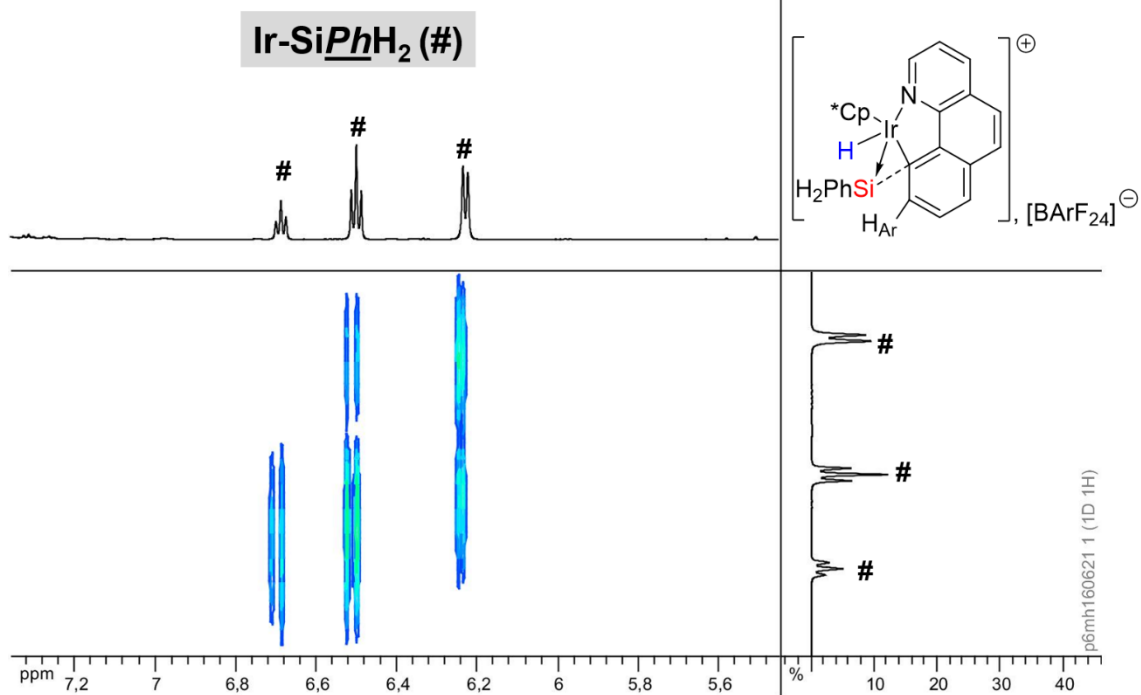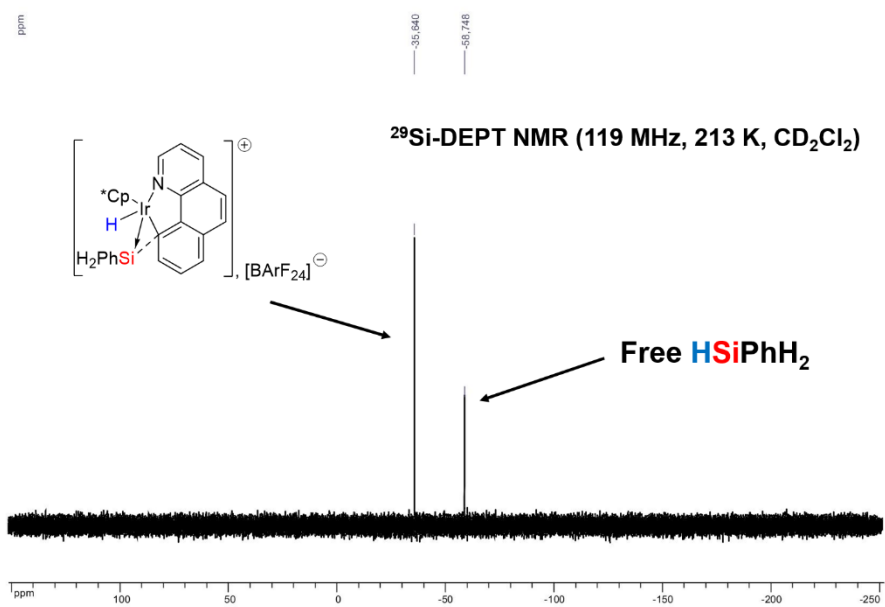
Ir-Si*Ph*H$_2$ (#)

Figure S- 9

Figure S- 10

^{29}Si-^{1}H NMR (continued)
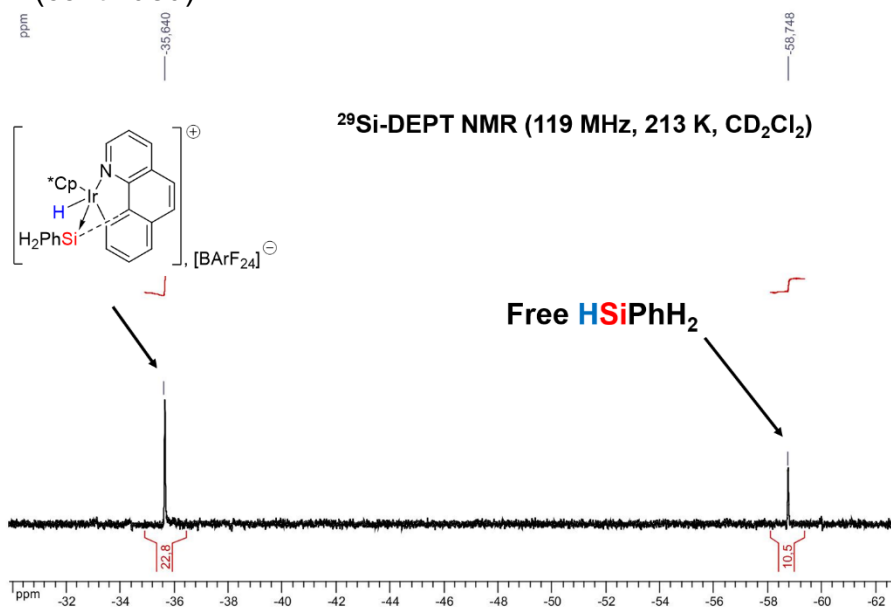
Figure S- 11

^{1}H,^{29}Si HMQC NMR
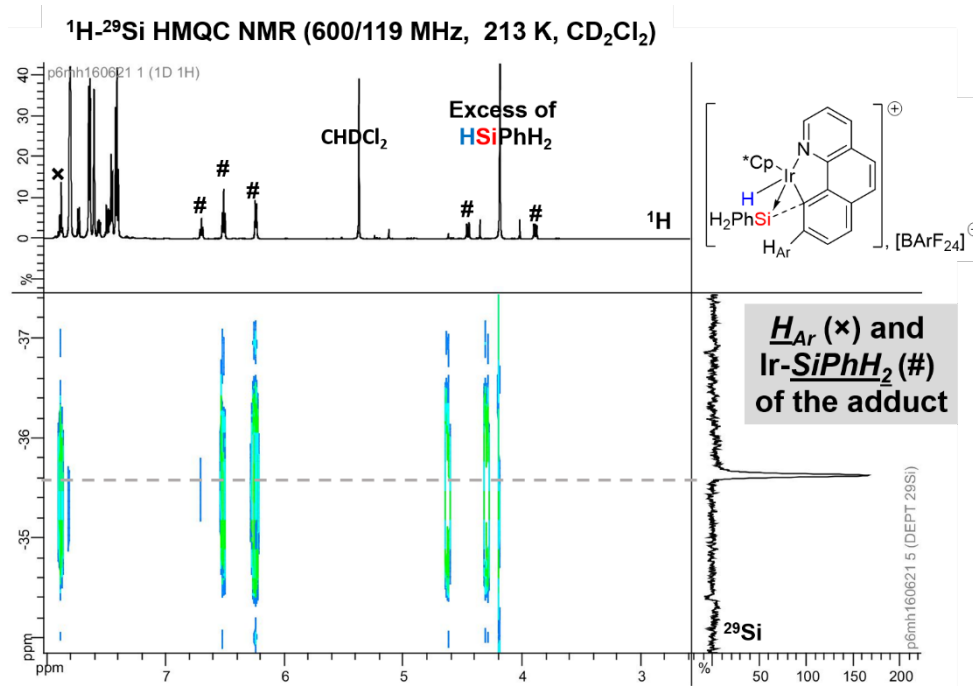
Figure S- 12
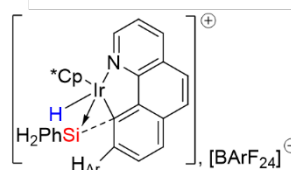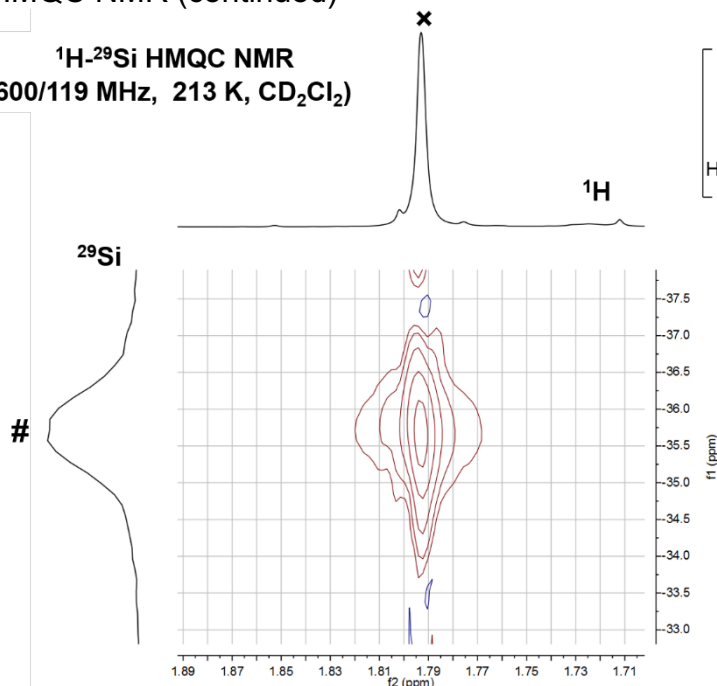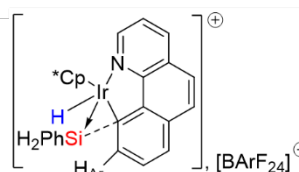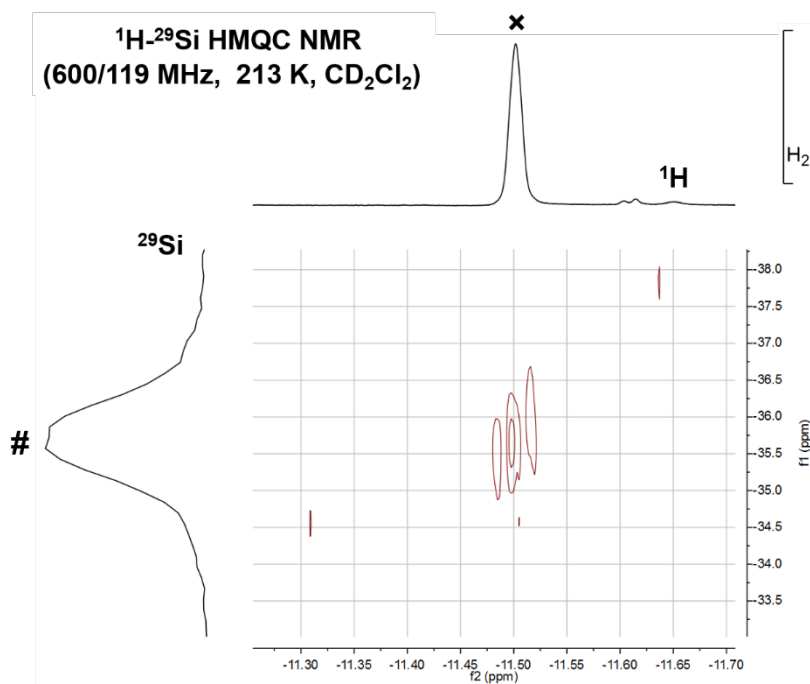
Figure S- 13
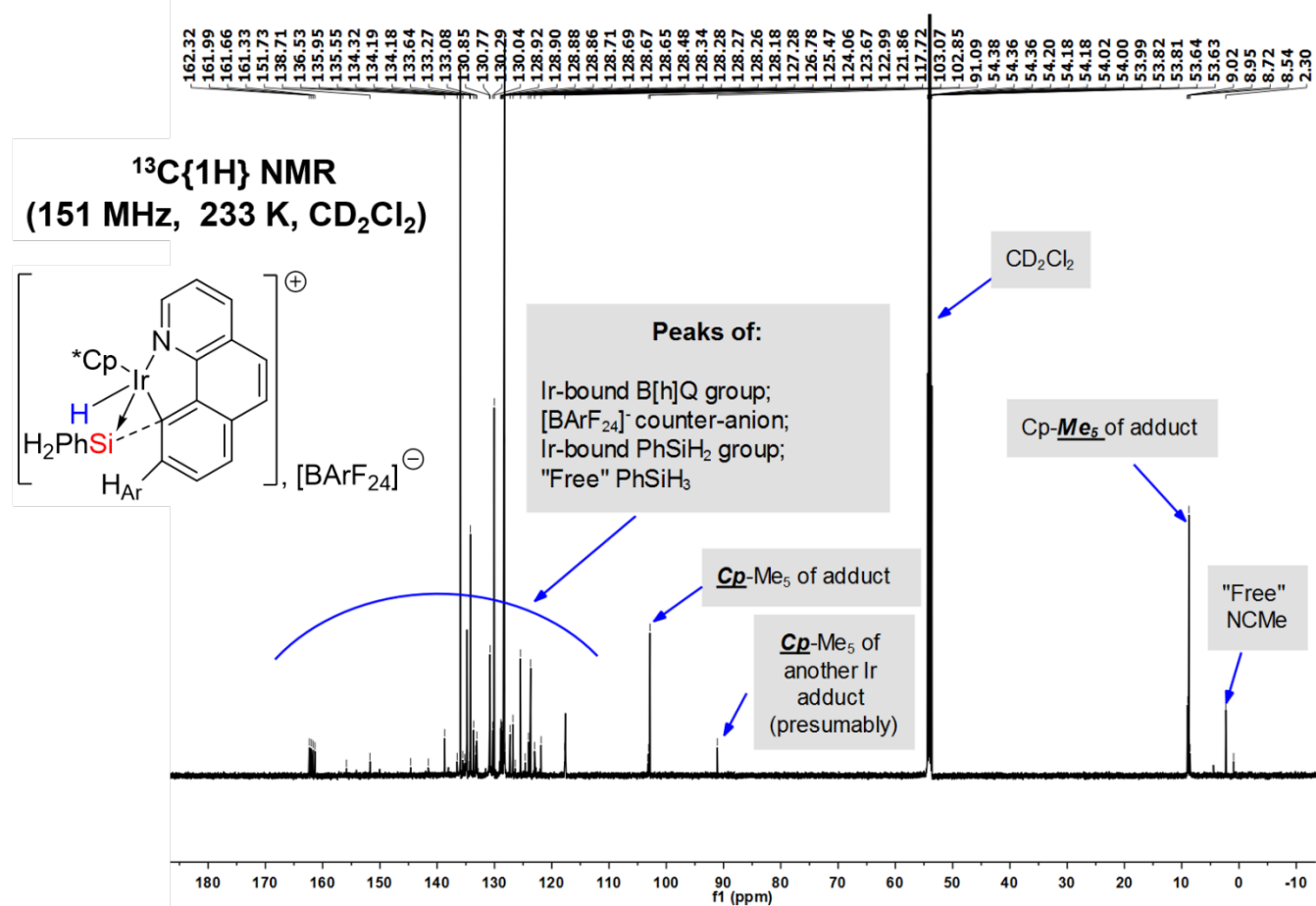
Figure S- 14

Figure S- 15

Formation of [2d][BArF$_{24}$] by Reaction of [1b][BArF$_{24}$] with HSi^{n}BuH$_2$: Procedure, NMR Data, and Spectra

Typical procedure for NMR analysis

In a glovebox, HSi^{n}BuH$_2$ (20.0 µL, 77.0 µmol) was added to a solution of [1b][BArF$_{24}$] (30 mg, 21.2 µmol) in CD$_2$Cl$_2$ (0.45 mL). The resulting solution was shaken and transferred into a J. Young NMR sample tube which was subsequently tightly sealed for analysis. After 25 minutes of reaction, the NMR tube was frozen at < -40 °C. Multinuclear NMR analysis (at -40 °C) of the reaction revealed the total conversion of [1b][BArF$_{24}$] to [2d][BArF$_{24}$], along with an unknown Ir-based side product (based on Cp*), the released CH$_3$CN (from [1b][BArF$_{24}$]) and excess of HSi^{n}BuH$_2$ with a relative ~1:1:6 ratio (see NMR spectra below). Isolation of pure [2d][BArF$_{24}$] was attempted in many circumstances by varying the conditions of the reaction and the methods of purification, all of which led to decomposition products of unidentified nature. Therefore, the characterization of [2d][BArF$_{24}$] was only possible *in situ* (solution NMR solvent). However, appropriate identification of all ^{1}H nuclei could not be realized due to the formation of a unidentified side-product [much likely of the formula[IrCp*(B[h]Q)X][BArF$_{24}$], where X may presumably be a solvent and certainly not NCMe or H)]. Nonetheless, ^{1}H and ^{29}Si chemical shifts that are diagnostic of the structure of [2d][BArF$_{24}$] could be unambiguously identified (vide infra). ^{13}C nuclei could not be assigned with certainty to the product of interest due to the complex nature of the reaction mixture and of the resulting NMR spectrum.

NMR data

Selected ^{1}H NMR data (600 MHz, 233 K, CD$_2$Cl$_2$): δ = 8.76 (broad m, 1H, H$_{Ar}$ B[h]Q), 8.43 (m, 1H, H$_{Ar}$ B[h]Q), 7.93 (m, 1H, H$_{Ar}$ B[h]Q), 7.86 (m, 1H, H$_{Ar}$ B[h]Q), 7.81 (m, 1H, H$_{Ar}$ B[h]Q), 7.73 (m, 8H, H$_{ortho}$ BArF$_{24}$), 7.70 (m, 1H, H$_{Ar}$ B[h]Q), 7.61 (m, 2H, H$_{Ar}$ B[h]Q), 7.54 (m, 4H, H$_{para}$ BArF$_{24}$), 3.65 (broad m, 1H, [Ir-H]-[SiH$_2$^{n}Bu]), 3.34 (broad m, 1H, [Ir-H]-[SiH$_2$^{n}Bu]), 1.74 (s, 15H, Cp-Me$_5$), −11.55 (bs, 1H, [Ir-H]-[SiH$_2$^{n}Bu]). **^{29}Si [indirect detection from ^{1}H,^{29}Si HMQC; 600/119 MHz, 233 K, CD$_2$Cl$_2$]**: δ = -31.60 (s, [Ir-H]-[SiH$_2$^{n}Bu]).

NMR spectra

¹H NMR
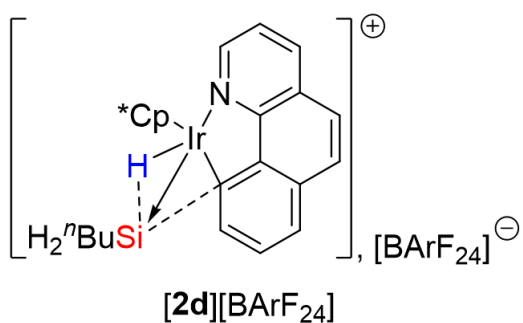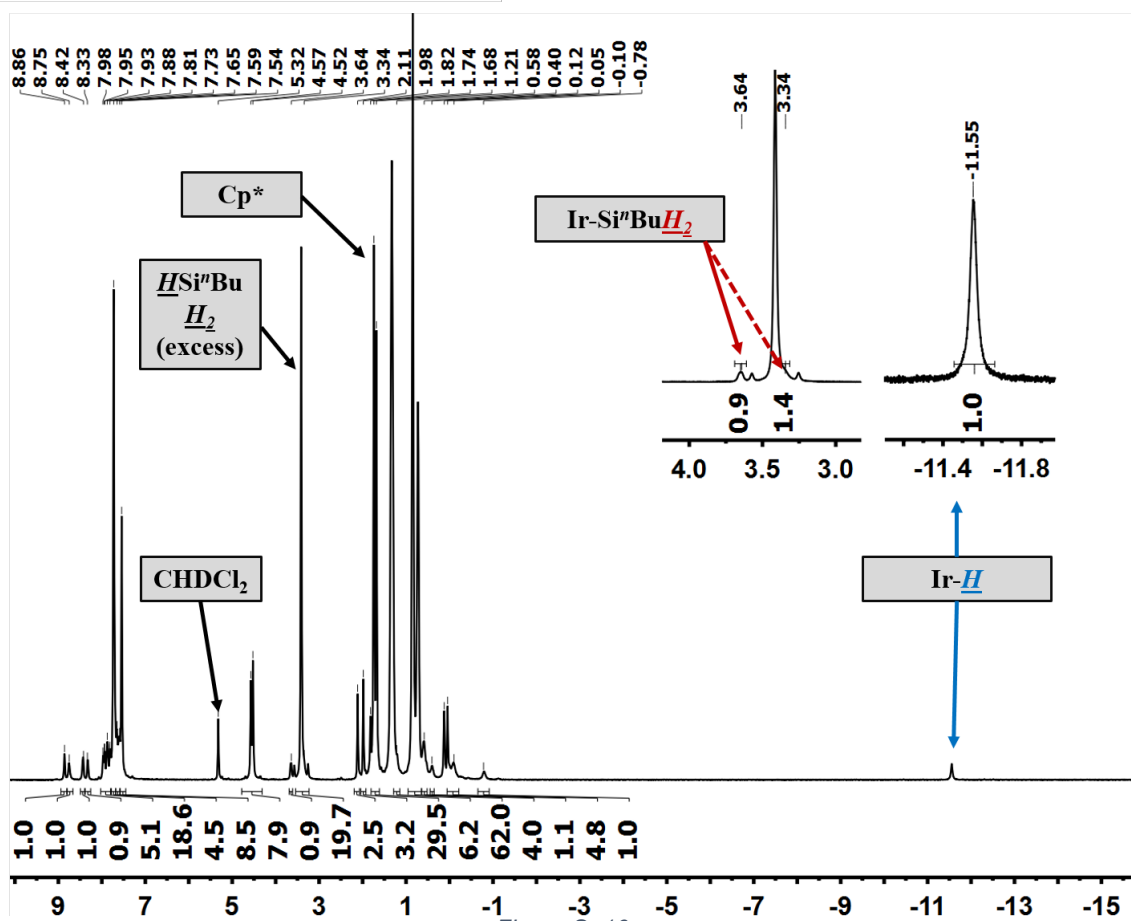
Figure S- 16

^{1}H,^{29}Si HMQC NMR

[2d][BArF$_{24}$]

^{1}H,^{29}Si HMQC (CD$_2$Cl$_2$, 233 K, 600/119 MHz)

Ir-Si^{n}Bu$\underline{H_2}$

Ir-$\underline{Si}^n$BuH$_2$
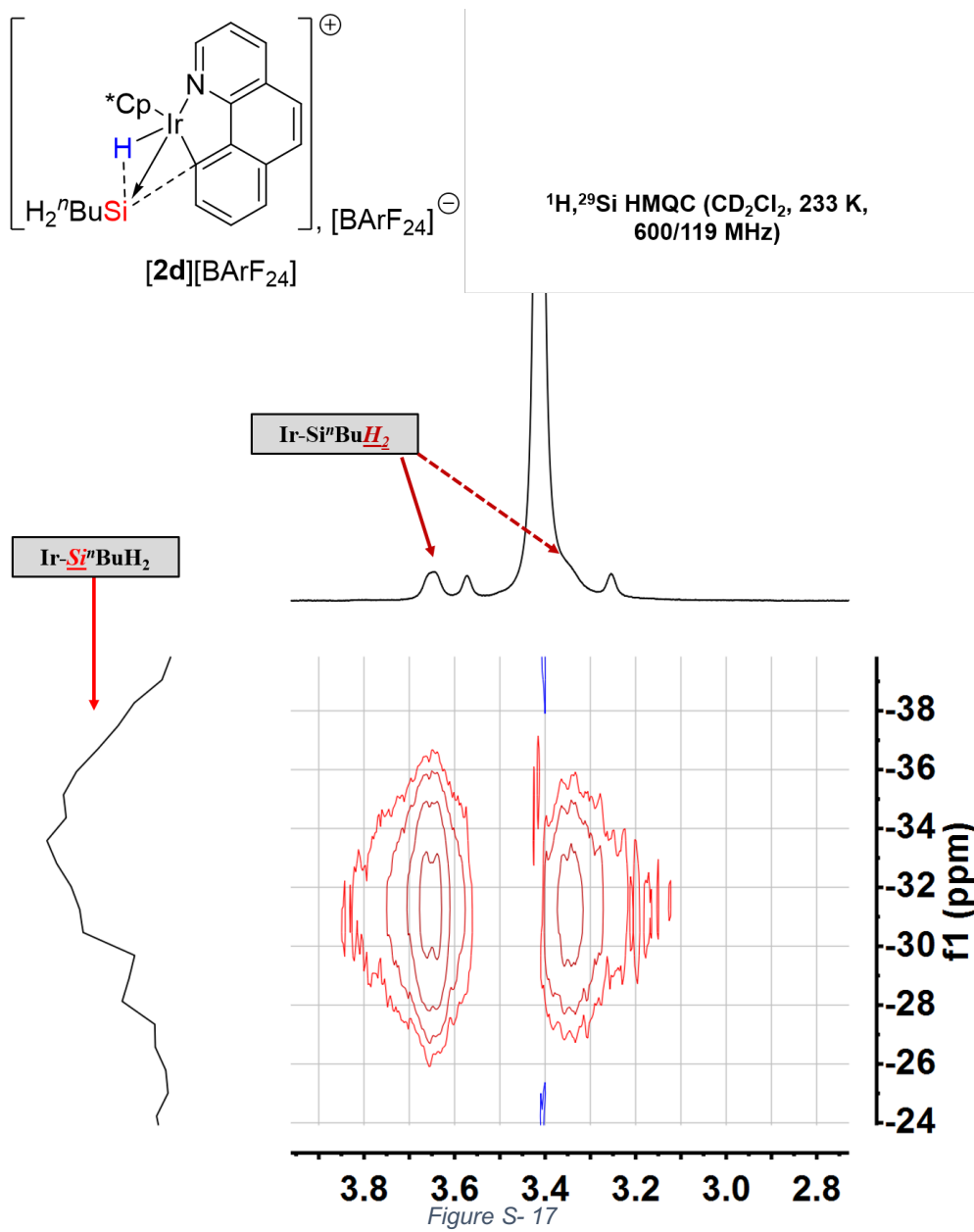
Figure S- 17

Synthesis of [2e][BArF$_{24}$] by Reaction of [1b][BArF$_{24}$] with HSi^{n}HexH$_{2}$: Procedure, NMR Data, and Spectra

Typical procedure for NMR analysis

In a glovebox, HSiHexH$_{2}$ (10.0 μL, 81.1 μmol) was added to a solution of [**1b**][BArF$_{24}$] (29 mg, 20.6 μmol) in CD$_{2}$Cl$_{2}$ (0.65 mL). The resulting solution was shaken and transferred into a J. Young NMR sample tube which was subsequently tightly sealed for analysis. After 25 minutes of reaction, the NMR tube was frozen at < -60 °C. Multinuclear NMR analysis (at -60 °C) of the reaction revealed the total and exclusive conversion of [**1b**][BArF$_{24}$] to [**2e**][BArF$_{24}$], along with the released CH$_{3}$CN (from [**1b**][BArF$_{24}$]) and excess of HSiHexH$_{2}$ (see NMR spectra below).

NMR data

^{1}H NMR (600 MHz, CD$_{2}$Cl$_{2}$) δ 8.46 (dd, J = 8.0, 1.2 Hz, 1H), 7.97 (d, J = 8.7 Hz, 1H), 7.90 (d, J = 8.0 Hz, 1H), 7.84 (t, J = 7.6 Hz, 1H), 7.74 (d, J = 8.7 Hz, 1H), 7.64 (dd, J = 7.9, 5.2 Hz, 1H), 3.72 – 3.66 (m, 1H), 3.40 (s, 1H), 1.76(s, 15H), 0.65(m, 1H), 0.1(m, 1H) -0.03 (s, 1H), -0.78 (s, 1H), -11.51 (s, 1H).

BArF$_{24}$

CH$_3$CN
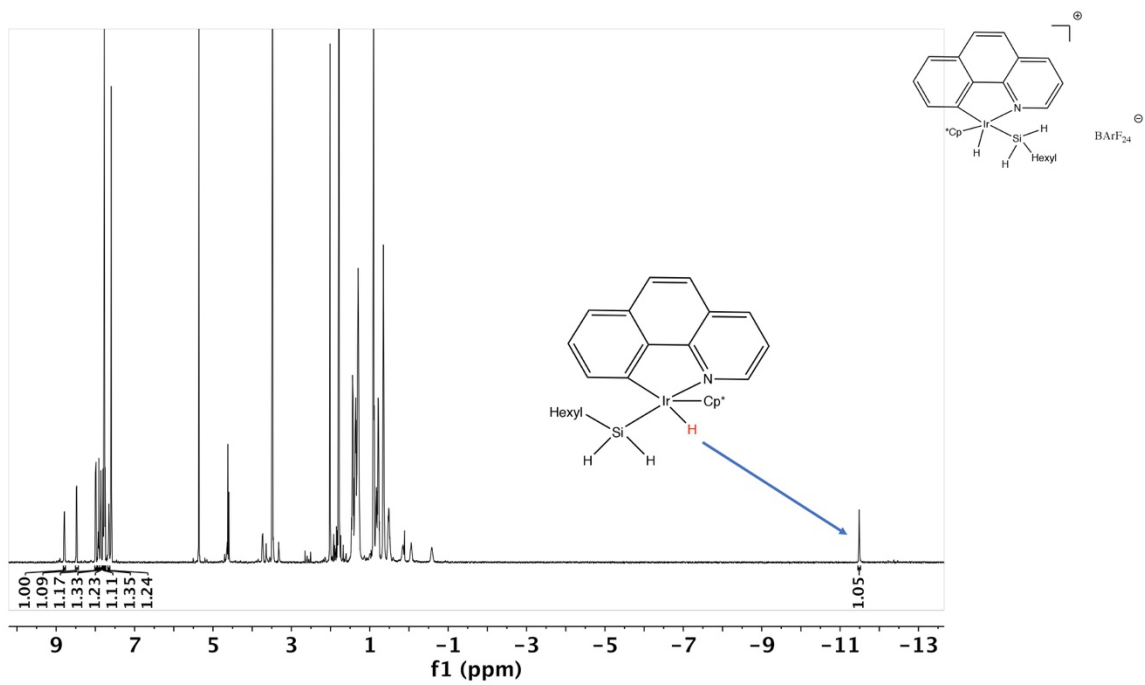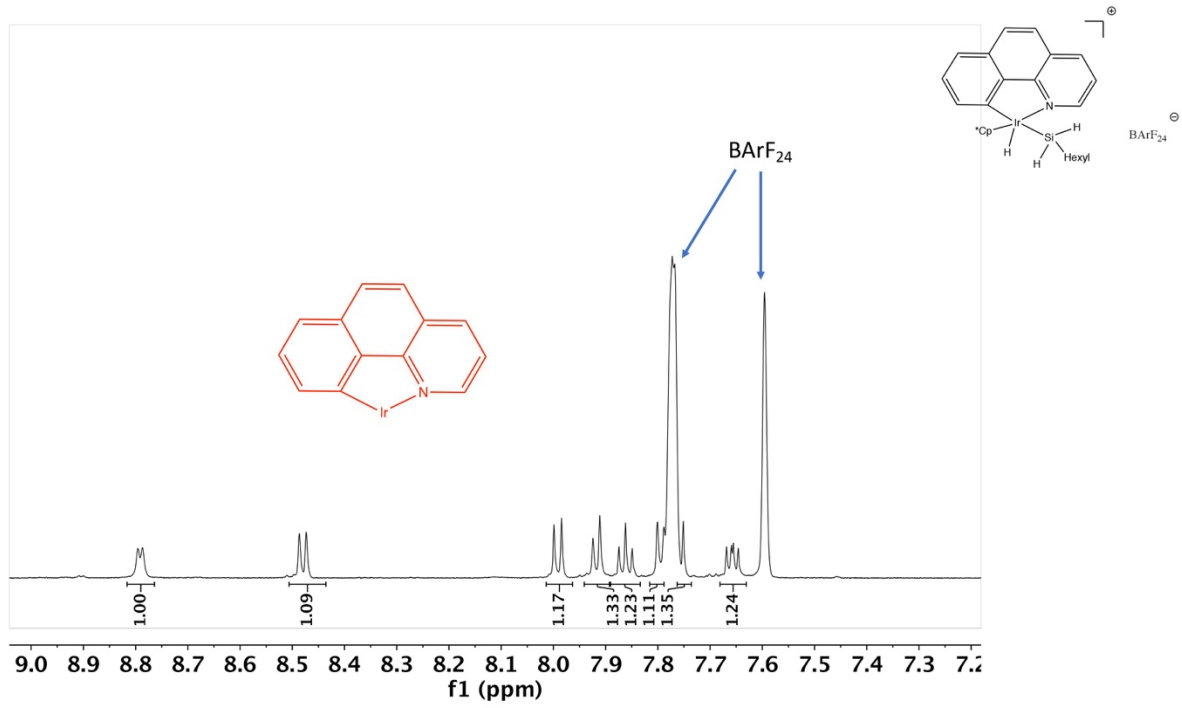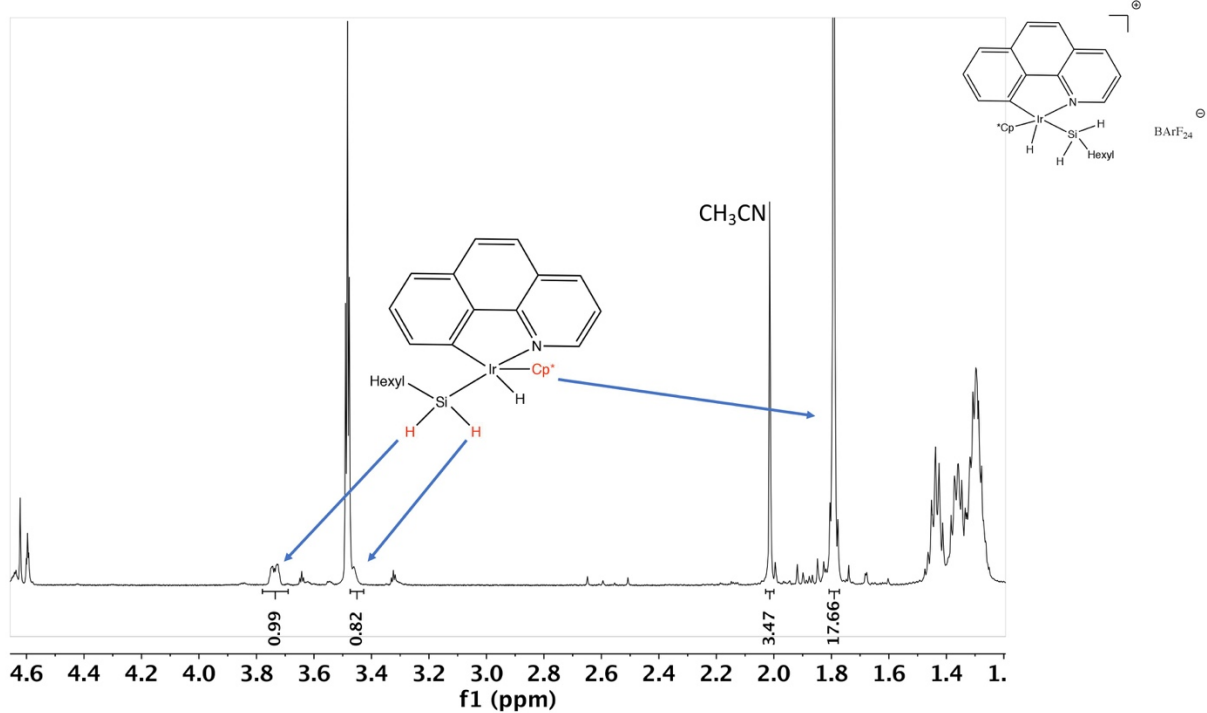
HMQC ^{1}H-^{29}Si

HMQC ^{1}H-^{29}Si

HMQC ^{1}H-^{29}Si

153

154

NOESY

NOESY

HSQC

COSY

HSQC

158
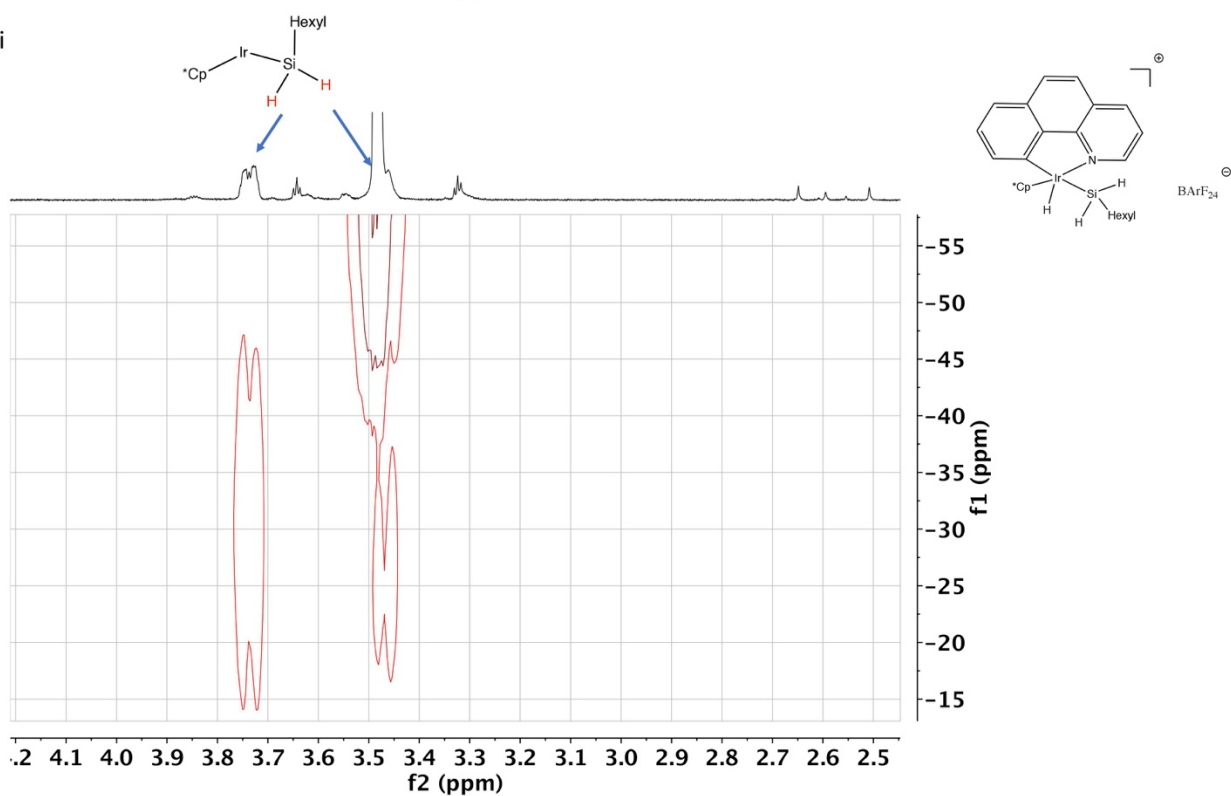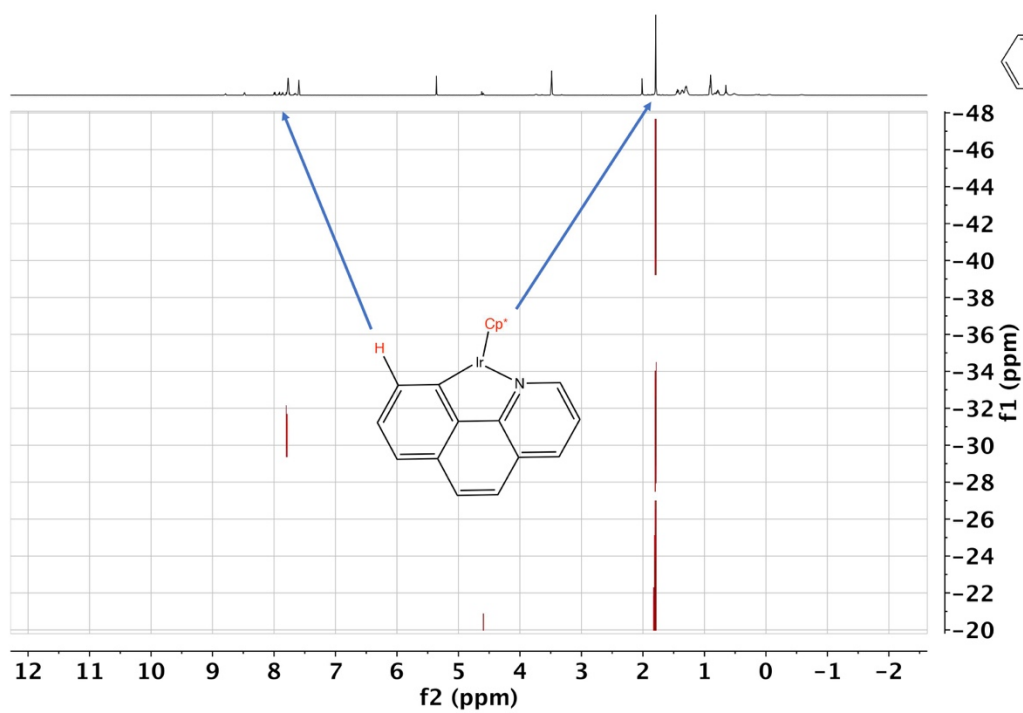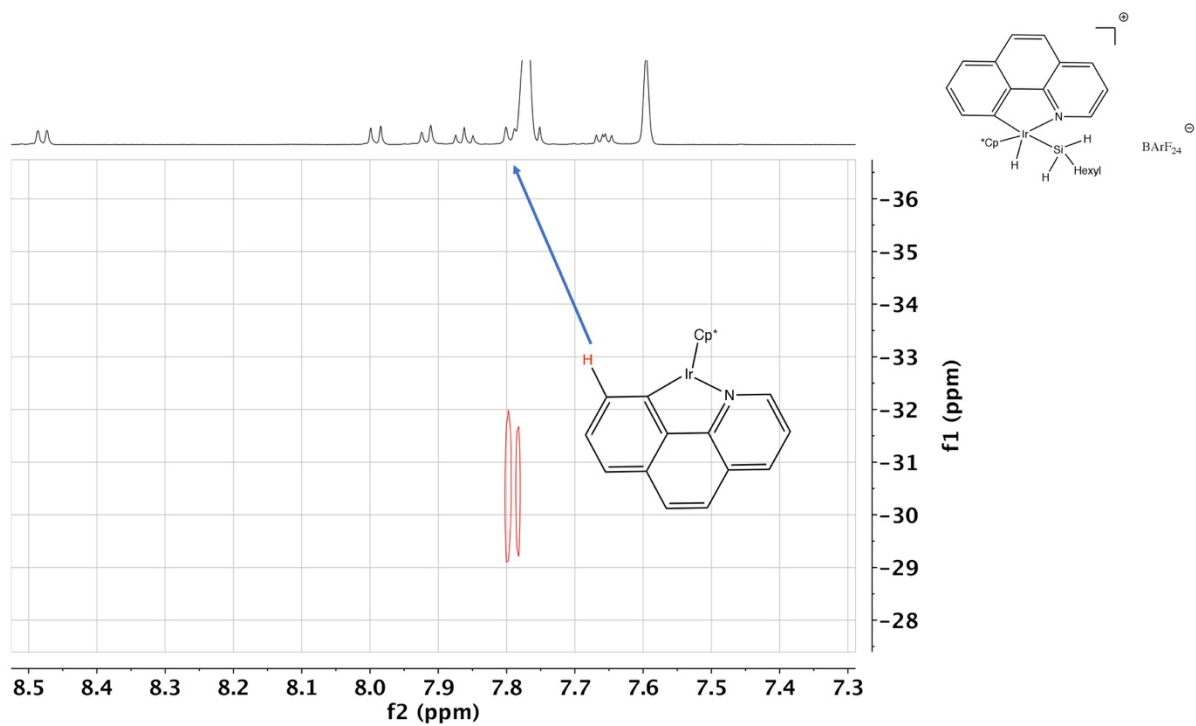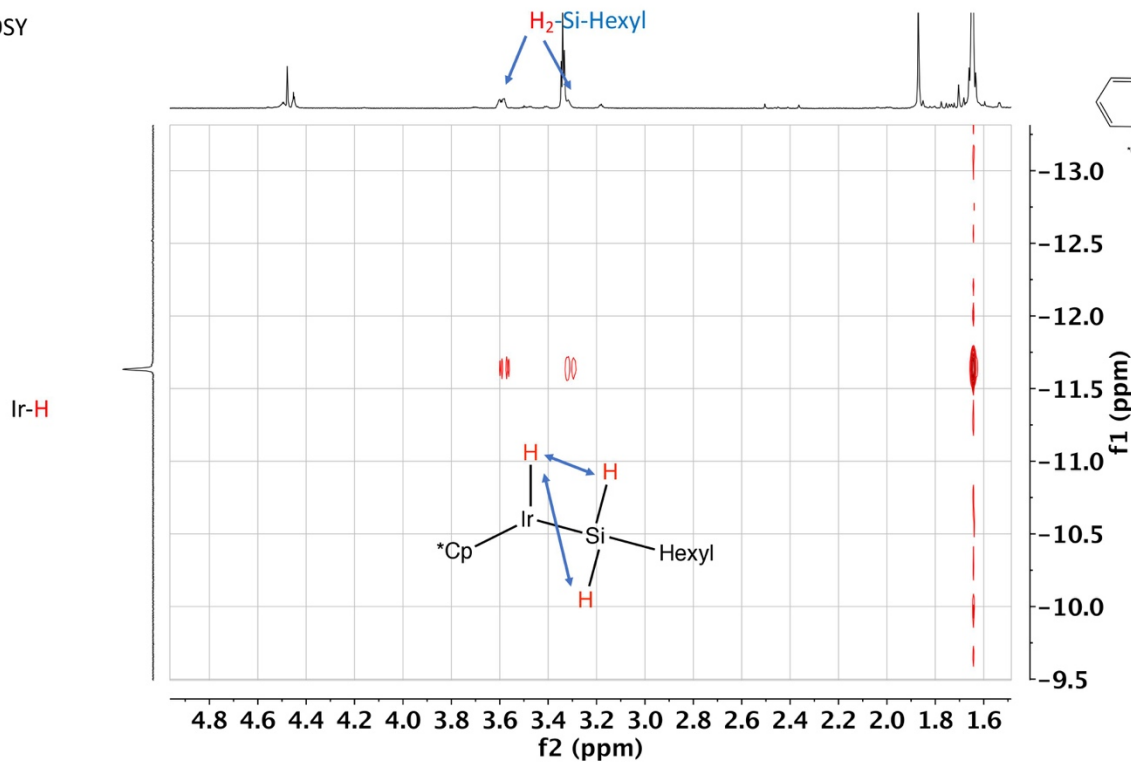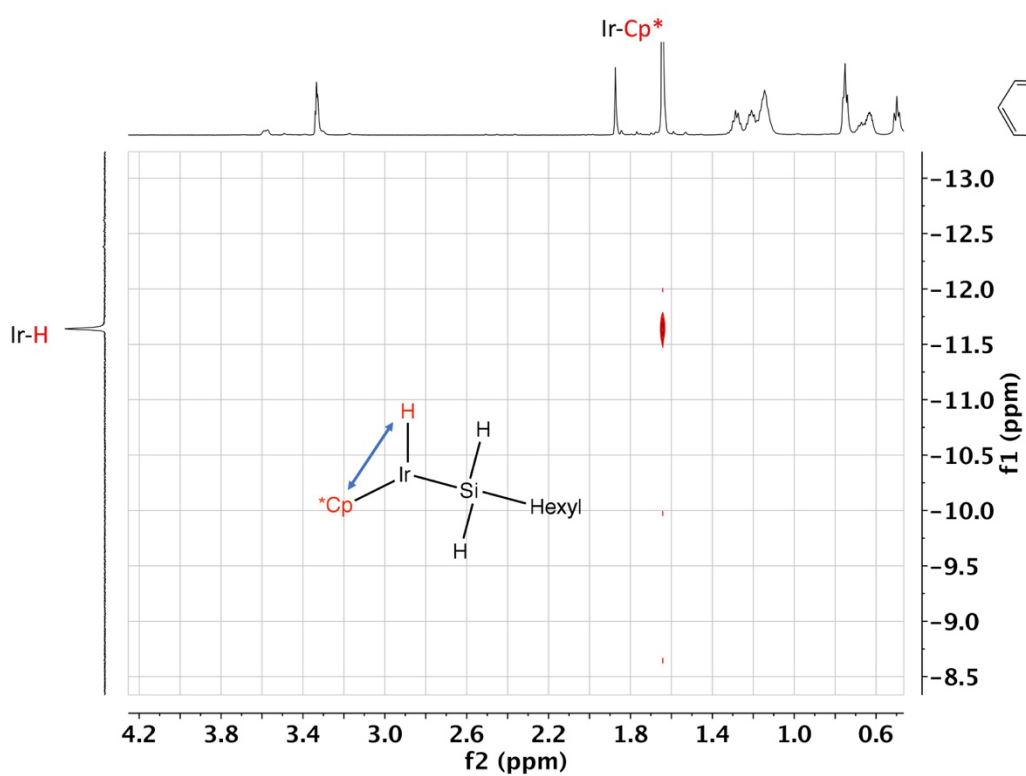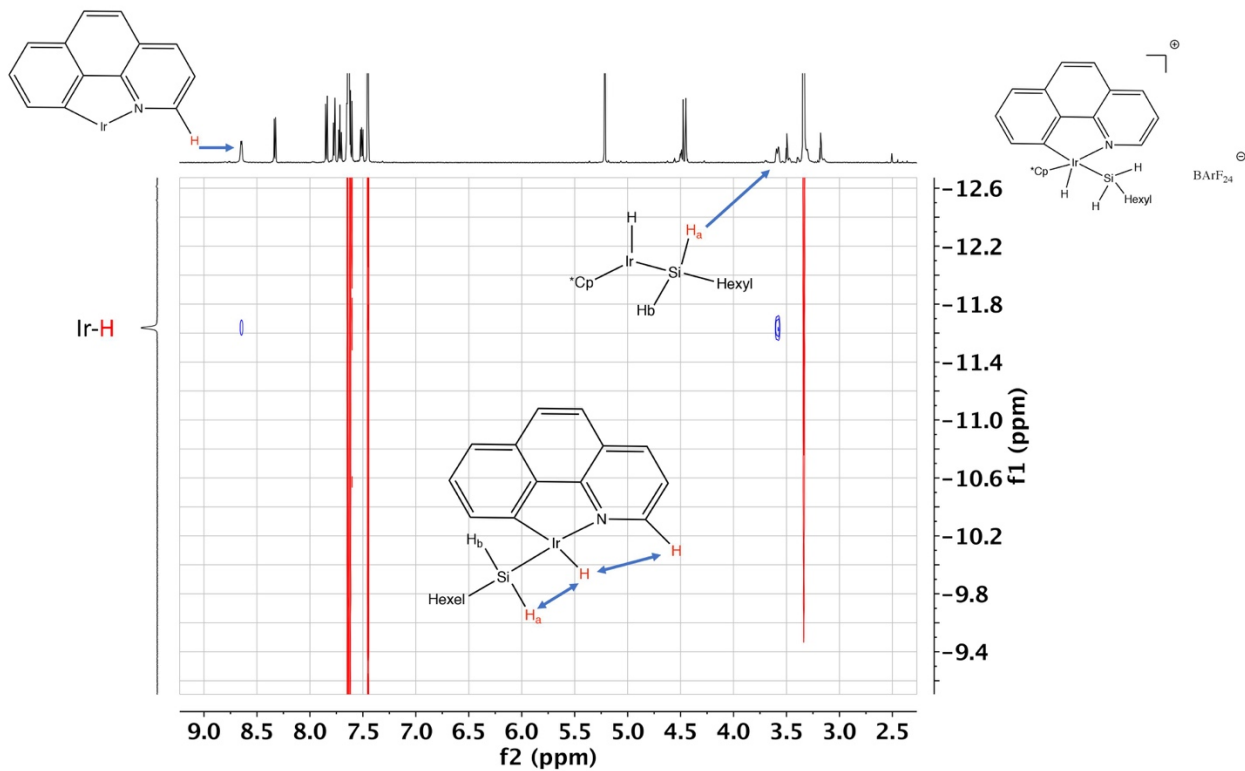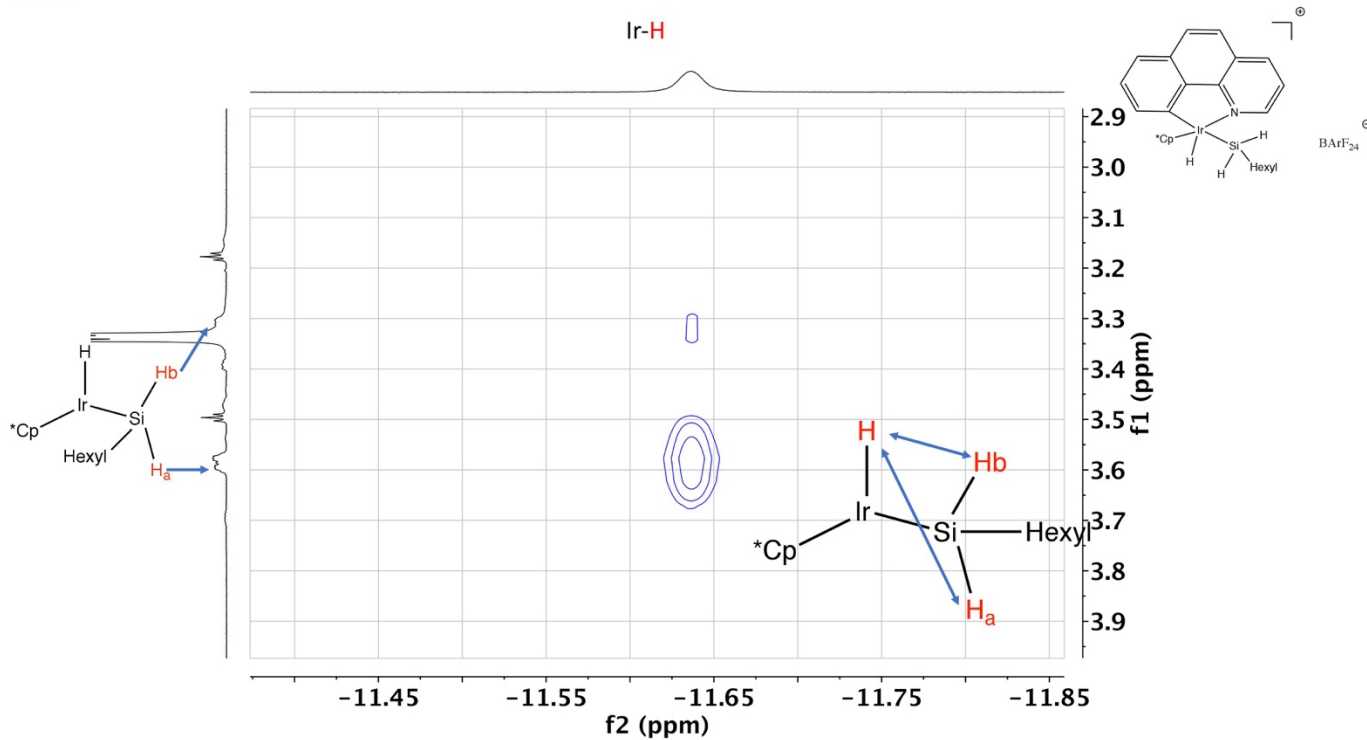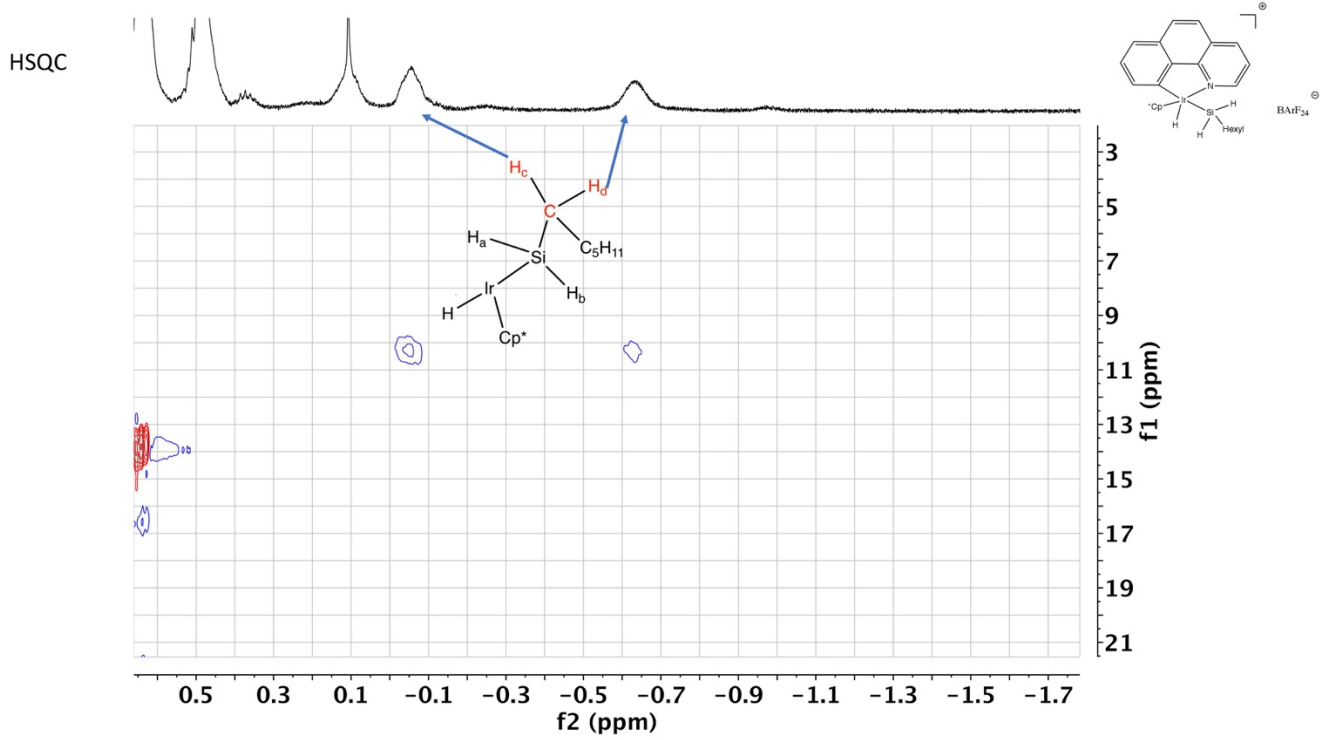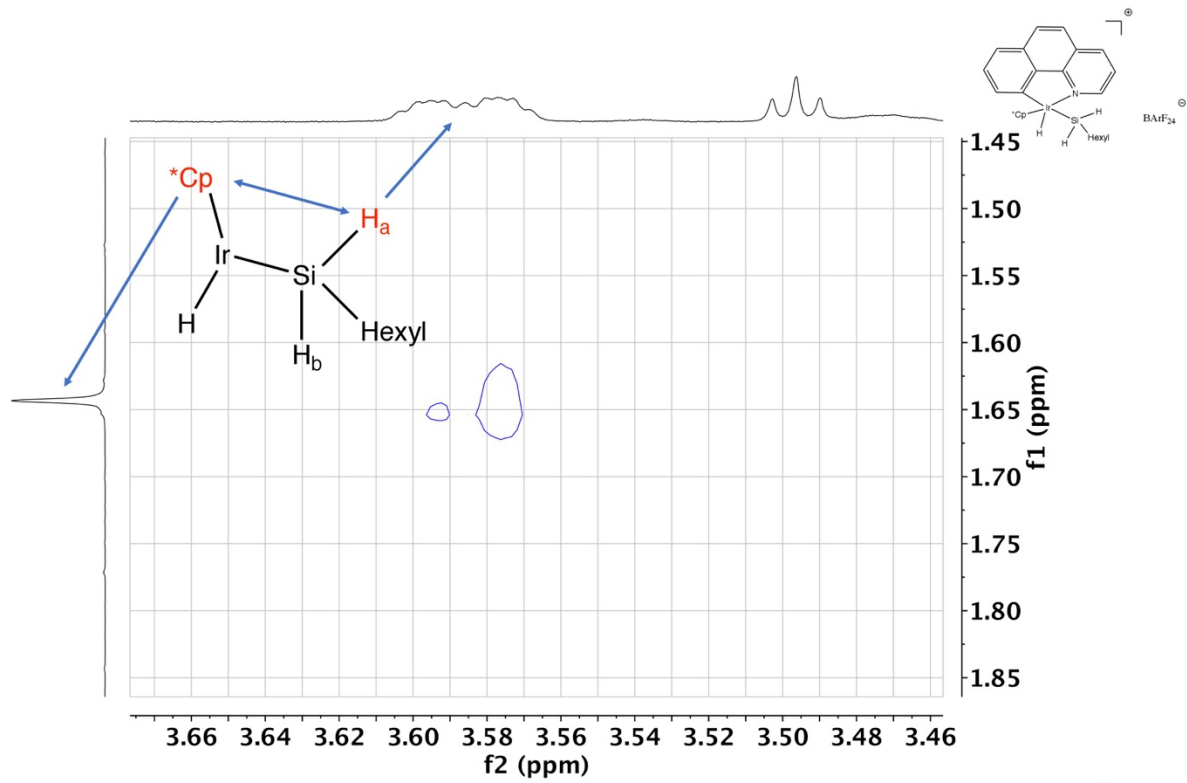
COSY
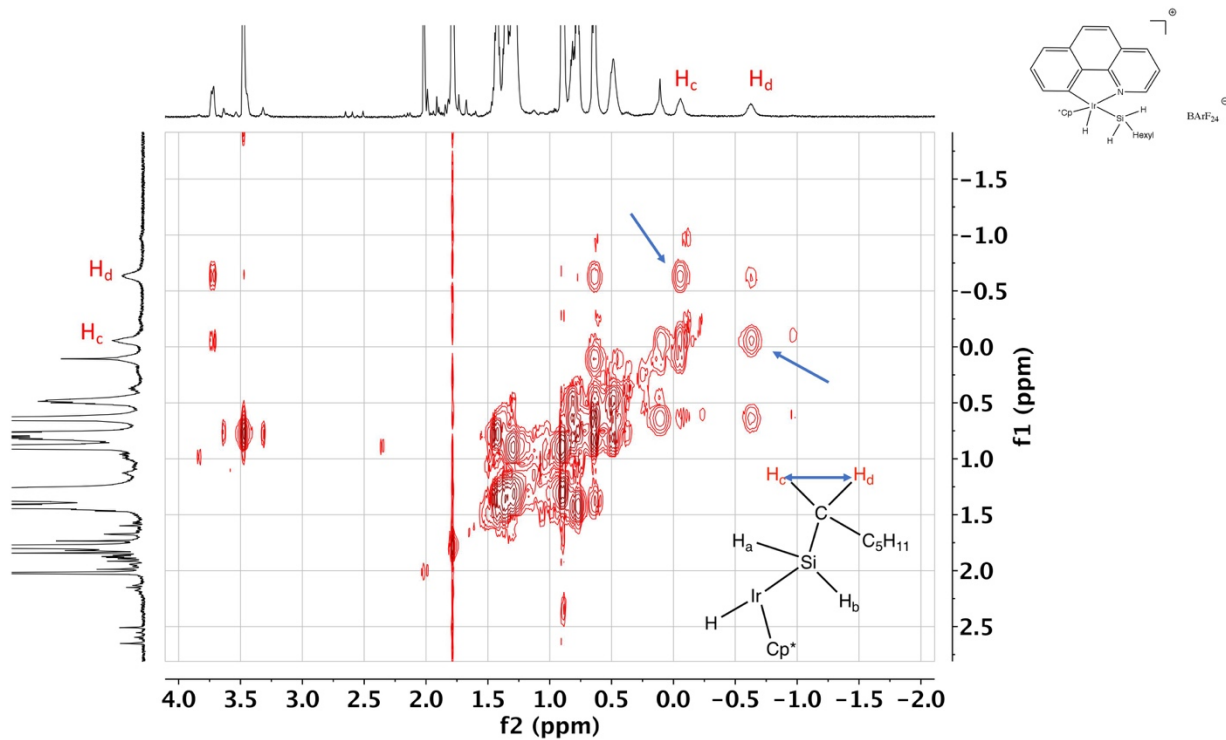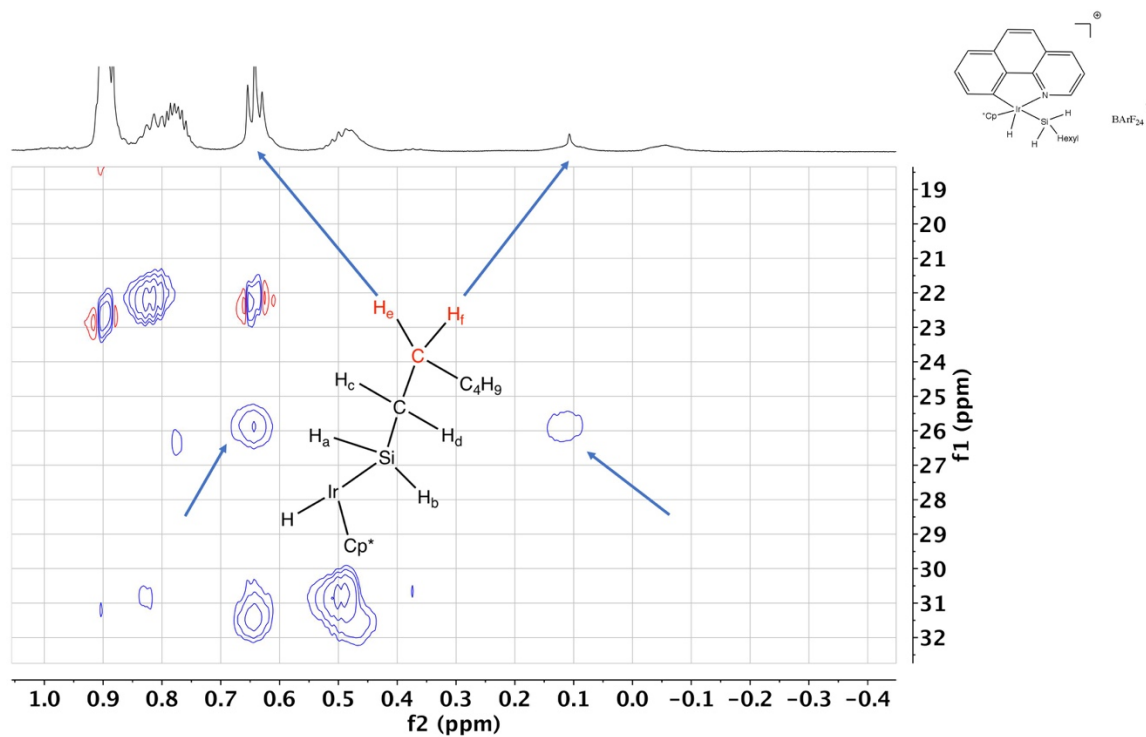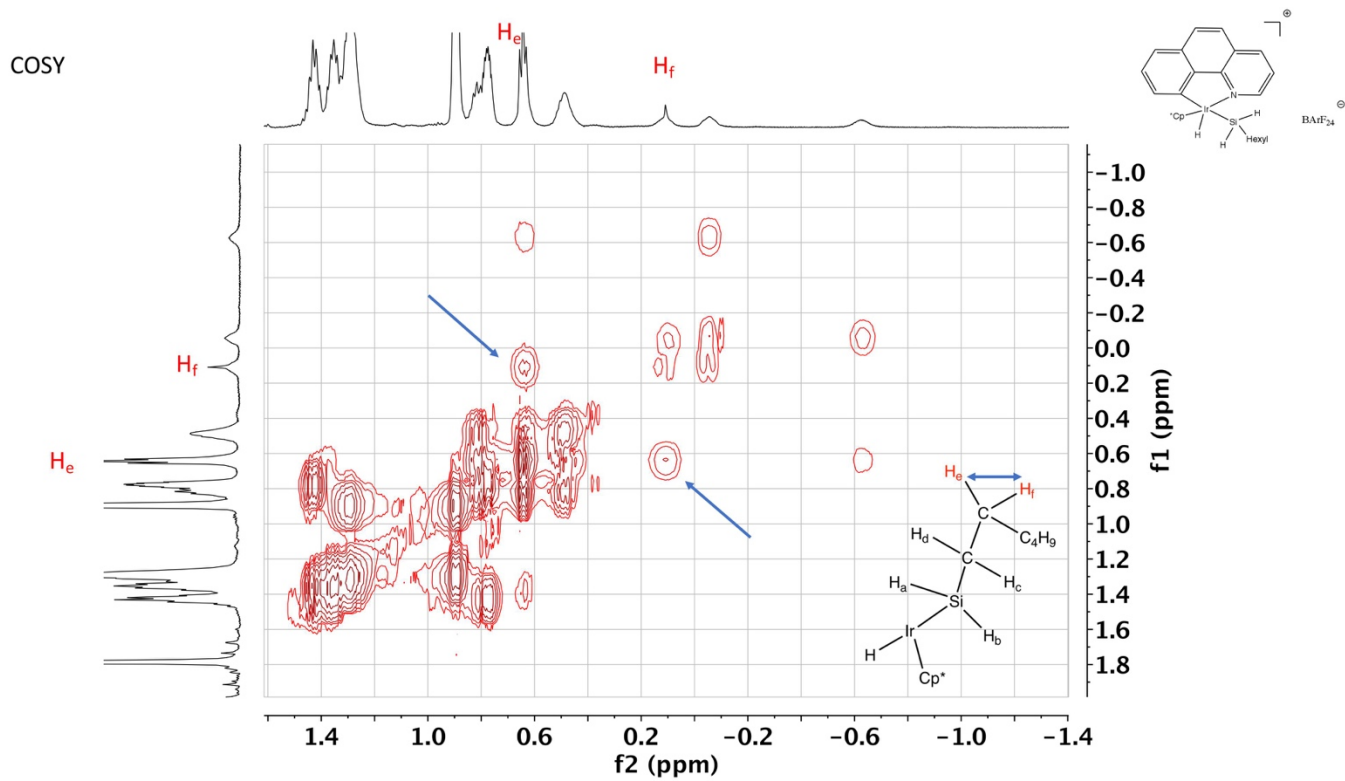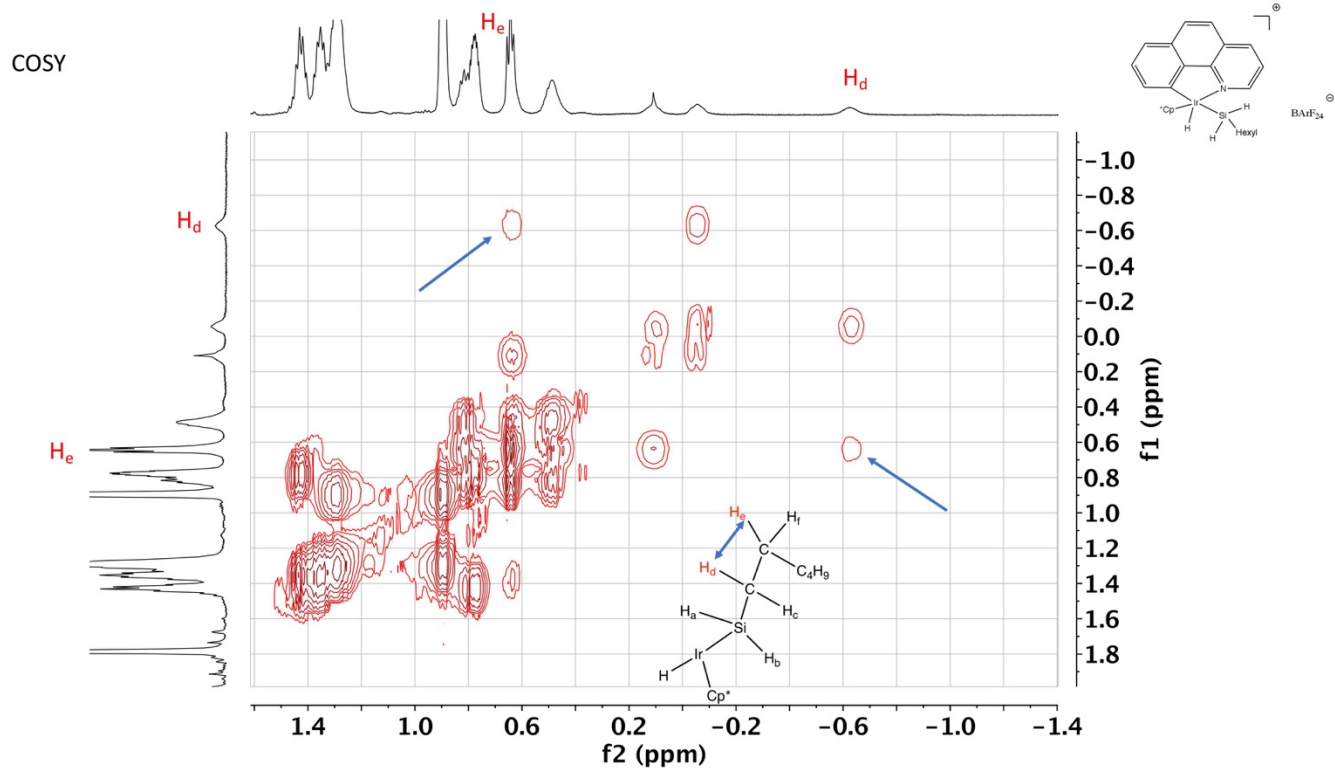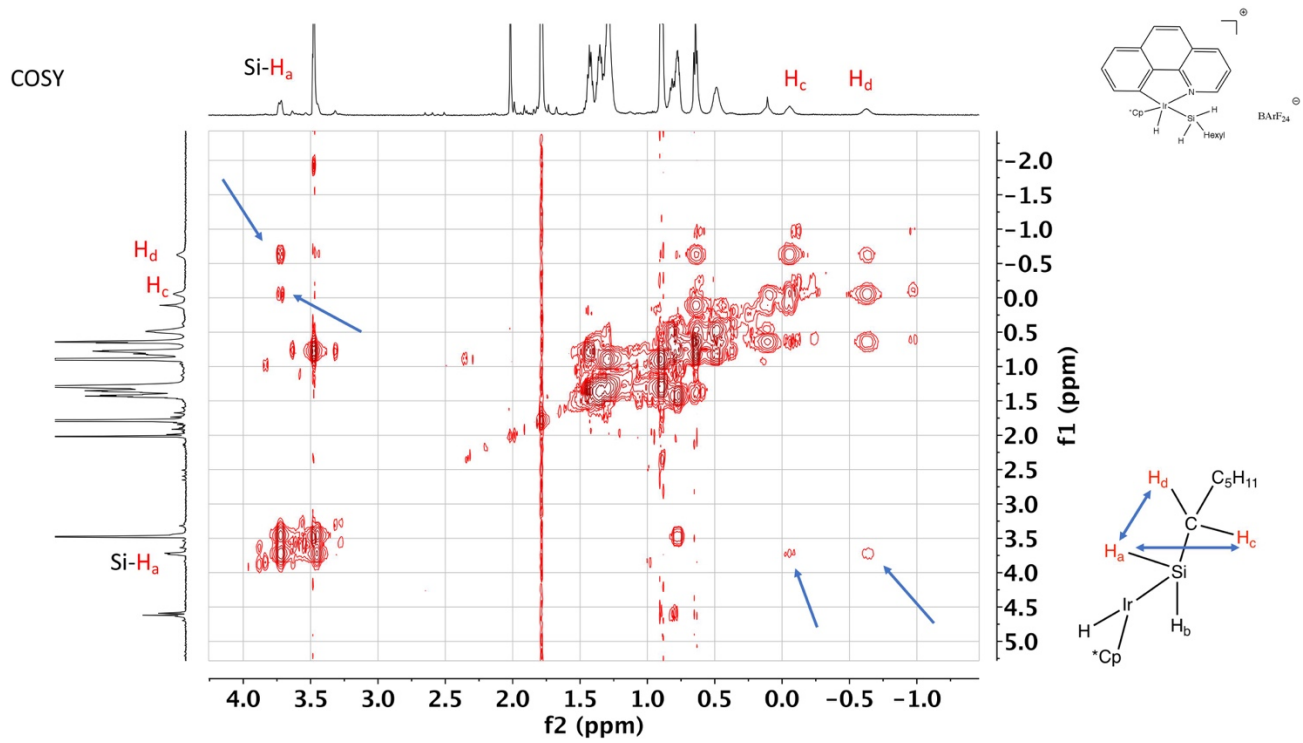
Synthesis of [2f][BArF$_{24}$] by Reaction of [1b][BArF$_{24}$] with SiEt$_2$H: Procedure, NMR Data, and Spectra

Typical procedure for NMR analysis

In a glovebox, Et$_2$SiH (10.0 μL, 81.1 μmol) was added to a solution of [**1b**][BArF$_{24}$] (29 mg, 20.6 μmol) in CD$_2$Cl$_2$ (0.65 mL). The resulting solution was shaken and transferred into a J. Young NMR sample tube which was subsequently tightly sealed for analysis. After 25 minutes of reaction, the NMR tube was frozen at < -60 °C. Multinuclear NMR analysis (at -60 °C) of the reaction revealed the total and exclusive conversion of [**1b**][BArF$_{24}$] to [**2f**][BArF$_{24}$] and excess of Et$_2$SiH (see NMR spectra below).

NMR data

^{1}H NMR (600 MHz, CD$_2$Cl$_2$) δ 8.82 (dd, J = 5.6, 1.3 Hz, 1H), 8.46 (dd, J = 8.0, 1.3 Hz, 1H), 8.00 (d, J = 8.7 Hz, 1H), 7.92 (dd, J = 6.8, 1.9 Hz, 1H), 7.88 – 7.84 (m, 1H), 7.75 (d, J = 8.7 Hz, 1H), 7.67 – 7.61 (m, 2H), 4.14 – 4.08 (m, 1H), 1.78 (s, 15H), 0.19 (t, J = 7.9 Hz, 3H), -0.01 – -0.15 (m, 1H), -0.44 (dqd, J = 15.6, 7.9, 3.5 Hz, 1H), -11.30 (s, 1H).
^{29}Si NMR (600 MHz, CD$_2$Cl$_2$) δ 0.00 ppm

CD$_2$Cl$_2$

Cp*

H-Si

Et-Si

BArF$_{24}$

0.98 0.91 1.11 1.43 2.33 1.79 1.34 0.94 17.19 3.46 1.20 1.07

8 7 6 5 4 3 2 1 0 −1

H-Ir

1.00

0.7 −10.9 −11.1 −11.3 −11.5 −11.7 −11.9 −12.1 −12.3

f1 (ppm)

BArF$_{24}$

BArF$_{24}$

[{C,N} ligand]

^{1}H-^{29}Si HMQC

HMQC

HSQC

Cp*-Ir

N,C ligand

BArF$_{24}$ $^{\ominus}$

NOESY

NOESY

H-Si-Ir

Ir-Cp*
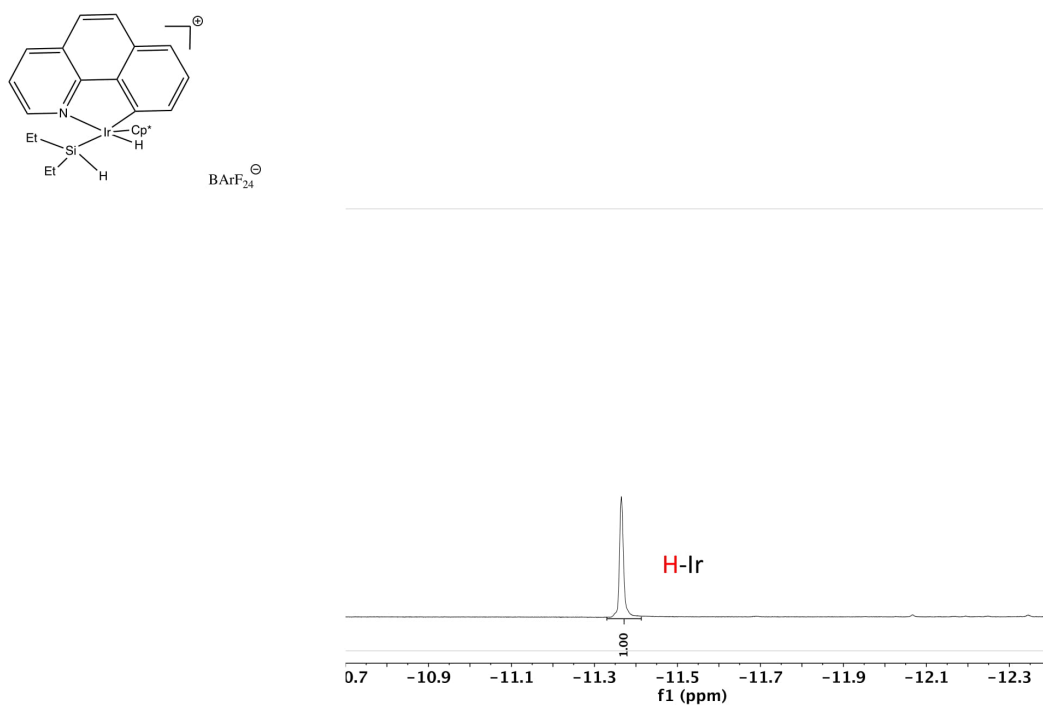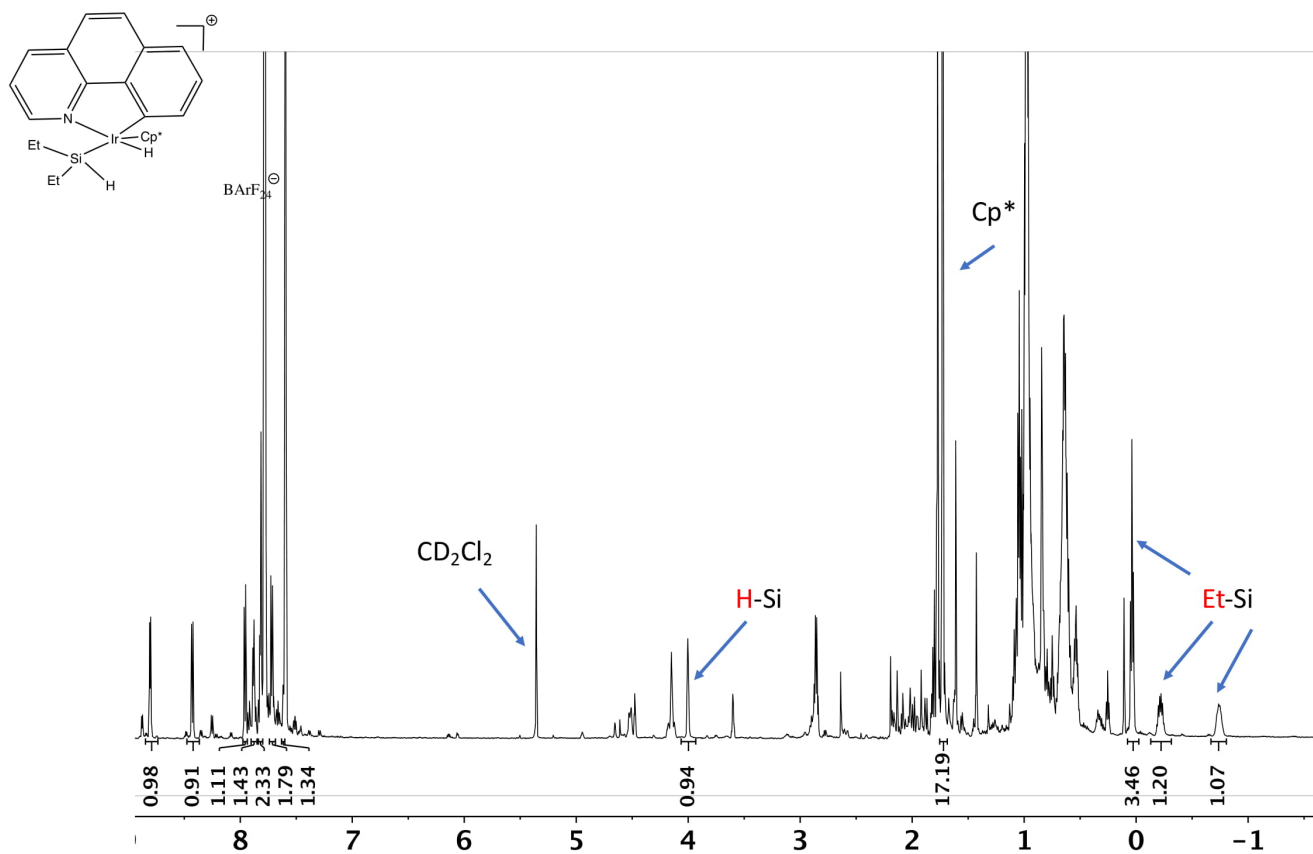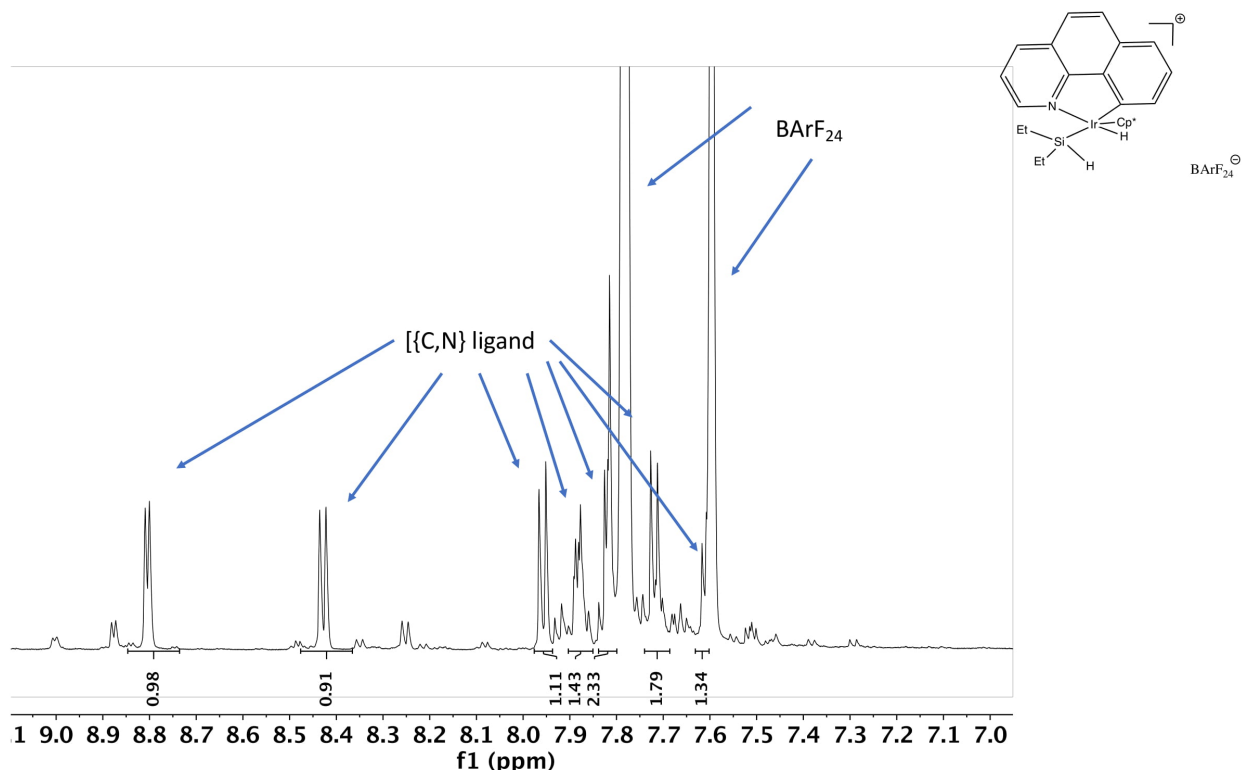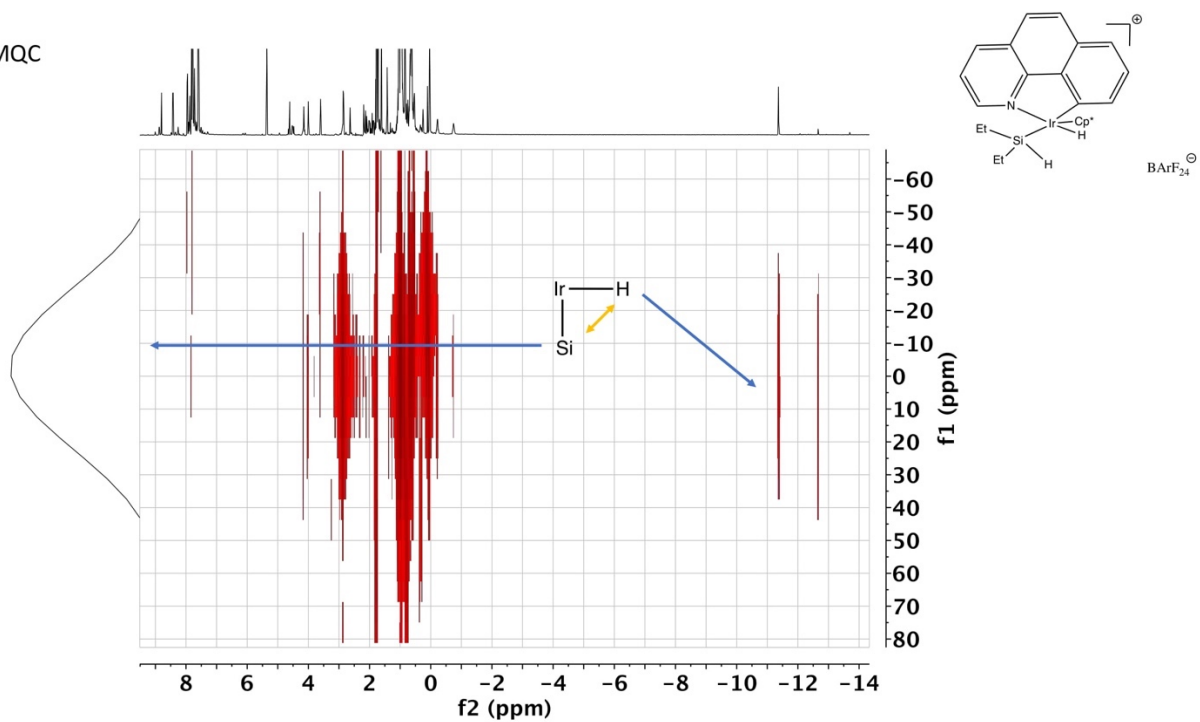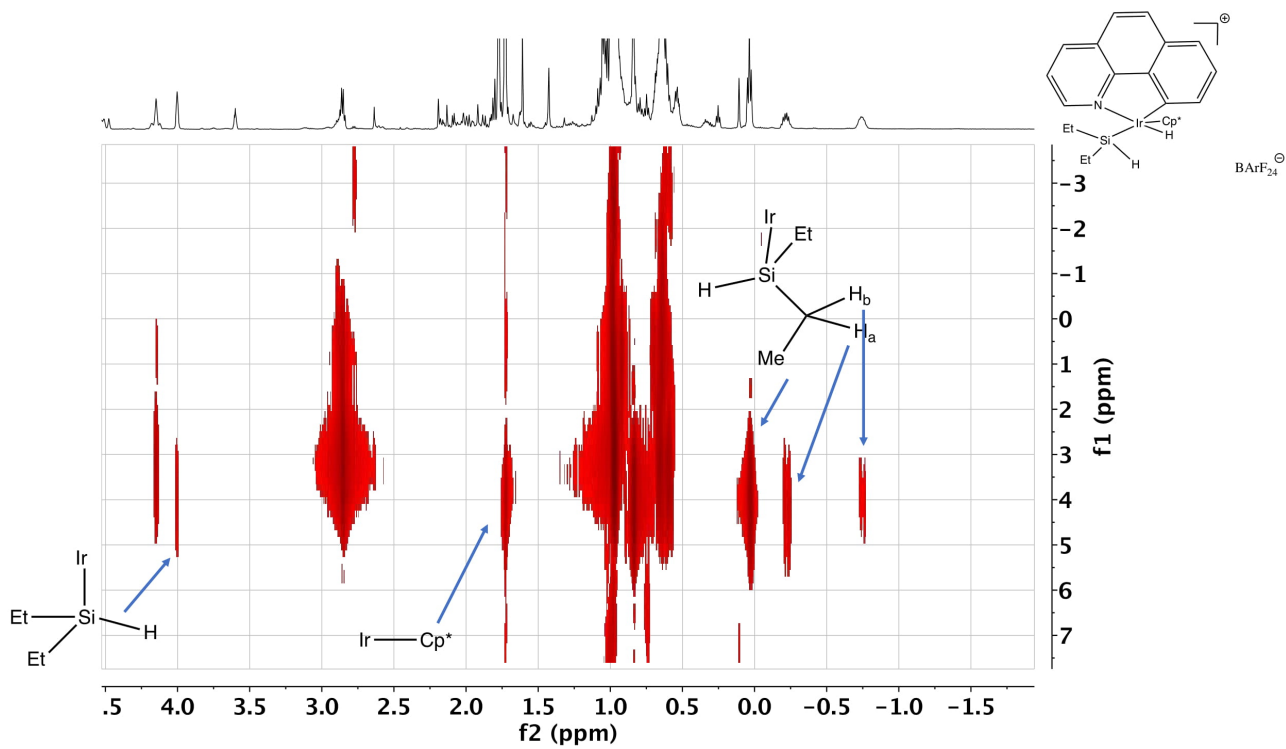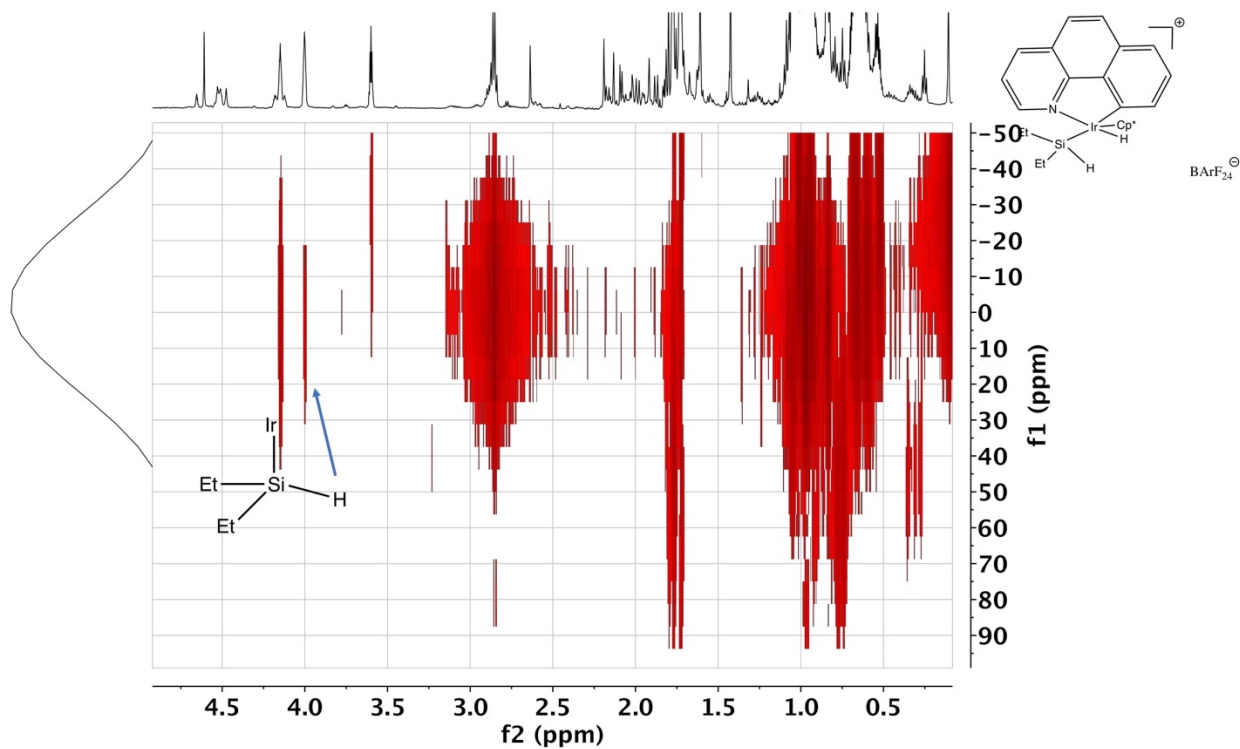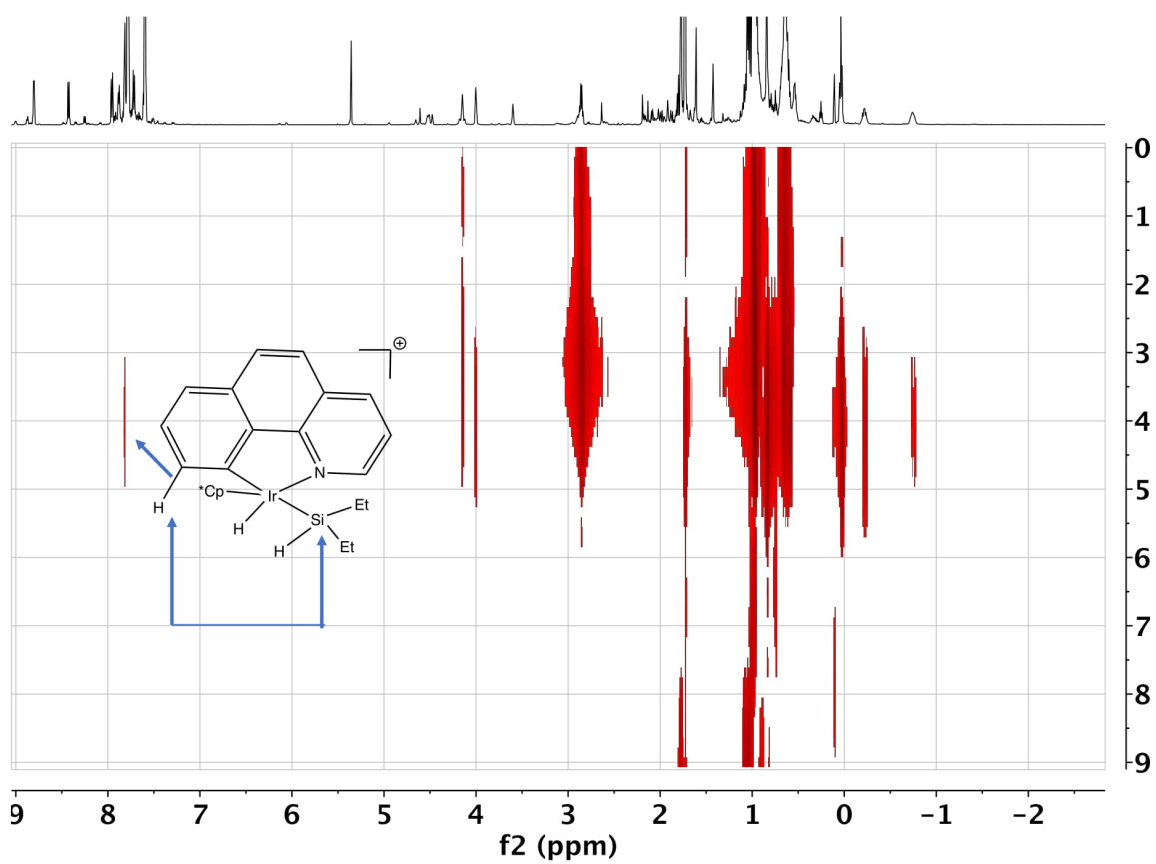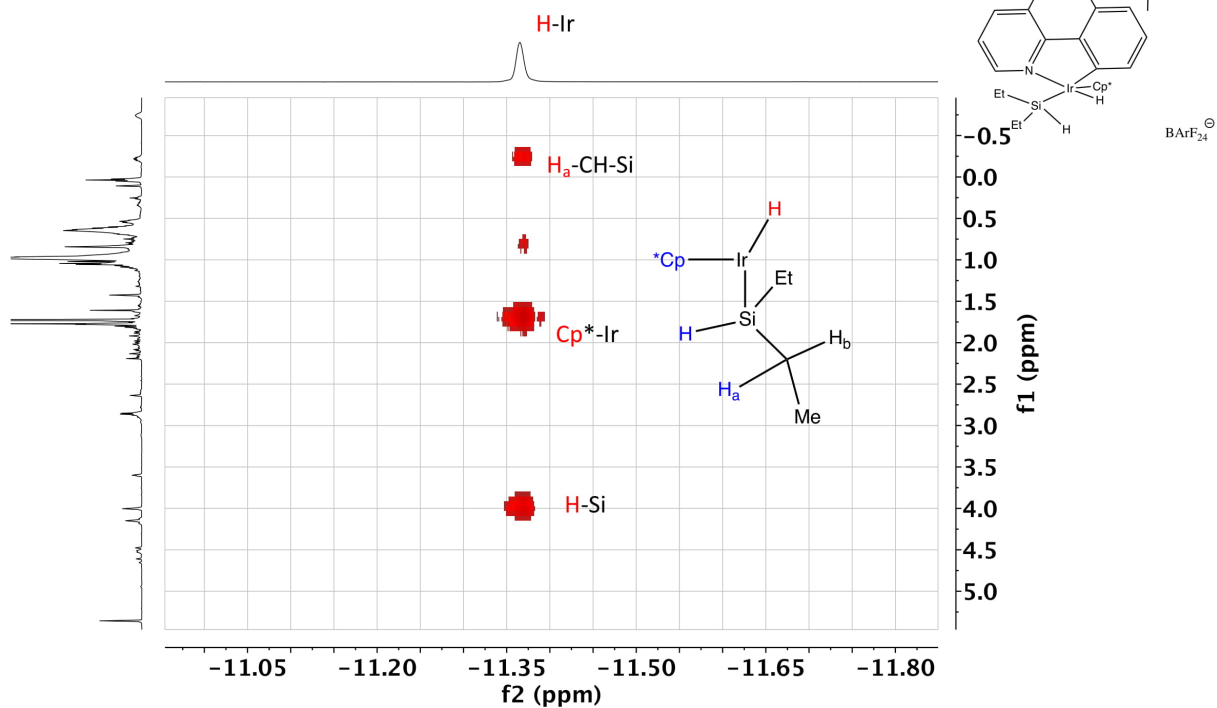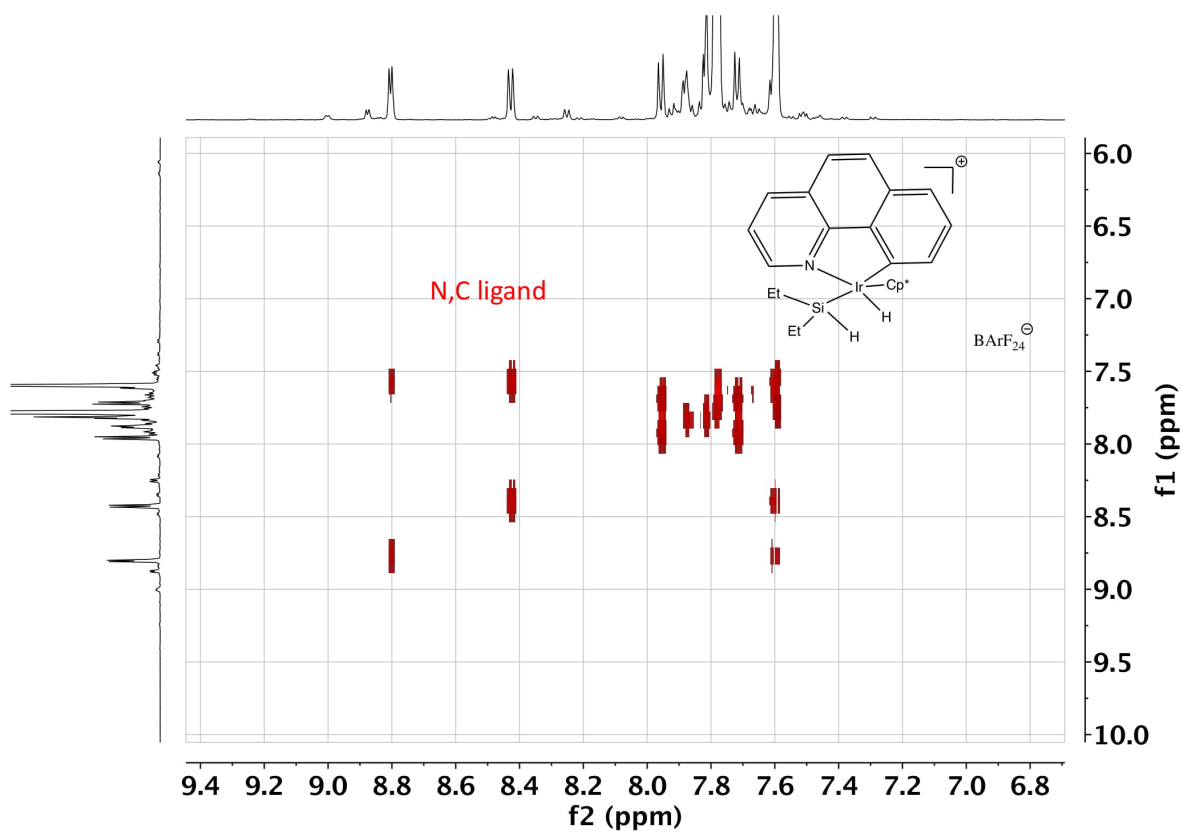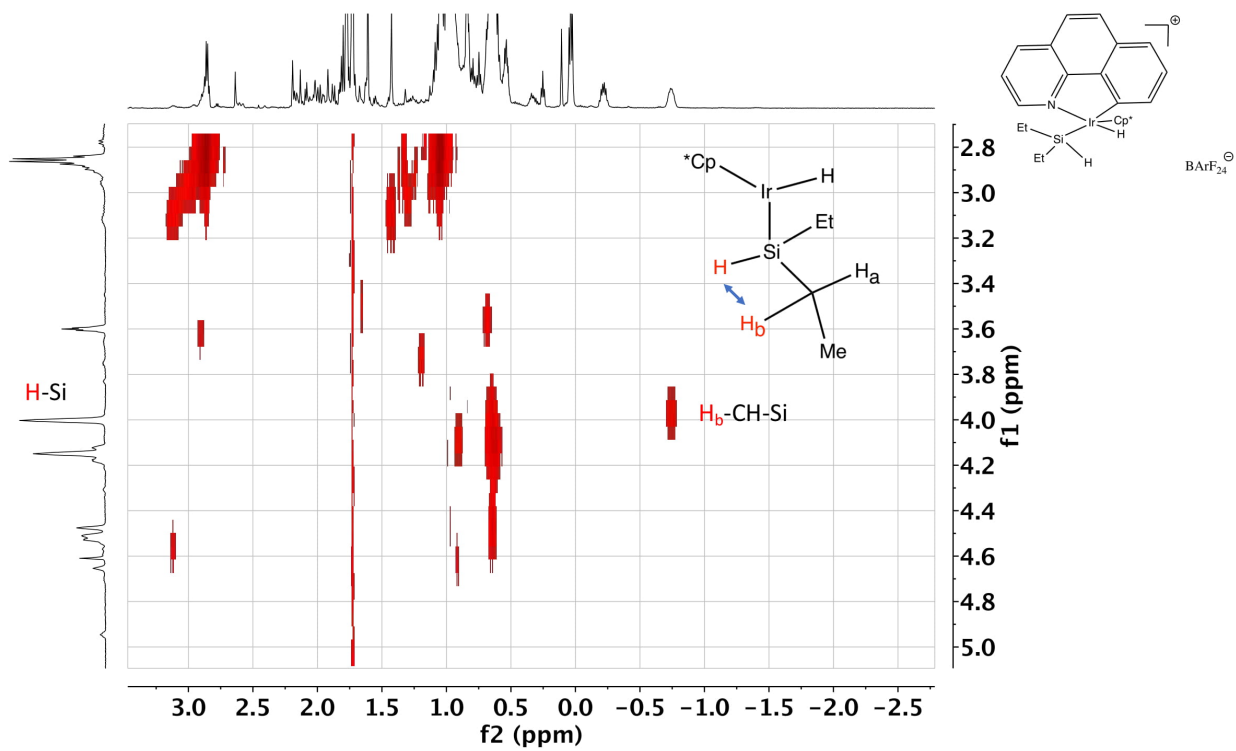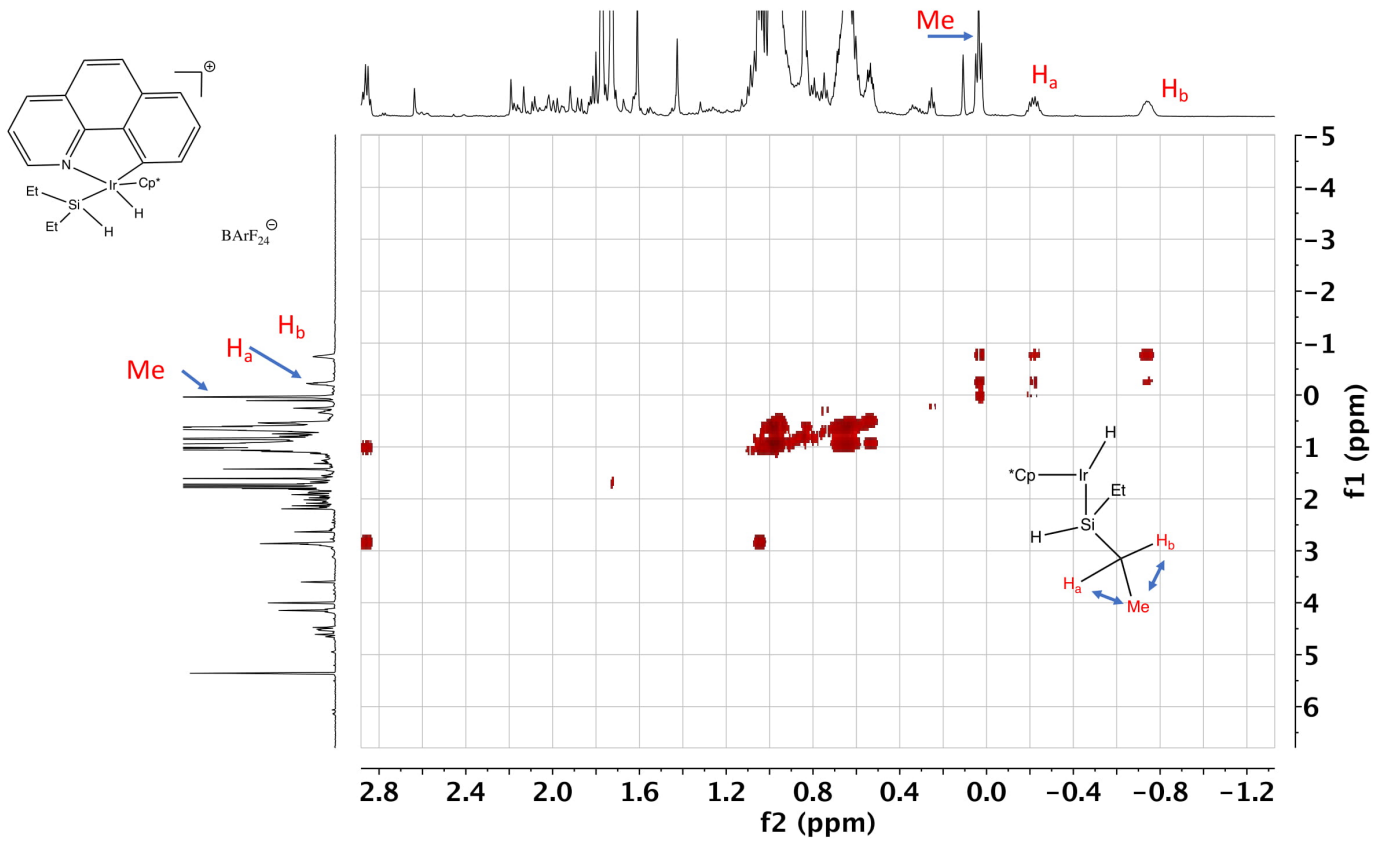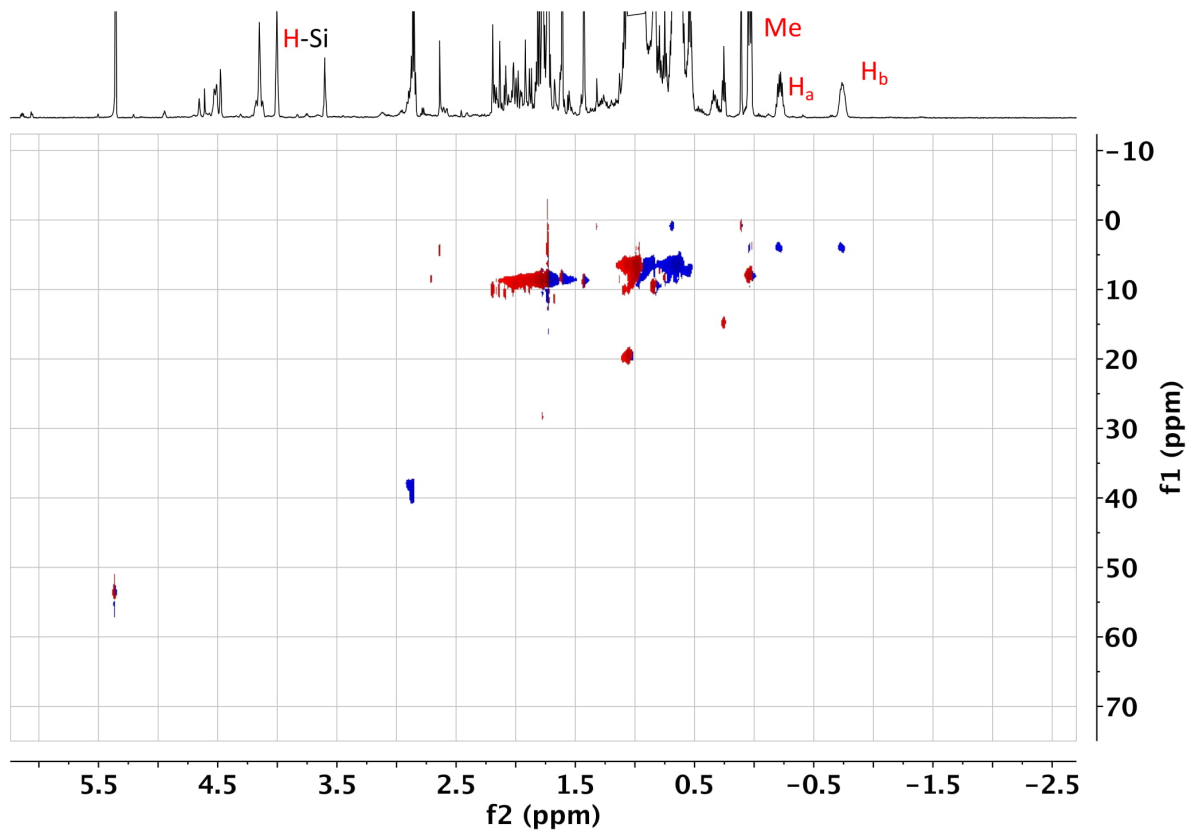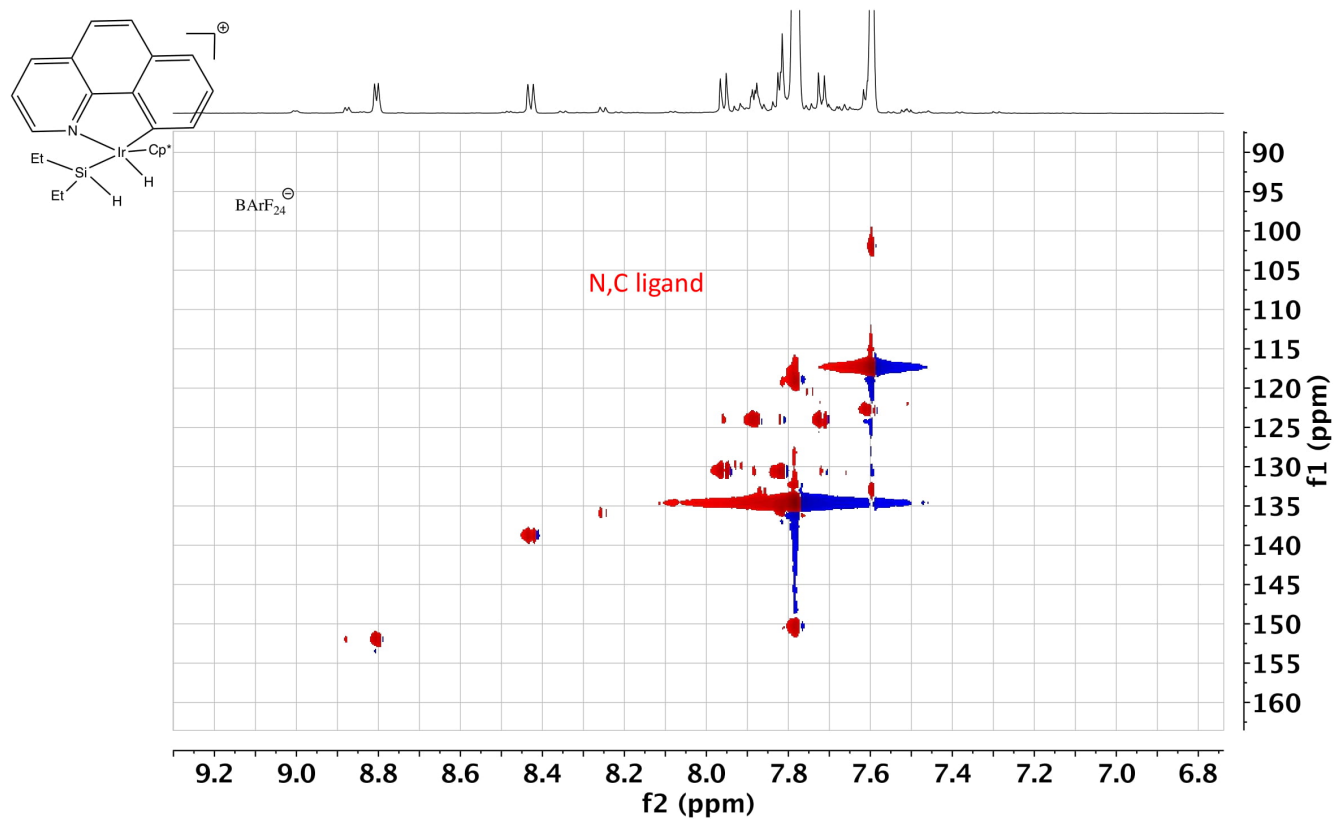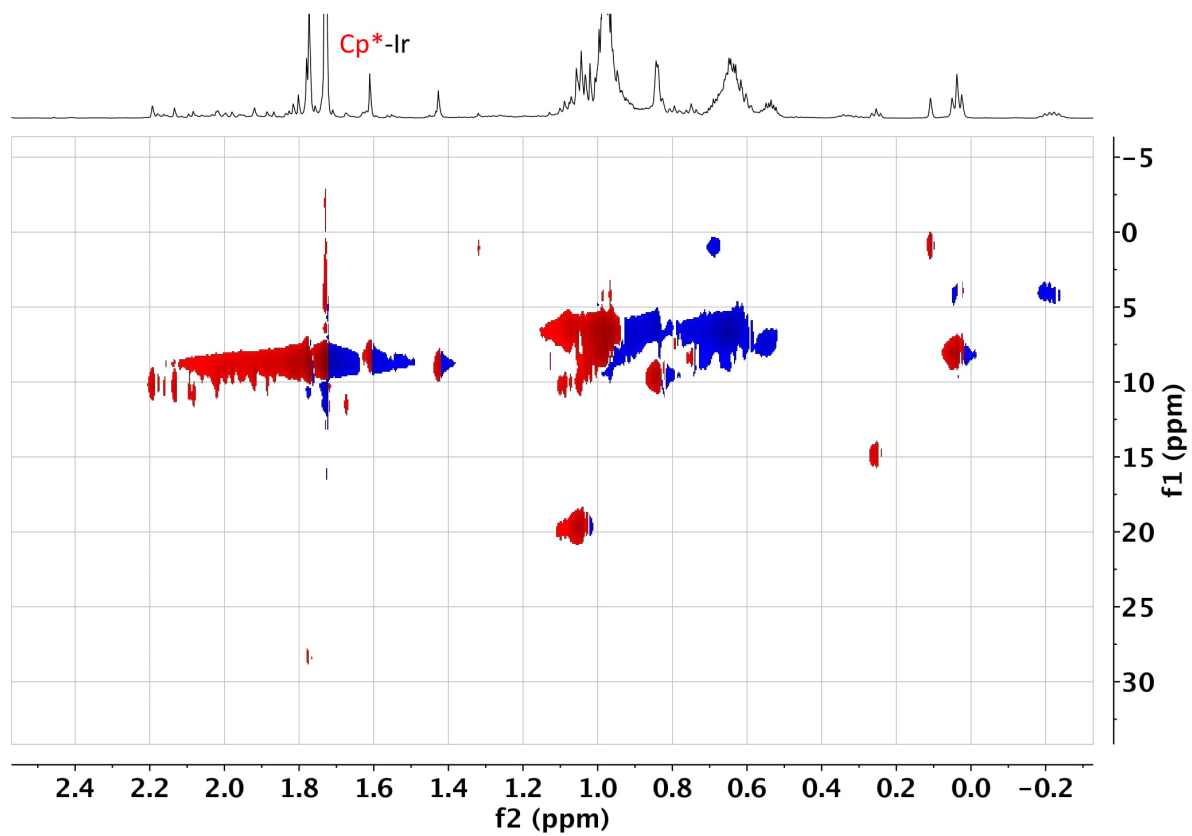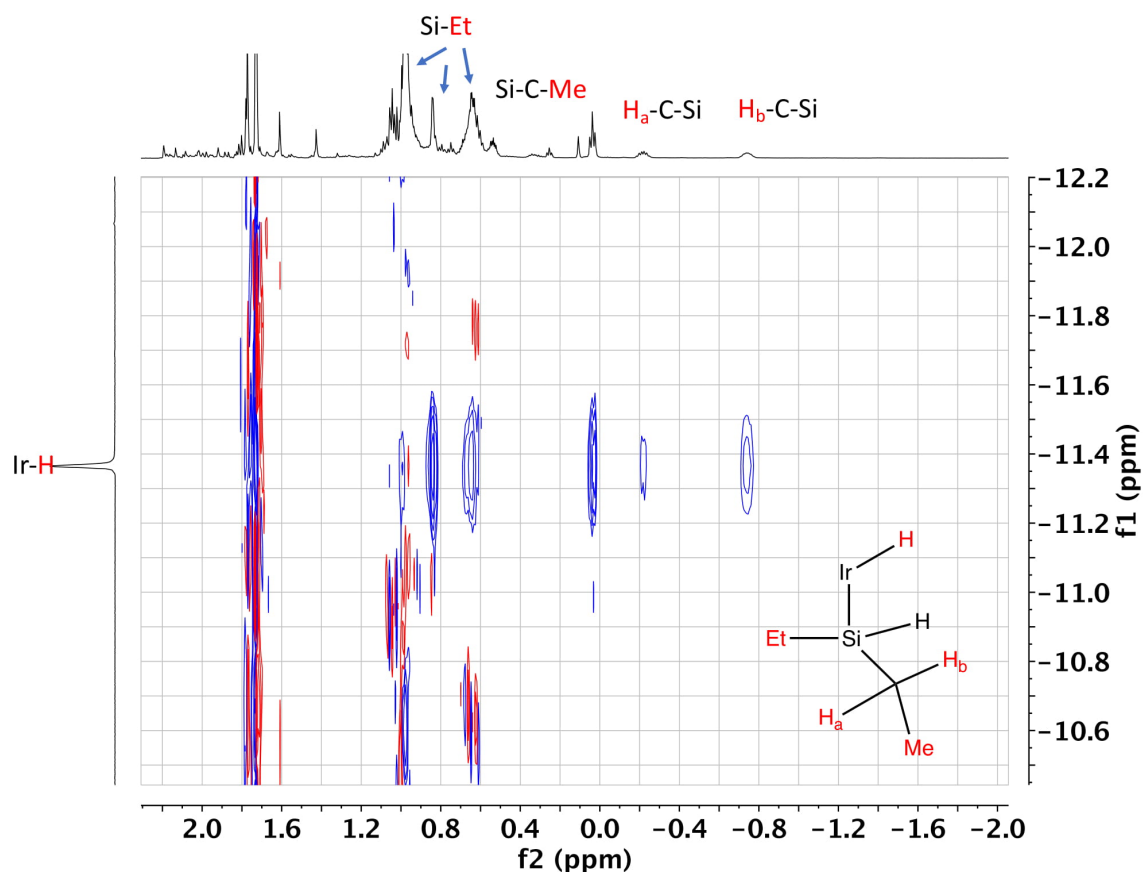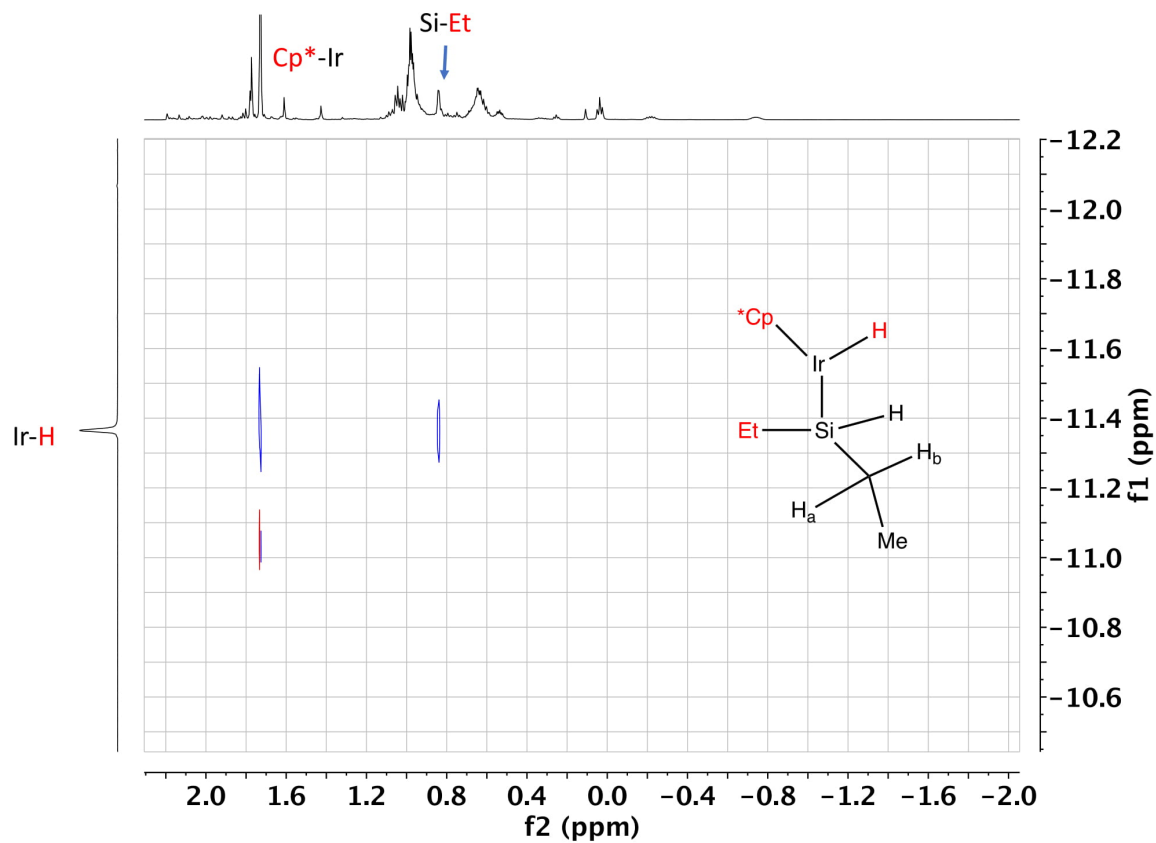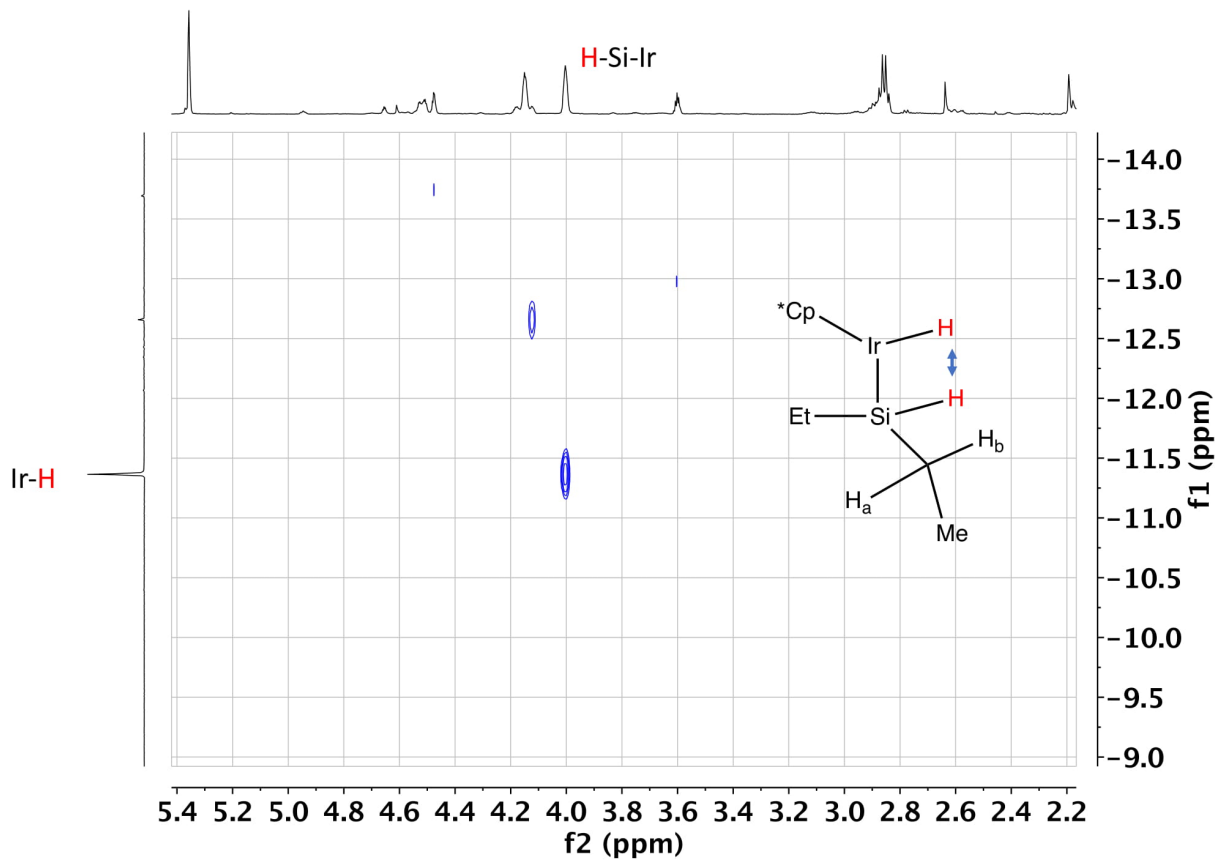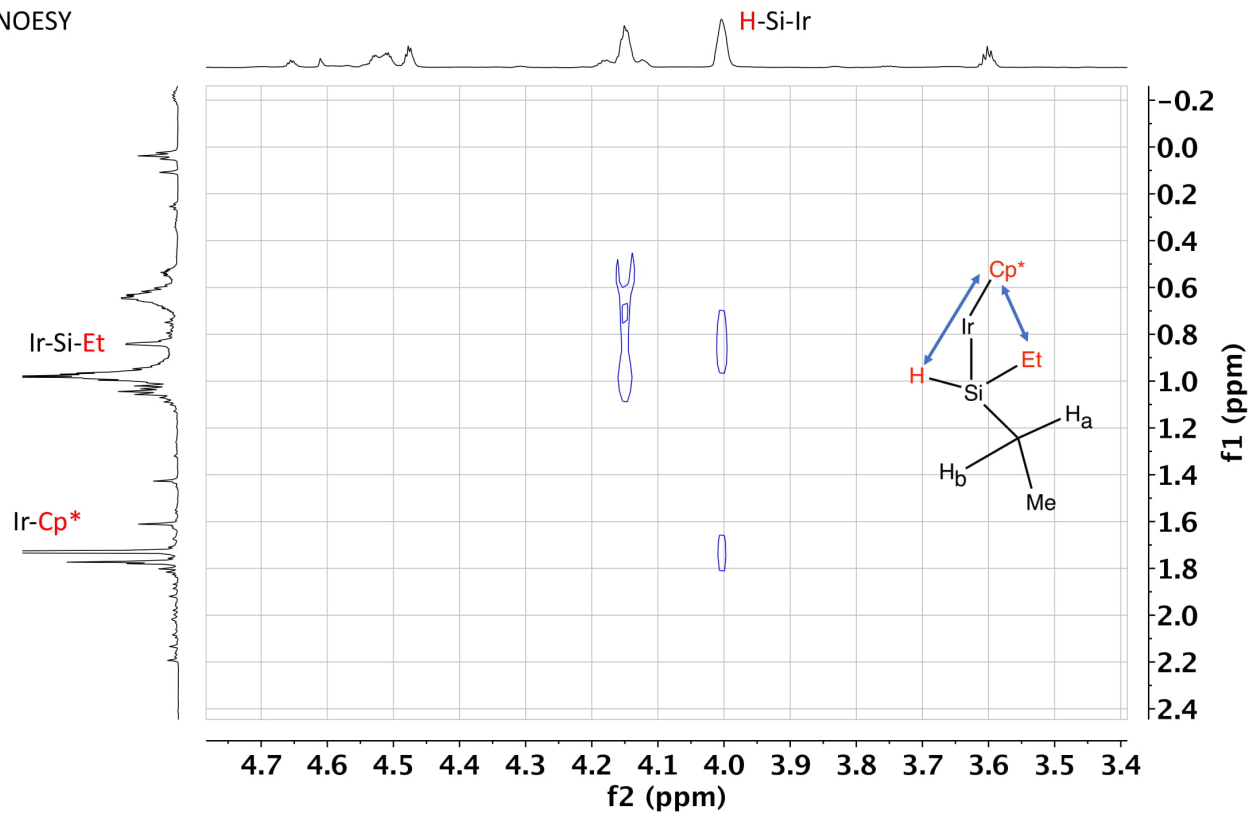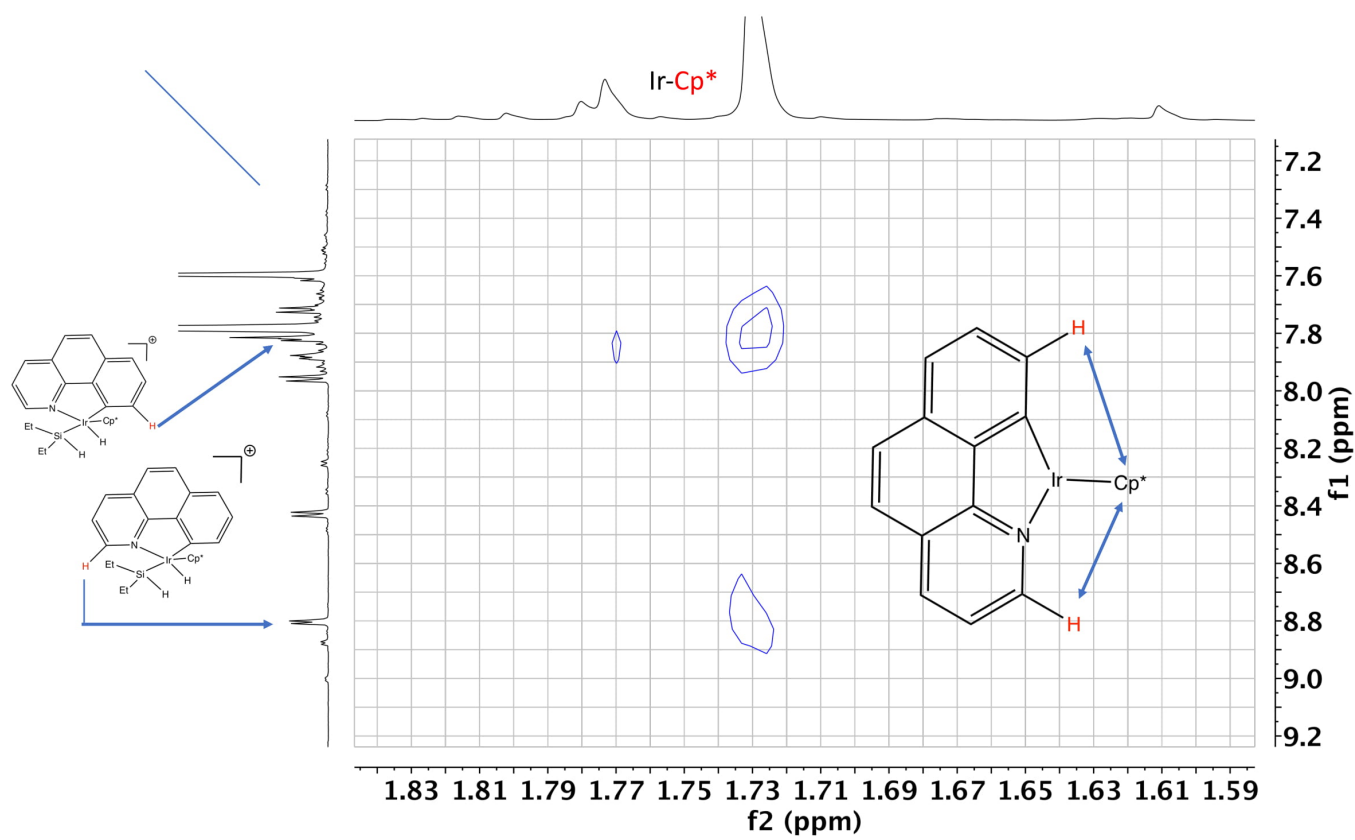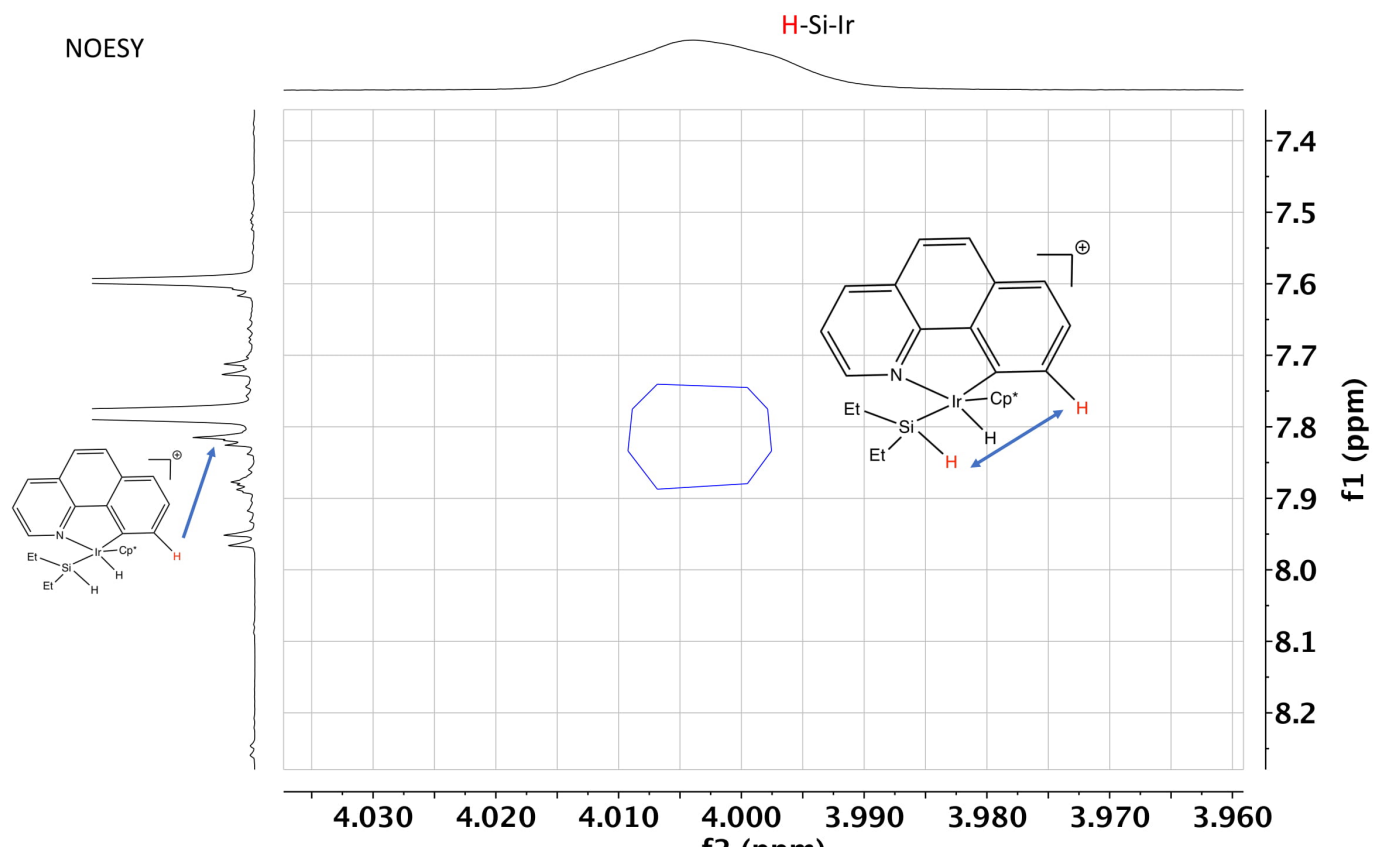
Synthesis of [2g][BArF$_{24}$] by Reaction of [1b][BArF$_{24}$] with Ph$_2$SiH$_2$: Procedure, NMR Data, and Spectra

Typical procedure for NMR analysis

In a glovebox, Et$_2$SiH (10.0 μL, 81.1 μmol) was added to a solution of [**1b**][BArF$_{24}$] (29 mg, 20.6 μmol) in CD$_2$Cl$_2$ (0.65 mL). The resulting solution was shaken and transferred into a J. Young NMR sample tube which was subsequently tightly sealed for analysis. After 25 minutes of reaction, the NMR tube was frozen at < -60 °C. Multinuclear NMR analysis (at -60 °C) of the reaction revealed the total and exclusive conversion of [**1b**][BArF$_{24}$] to [**2g**][BArF$_{24}$] and excess of Et$_2$SiH (see NMR spectra below).

NMR data

---

^{1}H NMR (600 MHz, CD$_2$Cl$_2$) δ 8.93 (d, J = 5.5 Hz, 1H), 8.28 (dd, J = 8.0, 1.2 Hz, 1H), 8.09 – 8.00 (m, 1H), 7.92 (t, J = 7.6 Hz, 1H), 7.79 (d, J = 7.8 Hz, 1H), 7.71 – 7.63 (m, 3H), 6.45 (t, J = 103.2 Hz, 5H), 4.96 (s, 1H, Si-H), 1.69(s, 15H) -11.06 (d, J = 2.8 Hz, 1H, Ir-H).

^{29}Si NMR (600 MHz, CD$_2$Cl$_2$) δ 0.00 ppm

174

COSY

175

HMQC + MSQC ^{1}H-^{13}C

176

COSY

H-Si

Ir-H

8

Ir-Cp*

Si-H

8

177

Ir-Cp*

1

8

6

2

f1 (ppm)

f2 (ppm)

H-Ir

7

1

f1 (ppm)

f2 (ppm)
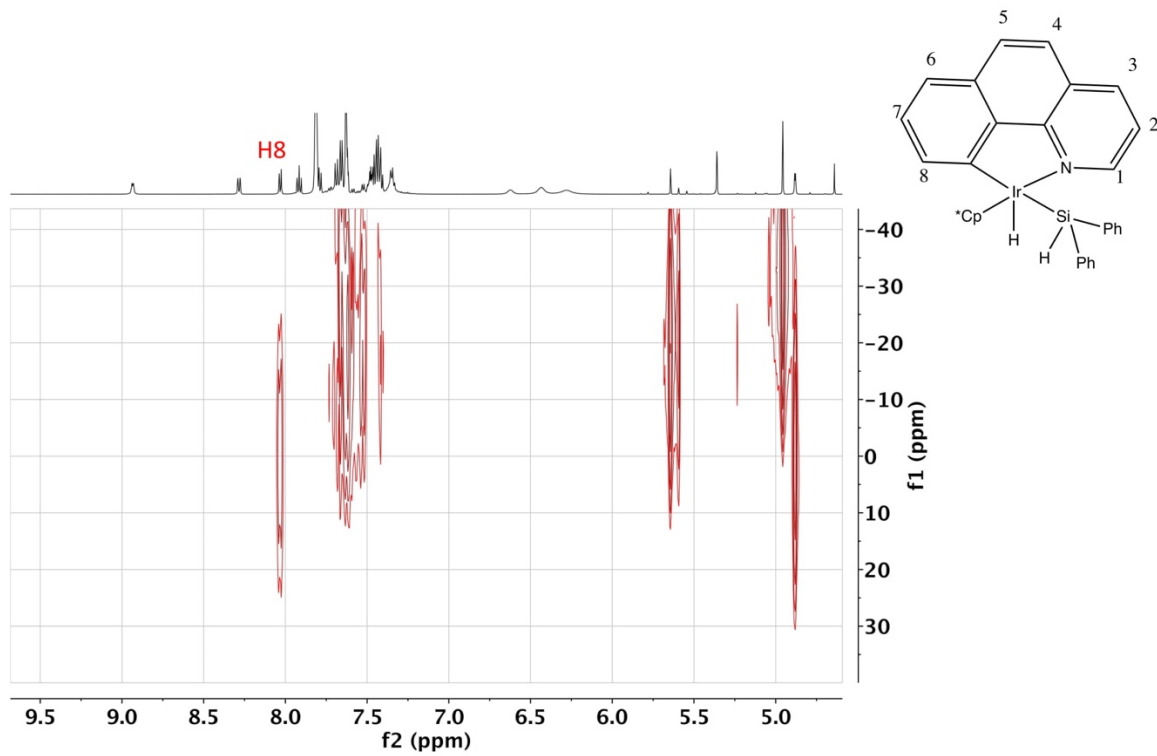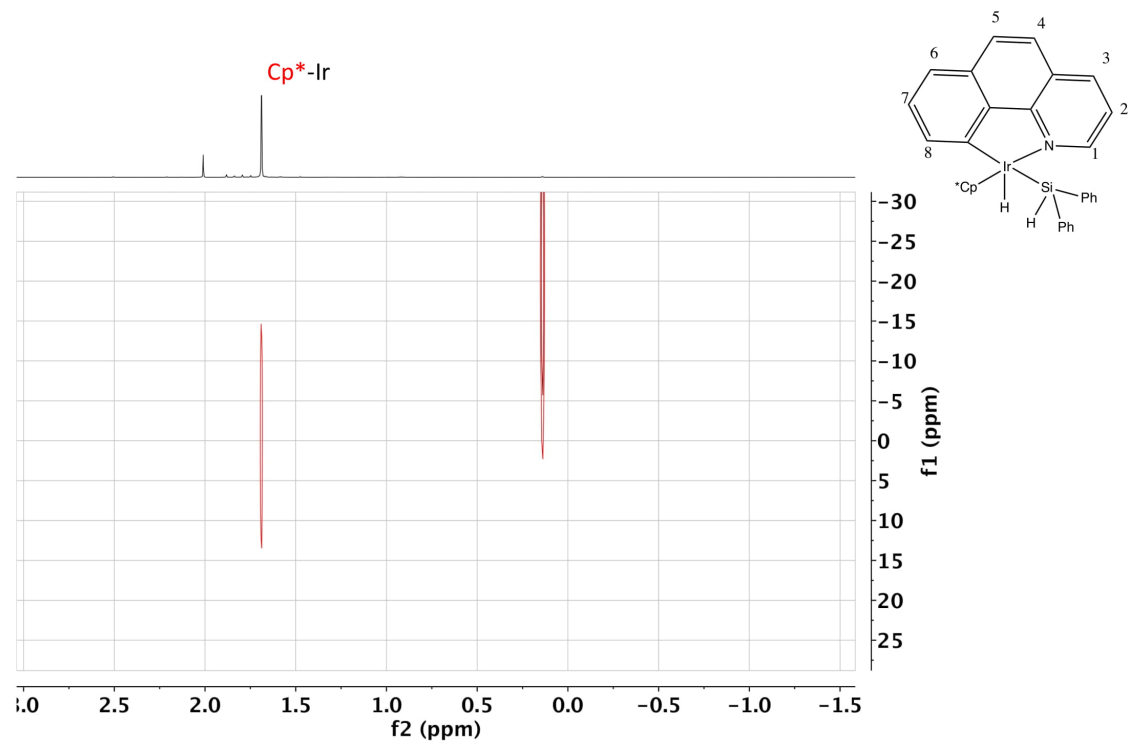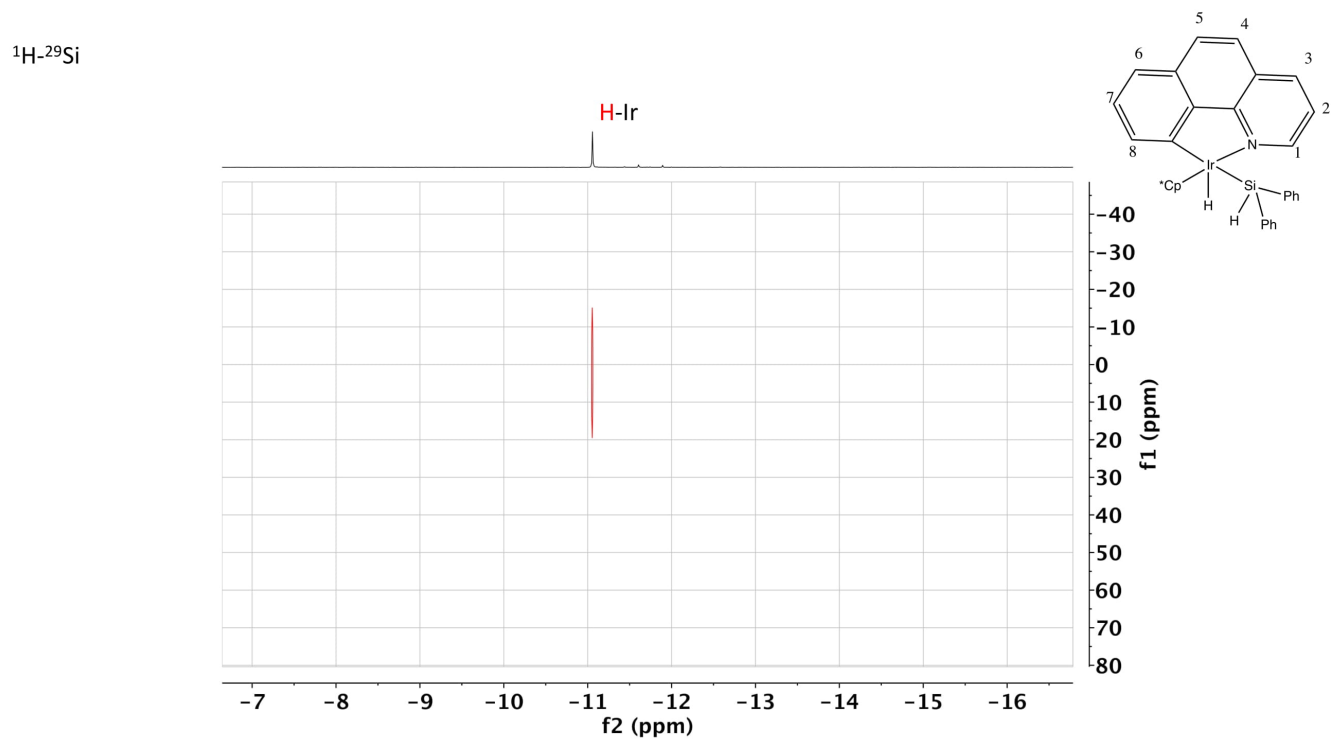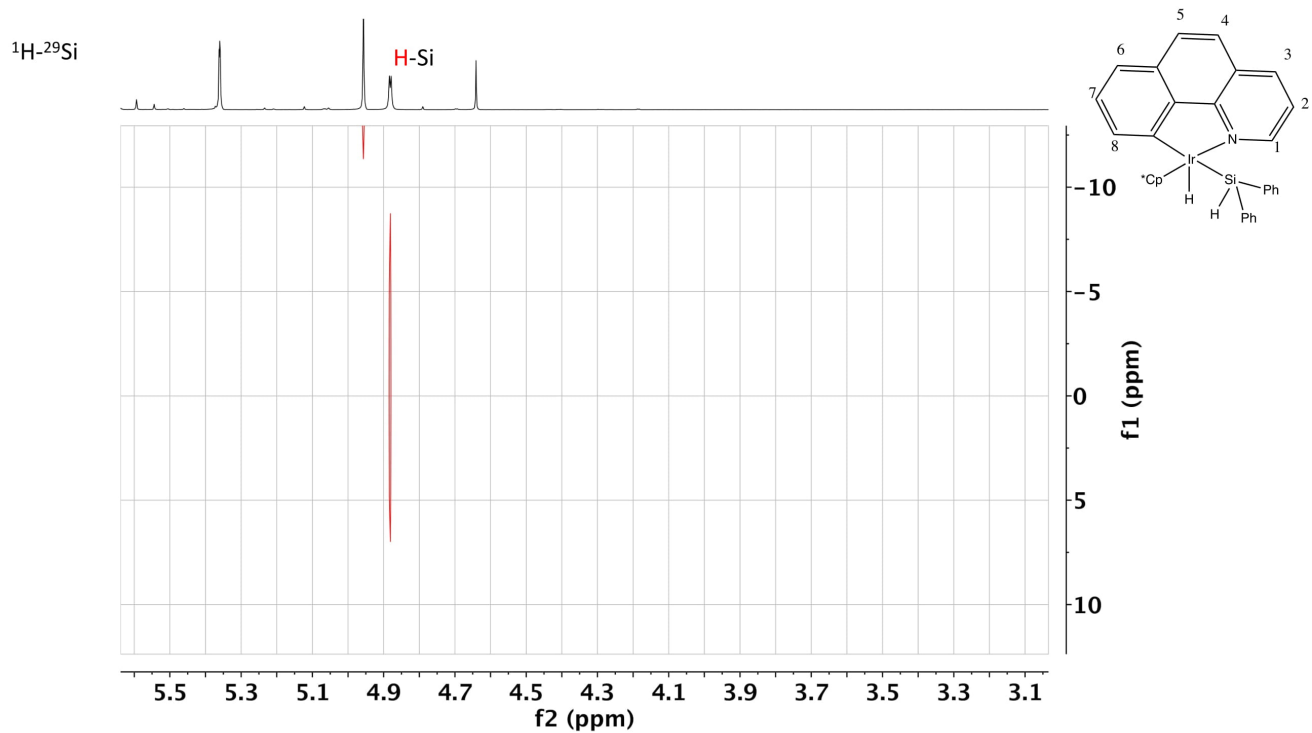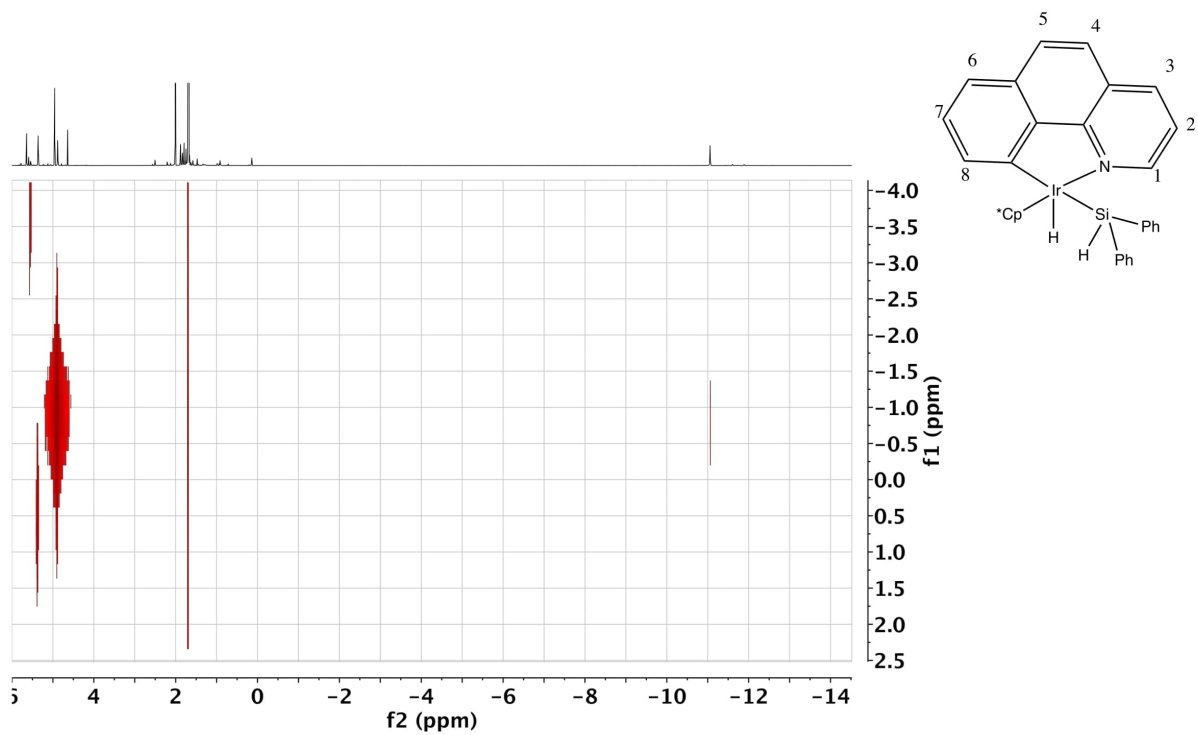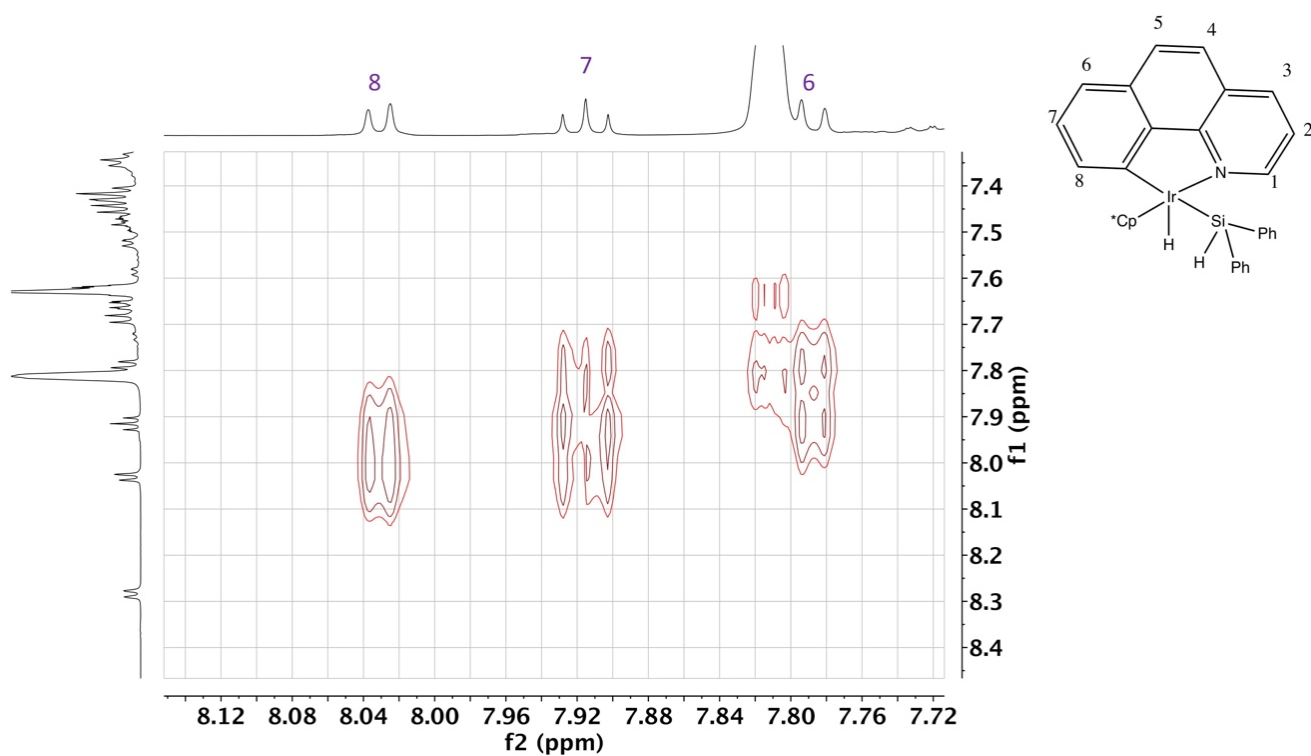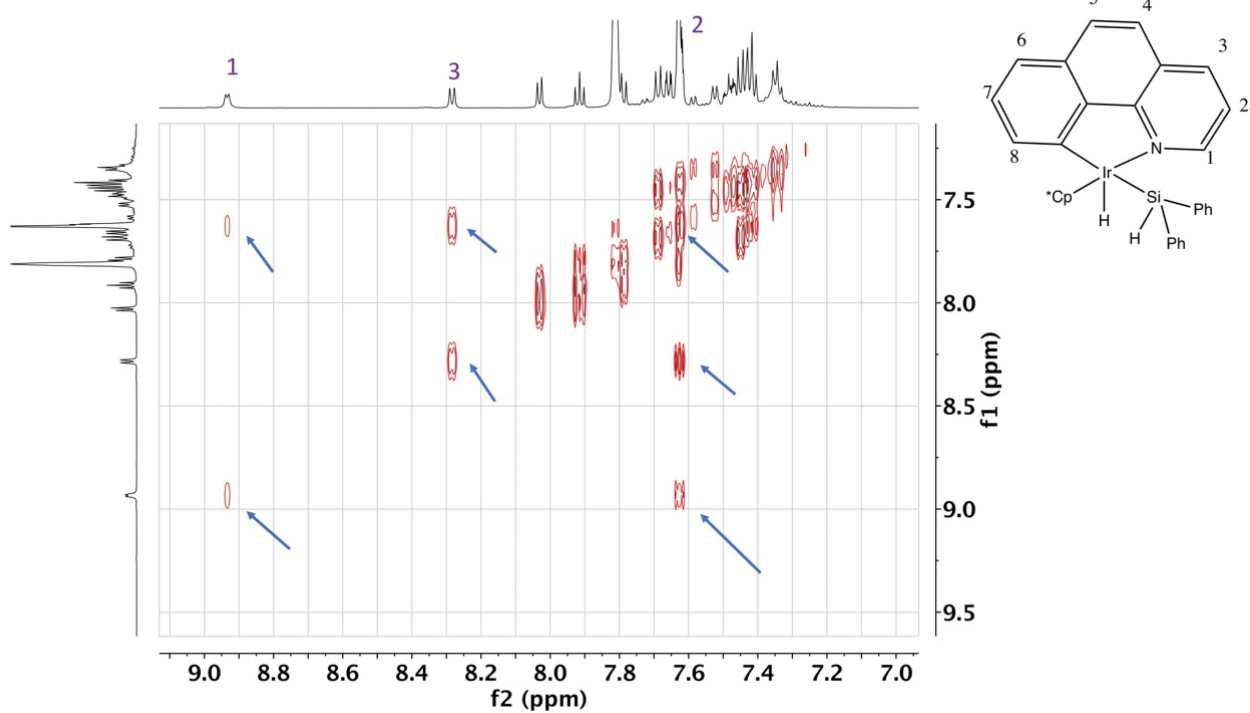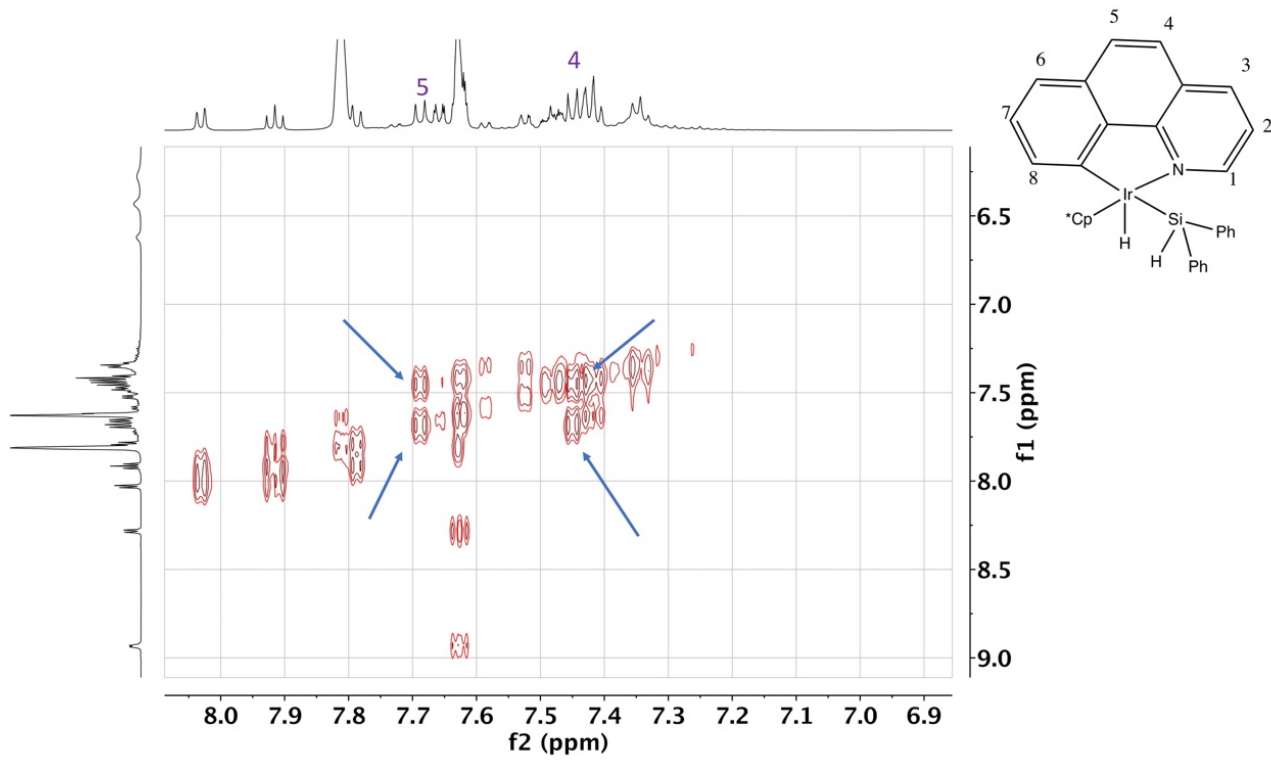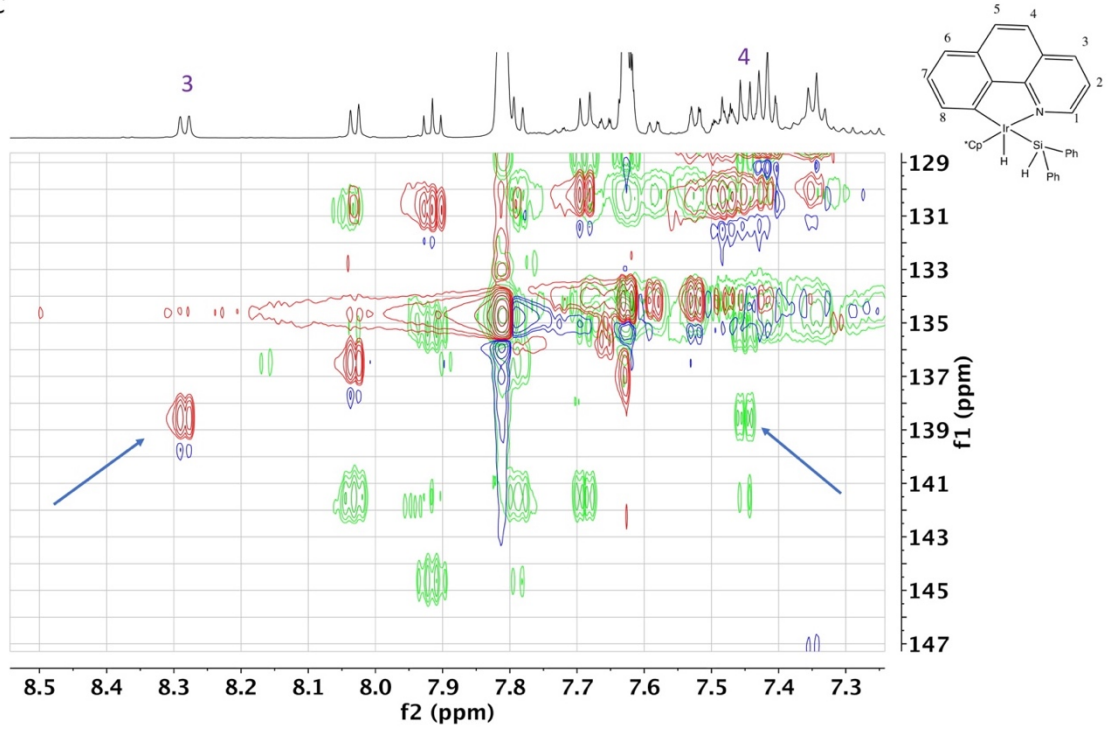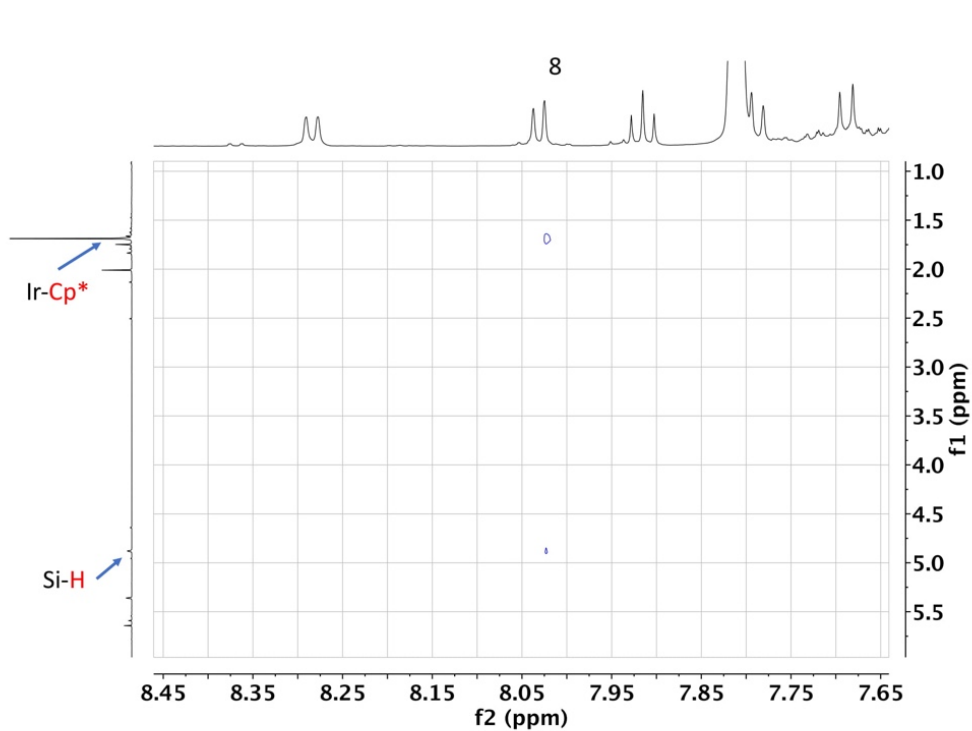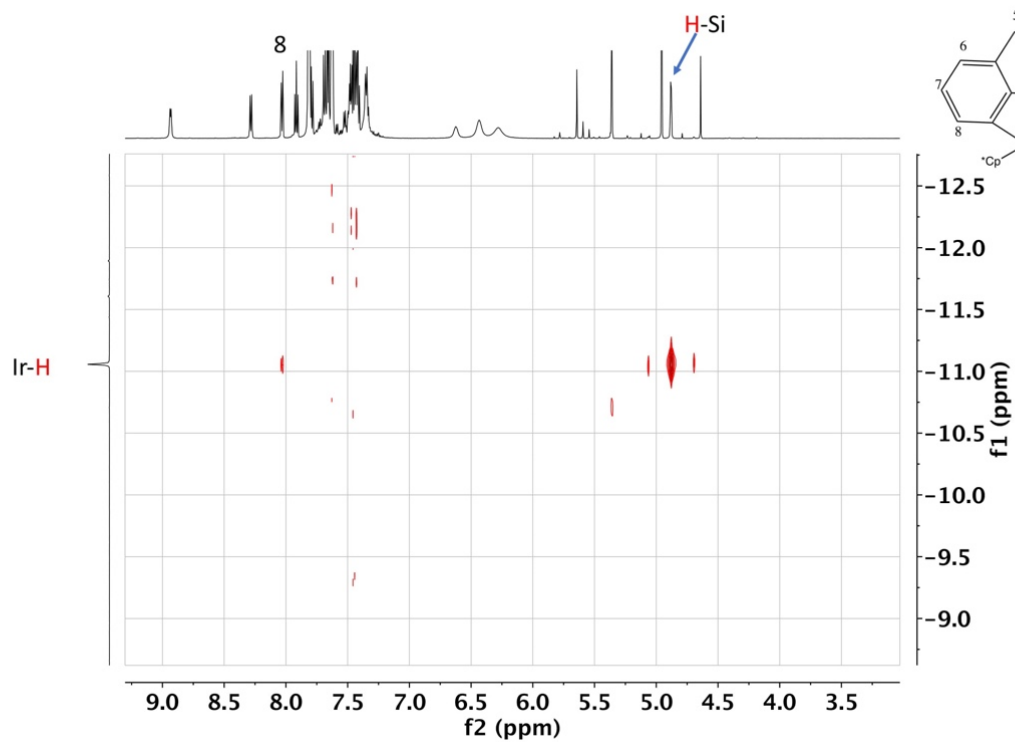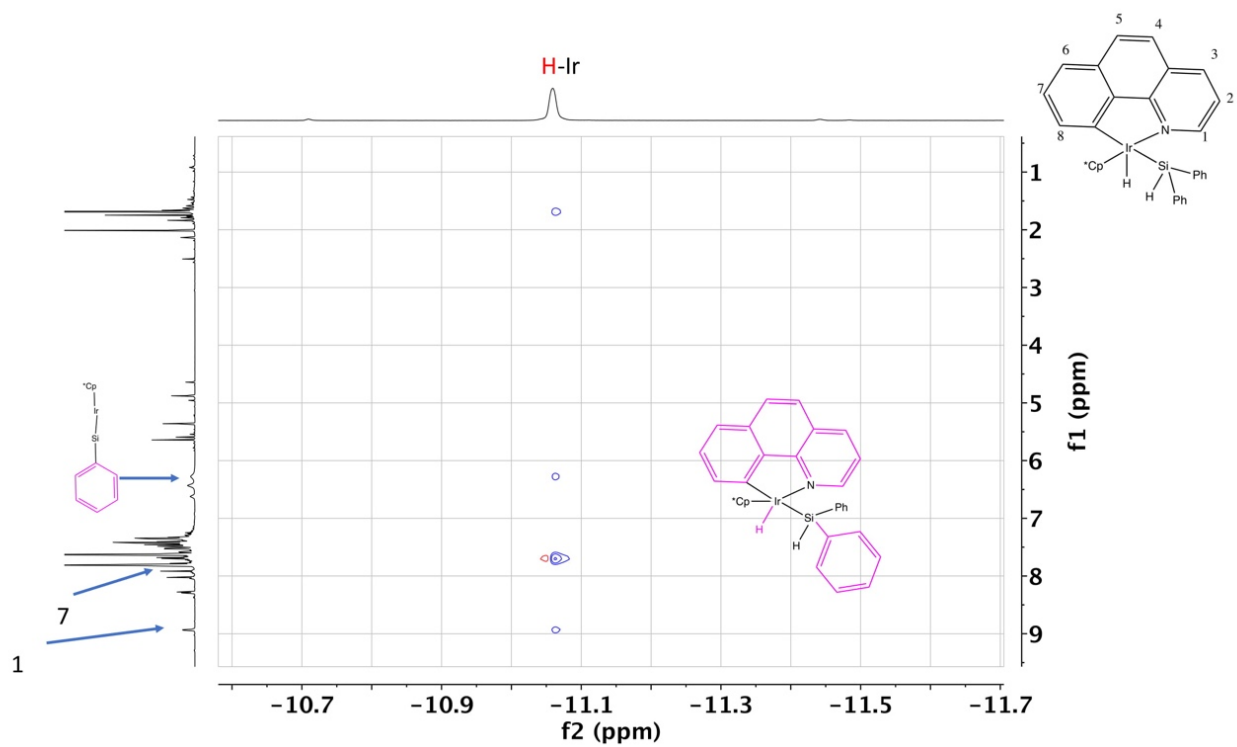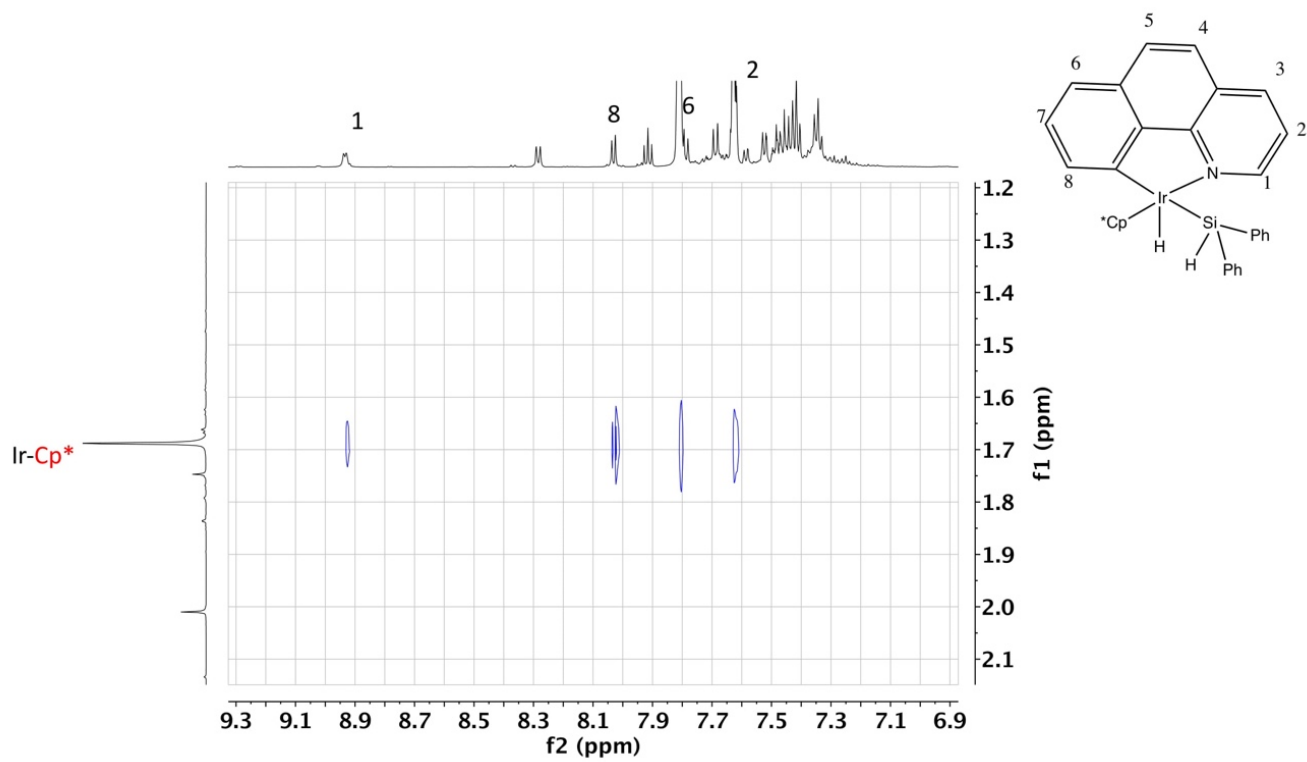
NOESY 1H-1H

HMQC + MSQC 1H-13C

H-Si
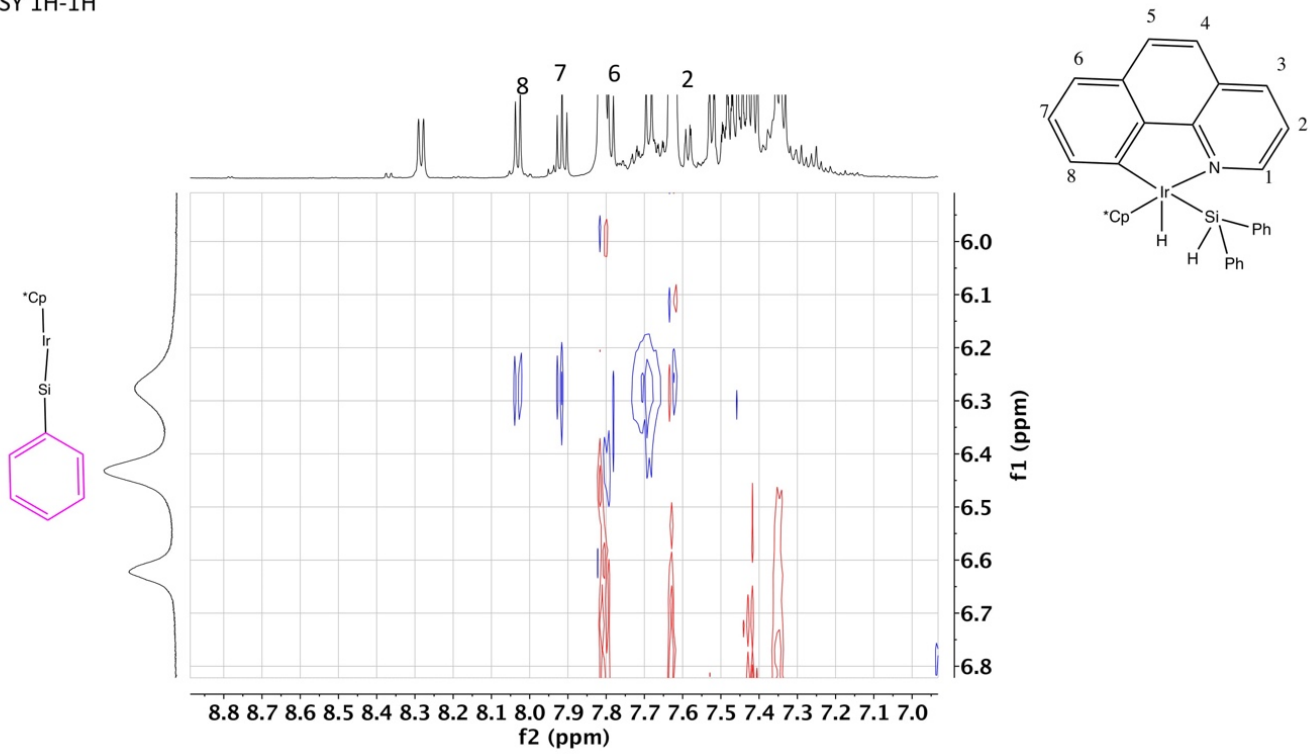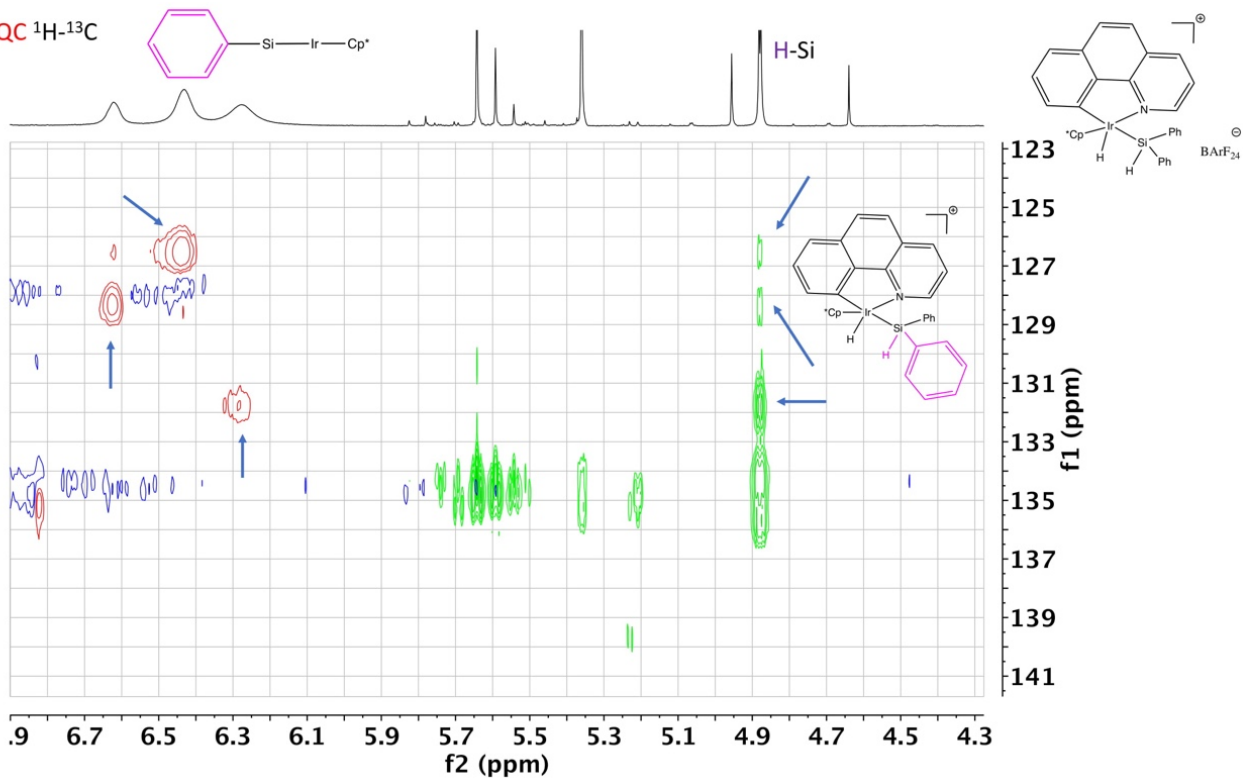
In situ Generation of [3][BArF$_{24}$] by Reaction of [1b][BArF$_{24}$] with HSiPhH$_2$ and THF: Procedures, NMR Data, and Spectra

Procedure 1 for NMR analysis (indirect; route 1, Figure 1)

In a glovebox, HSiPhH$_2$ (10.0 µL, 81.0 µmol) was added to a solution of [**1b**][BArF$_{24}$] (15 mg, 10.6 µmol) in CD$_2$Cl$_2$ (0.55 mL). The resulting solution was shaken and transferred into a J. Young NMR sample tube which was subsequently tightly sealed for analysis. After 25 minutes of reaction, the NMR tube was frozen at < -60 °C. ^{1}H NMR analysis (at -60 °C) of the reaction was carried to verify the total and exclusive conversion of [**1b**][BArF$_{24}$] to [**2c**][BArF$_{24}$]. Addition of THF (10 µL, 123.3 µmol) to the latter mixture resulted in immediate effervescence of the yellow solution that indicated H$_2$ gas evolution. To raise up the temperature from -60 °C to ~ 20 °C, it was found necessary to let the latter solution standing in the glovebox at room temperature for ~1-2 h. ^{1}H NMR analysis (at -60 °C) indicated complete consumption of [**2c**][BArF$_{24}$] and formation of [**3**][BArF$_{24}$] as the major Ir species along with H$_2$ (singlet at ca. δ 4.60 ppm) in a respective ca. 1:0.2 ratio (see NMR spectra below). A complex pattern of peaks of low-intensity were also observed in the range spanning δ 5.10-5.15 ppm (integrating roughly for 2H relative to [**3**][BArF$_{24}$]); part of the peaks, i.e., a singlet at δ 5.15 ppm, is assigned to the Si-bound hydrogen of an unidentified organosilicon derivative "Ph$_x$Si$_y$H$_z$" (on the basis of weak [29]Si satellites; vide infra). This procedure was found to be reproductible over (at least) ≥ 5 experiments.

Procedure 2 for NMR analysis

In a glovebox, $HSiPhH_2$ (10.0 µL, 81.0 µmol) was added to a solution of [**1b**][BArF$_{24}$] (15 mg, 10.6 µmol) in d_8-THF (0.55 mL). The resulting solution was shaken and transferred into a J. Young NMR sample tube which was subsequently tightly sealed for analysis. After 15 minutes of reaction at room-temperature, ^{1}H NMR analysis showed full consumption of [**1b**][BArF$_{24}$], but only partial conversion of [**2c**][BArF$_{24}$] to [**3**][BArF$_{24}$] (~ 50%; cf. spectrum 1 in Figure S28). After 1 h, this conversion was estimated to amount ~75% (cf. spectrum 2 in Figure S28). Full conversion was obtained after 2 h of reaction; cf. spectrum 3 in Figure S28. Indeed, the latter ^{1}H NMR spectrum indicated complete consumption of [**2c**][BArF$_{24}$] and selective formation of [**3**][BArF$_{24}$] along with H_2 (singlet at ca. δ 4.55 ppm) in a respective ca. 1:0.3 ratio. A complex pattern of peaks of low-intensity were also observed in the range spanning δ 5.00-5.25 ppm (integrating roughly for 6H relative to [**3**][BArF$_{24}$]. Also detected are the two peaks resonating at δ 1.53 and 3.33 ppm, which are assigned to the product of polymerization of THF inititated by the cationic [Cp*Ir(C,N)(PhHSi•*thf*]$^+$ species.[17]

NMR data

Data recorded at 298 K for [**3**][BArF$_{24}$] are as follows: ^{1}H NMR (400 MHz, 298 K, CD$_2$Cl$_2$): δ = 9.01 (d, 1H, H$_{Ar}$ B[*h*]Q, *J* = 5.3 Hz), 8.24 (d, 1H, H$_{Ar}$ B[*h*]Q, *J* = 8.0 Hz), 8.02 (d, 1H, H$_{Ar}$ B[*h*]Q, *J* = 7.0 Hz), 7.80 (m, 1H, H$_{Ar}$ B[*h*]Q), 7.75 (m, 8H, H$_{ortho}$ BArF$_{24}$), 7.67-7.71 (m, 3H, H$_{Ar}$ B[*h*]Q), 7.57 (m, 4H, H$_{para}$ BArF$_{24}$), 7.52 (m, 1H, H$_{Ar}$ B[*h*]Q), 7.24-7.26 (bs, 5H, [SiH*Ph*]), 5.73 (s, 1H, [Si*H*Ph], $^1J_{\text{H-Si}}$ = 99.3 Hz), 1.74 (s, 15H, Cp-*Me$_5$*). Two broad peaks of THF were detected at respectively δ 3.66 and 1.79 ppm, indicating fast-exchange of bulk THF molecules with those coordinated to the Si centre of [**3**][BArF$_{24}$] (cf. Figure S16). ^{13}C (126 Hz, 298 K, CD$_2$Cl$_2$): δ = 162.3 (1:1:1:1 quartet, $^1J_{\text{C-B}}$ = 49.9 Hz, $\underline{C}$–B in BArF$_{24}$), 158.1 (B[*h*]Q), 152.1 (broad, H-$\underline{C}$=N, B[*h*]Q), 141.9 (B[*h*]Q), 136.6 ($\underline{C}$-H, B[*h*]Q), 135.2 (B[*h*]Q), 134.6 (broad, $\underline{C}$-H, B[*h*]Q), 135.4 (m, $\underline{C}$–H$_{ortho}$ in BArF$_{24}$), 130.88 ($\underline{C}$-H, B[*h*]Q), 130.85 ($\underline{C}$-H, B[*h*]Q), 130 ($\underline{C}$-H, B[*h*]Q), 129.5 (qq, $^2J_{\text{C-F}}$ = 31.9 Hz, $^3J_{\text{C-F}}$ = 2.9 Hz, $\underline{C}_{Ar}$-CF$_3$ in BArF$_{24}$), 128.88 (B[*h*]Q), 128.82 (C-Si, IrSi$\underline{Ph}$H$_2$), 128.80 (broad, $\underline{C}$-H, IrSi$\underline{Ph}$H$_2$), 128.09 (B[*h*]Q), 124.6 ($\underline{C}$-H, B[*h*]Q), 122.4 ($\underline{C}$-H, B[*h*]Q), 124.6 (q, $^1J_{\text{C-F}}$ = 272.4 Hz, $\underline{C}$F$_3$ in BArF$_{24}$), 118.1 (m, C-H^{para} in BArF$_{24}$), 94.7 ($\underline{Cp}$-Me$_5$), 9.0 (Cp-$\underline{Me_5}$), [Remaining ^{13}C resonances of IrSi$\underline{Ph}$H$_2$ could not be assigned with certainty as their corresponding ^{1}H resonances overlapped with some peaks of the C,N-ligand and those of the BArF$_{24}$ anion]. ^{29}Si [obtained indirectly by ^{1}H,^{29}Si HMQC cross-peak correlation with the ^{1}H singlet at 5.73 ppm; 500/99 Hz, 298 K, CD$_2$Cl$_2$)]: δ = 73.1 ppm.

Data recorded at 213 K for [**3**][BArF$_{24}$] are as follows: ^{1}H NMR (600 MHz, 213 K, CD$_2$Cl$_2$): δ = 9.12 (bs, 1H, H$_{Ar}$ B[*h*]Q), 8.23 (d, 1H, H$_{Ar}$ B[*h*]Q, *J* = 8.0 Hz), 8.0 (bs, 1H, H$_{Ar}$ B[*h*]Q), 7.91 (bs, 1H, H$_{Ar}$ B[*h*]Q), 7.76 (m, 8H, H$_{ortho}$ BArF$_{24}$), 7.57 (m, 4H, H$_{para}$ BArF$_{24}$), 7.54 (m, 1H, H$_{Ar}$ B[*h*]Q), 5.61 (bs, 1H, [Si*H*Ph], $^1J_{\text{H-Si}}$ = 100.4 Hz), 2.31 (bs, 2H, Si-*THF*), 2.07 (bs, 2H, Si-*THF*), 1.68 (bs, 15H, Cp-*Me$_5$*), 0.86 (bs, 2H, Si-*THF*), 0.67 (bs, 2H, Si-*THF*). The new ^{1}H NMR spectrum recorded at 213 K allowed the detection of peaks characterizing the Si-coordinated THF. However, some peaks of the C,N-ligand and those of the Ir-bound "*Ph*SiH$_2$" moiety could not be clearly detected in this new experiment (due to overlapping with peaks of [BArF$_{24}$]$^-$ and of the Ph group belonging to excess HPhSiH$_2$). Due to chirality at the Si centre, [**3**][BArF$_{24}$] is one of two possible diastereoisomers. Thus, the typical peaks of Si-coordinated THF of the other diastereoisomer (found to be the minor one) were also detected by the ^{1}H NMR experiment recorded at 213 K (as also confirmed by ^{1}H,^{1}H

COSY and NOESY NMR spectra; cf. spectra section). Selected data are as follow: ^{1}H NMR (600 MHz, 213 K, CD_2Cl_2): δ = 2.96 (bs, 2H, Si-*THF*), 2.72 (bs, 2H, Si-*THF*), 1.23 (bs, 2H, Si-*THF*), 1.06 ppm (bs, 2H, Si-*THF*).

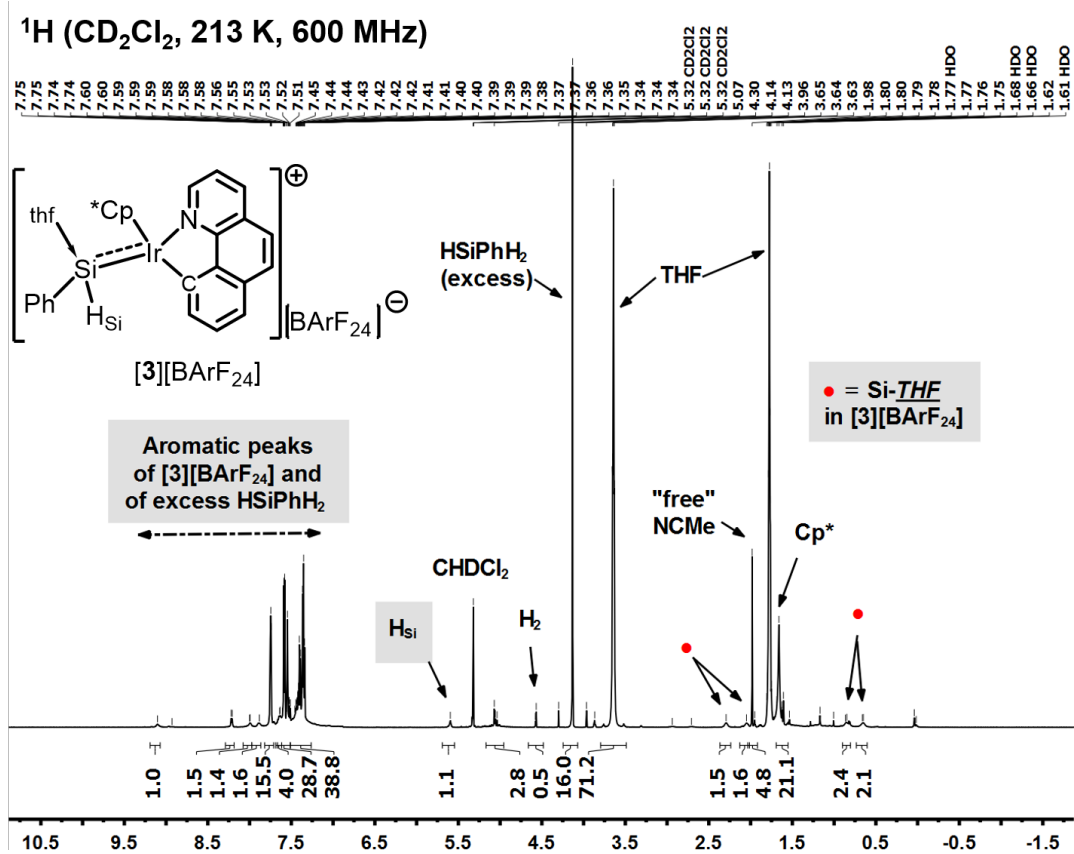# NMR spectra

^{1}H NMR (procedure 1, 298 K)

Figure S- 18
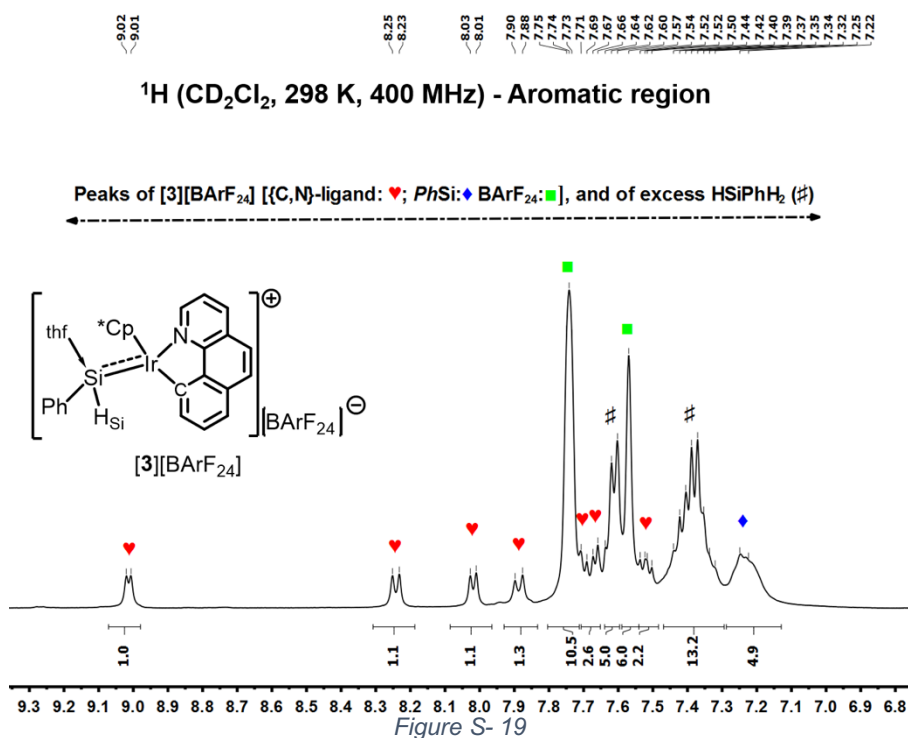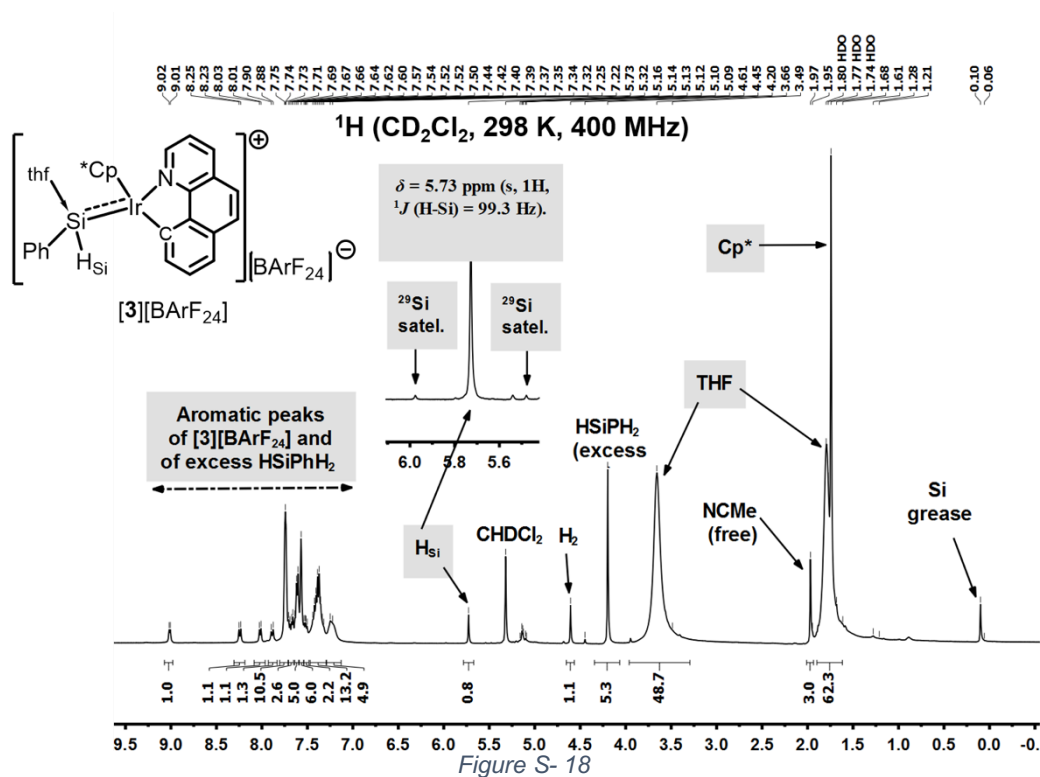
Figure S- 19

^{1}H NMR (procedure 1, 213 K)
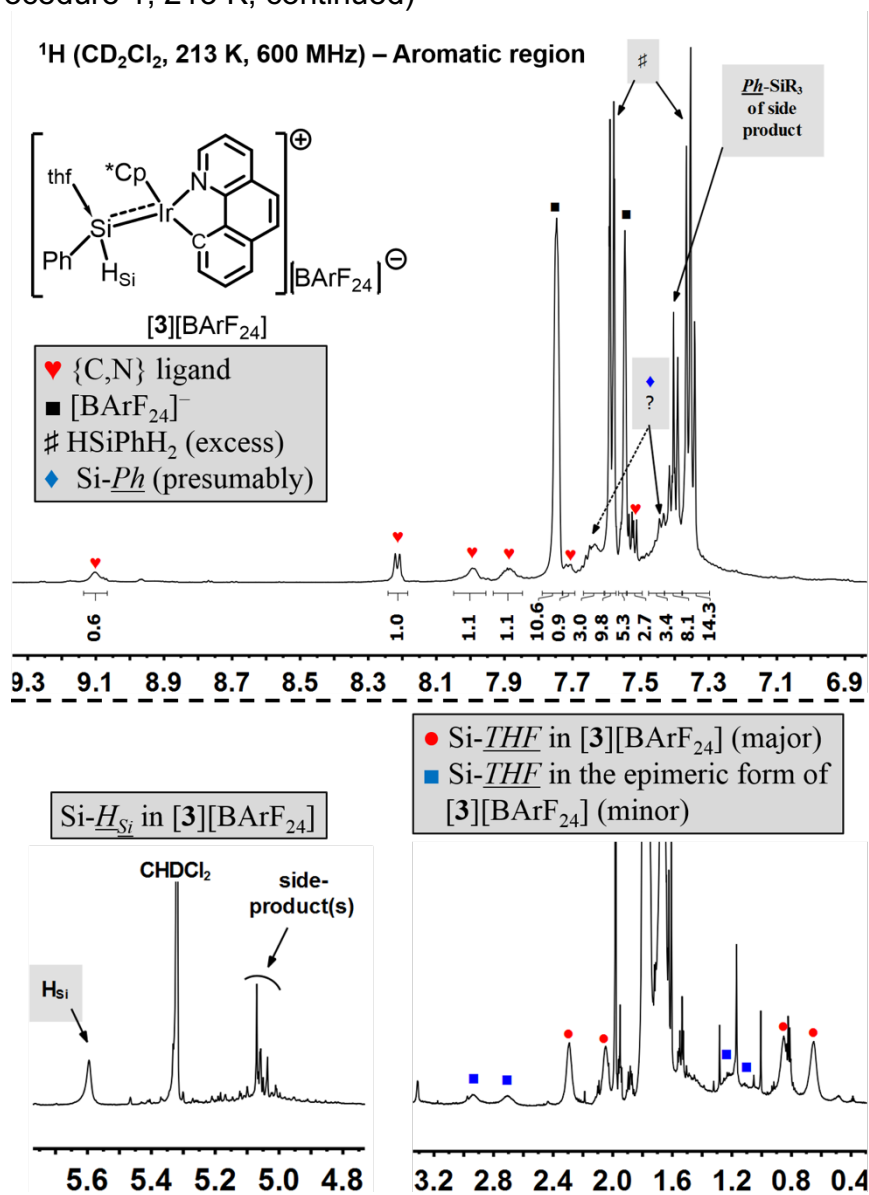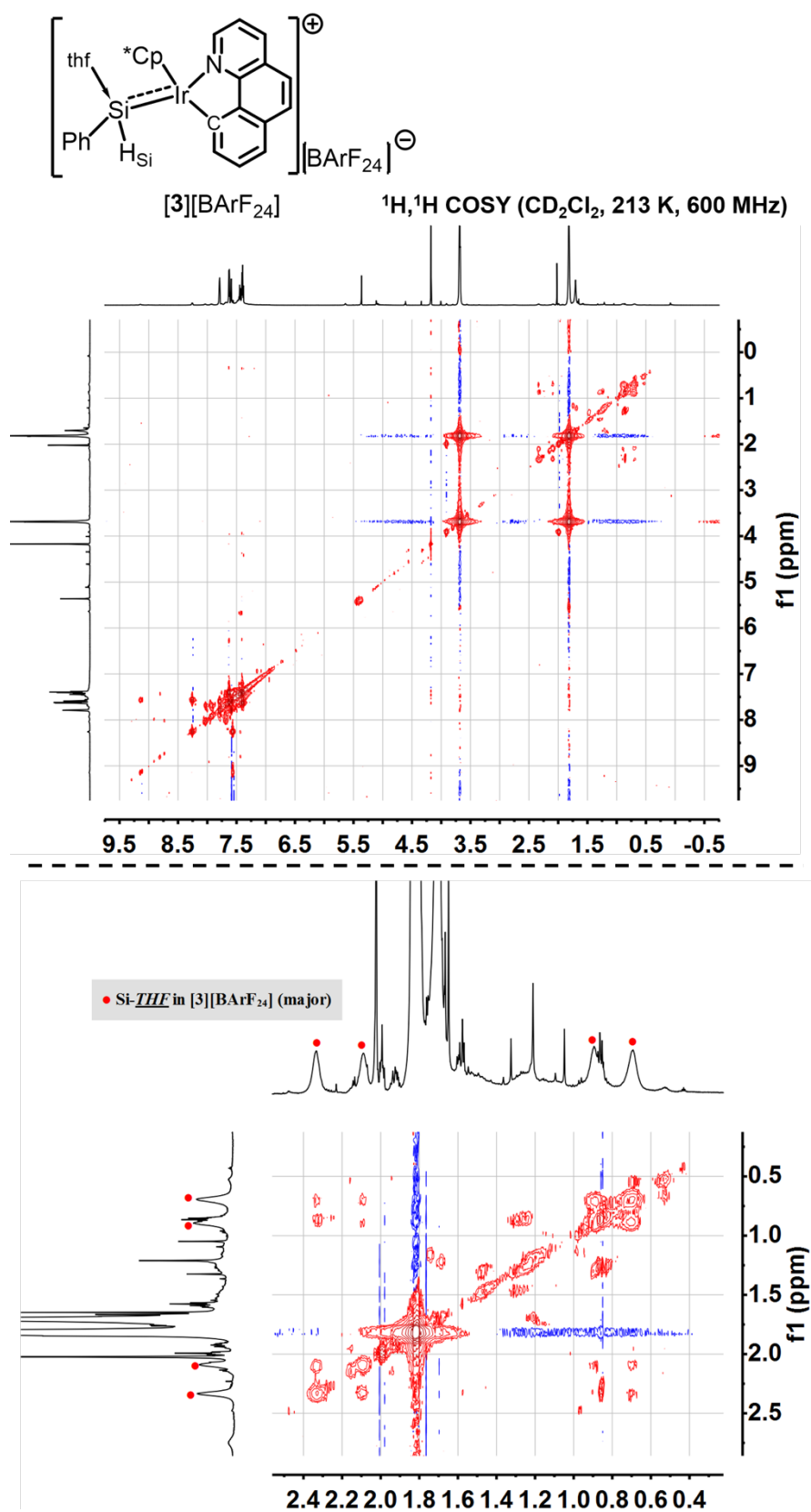
Figure S- 20

Figure S- 21
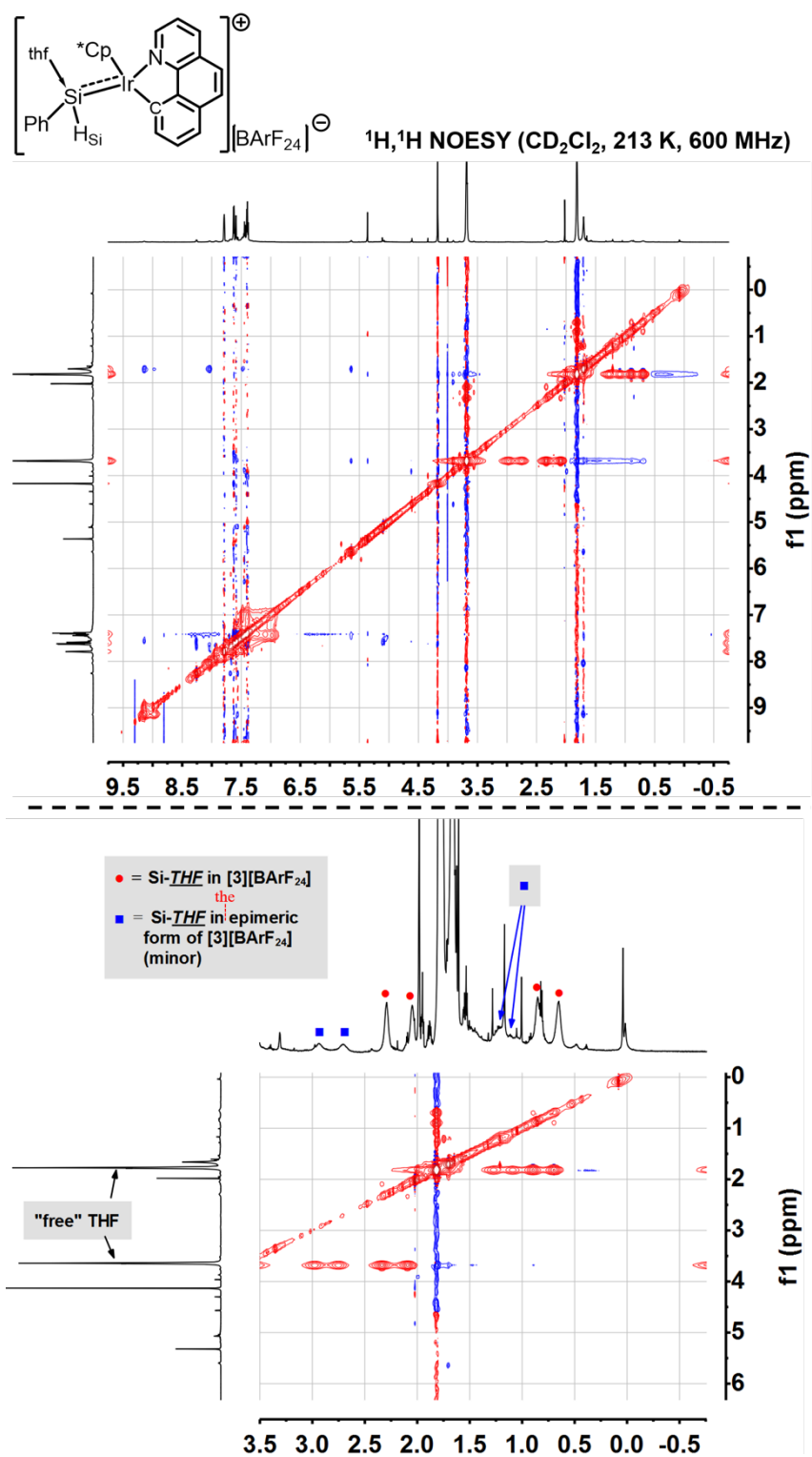
Figure S- 22

Figure S- 23

^{1}H,^{29}Si HMQC NMR (procedure 1, 213 K)
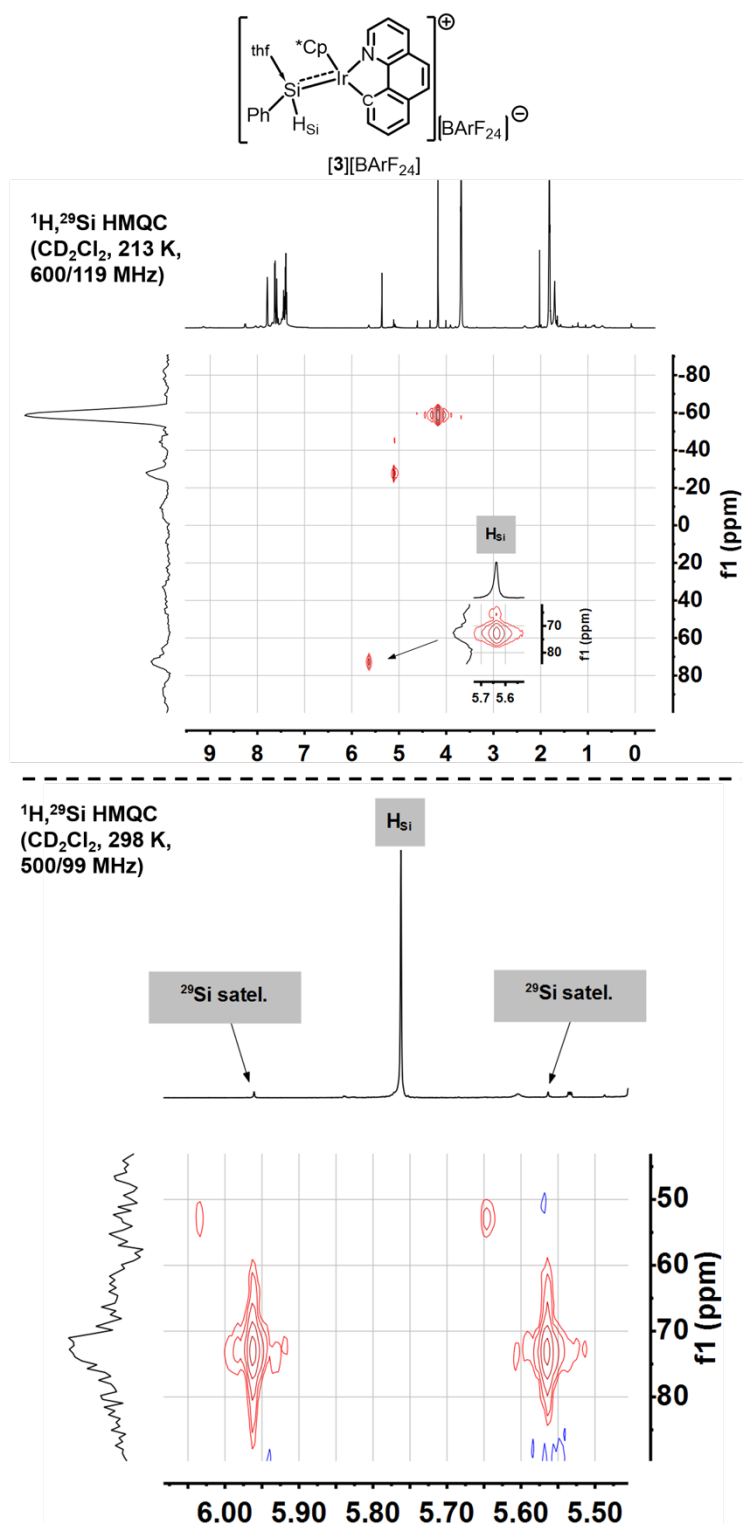
Figure S- 24

^{1}H,^{29}Si HMQC NMR (continued)

[3][BArF$_{24}$] ^{1}H,^{29}Si HMQC (CD$_2$Cl$_2$, 213 K, 600/119 MHz)
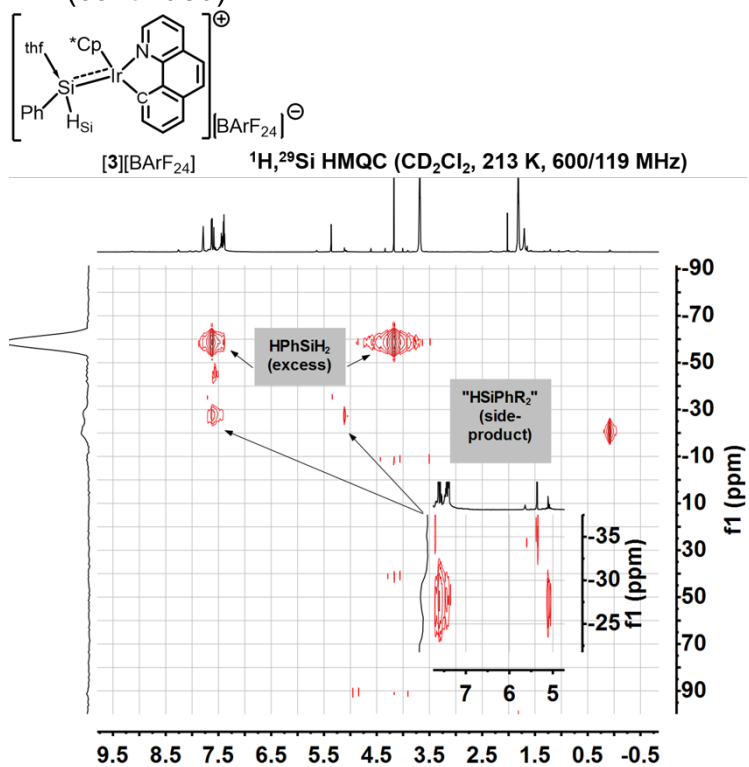
Figure S- 25

^{13}C-^{1}H NMR (procedure 1, 298 K)
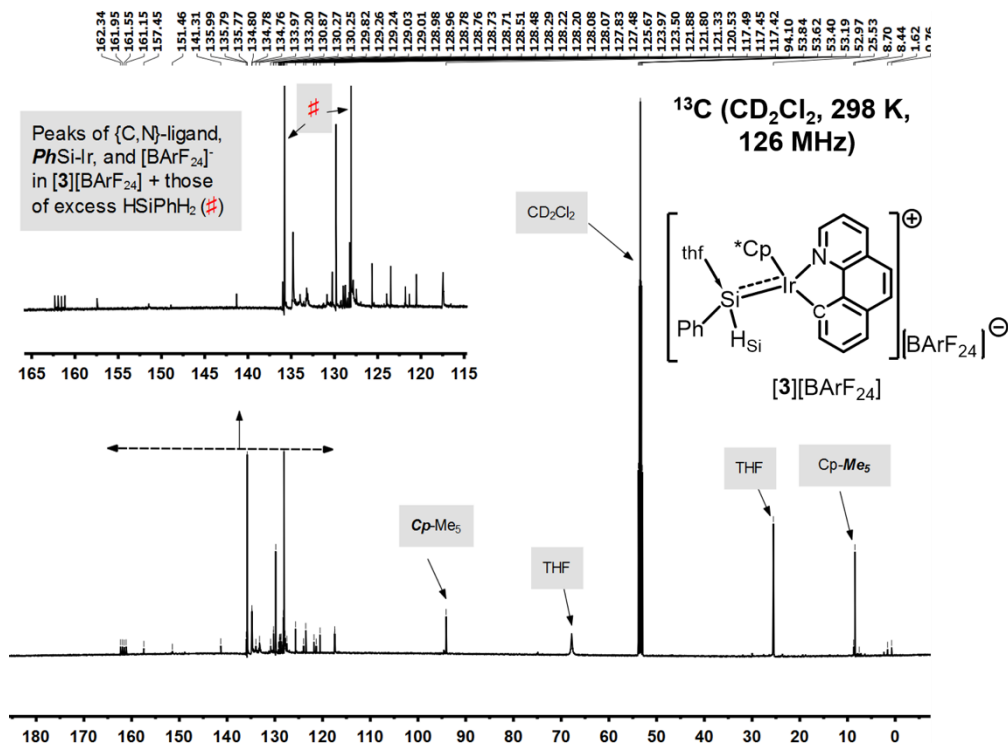
Figure S- 26

¹H NMR (procedure 2, 298 K)

¹H NMR (procedure 2, 298 K)

Figure S- 27

¹H (d_8-THF, 298 K, 400 MHz)
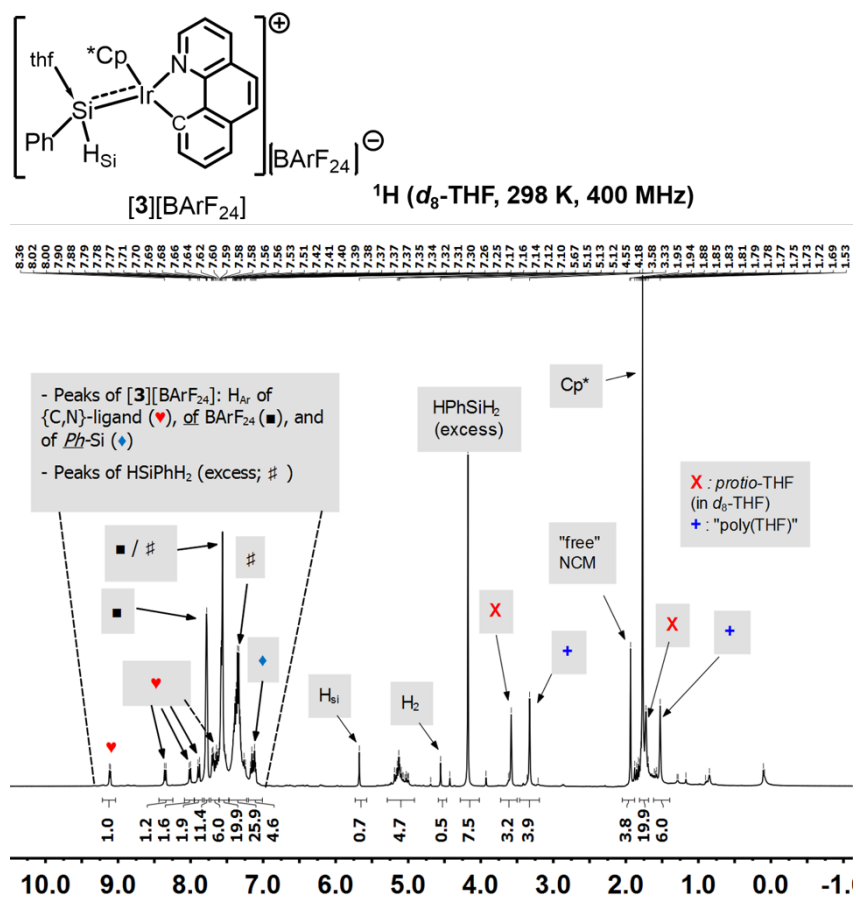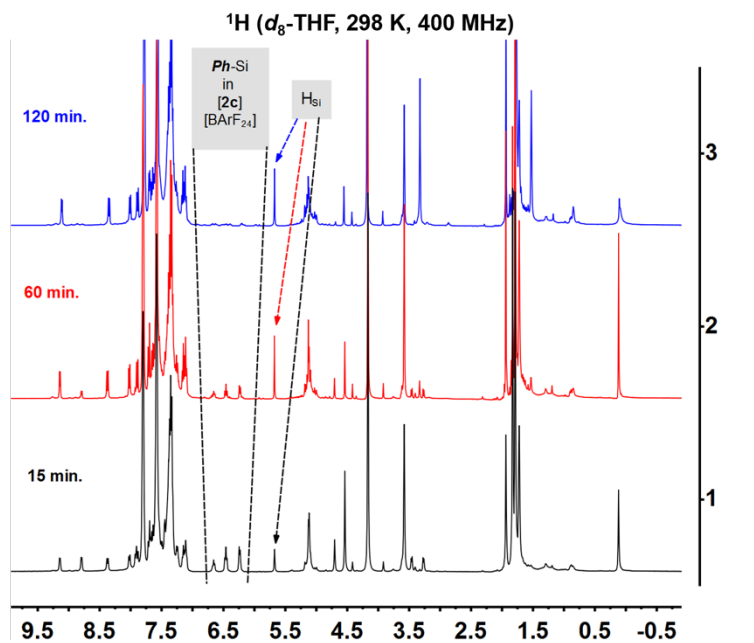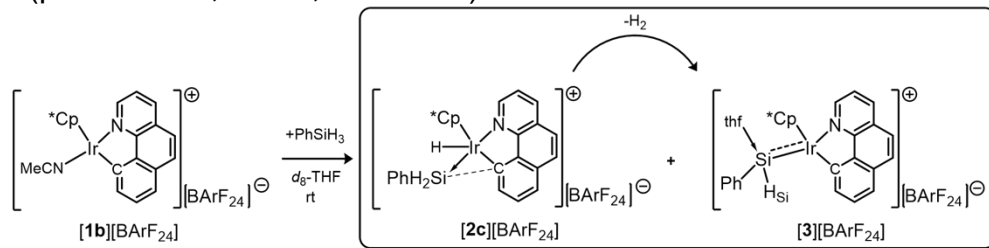
Figure S- 28

¹H NMR (on the reproducibility of procedure 1)
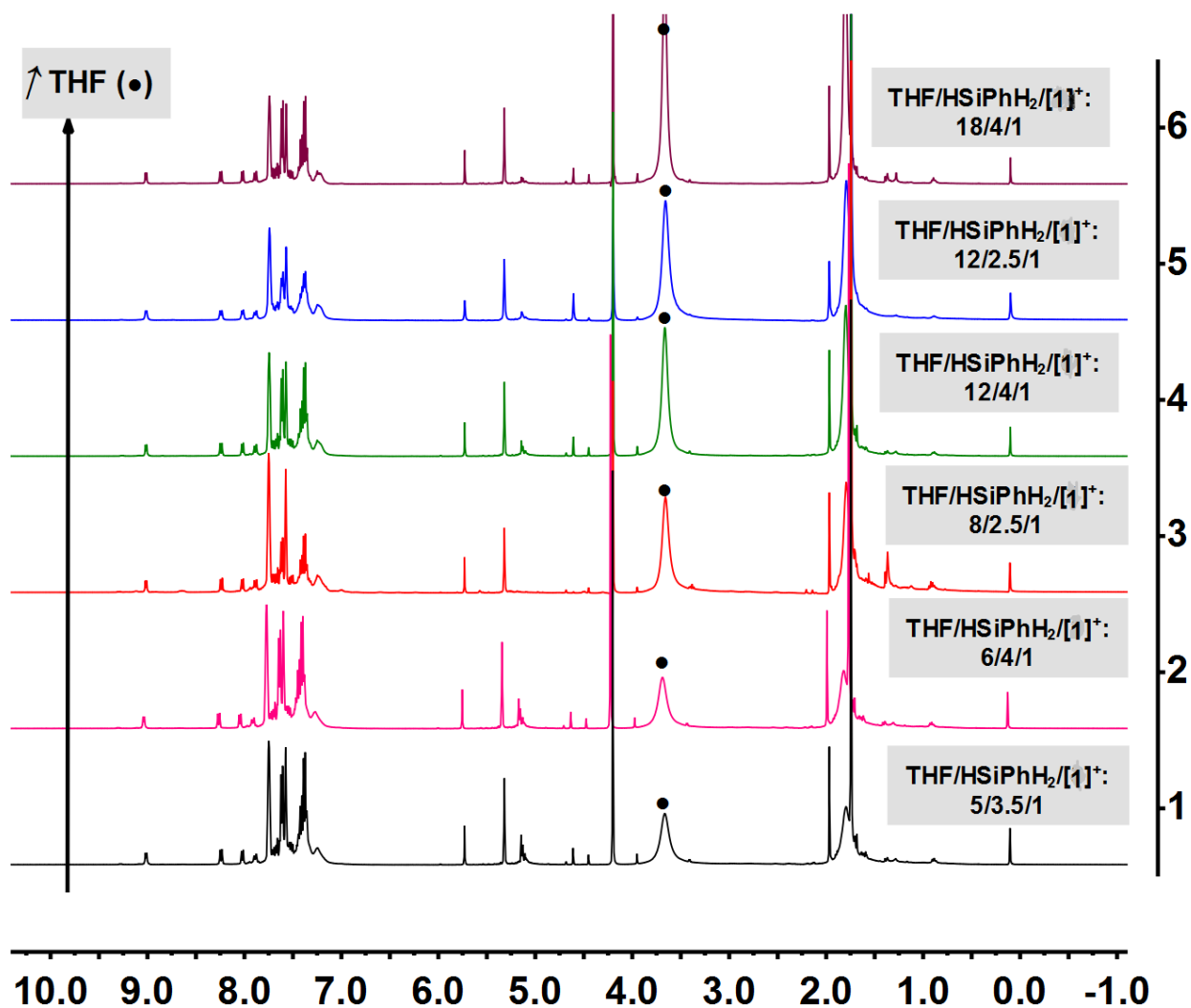
Figure S- 29 Evidence for the reproducibility of procedure 1 desbribed above for the in-situ generation of [**3**][BArF$_{24}$]: Stacked spectra correponding to six independent experiments leading in each case to complete conversion of [**1b**][BArF$_{24}$] to [**3**][BArF$_{24}$]; these latter experiments [referred to as **1** to **6** on going from down (black line) to top (purple line) of the figure] differ only by the THF/HSiPhH$_2$/[**1**]$^+$ ratio initially used. Notice that an excess of up to 12 eq. of THF relative to [**1**]$^+$ may be used without consequently changing the outcome of the reaction (at least in the time range of the experiment).

In-situ Generation of [4][BArF$_{24}$] by Reaction of [1b][BArF$_{24}$] with HSi^{n}BuH$_2$ and THF: Procedures, NMR Data, and Spectra

Procedure 2 for NMR analysis (indirect; route 1, Figure 1)

Compound [4][BArF$_{24}$] was generated in solution using the procedure 2 previously described for [3][BArF$_{24}$] (cf. previous section): HSi^{n}BuH$_2$ (20.0 µL, 77.0 µmol) was added to a solution of [1b][BArF$_{24}$] (30 mg, 21.2 µmol) in d_8-THF (0.45 mL). The resulting solution was shaken and transferred into a J. Young NMR sample tube which was subsequently tightly sealed for analysis at -40 °C. Full conversion was obtained after 2 h of reaction, as verified by ^{1}H NMR analysis (cf. spectra in the next sub-section). Indeed, the latter ^{1}H NMR spectrum indicated complete consumption of [1b][BArF$_{24}$] and selective formation of [4][BArF$_{24}$] along with H$_2$ (singlet at ca. δ 4.55 ppm) in a respective ca. 1:0.3 ratio. A complex pattern of unresolved and unidentified peaks of low-intensity were also observed in the range spanning δ 4.59-4.66 ppm (integrating roughly for 2H relative to [3][BArF$_{24}$]).

NMR data

^{1}H, ^{13}C-^{1}H and ^{1}H,^{29}Si HMQC

One arbitrary representation of the molecular structure of [4][BArF$_{24}$] is drawn below for indicating the labelling pattern which was chosen for assigning spin-active nuclei to their corresponding chemical shifts.
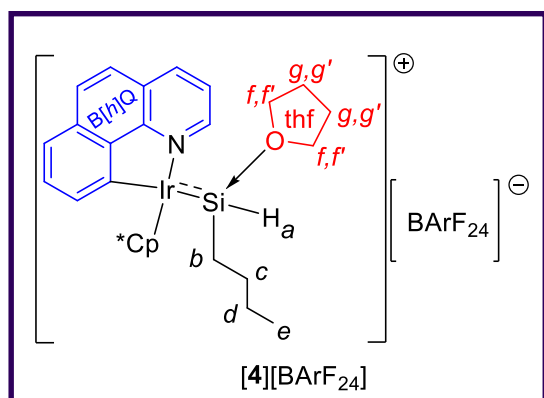
[4][BArF$_{24}$]

^{1}H (600 MHz, 233 K, d_8-THF): δ = 9.01 (d, 1H, H$_{Ar}$ B[h]Q, J = 5.4 Hz), 8.49 (d, 1H, H$_{Ar}$ B[h]Q, J = 7.9 Hz), 7.98 (d, 1H, H$_{Ar}$ B[h]Q, J = 8.7 Hz), 7.82 (d, 1H, H$_{Ar}$ B[h]Q, J = 8.7 Hz), 7.86 (m, 8H, H$_{ortho}$ BArF$_{24}$), 7.76 (d, 1H, H$_{Ar}$ B[h]Q, J = 7.8 Hz), 7.66 (m, 4H, H$_{para}$ BArF$_{24}$), 7.60-7.65 (m, 3H, H$_{Ar}$ B[h]Q), 4.78 (t, 1H, H$_a$, $^1J_{H-Si}$ = 95.4 Hz, $^1J_{H-H}$ = 2.8 Hz),

2.31 (bs, 2H, Si-*thf*), 2.07 (bs, 2H, Si-*thf*), 1.88 (bs, 15H, Cp-*Me$_5$*), 1.34-1.44 [m, 4H, Si-*thf* (overlap with H$_{c,d}$ peaks of free silane)], 0.83 (bs, 2H, H$_g$ or H$_{g'}$), 0.75 (broad m, 2H, H$_d$), 0.60-0.69 [broad m, 4H, (H$_g$ or H$_{g'}$) + H$_c$], 0.53 (t, 3H, H$_e$, J = 8.7 Hz), -0.1 (m,

2H, H_b). **^{13}C (151 Hz, 233 K, d_8-THF)**: δ = 163.0 (1:1:1:1 quartet, $^1J_{C-B}$ = 49.7 Hz, $\underline{C}$–B in BArF$_{24}$), 158.2 (B[*h*]Q), 153.3 (broad, H-$\underline{C}$=N, B[*h*]Q), 142.6 (B[*h*]Q), 137.2 ($\underline{C}$-H, B[*h*]Q), 135.8 (B[*h*]Q), 135.6 (m, B[*h*]Q + $\underline{C}$–H$_{ortho}$ in BArF$_{24}$), 134.7 (B[*h*]Q), 131.0 ($\underline{C}$-H, B[*h*]Q), 130.8 ($\underline{C}$-H, B[*h*]Q), 130.1 (qq, $^2J_{C-F}$ = 31.0 Hz, $^3J_{C-F}$ = 2.8 Hz, $\underline{C}_{Ar}$-CF$_3$ in BArF$_{24}$), 128.6 (B[*h*]Q), 125.6 (q, $^1J_{C-F}$ = 272.6 Hz, $\underline{C}$F$_3$ in BArF$_{24}$), 125.2 ($\underline{C}$-H, B[*h*]Q), 123.1 ($\underline{C}$-H, B[*h*]Q), 121.3 ($\underline{C}$-H, B[*h*]Q), 118.5 (m, C-H^{para} in BArF$_{24}$), 94.7 ($\underline{Cp}$-Me$_5$), 14.5 (broad m, C_b), 13.9 (s, C_e), 9.0 (Cp-$\underline{Me_5}$), [remaining ^{13}C resonances of IrSi^n$\underline{Bu(thf)}$ could not be assigned with certainty as their corresponding ^{13}C resonances, being weak in intensity, overlapped with peaks of excess HSi^{n}BuH$_2$].

^{29}Si [obtained indirectly by ^{1}H,^{29}Si HMQC cross-peak correlation with the ^{1}H triplet at 4.78 ppm; 600/119 Hz, 233 K, d_8-THF]: δ = 71.3 ppm.

¹H, ¹H NOESY

Below is shown one possible representation of the molecular structure of [**4**][BArF$_{24}$] (asymmetry at Ir and Si centres makes possible the co-existence of two pairs of epimeric forms with four relative diastereomers), which is drawn here for pointing out the various NOESY through-space correlations observed in the 2D spectrum shown in the spectra section.


[**4**][BArF$_{24}$]
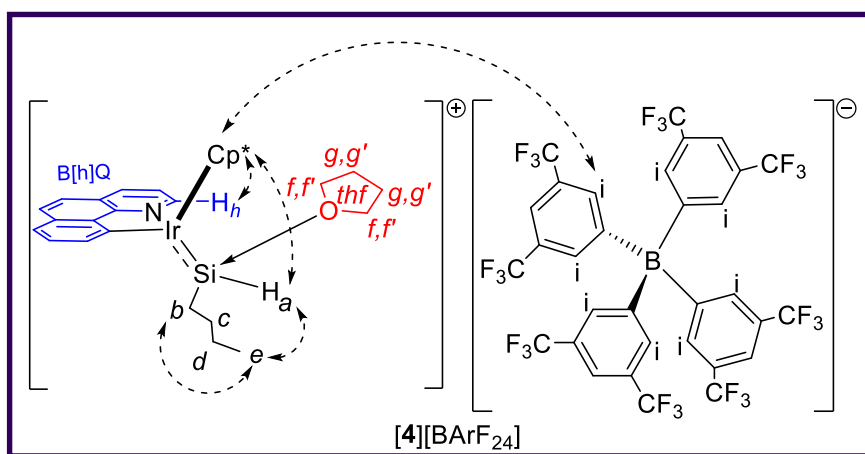
2-D ¹H,¹H NOESY NMR spectroscopy was recorded (600 MHz, 233 K, d_8-THF) in order to help with the assignment of *spatially correlated* ¹H nuclei. This method of analysis allowed us to obtain (together with all other NMR analyses) additional strong evidence for the structural assignment that we attribute to compound [**4**][BArF$_{24}$] *in solution*. Also, this further confirms that the molecular structure adopted by [**4**][BArF$_{24}$] in the solid-state (X-ray diffraction analysis of single crystals) is also maintained in solution. Most importantly, through-space cross-peak correlations are observed between H_a (i.e. hydrogen bound directly to Si) and nuclei belonging to Cp* (CH_3) and *n*-butyl (H_{b-e}), as well as between CH_3 of Cp* and nuclei belonging to B[*h*]Q (H_h) and [BArF$_{24}$]$^-$ (H_i); thus unambiguously establishing the long-range interactions between these groups (through either covalent bonds or noncovalent interactions) and hence the overall molecular cohesion of the ionic Ir-"silylene" metallacycle [**4**][BArF$_{24}$].

NMR spectra

^{1}H NMR (procedure 2)
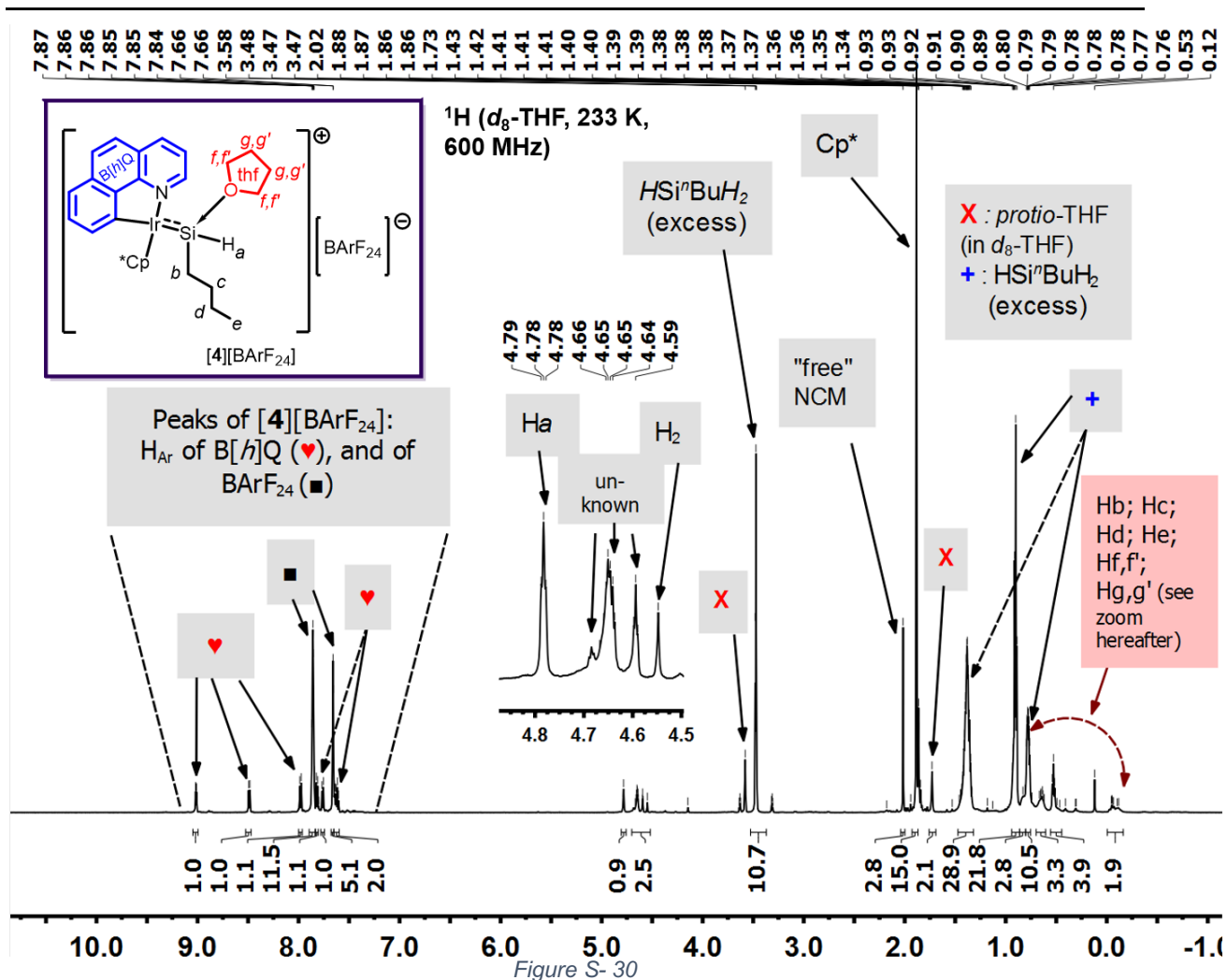
Figure S- 30

^{1}H (d_8-THF, 233 K, 600 MHz)
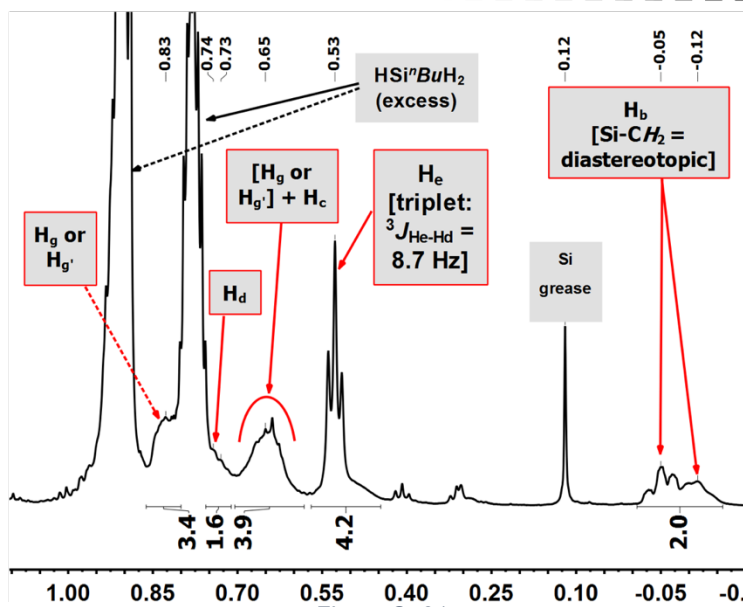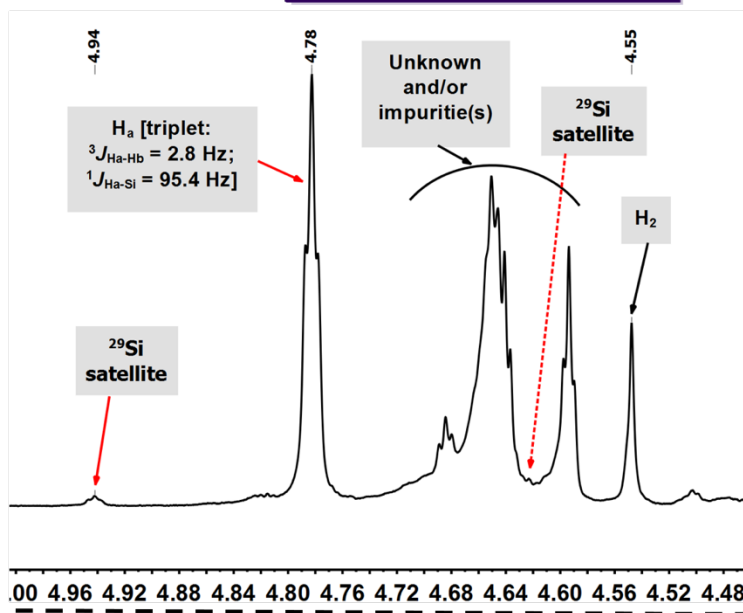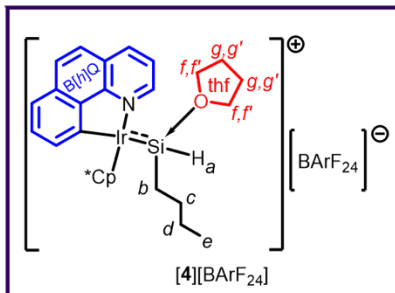
Figure S- 31
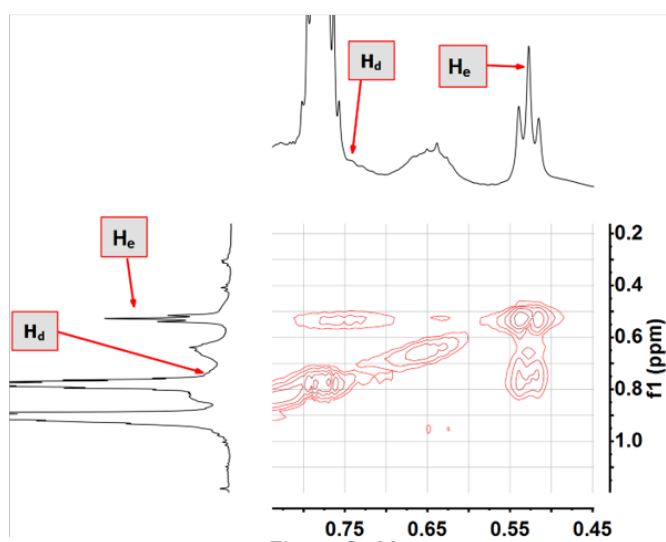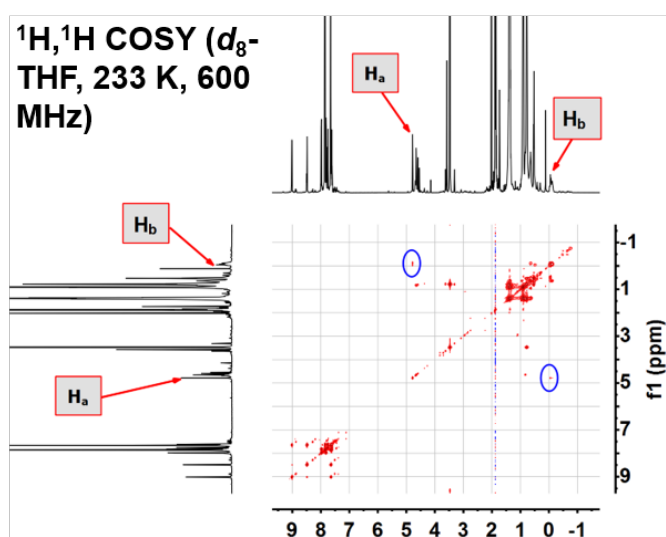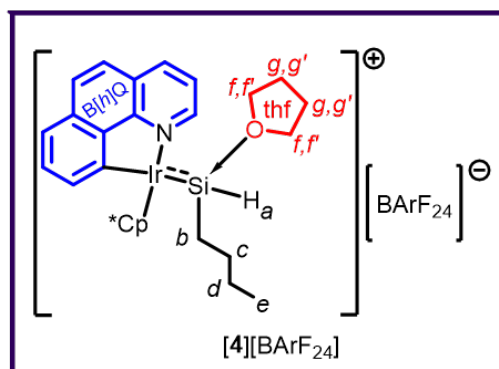
Figure S- 32

^{1}H,^{1}H NOESY NMR (procedure 2)
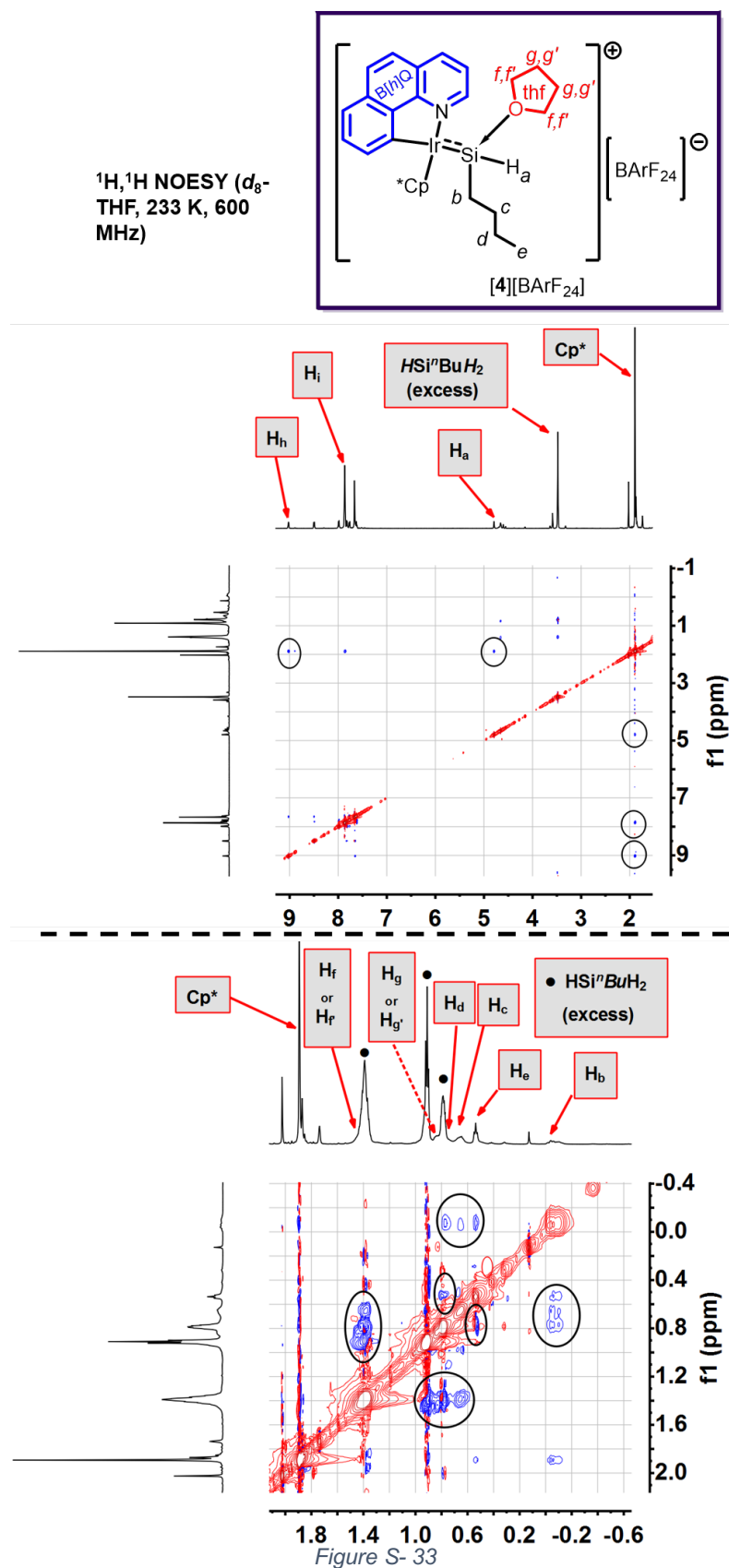
Figure S- 33

Figure S- 34

^{1}H,^{29}Si HMQC (d_8-THF, 233 K, 600/119 MHz)
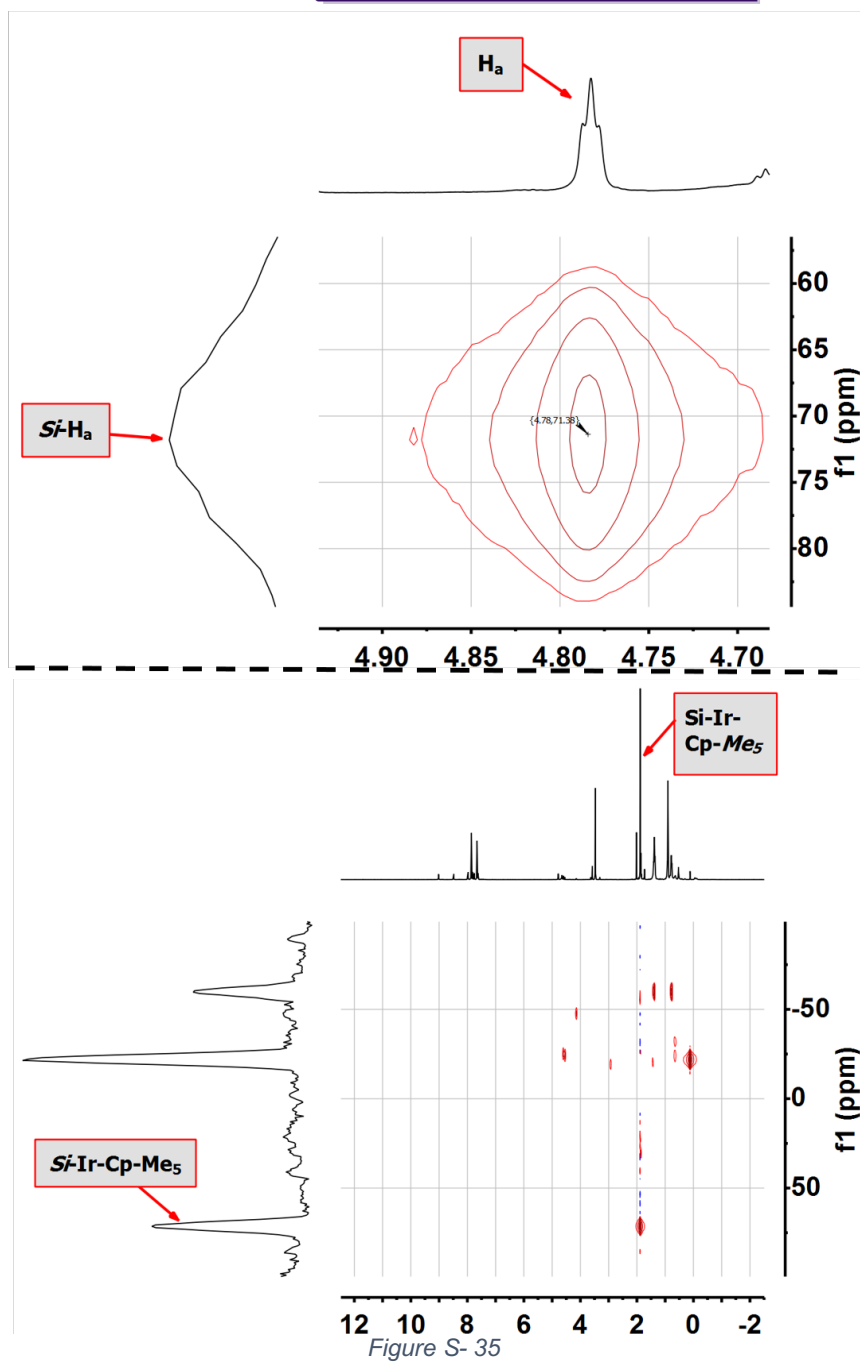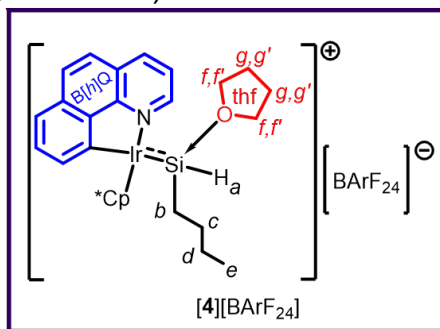
Figure S- 35

^{13}C-^{1}H NMR (procedure 2)

Figure S- 36
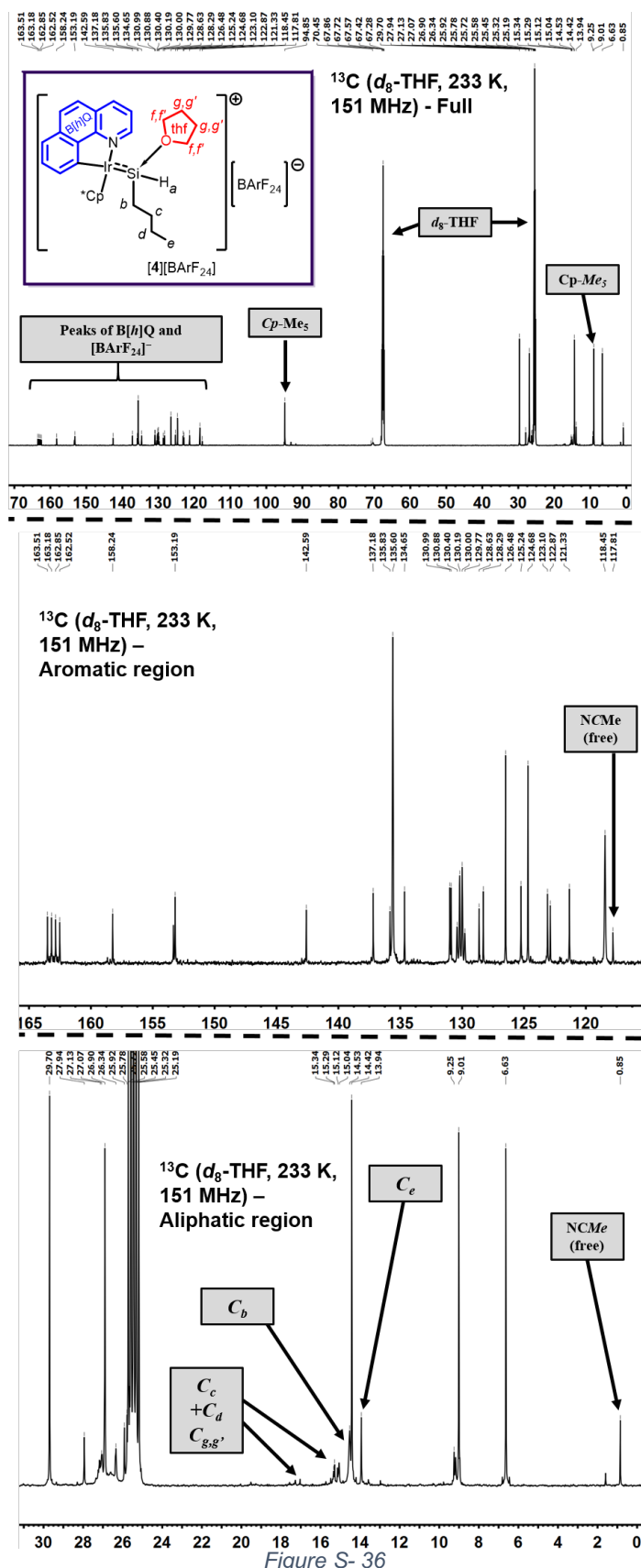
In-situ Generation of [5][BArF$_{24}$] by Reaction of [1b][BArF$_{24}$] with HSi^{n}HexH$_2$ and THF: Procedures, NMR Data, and Spectra

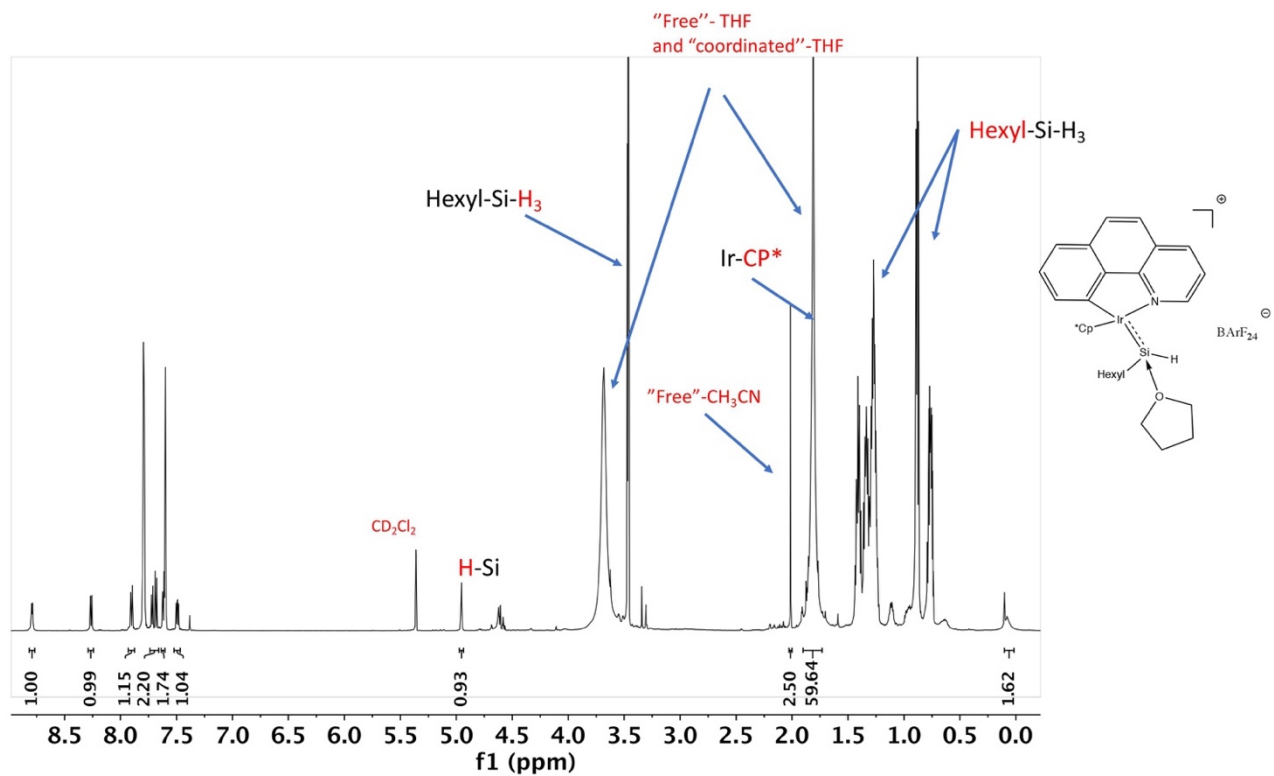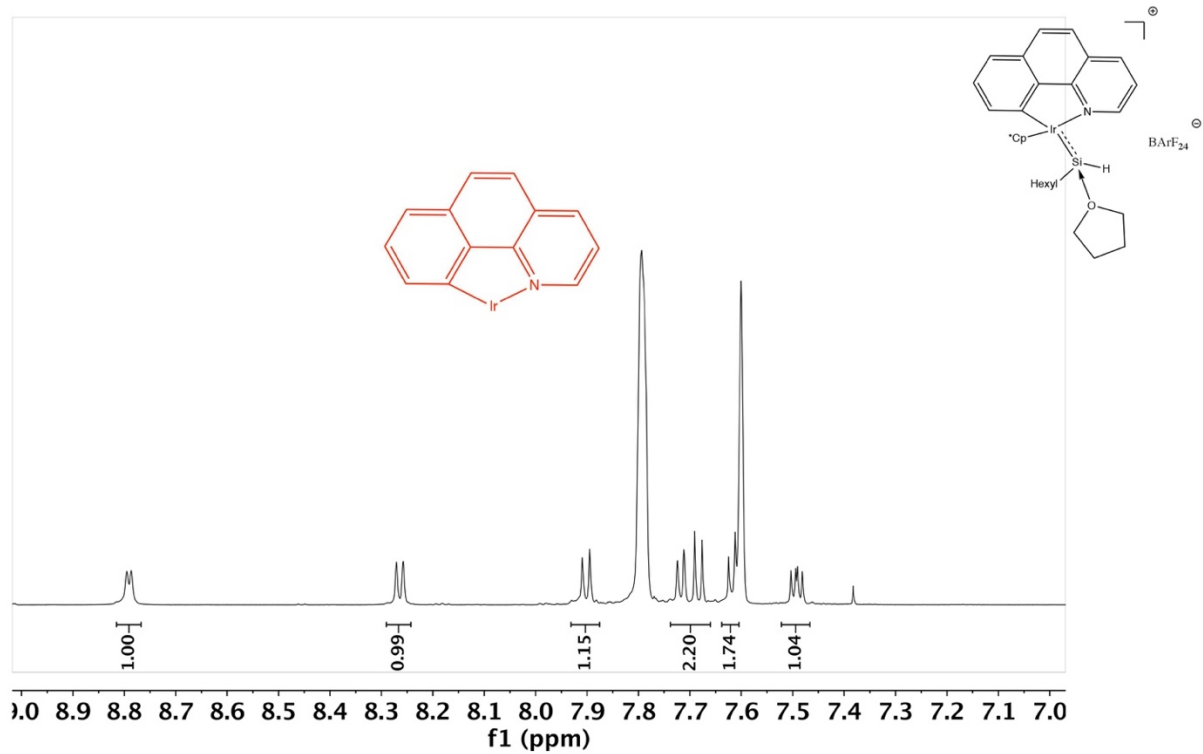Compound [**5**][BArF$_{24}$] was generated in solution using the procedure 2 previously described for [**3**][BArF$_{24}$] (cf. previous section): HSi^{n}HexH2 (20.0 μL, 77.0 μmol) was added to a solution of [**1b**][BArF$_{24}$] (30 mg, 21.2 μmol) in d_8-THF (0.45 mL). The resulting solution was shaken and transferred into a J. Young NMR sample tube which was subsequently tightly sealed for analysis at -40 °C. Full conversion was obtained after 2 h of reaction, as verified by ^{1}H NMR analysis (cf. spectra in the next sub-section). Indeed, the latter ^{1}H NMR spectrum indicated complete consumption of [**1b**][BArF$_{24}$] and selective formation of [**5**][BArF$_{24}$] along with H$_2$ (singlet at ca. *δ* 4.55 ppm).

NMR data

---

^{1}H, ^{13}C-^{1}H and ^{1}H,^{29}Si HMQC

^{1}H NMR (600 MHz, CD$_2$Cl$_2$) δ 8.79 (d, J = 5.4 Hz, 1H), 8.30 – 8.23 (m, 1H), 7.90 (d, J = 8.8 Hz, 1H), 7.70 (dd, J = 20.6, 8.3 Hz, 2H), 7.62 (d, J = 7.5 Hz, 2H), 7.49 (dd, J = 7.9, 5.4 Hz, 1H), 4.95 (t, J = 3.1 Hz, 1H, H-Si), 3.67 (J = 3.68 Hz, 2H, Si-*thf*), this peak is overlap of Ir-Cp*, excess of THF and coordinated-THF, 1.82 (d, J = 6.3 Hz, 15H), 1.82 (d, J = 6.3 Hz, 2H, Si-*thf*), 0.14 – 0.01 (m, 2H, alkyl group of Ir-Si-Hexyl), the rest of Si-alkyl group is undetected.

^{29}Si NMR (600 MHz, CD$_2$Cl$_2$) δ 79.89 ppm

Hexyl-Si-H₃ labels, "Free"- THF and "coordinated"-THF, Ir-CP*, "Free"-CH₃CN, CD₂Cl₂, H-Si

Top spectrum integrations: 1.00, 0.99, 1.15, 2.20, 1.74, 1.04

f1 (ppm)

Bottom spectrum labels:

"Free"- THF and "coordinated"-THF

Hexyl-Si-H₃

Hexyl-Si-H₃

Ir-CP*

"Free"-CH₃CN

CD₂Cl₂

H-Si

Integrations: 1.00, 0.99, 1.15, 2.20, 1.74, 1.04, 0.93, 2.50, 59.64, 1.62

f1 (ppm)

BArF₂₄

¹H-²⁹Si HMQC

¹H-²⁹Si HMQC

NOESY

H-Si

NOESY

Si-H

Cp*-Ir

COSY

H-Si-CH₂-C₄H₁₁

Si-H
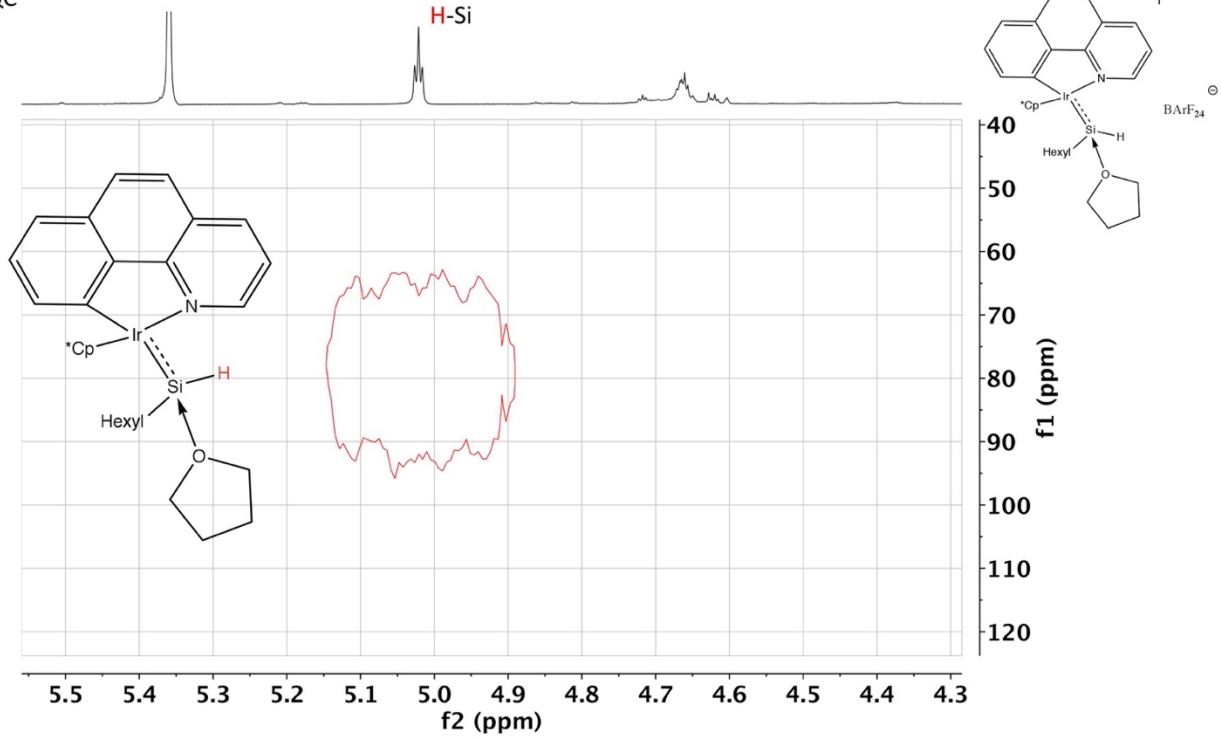
HSQC
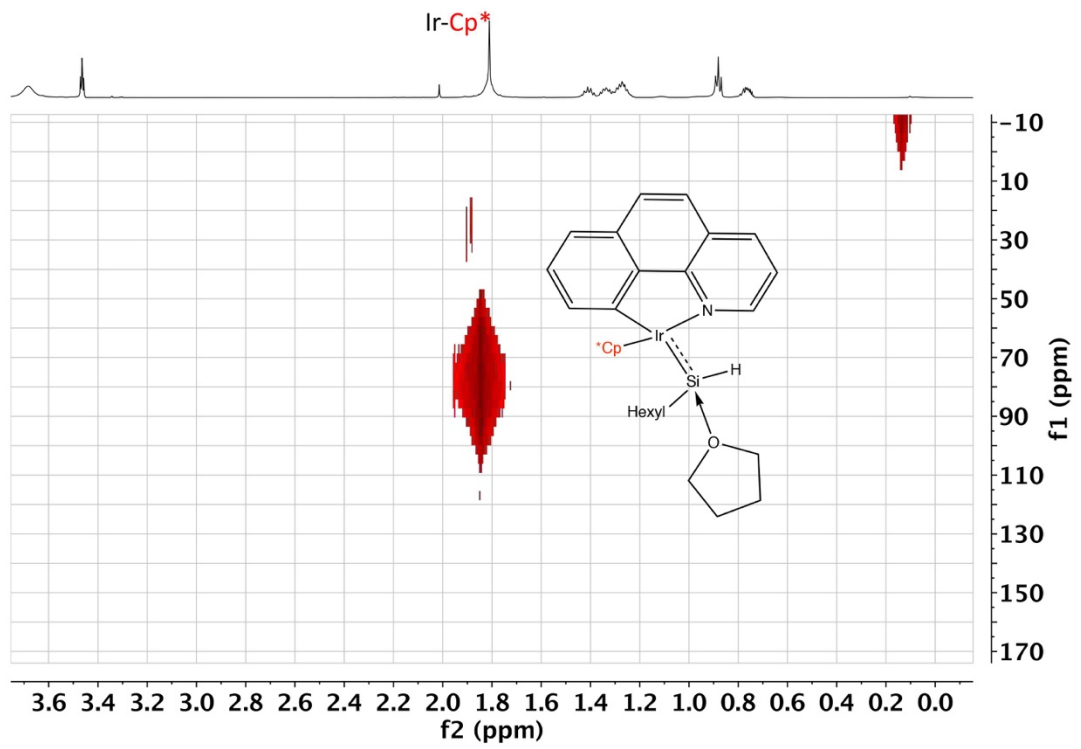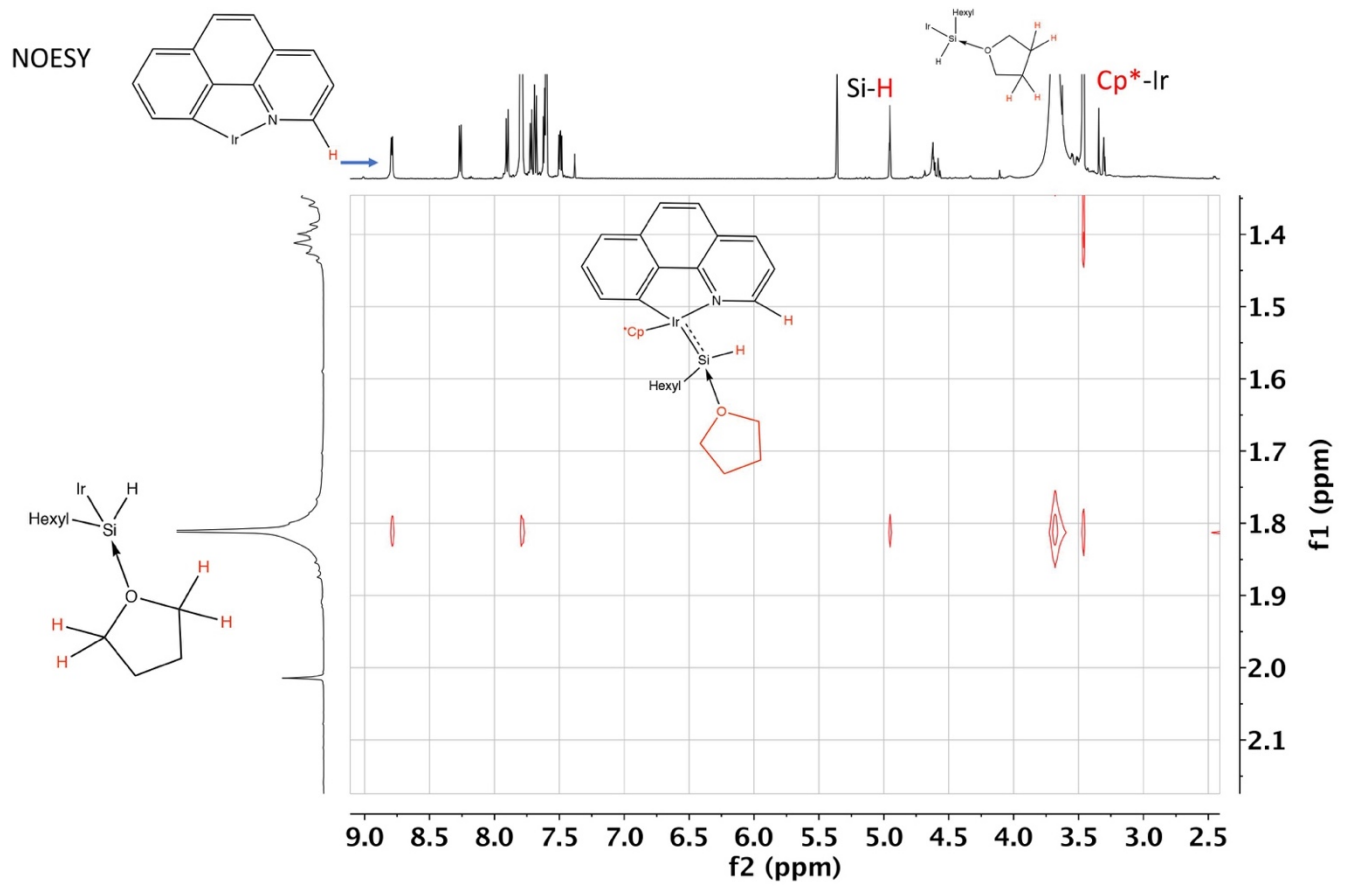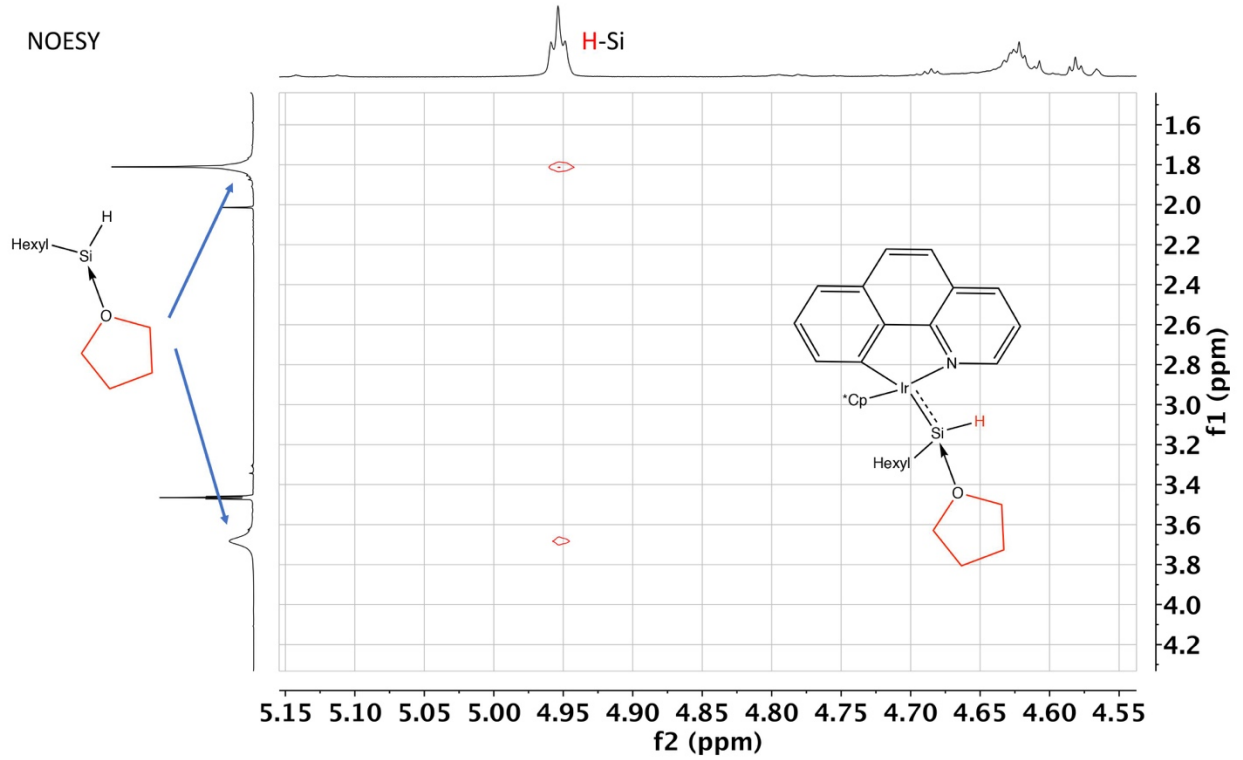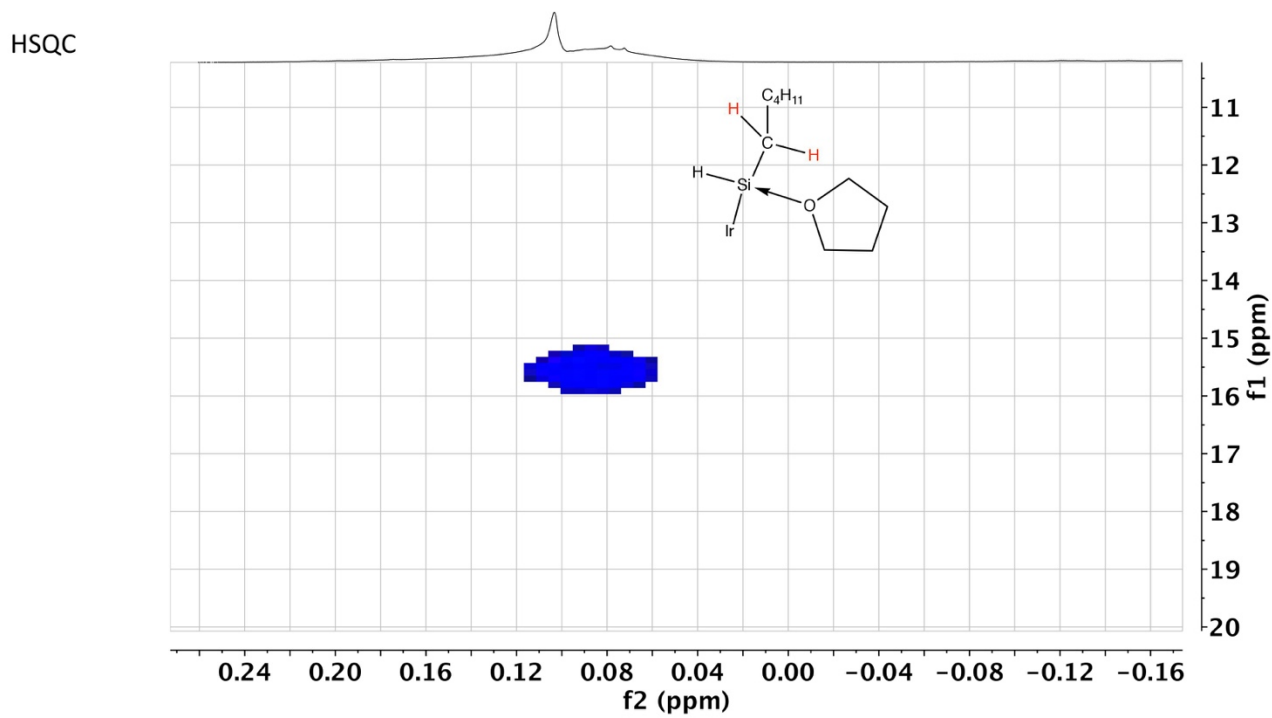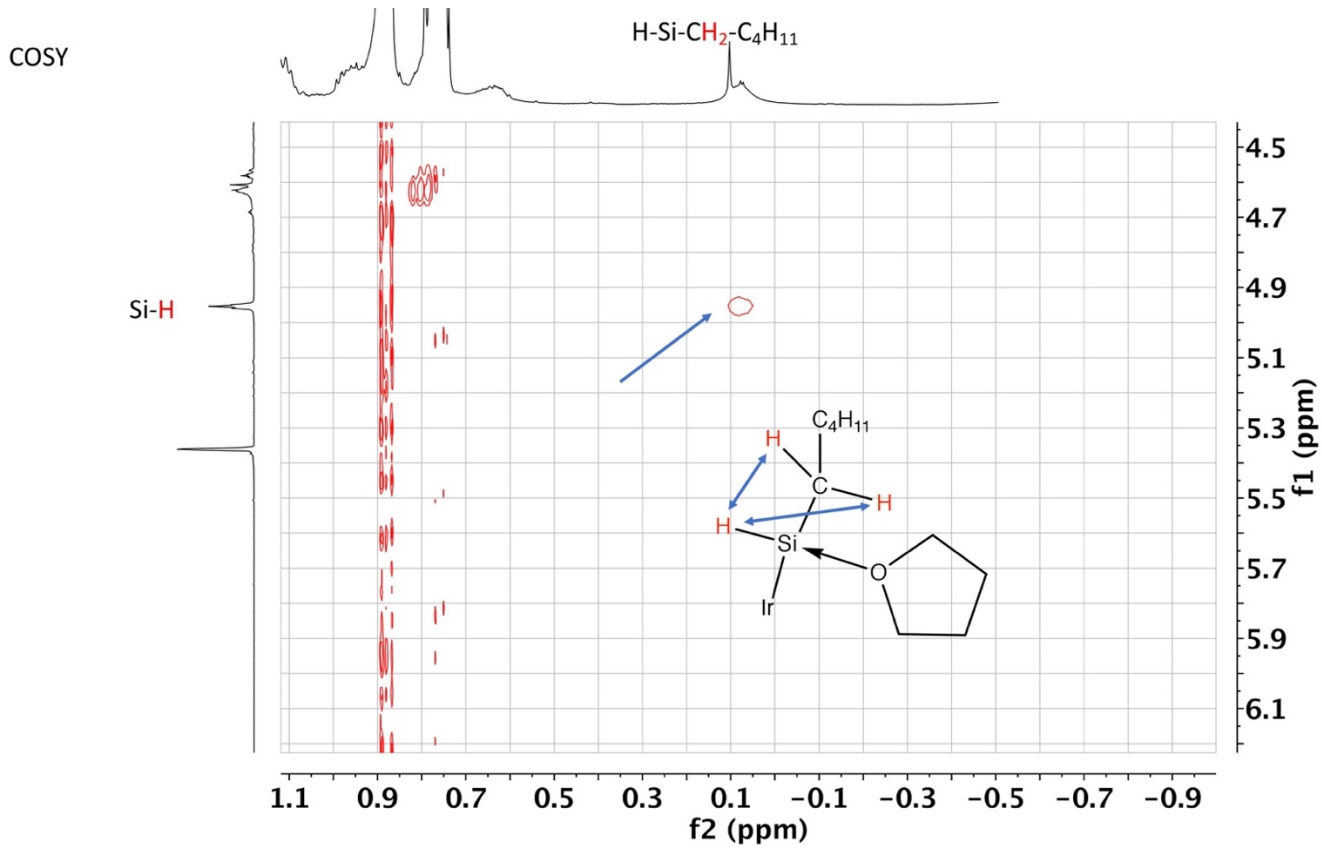
Synthesis of **F-2**

A mixture of [Cp*IrCl$_2$]$_2$ (50.0 mg, 0.081mmol), NaOAc (40.0 mg, 0.49 mmol), F-phenyl pyridine (21.4 mg, 0.17 mmol), was stirred vigorously at room temperature (RT) in 20 mL of dichloromethane for 5 days. The mixture was filtered through Celite and evaporated to dryness[16,17]. The solid obtained was washed with hexane to remove excess ligand. Cyclometalated compound **F-2** was isolated as a red-orange solid (60.0 mg, 80%).

^{1}H NMR (500 MHz, CD$_2$Cl$_2$) δ 7.86 (d, J = 7.0 Hz, 1H), 7.84 – 7.79 (m, 1H), 7.74 (d, J = 6.6 Hz, 2H), 7.25 (t, J = 7.4 Hz, 1H), 7.08 (d, J = 7.1 Hz, 1H), 6.95 (s, 1H), 1.73 (s, 15H).

^{13}C NMR (500 MHz, CD$_2$Cl$_2$) δ 105.55 (C1), 114.70(C3), 122.05(C5), 124.59(C4), 130.89 (C6), 136.02(C7), 141, 47(C2), 53.23 (Cp*),

^{19}F NMR (500 MHz, CD$_2$Cl$_2$) δ -58.21 ppm

HSQC ^{1}H-^{13}C

H1

COSY

H1

H2

COSY

H3

H2

NOESY

Ir-Cp*

H7

COSY

COSY

2H

HSQC

H3   H4

COSY

COSY

216
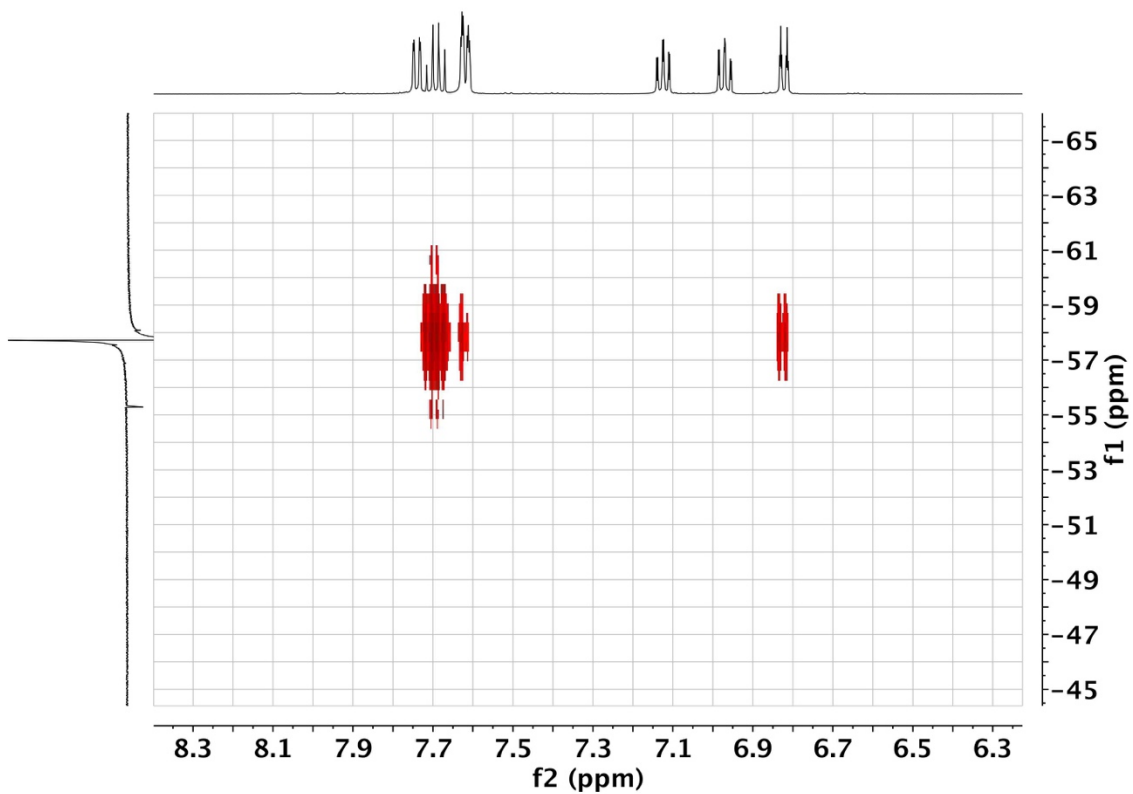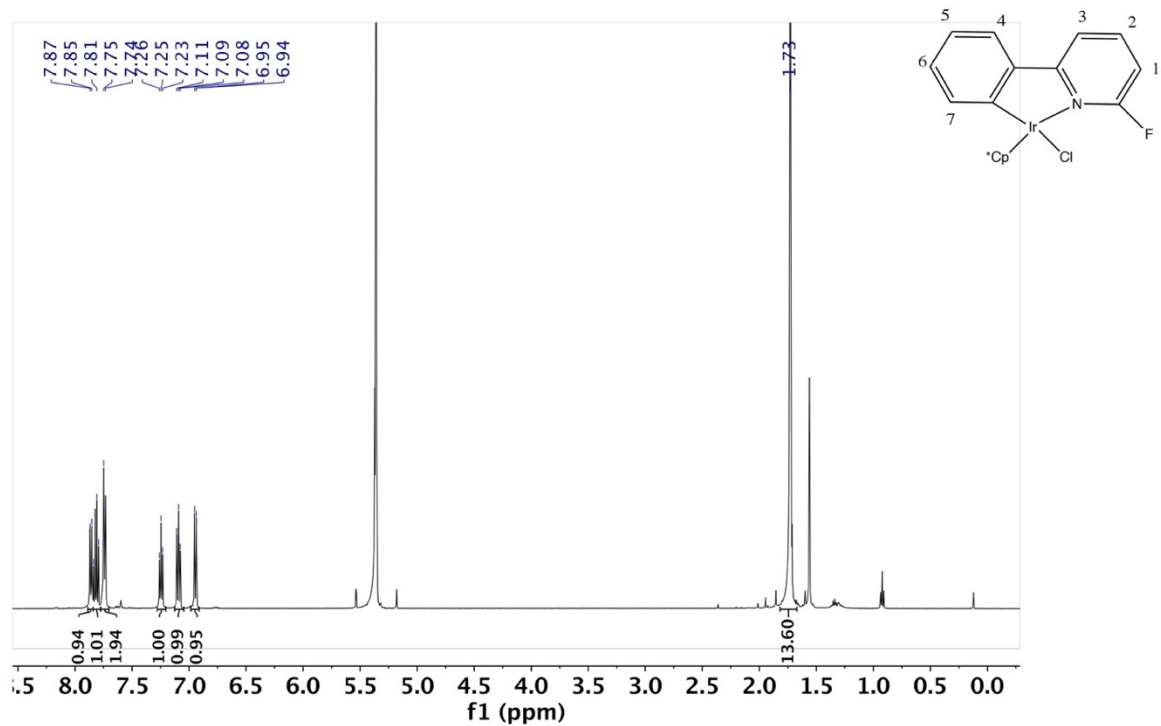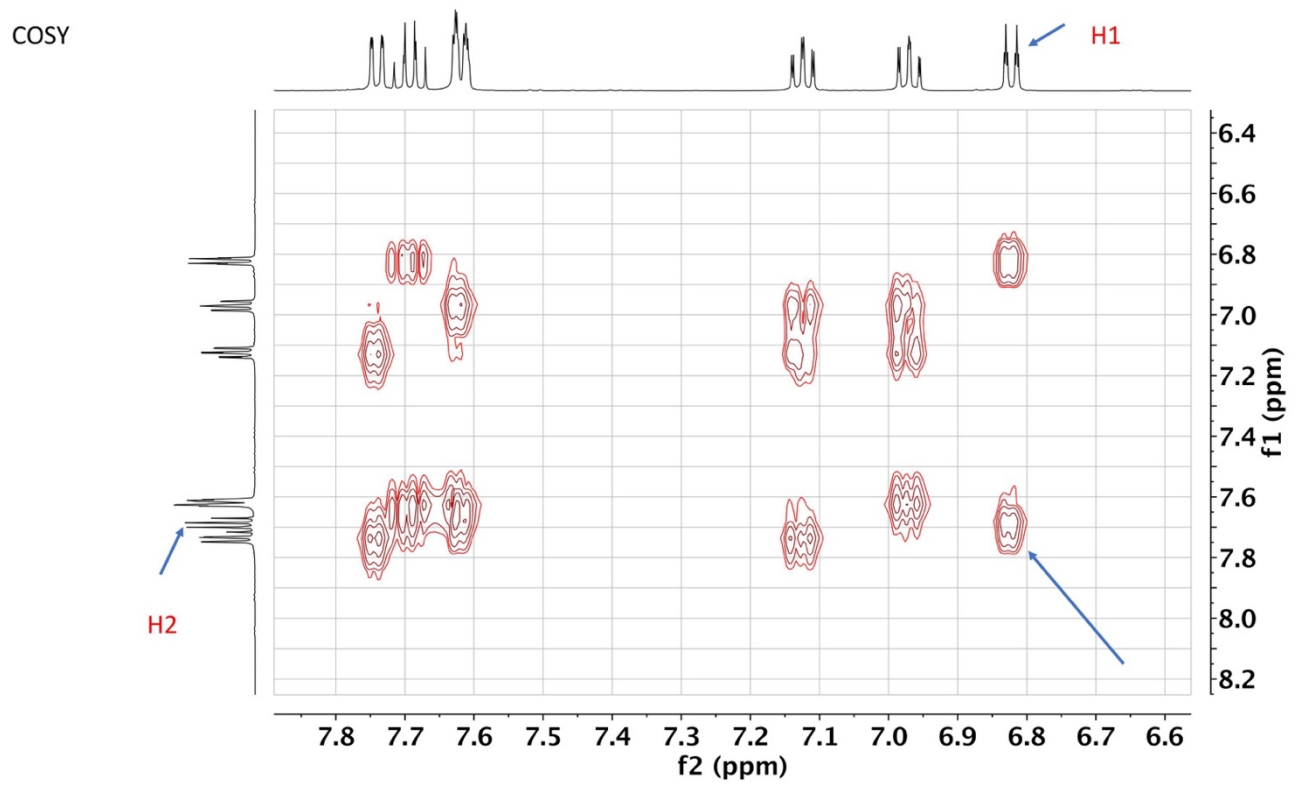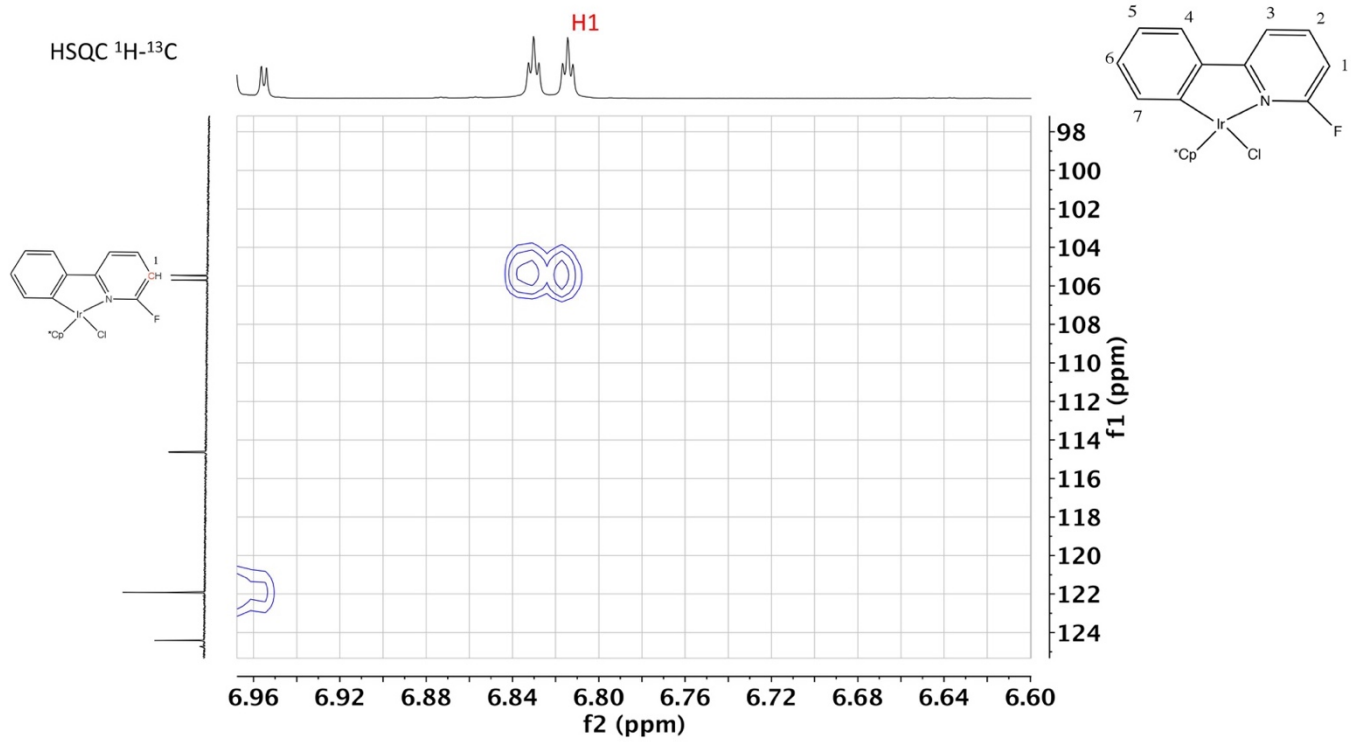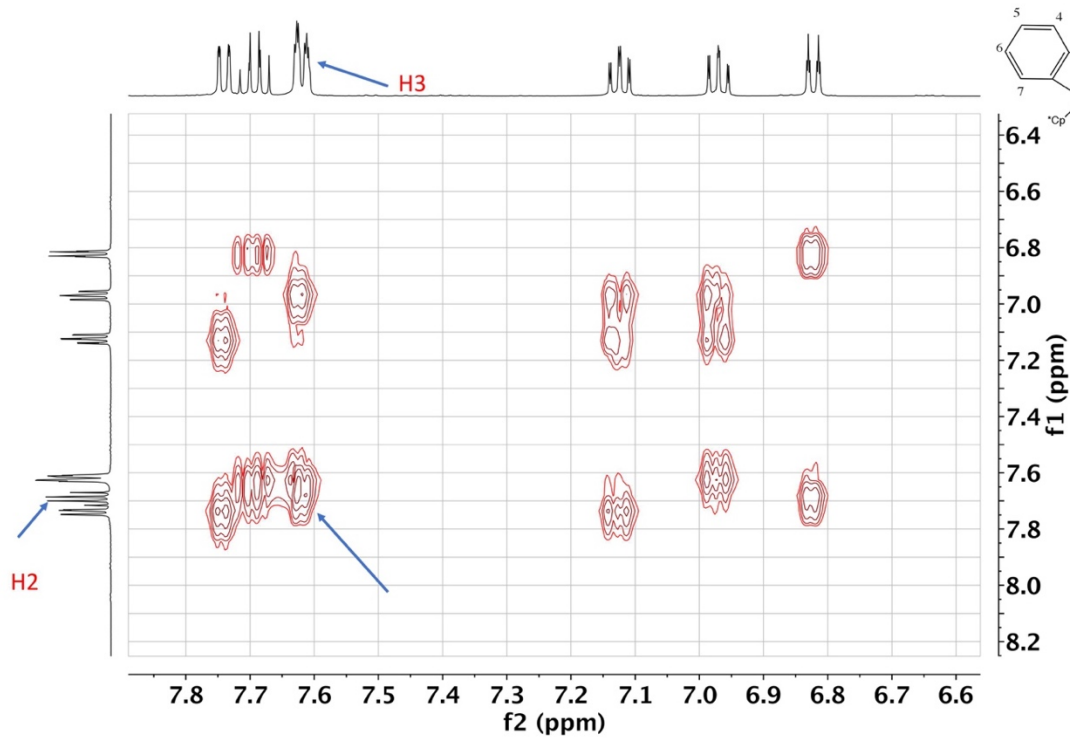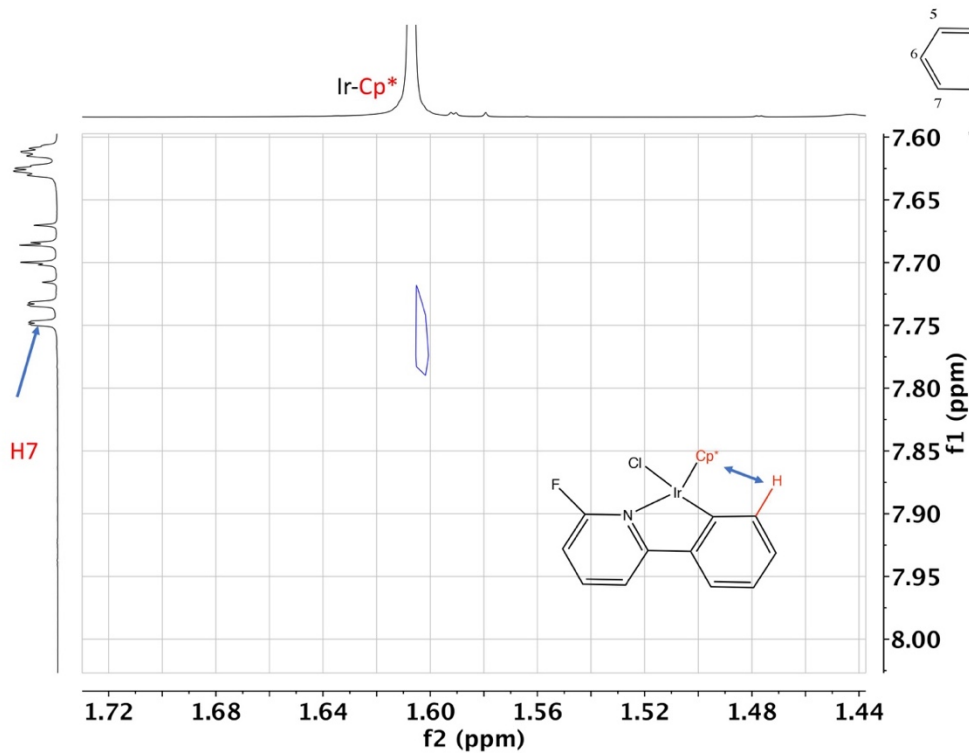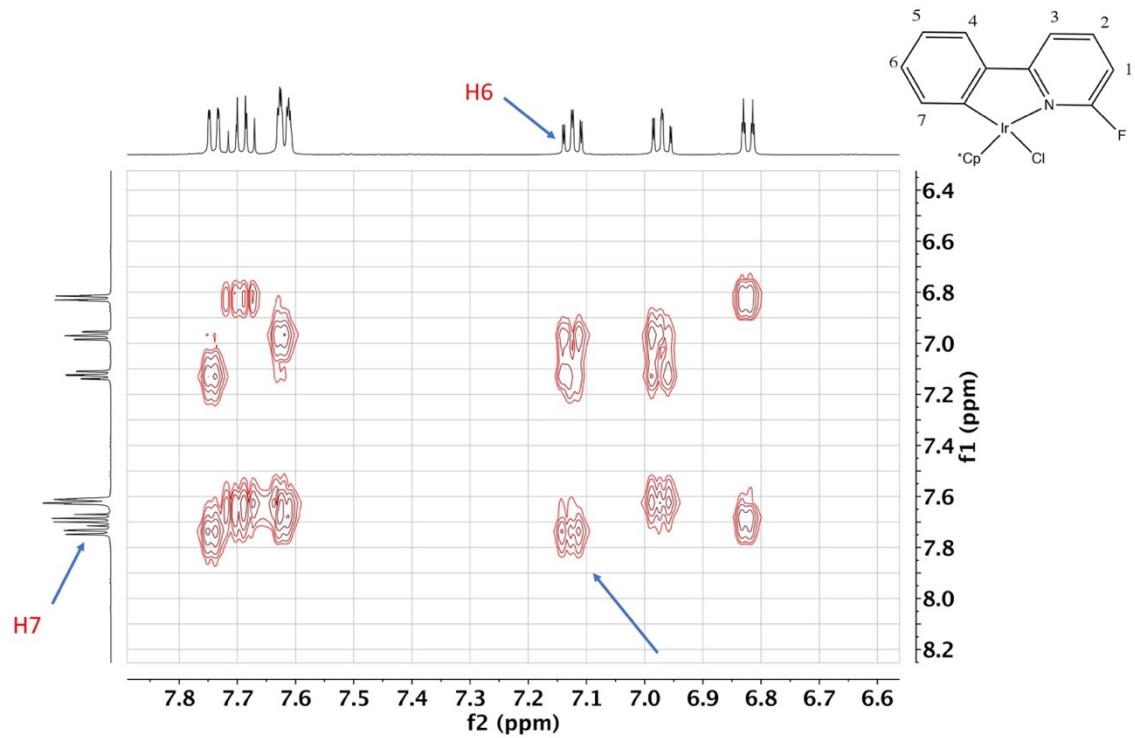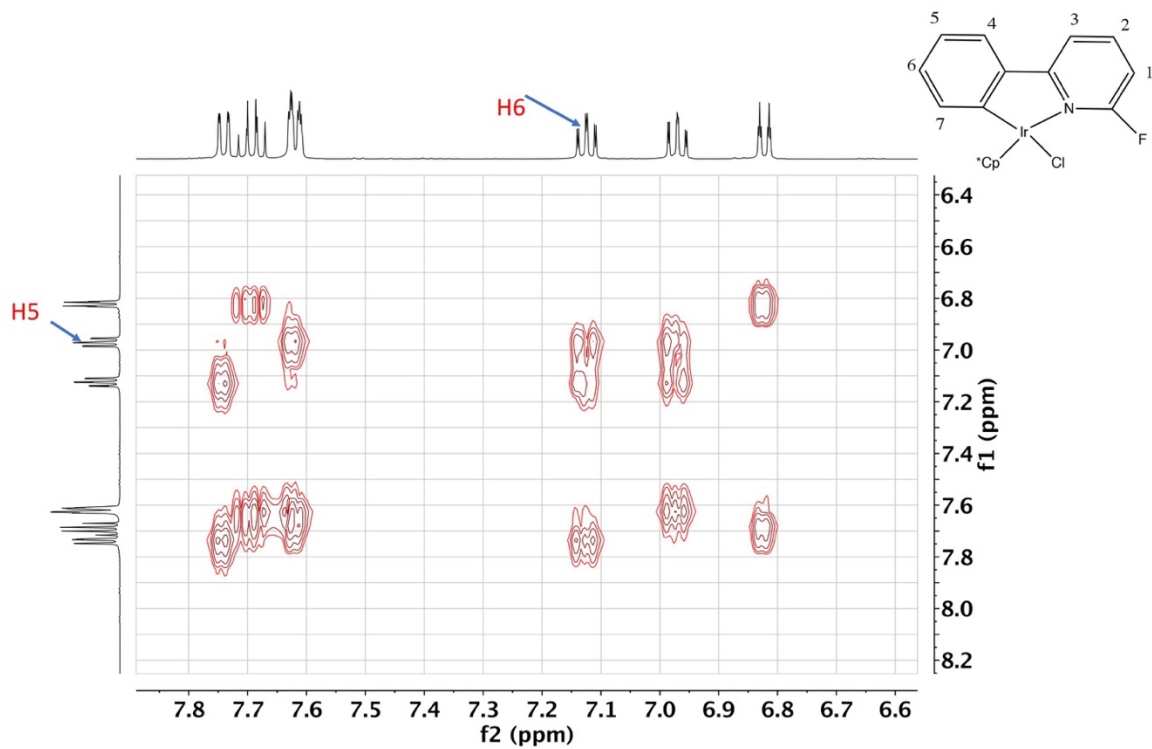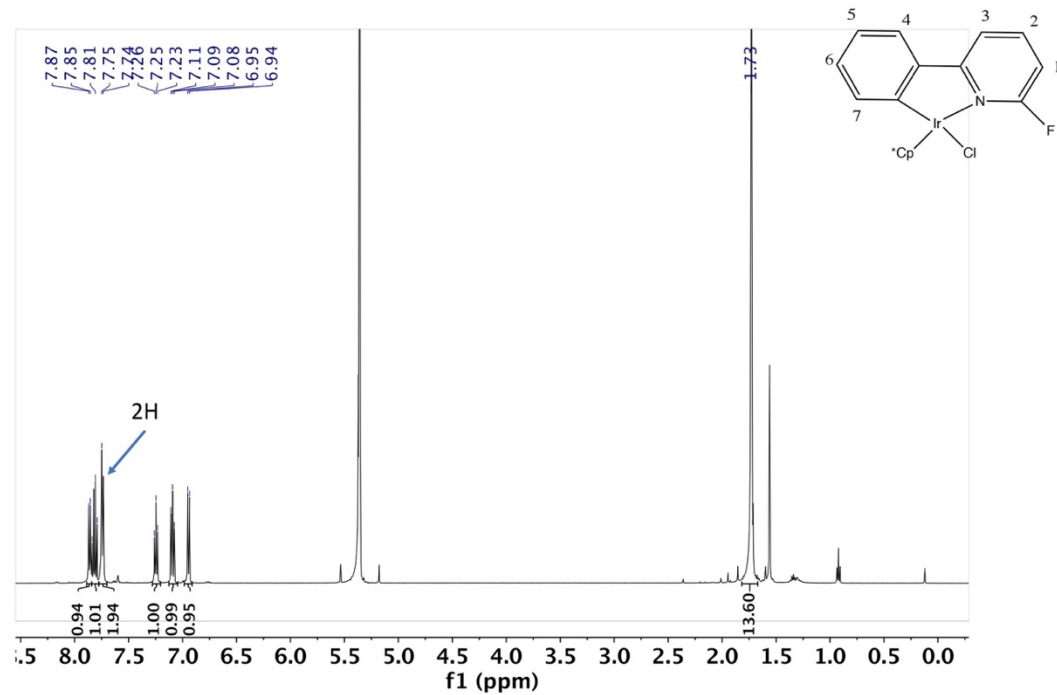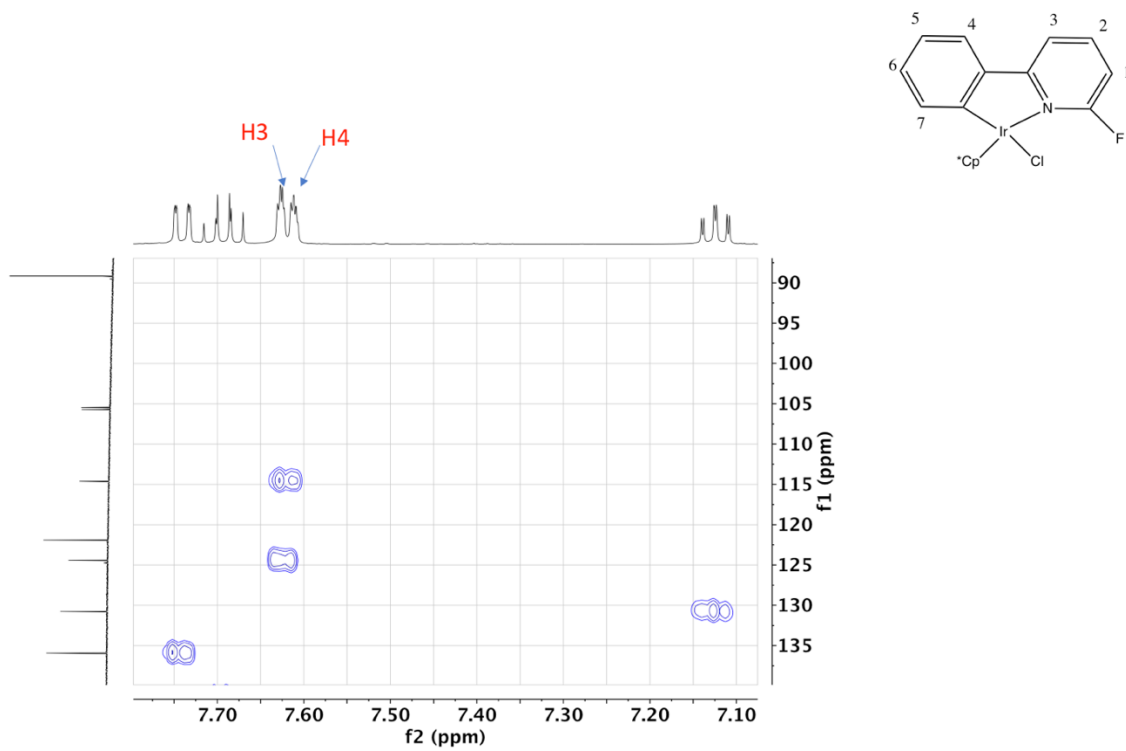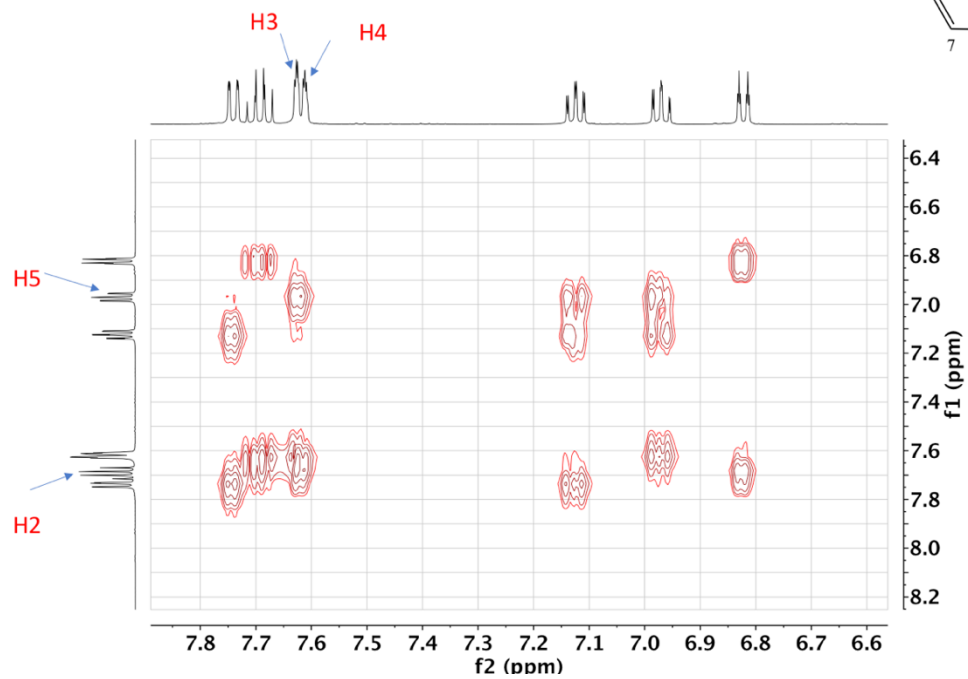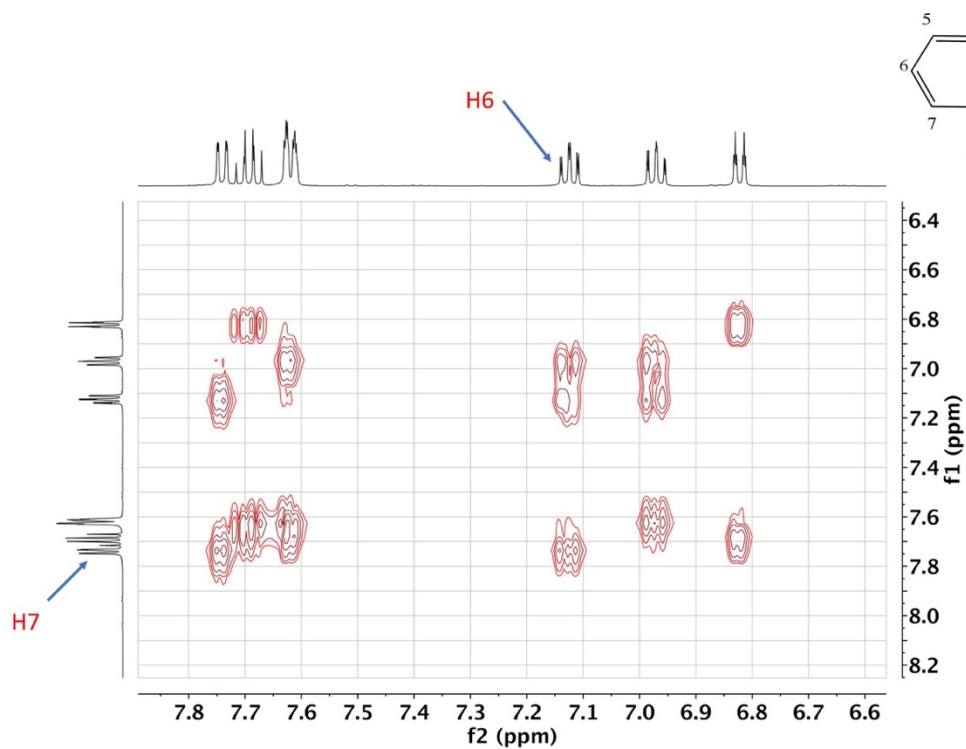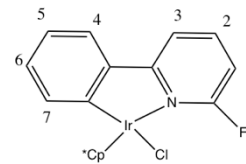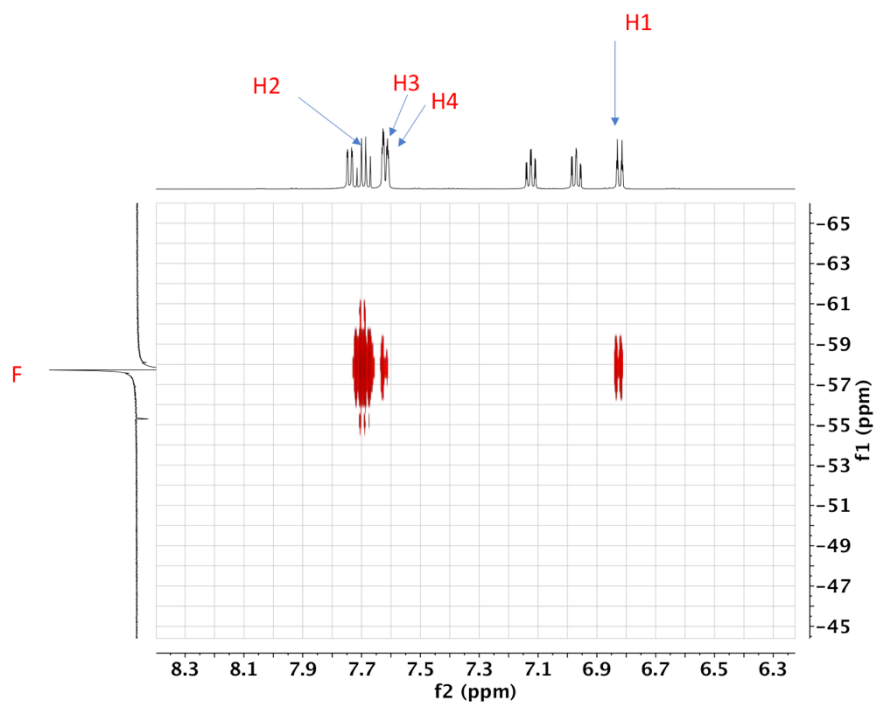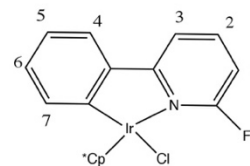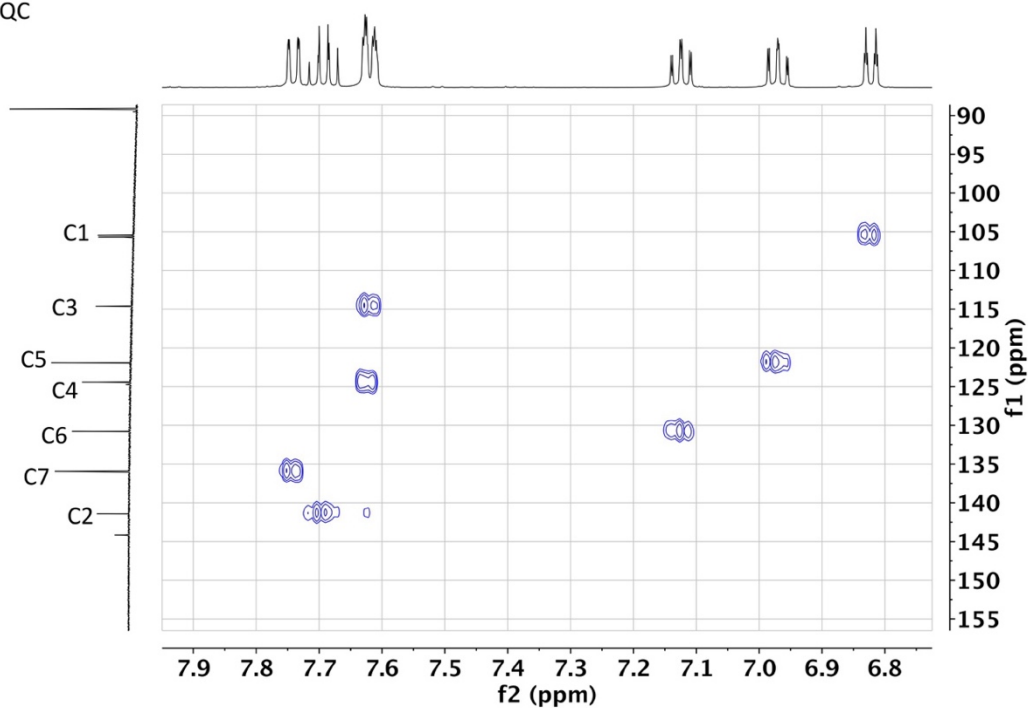
HSQC

HSQC
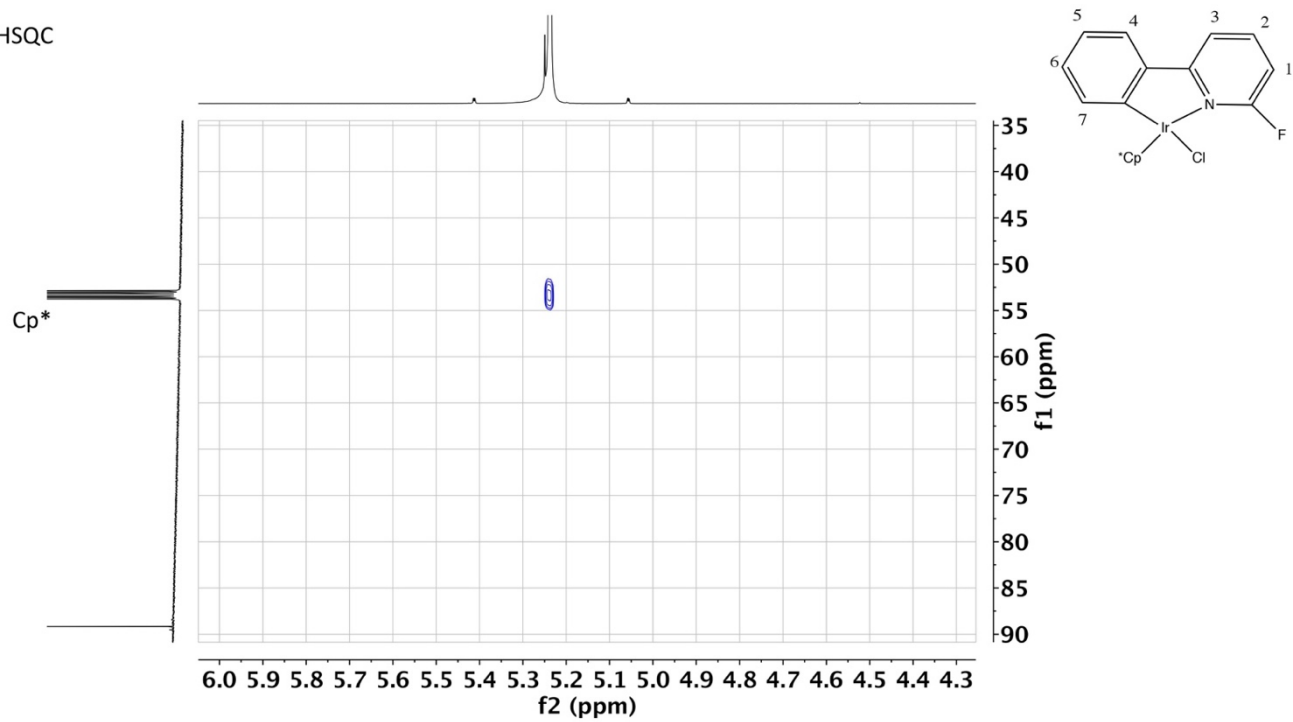
HMBC
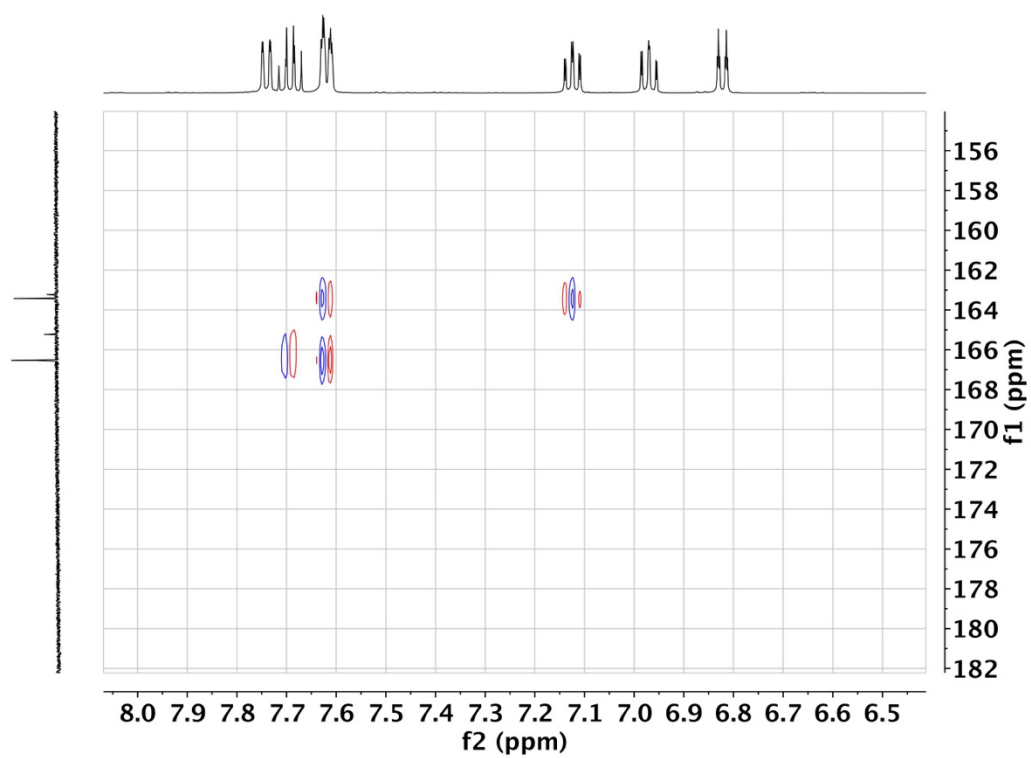
Synthesis of **F-1a**

In a Schlenk flask an equimolar mixture of **F-2** and Na[BArF$_{24}$], was dissolved in acetonitrile ($\sim$7−10 mL). The resulting mixture was vigorously stirred at room temperature for 2 h. The resulting suspension was filtered through a pad of celite, and the solvent was removed from the filtrate under reduced pressure. The solid was either recrystallized in a mixture of CH_2Cl_2 and n-hexane or n-pentane or washed with n-hexane or n-pentane[16,17], to afford an analytically pure compound. (90%)

^{1}H NMR (500 MHz, CD$_2$Cl$_2$) δ 7.90 – 7.81 (m, 1H), 7.73 – 7.68 (m, 3H), 7.22 (td, J = 7.4, 1.4 Hz, 1H), 7.12 (td, J = 7.5, 1.3 Hz, 1H), 6.93 (dt, J = 8.0, 1.2 Hz, 1H), 2.21 (s, 3H), 1.60 (s, 15H).

^{13}C NMR (500 MHz, CD$_2$Cl$_2$) δ 144.50 (C2), 135.04 (C3, C4,C7), 132.58 (C5), 124.1(C6), 106.78 (C1).

^{19}F NMR (500 MHz, CD$_2$Cl$_2$) -57.65

Référence Produit	%N	%C	%H
F-1a	1.45	36.63	2.30
	1.80	44.73	2.77
	1.86	45.45	2.63
Valeur Théorique Attendue	2.00	47.05	2.66

Référence Produit	%N	%C	%H
F-2	2.53	46.35	4.15
	2.50	46.32	4.17
Valeur Théorique Attendue	2.62	47.14	4.14

Table: Elementary analysis of **F-1a** and **F2**

COSY ^{1}H-^{19}F

COSY

220

COSY

HSQC

221
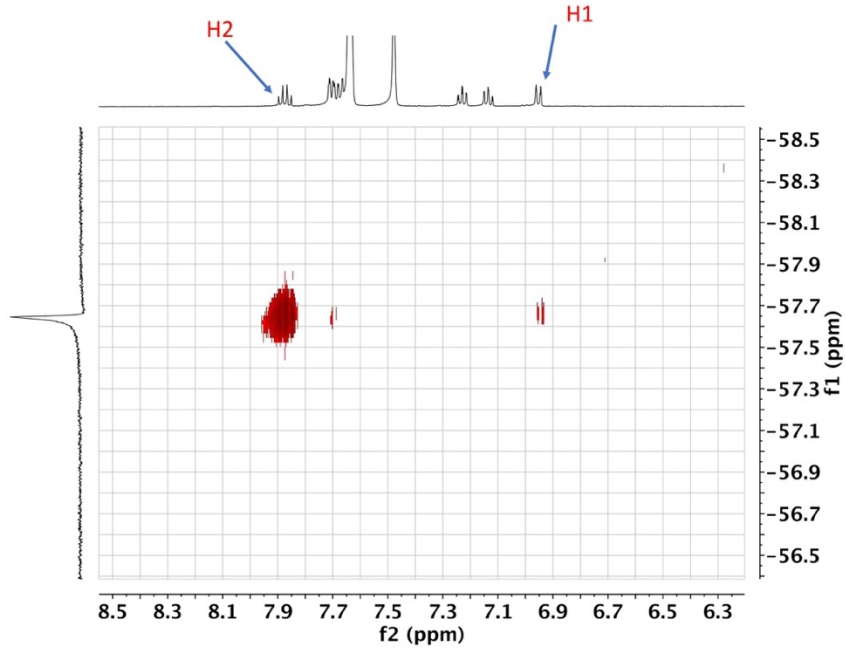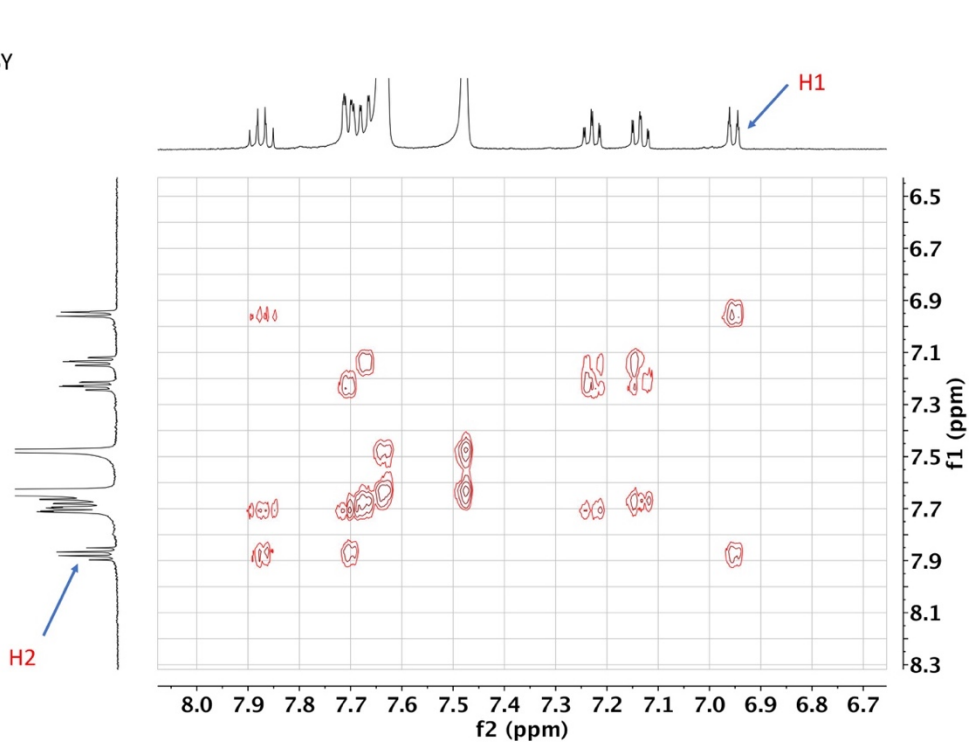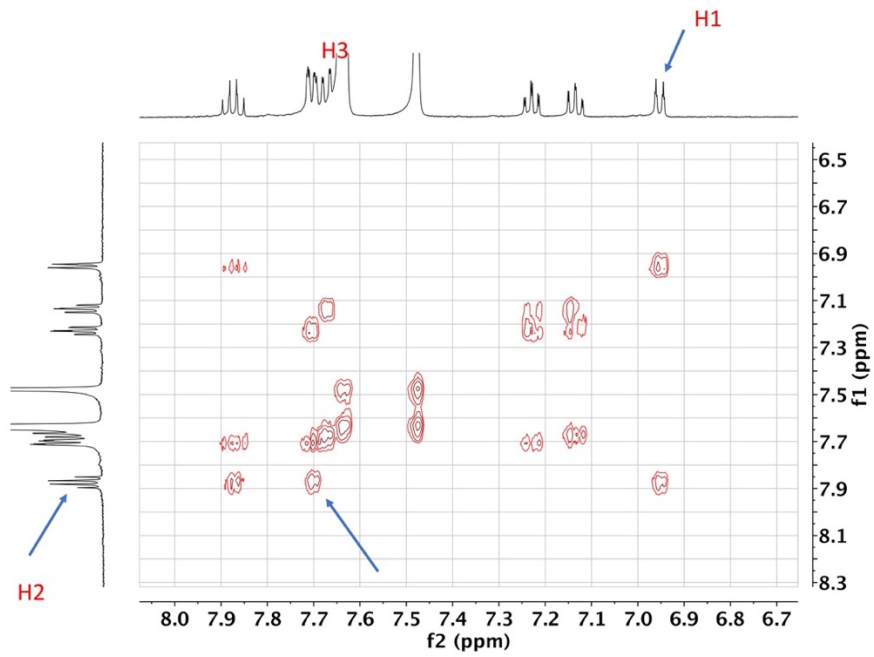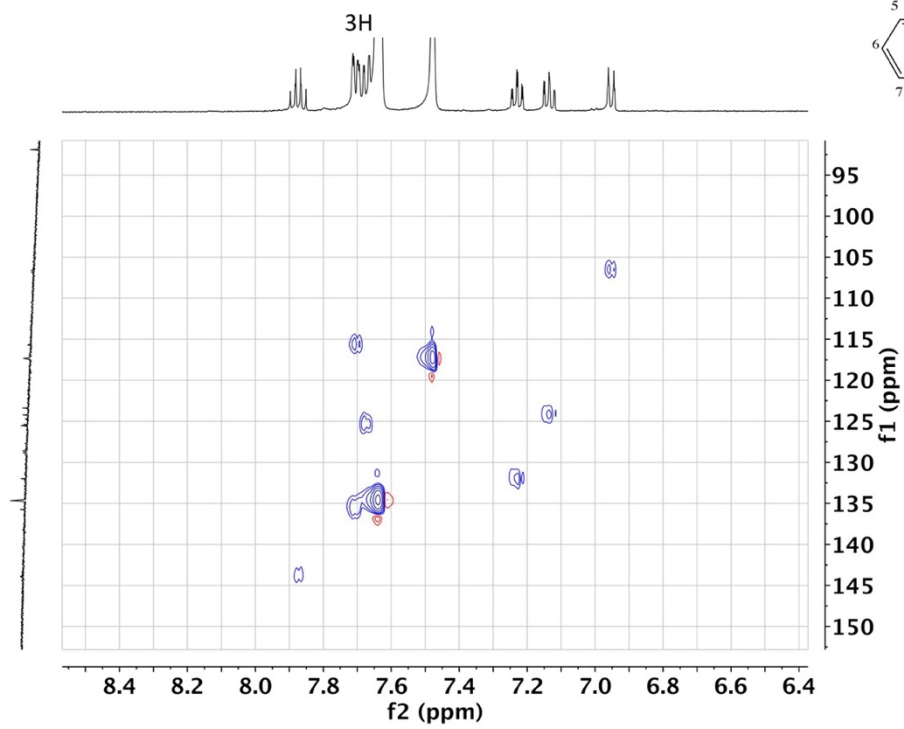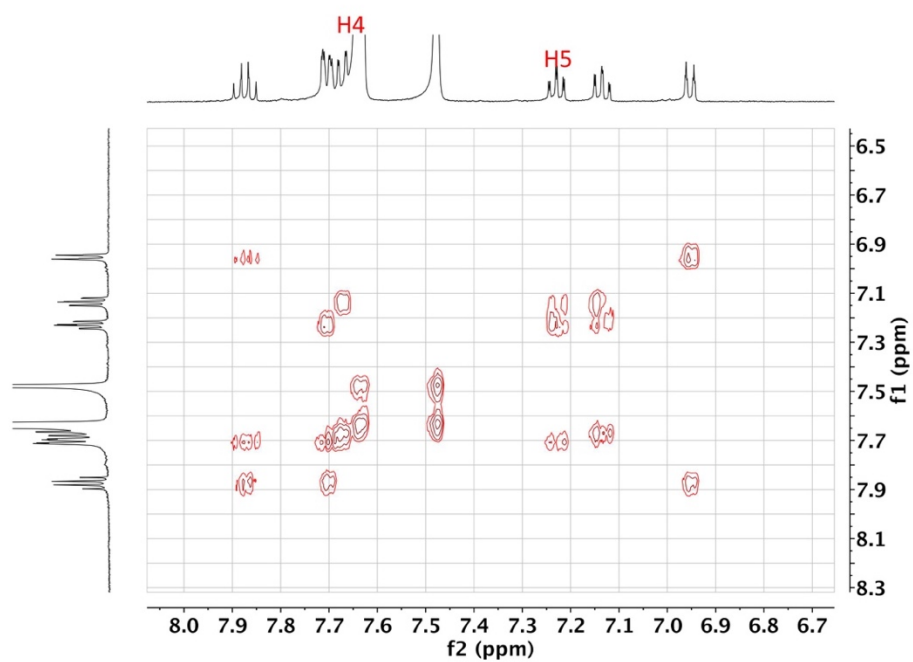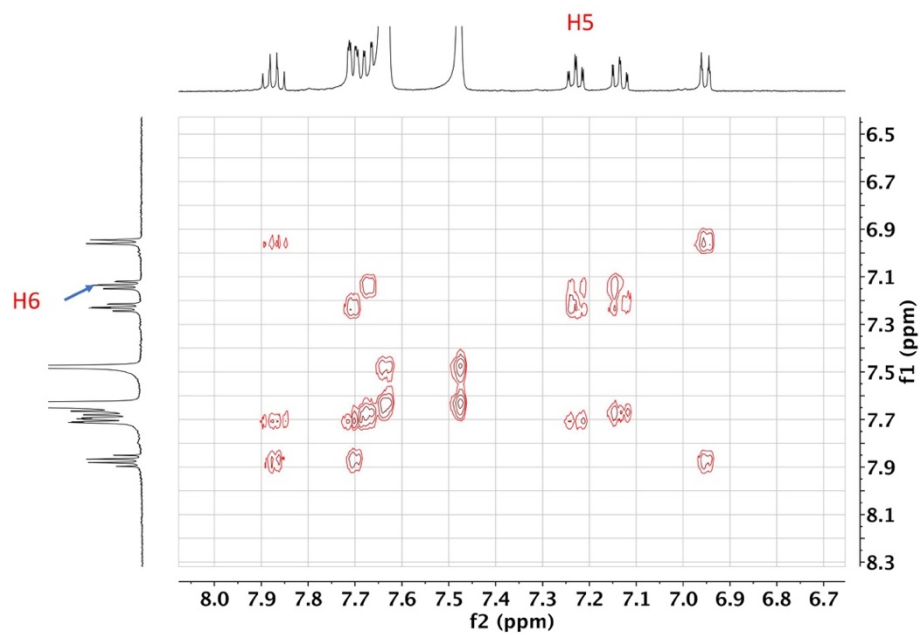
COSY

COSY

COSY
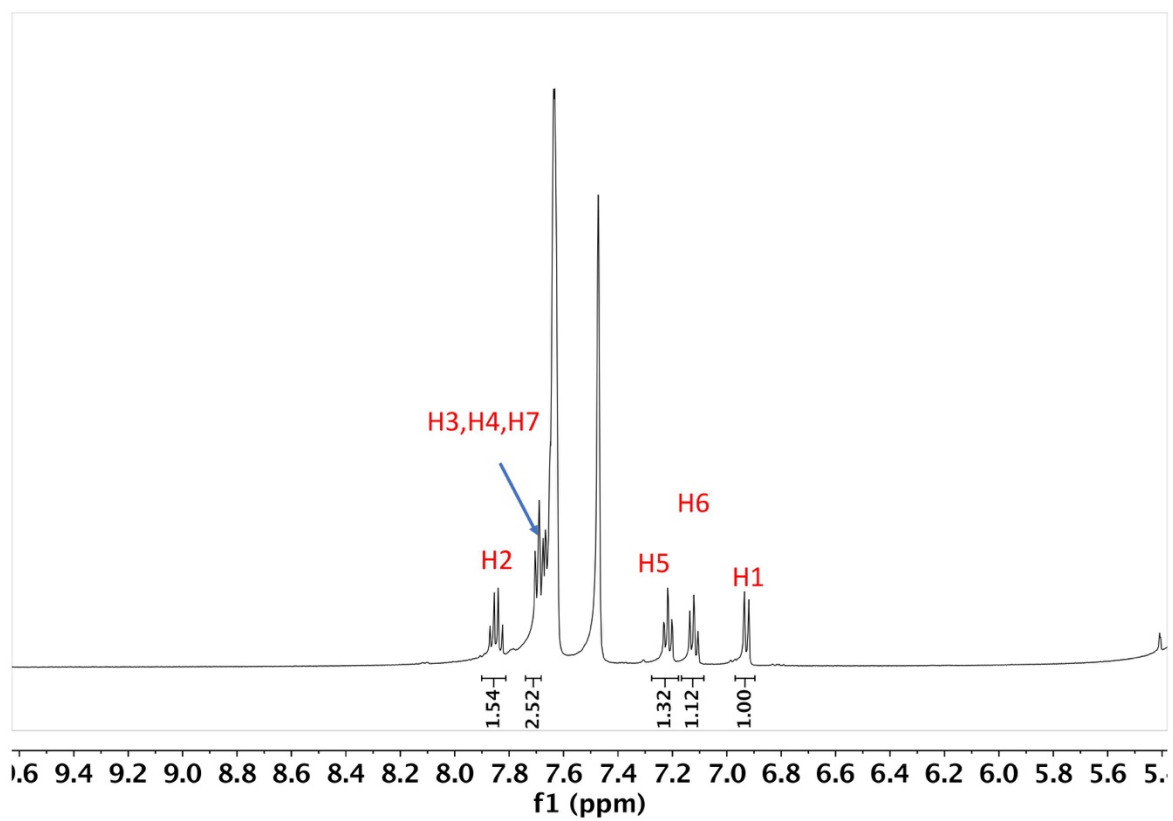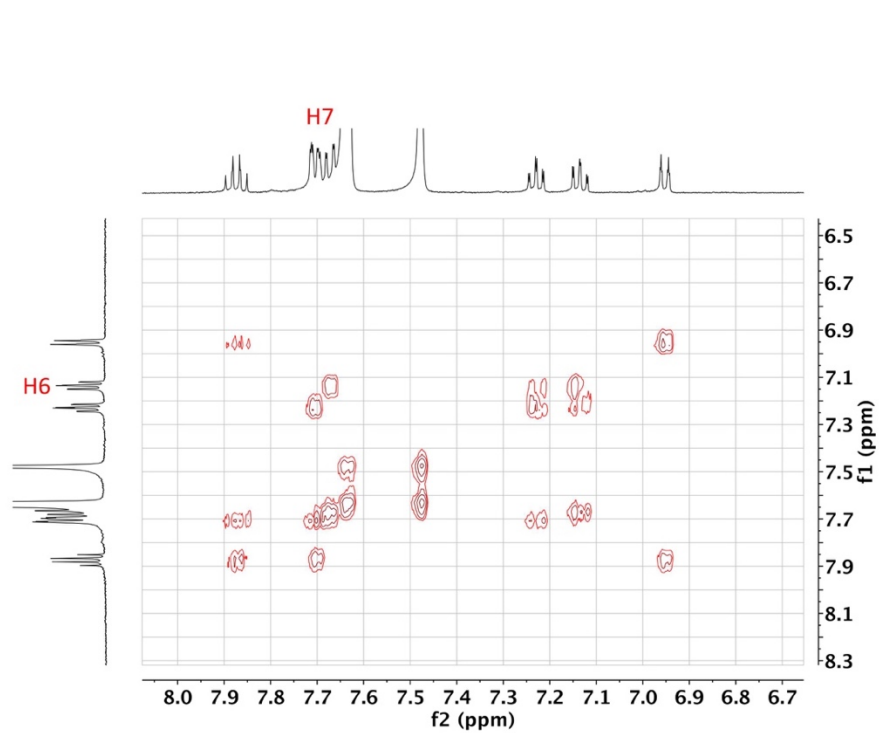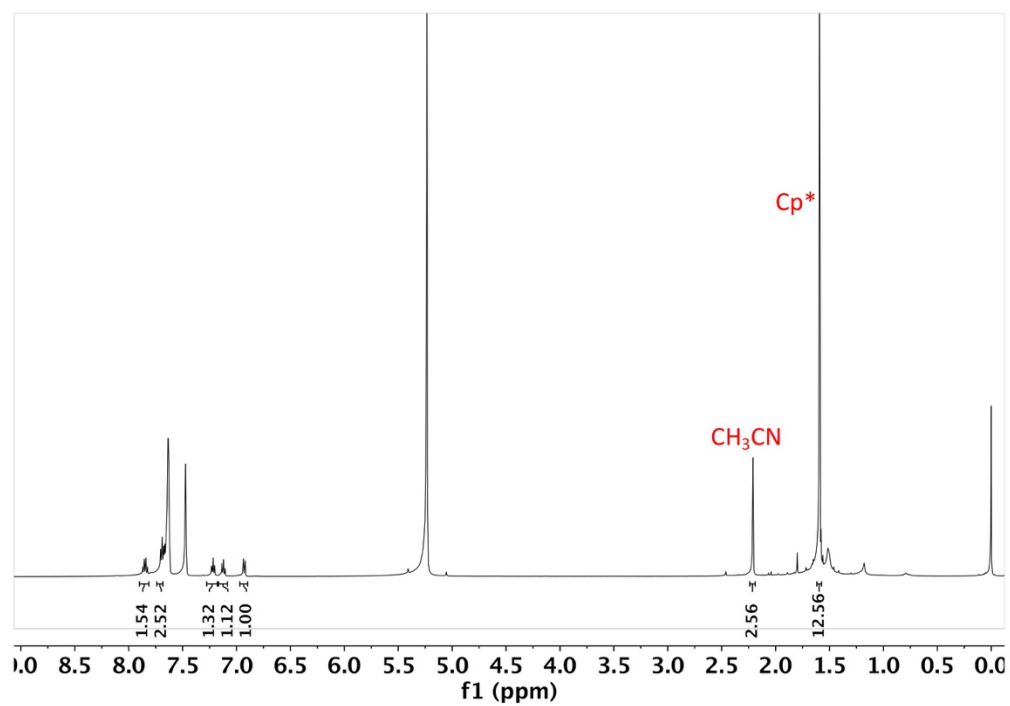
HSQC ^{1}H-^{13}C
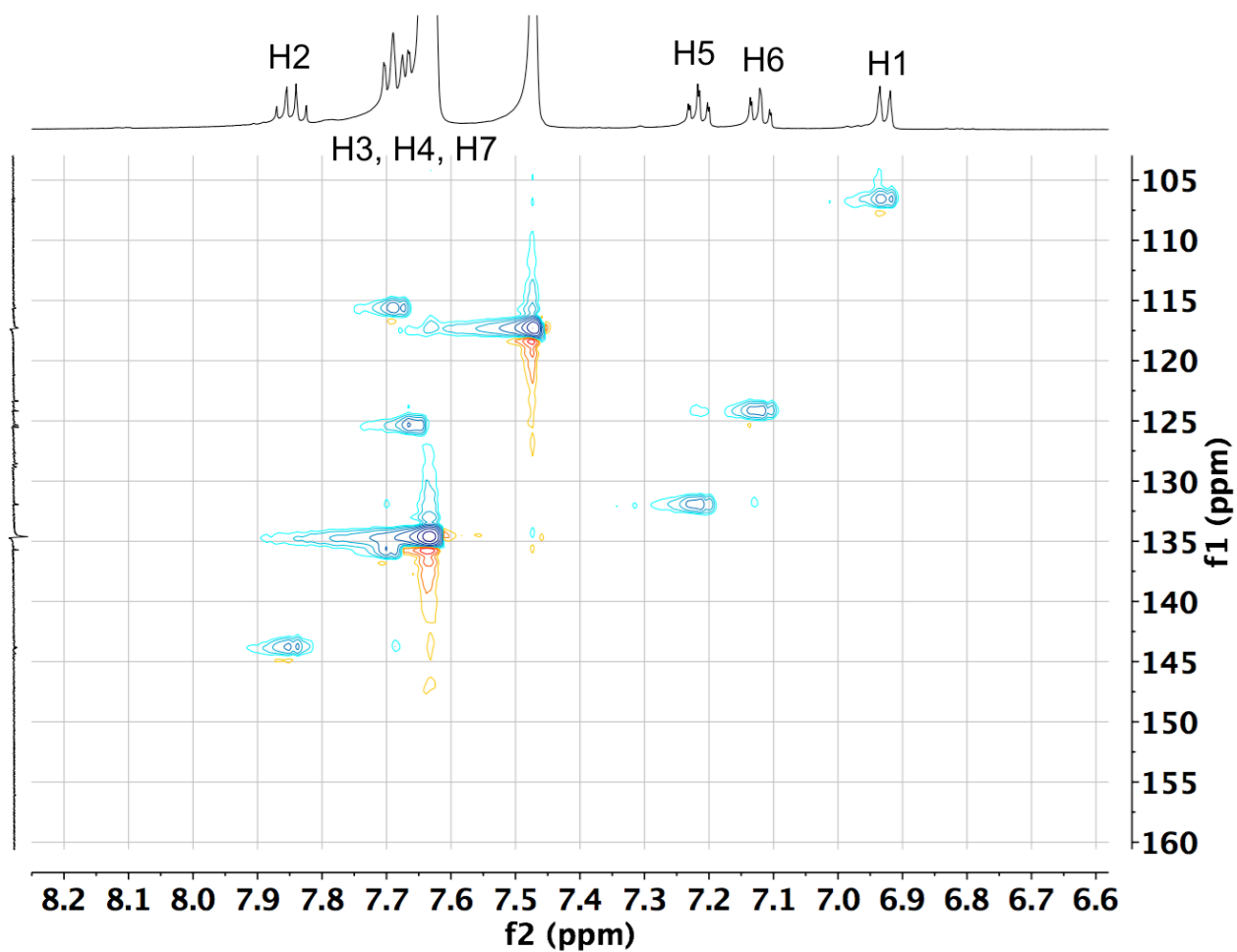
DFT Energies of Models and Analytical Data

(for the geometries please refer to the web-oriented object file under the .xyz format)

Natural Charge distribution and Wiberg bond indices for selected interatomic interactions in [**2c-r2**]$^+$
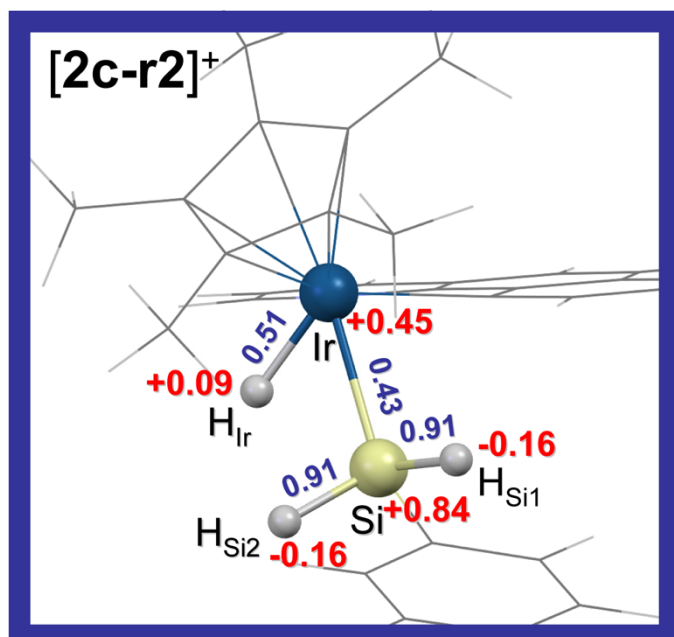
Figure S- 37

ETS-NOCV analysis of $[\mathbf{2d}]^+$ assuming the $[Si(H_2)R]^+$ (R= nBu) ligand as a closed shell fragment

$\Delta\rho_1$ $\;$ -109 kcal/mol

75 % of ΔE_{orb}
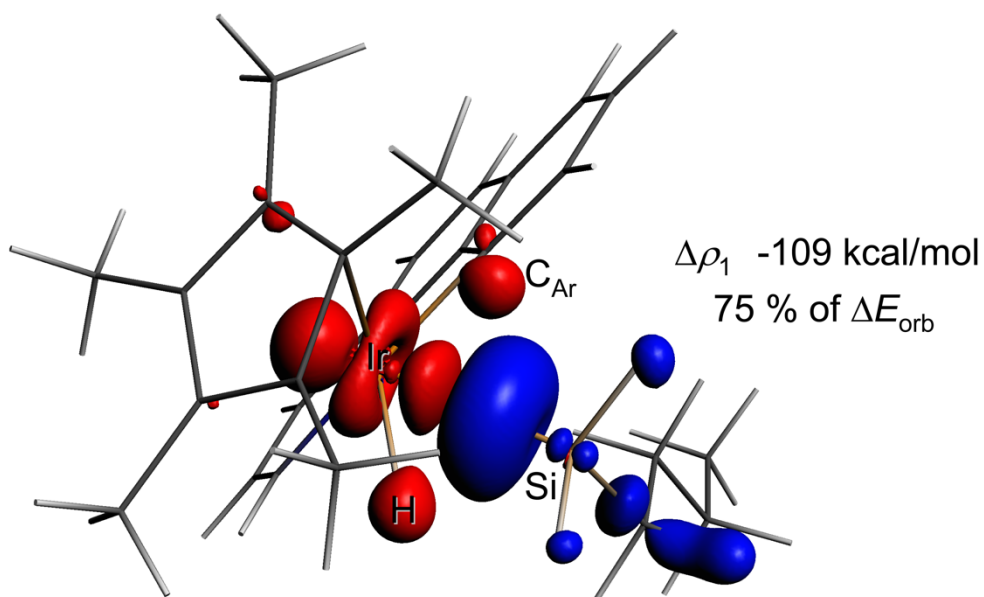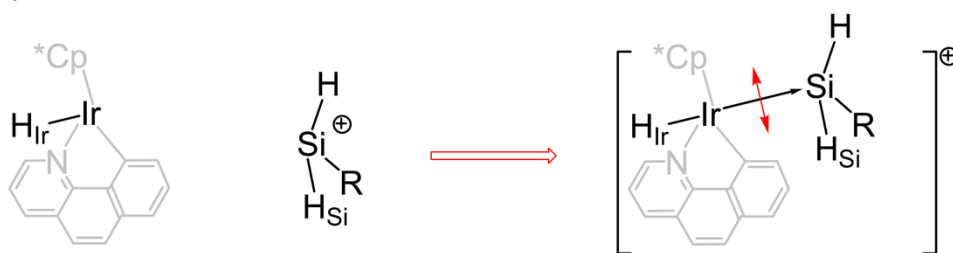
ΔE_{orb} = -145 kcal/mol

Figure S- 38 $\Delta\rho_1$ shows that most of the donation of electron density operates mainly from a delocalized interaction of the Si centre with the Ir, hydridic H and carbanionic C_{Ar} centres to build up a rather delocalized 4 centre interaction where the Ir-Si component dominates. Red and blue lobes are associated to donating and accepting orbitals respectively. Identical interactions are noticed for the low lying rotamer $[\mathbf{2c\text{-}r2}]^+$.

ETS-NOCV analysis of THF-devoid [**3**]$^+$ assuming the :Si(H)Ph ligand as a closed shell neutral fragment

ΔE_{orb} = -101 kcal/mol
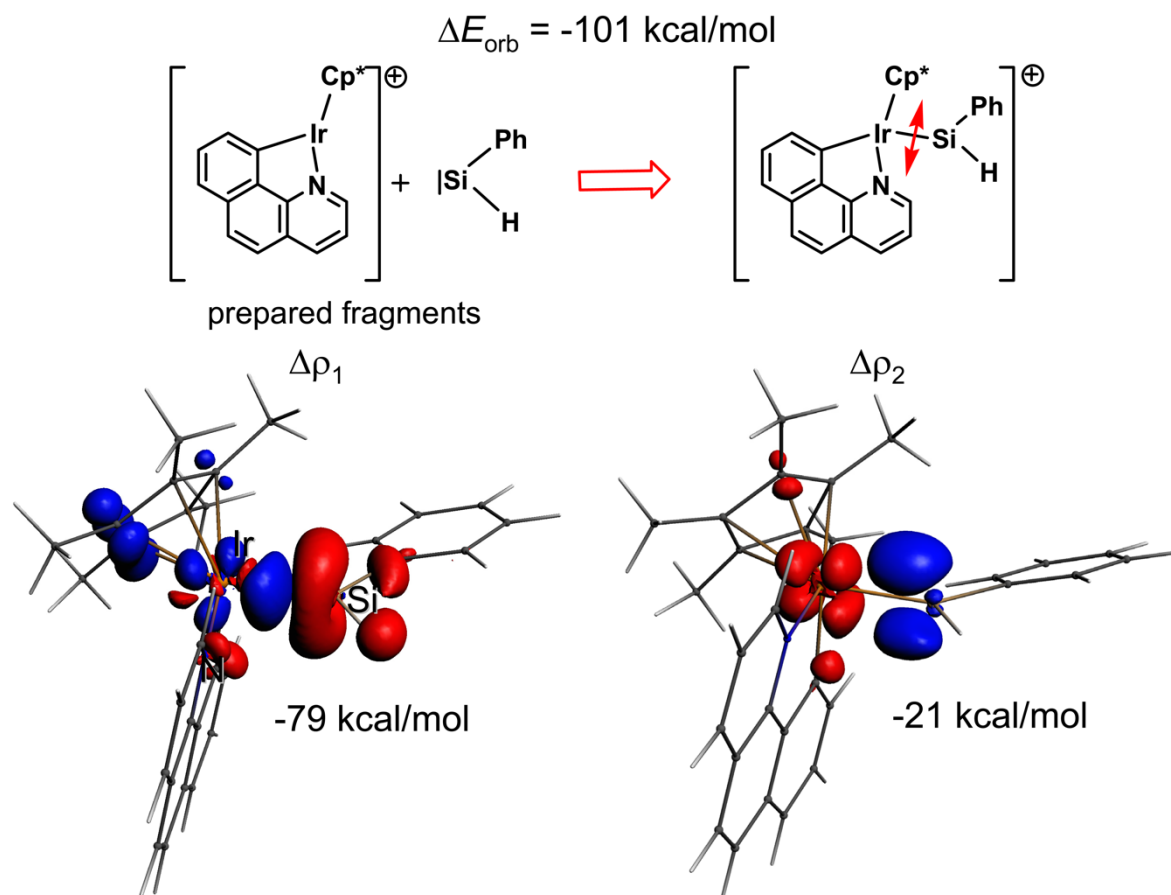
Figure S- 39 Isosurface plots of deformation densities $\Delta\rho_1$ (σ Si→Ir bond) and $\Delta\rho_2$ (π Ir→Si „backdonation") associated respectively to interaction energies ΔE_1= -79 kcal/mol and ΔE_2= -21 kcal/mol representing about 80% and 20% of the orbital interfragment interaction energy ΔE_{orb} (-101 kcal/mol). Red and blue lobes are associated to donating and accepting orbitals respectively. The red double arrow indicates the broken bond in the fragmentation scheme.

ETS-NOCV analysis of [**3**]$^+$ assuming the :Si(H)Ph ligand as a closed shell neutral fragment
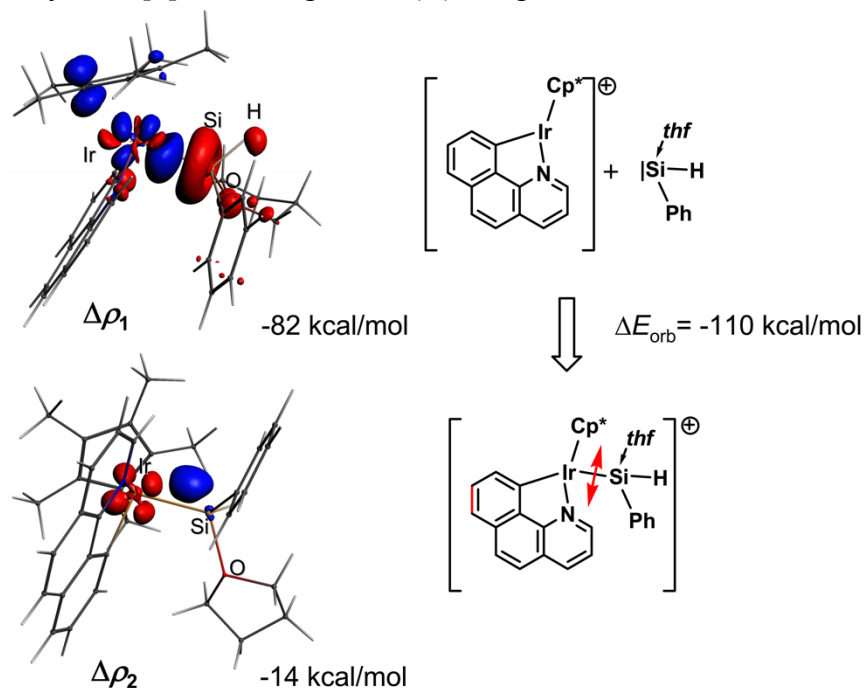
Figure S- 40 $\Delta\rho_1$ corresponds to the σ-bond Ir$\leftarrow$Si component of the interaction representing about 70 % of the bonding orbiatl interaction energy, whereas $\Delta\rho_2$ materializes the residual π-Ir$\rightarrow$Si back bonding interaction, representing about 10% of the orbital interaction energy. Red and blue lobes are associated to donating and accepting orbitals respectively. The red double arrow indicates the broken bond in the fragmentation scheme.

ETS-NOCV analysis of [**4**]$^+$ assuming the :Si(H)(nBu) ligand as a closed shell neutral fragment
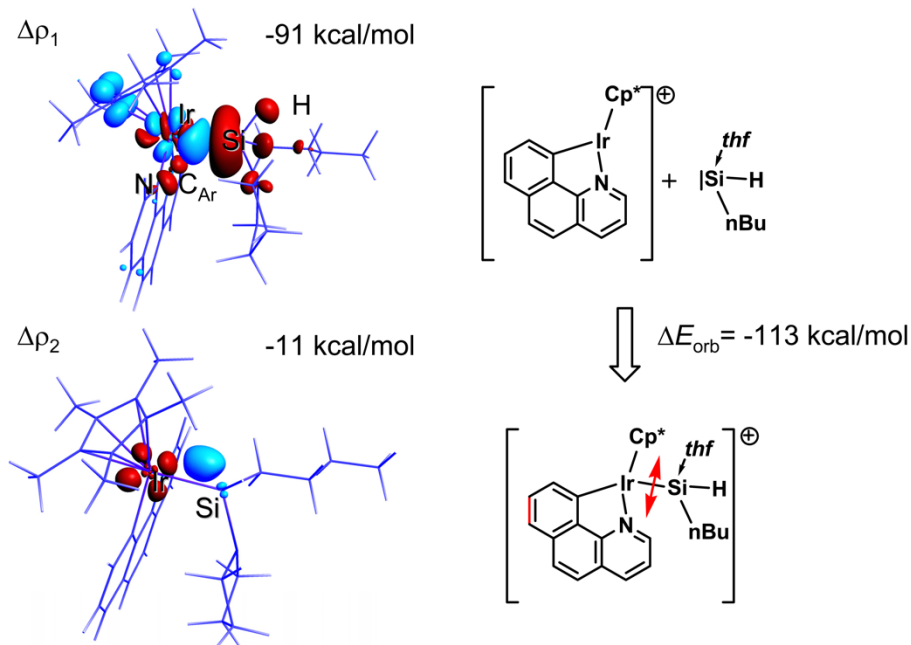
Figure S- 41 $\Delta\rho_1$ corresponds to the σ-bond Ir-Si component of the interaction representing about 85 % of the bonding orbiatl interaction energy, whereas $\Delta\rho_2$ materializes the residual π-metal-to-Si back bonding interaction, representing about 7% of the orbital interaction energy. Red and blue lobes are associated to donating and accepting orbitals respectively. The red double arrow indicates the broken bond in the fragmentation scheme.

Detailed analysis of transition states.

a)
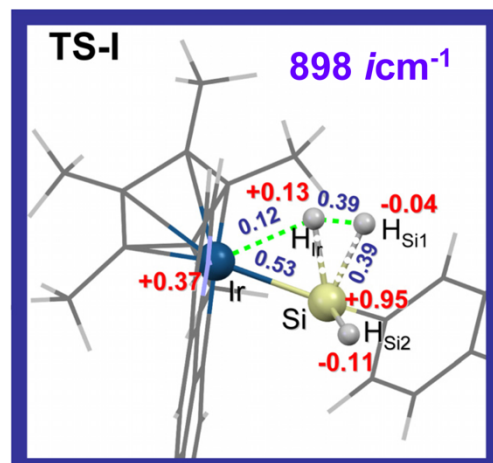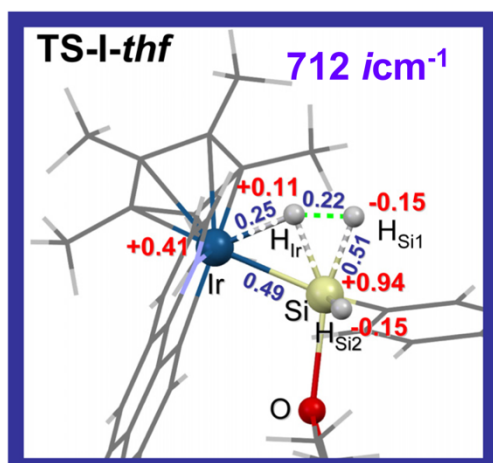
b)
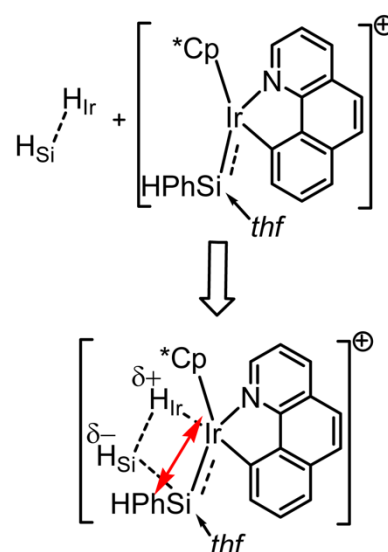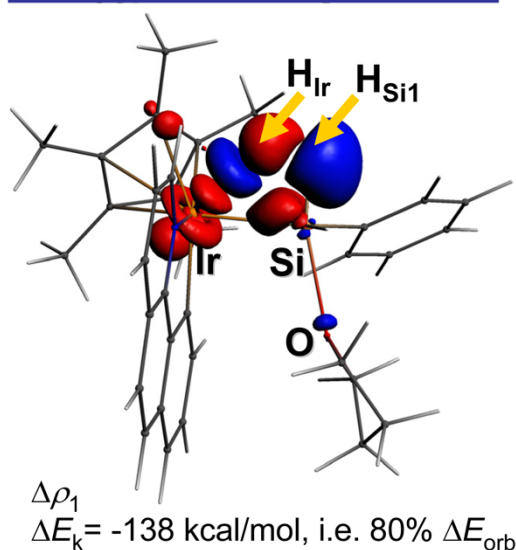
Figure S- 42 a) Enlarged views of the geometries of transition states **TS-I-*thf*** and **TS-I** with the associated imaginary vibrational mode frequency; Natural partial charges[198, 199] at selected atoms and relevant Wiberg[200] bond indice (abbr. wbi) are printed in red and blue colour respectively. b) ETS-NOCV analysis[201, 202] of orbital interactions between closed-shell fragments in their prepared geometry in **TS-I-thf**. The colored isosurface (0.005 e/bohr^3) deformation density plot $\Delta\rho_1$ depicts density transfers occurring upon interaction. The red double arrow indicates the broken interactions in the fragmentation scheme.

Note on Figure S48b: The interaction of "prepared" H_2 with the silanediyl-iridacycle gives deformation density $\Delta\rho_1$, which suggests that most of the density donation operates from the Ir and the Ir-Si bond towards the H_{Ir}-Ir and the H_{Si}-Si segments. The donation from H_{Ir} correlates consistently with the polarization of the H_{Ir}-H_{Si1} interaction in **TS-I-*thf***.

Table 1. Crystal data and structure refinement for [**2c**][BArF$_{24}$]

Identification code   jpdbdh190228

Empirical formula   C61 H43 B F24 Ir N Si

Formula weight   1477.06

Temperature   173(2) K

Wavelength   0.71073 A

Crystal system, space group   Triclinic, P -1

Unit cell dimensions a = 12.4323(9) A   alpha = 101.912(3) deg.
                      b = 13.4390(9) A   beta = 102.129(3) deg.
                      c = 22.4993(17) A   gamma = 104.614(2) deg.

Volume   3420.0(4) A^3

Z, Calculated density   2, 1.434 Mg/m^3

Absorption coefficient   2.070 mm^-1

F(000)   1456

Crystal size   0.200 x 0.120 x 0.080 mm

Theta range for data collection   2.198 to 33.117 deg.

Limiting indices   -19<=h<=19, -20<=k<=20, -34<=l<=34

Reflections collected / unique 280462 / 25896[R(int)= 0.0552]

Completeness to theta = 25.242   99.9 %

Absorption correction   Semi-empirical from equivalents

Max. and min. transmission   0.7465 and 0.6184

Refinement method   Full-matrix least-squares on F^2

Data / restraints / parameters   25896 / 1 / 801

Goodness-of-fit on F^2   1.130

Final R indices [I>2sigma(I)]   R1 = 0.0676, wR2 = 0.1716

R indices (all data)   R1 = 0.0761, wR2 = 0.1759

Extinction coefficient   n/a

Largest diff. peak and hole   4.785 and -4.616 e.A^-3

Table 2. Crystal data and structure refinement for [**2e**][BArF24].

Identification code   jpdhbd190411

Empirical formula   C61 H51 B F24 Ir N Si

Formula weight   1485.12

Temperature   120(2) K

Wavelength   0.71073 A

Crystal system, space group   Triclinic, P -1

Unit cell dimensions   a = 14.3167(6) A   alpha = 99.0010(10) deg.
                        b = 15.2182(7) A   beta = 112.6430(10) deg.
                        c = 15.2213(6) A   gamma = 97.763(2) deg.

Volume   2952.8(2) A^3

 Z, Calculated density   2, 1.670 Mg/m^3

 Absorption coefficient   2.398 mm^-1

  F(000)   1472

  Crystal size   0.250 x 0.200 x 0.180 mm

  Theta range for data collection   2.163 to 33.757 deg.

  Limiting indices   -22<=h<=22, -23<=k<=23, -23<=l<=23

  Reflections collected / unique 304576 / 23610 [R(int) = 0.0226]

  Completeness to theta = 25.242   99.8 %

  Absorption correction   Semi-empirical from equivalents

  Max. and min. transmission   0.7467 and 0.6754

 Refinement method   Full-matrix least-squares on F^2

Data / restraints / parameters   23610 / 0 / 814

Goodness-of-fit on F^2   1.055

Final R indices [I>2sigma(I)]   R1 = 0.0246, wR2 = 0.0650

R indices (all data)   R1 = 0.0252, wR2 = 0.0654

Extinction coefficient   n/a

Largest diff. peak and hole   2.487 and -2.140 e.A^-3

Table 3. Crystal data and structure refinement for [**2f**][BArF₂₄].

Identification code	jpdhbd180419_02
Empirical formula	C59 H47 B F24 Ir N Si
Formula weight	1457.07
Temperature	173(2) K
Wavelength	0.71073 A
Crystal system, space group	Triclinic, P -1
Unit cell dimensions	a = 12.525(9) A alpha = 92.37(3) deg.
	b = 13.582(9) A beta = 101.368(15) deg.
	c = 17.909(14) A gamma = 103.672(15) deg.
Volume	2890(4) A^3
Z, Calculated density	2, 1.675 Mg/m^3
Absorption coefficient	2.449 mm^-1
F(000)	1440
Crystal size	0.300 x 0.240 x 0.200 mm
Theta range for data collection	1.165 to 34.122 deg.
Limiting indices	-19<=h<=19, -21<=k<=21, -28<=l<=28
Reflections collected / unique	120972 / 23579 [R(int) = 0.0463]
Completeness to theta = 25.242	100.0 %
Absorption correction	Semi-empirical from equivalents
Max. and min. transmission	0.7467 and 0.6585
Refinement method	Full-matrix least-squares on F^2
Data / restraints / parameters	23579 / 2 / 775
Goodness-of-fit on F^2	1.048
Final R indices [I>2sigma(I)]	R1 = 0.0577, wR2 = 0.1431
R indices (all data)	R1 = 0.0765, wR2 = 0.1549
Extinction coefficient	n/a
Largest diff. peak and hole	3.174 and -2.817 e.A^-3

Table 4. Crystal data and structure refinement for [**2g**][BArF24].

Identification code   jpdbdh190221

Empirical formula   C67 H47 B F24 Ir N Si

Formula weight   1553.15

Temperature   120(2) K

Wavelength   0.71073 A

Crystal system, space group   Triclinic, P -1

Unit cell dimensions a = 15.5519(8) A   alpha = 110.859(2) deg.
                      b = 16.6310(8) A   beta = 90.904(2) deg.
                      c = 17.1243(9) A   gamma = 108.469(2) deg.

Volume   3884.1(3) A^3

Z, Calculated density   2, 1.328 Mg/m^3

Absorption coefficient   1.827 mm^-1

F(000)   1536

Crystal size   0.180 x 0.100 x 0.080 mm

Theta range for data collection   2.248 to 32.031 deg.

Limiting indices   -23<=h<=23, -21<=k<=24, -25<=l<=25

Reflections collected / unique 295977 / 26948 [R(int) = 0.0766]

Completeness to theta = 25.242   99.9 %

Absorption correction   Semi-empirical from equivalents

Max. and min. transmission   0.7463 and 0.6157

Refinement method   Full-matrix least-squares on F^2

Data / restraints / parameters   26948 / 0 / 847

Goodness-of-fit on F^2   1.036

Final R indices [I>2sigma(I)]   R1 = 0.0509, wR2 = 0.1227

R indices (all data)   R1 = 0.0711, wR2 = 0.1351

Extinction coefficient   n/a

Largest diff. peak and hole   2.821 and -2.500 e.A^-3

Table 5. Crystal data and structure refinement for [**3**][BArF₂₄].

```
Identification code              jpdhbd170628

Empirical formula                C65 H49 B F24 Ir N O Si

Formula weight                   1547.15

Temperature                      173(2) K

Wavelength                       1.54178 A

Crystal system, space group      Monoclinic,  P 21

Unit cell dimensions  a = 12.6875(3) A    alpha = 90 deg.
                      b = 18.6774(4) A    beta = 90.1210(10) deg.
                      c = 13.2649(3) A    gamma = 90 deg.

Volume                           3143.37(12) A^3

Z, Calculated density            2,  1.635 Mg/m^3

Absorption coefficient           5.327 mm^-1

F(000)                           1532

Crystal size                     0.400 x 0.250 x 0.220 mm

Theta range for data collection  3.332 to 66.804 deg.

Limiting indices          -14<=h<=15, -22<=k<=16, -15<=l<=15

Reflections collected / unique   31109 / 8412 [R(int) = 0.0276]

Completeness to theta = 66.804   99.3 %

Absorption correction            Semi-empirical from equivalents

Max. and min. transmission       0.7528 and 0.5294

Refinement method             Full-matrix least-squares on F^2

Data / restraints / parameters   8412 / 1 / 784

Goodness-of-fit on F^2           1.072

Final R indices [I>2sigma(I)]    R1 = 0.0430, wR2 = 0.1114

R indices (all data)             R1 = 0.0446, wR2 = 0.1125

Absolute structure parameter     0.017(5)

Extinction coefficient           n/a

Largest diff. peak and hole      1.193 and -0.605 e.A^-3
```

Table 6. Crystal data and structure refinement for [**4**][BArF$_{24}$].

```
Identification code              jpdhbd180118

Empirical formula                C67 H58 B Cl2 F24 Ir N O Si

Formula weight                   1651.14

Temperature                      173(2) K

Wavelength                       0.71073 A

Crystal system, space group      Triclinic,  P -1

Unit cell dimensions   a = 12.8202(5) A    alpha = 103.9200(10) deg.
                       b = 13.7546(6) A     beta = 97.2070(10) deg.
                       c = 20.3626(9) A    gamma = 92.2020(10) deg.

Volume                           3448.9(3) A^3

Z, Calculated density            2,  1.590 Mg/m^3

Absorption coefficient           2.138 mm^-1

F(000)                           1642

Crystal size                     0.450 x 0.300 x 0.200 mm

Theta range for data collection  1.040 to 32.154 deg.

Limiting indices            -19<=h<=19, -20<=k<=20, -30<=l<=30

Reflections collected / unique   214858 / 24102 [R(int) = 0.0629]

Completeness to theta = 25.242   100.0 %

Absorption correction            Semi-empirical from equivalents

Max. and min. transmission       0.7463 and 0.5921

Refinement method            Full-matrix least-squares on F^2

Data / restraints / parameters   24102 / 2 / 884

Goodness-of-fit on F^2           1.088

Final R indices [I>2sigma(I)]    R1 = 0.0650, wR2 = 0.1534

R indices (all data)             R1 = 0.0954, wR2 = 0.1748

Extinction coefficient           n/a

Largest diff. peak and hole      4.308 and -3.540 e.A^-3
```

Table 7. Crystal data and structure refinement for [**5**][BArF₂₄].

Identification code   jpdhbd190314

Empirical formula   C66 H59 B Cl2 F24 Ir N O Si

Formula weight   1640.14

Temperature   120(2) K

Wavelength   0.71073 A

Crystal system, space group   Monoclinic, C 2/c

Unit cell dimensions   a = 42.662(2) A   alpha = 90 deg.
                        b = 12.4134(6) A   beta = 124.997(2) deg.
                        c = 32.7773(18) A   gamma = 90 deg.

Volume   14219.7(13) A^3

Z, Calculated density   8, 1.532 Mg/m^3

Absorption coefficient   2.074 mm^-1

F(000)   6528

Crystal size   0.220 x 0.200 x 0.180 mm

Theta range for data collection 2.191 to 32.048 deg.

Limiting indices   -62<=h<=63, -18<=k<=18, -48<=l<=48

Reflections collected / unique 323308 / 24767 [R(int) = 0.0732]

Completeness to theta = 25.242   99.9 %

Absorption correction   Semi-empirical from equivalents

Max. and min. transmission   0.7463 and 0.6457

Refinement method   Full-matrix least-squares on F^2

Data / restraints / parameters 24767 / 0 / 885

Goodness-of-fit on F^2   1.090

Final R indices [I>2sigma(I)]   R1 = 0.0671, wR2 = 0.1554

R indices (all data)   R1 = 0.0911, wR2 = 0.1686

Extinction coefficient   n/a

Largest diff. peak and hole   2.472 and -2.467 e.A^-3

Table 8. Crystal data and structure refinement for [**6**][BArF$_{24}$].

Identification code   jpdhbd180801

Empirical formula   C63 H53 B F24 Ir N O Si

Formula weight   1527.16

Temperature   173(2) K

Wavelength   0.71073 A

Crystal system, space group   Triclinic, P -1

Unit cell dimensions   a = 12.6227(6) A   alpha = 99.426(2) deg.
                              b = 14.4823(7) A   beta = 93.060(2) deg.
                              c = 18.7658(9) A   gamma = 99.782(2) deg.

Volume   3323.3(3) A^3

Z, Calculated density   2, 1.526 Mg/m^3

Absorption coefficient   2.134 mm^-1

F(000)   1516

Crystal size   0.350 x 0.250 x 0.150 mm

Theta range for data collection   1.104 to 30.267 deg.

Limiting indices   -17<=h<=17, -20<=k<=20, -26<=l<=26

Reflections collected / unique   157402 / 19695 [R(int) = 0.1236]

Completeness to theta = 25.242   100.0 %

Absorption correction   Semi-empirical from equivalents

Max. and min. transmission   0.7460 and 0.6309

Refinement method   Full-matrix least-squares on F^2

Data / restraints / parameters   19695 / 1 / 806

Goodness-of-fit on F^2   1.004

Final R indices [I>2sigma(I)]   R1 = 0.0662, wR2 = 0.1539

R indices (all data)   R1 = 0.1092, wR2 = 0.1724

Extinction coefficient   n/a

Largest diff. peak and hole   3.094 and -1.161 e.A^-3

Table 9. Crystal data and structure refinement for [**7**][BArF$_{24}$].

```
Identification code              jpdhbd180823

Empirical formula                C71 H53 B F24 Ir N O Si

Formula weight                   1623.24

Temperature                      173(2) K

Wavelength                       0.71073 A

Crystal system, space group      Triclinic,  P -1

Unit cell dimensions   a = 12.8122(13) A   alpha = 81.036(3) deg.
                       b = 15.3980(16) A    beta = 78.121(3) deg.
                       c = 19.918(2) A    gamma = 84.569(3) deg.

Volume                           3790.4(7) A^3

Z, Calculated density            2,  1.422 Mg/m^3

Absorption coefficient           1.876 mm^-1

F(000)                           1612

Crystal size                     0.360 x 0.200 x 0.080 mm

Theta range for data collection  1.342 to 31.045 deg.

Limiting indices         -18<=h<=18, -22<=k<=22, -28<=l<=28

Reflections collected / unique   170898 / 24182 [R(int) = 0.0876]

Completeness to theta = 25.242   99.9 %

Absorption correction            Semi-empirical from equivalents

Max. and min. transmission       0.7462 and 0.6161

Refinement method                Full-matrix least-squares on F^2

Data / restraints / parameters   24182 / 1 / 849

Goodness-of-fit on F^2           1.026

Final R indices [I>2sigma(I)]    R1 = 0.0551, wR2 = 0.1374

R indices (all data)             R1 = 0.0815, wR2 = 0.1512

Extinction coefficient           n/a

Largest diff. peak and hole      2.477 and -1.381 e.A^-3
```

Table 10. Crystal data and structure refinement for [**F-1a**][BArF$_{24}$].

Identification code	jpdhbd180319
Empirical formula	C55 H37 B F25 Ir N2
Formula weight	1403.87
Temperature	173(2) K
Wavelength	0.71073 A
Crystal system, space group	Triclinic, P -1

Unit cell dimensions   a = 12.7646(6) A   alpha = 91.941(2) deg.

b = 13.1773(6) A   beta = 97.366(2) deg.

c = 17.0173(8) A   gamma = 106.942(2) deg.

Volume   2707.9(2) A^3

Z, Calculated density   2, 1.722 Mg/m^3

Absorption coefficient   2.592 mm^-1

F(000)   1376

Crystal size   0.200 x 0.120 x 0.080 mm

Theta range for data collection   1.210 to 28.143 deg.

Limiting indices   -16<=h<=16, -17<=k<=17, -22<=l<=22

Reflections collected / unique   96515 / 13119 [R(int) = 0.0980]

Completeness to theta = 25.242   99.9 %

Absorption correction   Semi-empirical from equivalents

Max. and min. transmission   0.7456 and 0.6074

Refinement method   Full-matrix least-squares on F^2

Data / restraints / parameters   13119 / 0 / 742

Goodness-of-fit on F^2   1.022

Final R indices [I>2sigma(I)]   R1 = 0.0627, wR2 = 0.1194

R indices (all data)   R1 = 0.0890, wR2 = 0.1284

Extinction coefficient   n/a

Largest diff. peak and hole   1.964 and -1.607 e.A^-3

Table 11. Crystal data and structure refinement for [**F-5a**][BArF$_{24}$].
Identification code   jpdbdh180911

Empirical formula   C57 H46 B F25 Ir N Si

Formula weight   1451.05

Temperature   173(2) K

Wavelength   0.71073 A

Crystal system, space group   Triclinic, P -1

Unit cell dimensions   a = 12.6306(4) A   alpha = 92.3020(10) deg.

                          b = 13.4234(5) A   beta = 102.2550(10) deg.

                          c = 17.8719(6) A   gamma = 103.0050(10) deg.

Volume   2872.77(17) A^3

Z, Calculated density   2, 1.677 Mg/m^3

Absorption coefficient   2.465 mm^-1

F(000)   1432

Crystal size   0.300 x 0.200 x 0.180 mm

Theta range for data collection 1.171 to 30.085 deg.

Limiting indices   -17<=h<=17, -18<=k<=18, -25<=l<=25

Reflections collected / unique 135723 / 16864 [R(int) = 0.0550]

Completeness to theta = 25.242   100.0 %

Absorption correction   Semi-empirical from equivalents

Max. and min. transmission   0.7460 and 0.6695

Refinement method   Full-matrix least-squares on F^2

Data / restraints / parameters 16864 / 0 / 775

Goodness-of-fit on F^2   1.037

Final R indices [I>2sigma(I)]   R1 = 0.0457, wR2 = 0.1173

R indices (all data)   R1 = 0.0588, wR2 = 0.1245

Extinction coefficient   n/a

Largest diff. peak and hole   2.460 and -1.572 e.A^

Résumé en anglais

The scope of this thesis spans the most recent advances in the investigation of chemical bonds of iridium-silicon complexes, in which a metal-bound silyl group behaves as a Z ligand that maintains a dative bond with the metal centre. This contrasts greatly with the case where this group behaves like an X ligand, that is where this silyl group binds to Ir through a covalent bond. Finally, and most interestingly are silylene ligands that in principle should establish a double bond with the Ir centre.

The idea of evaluating and tuning the electrophilic character of the silyl moiety and adjuncts its "silylicity" was probed by experimental and theoretical means. To conduct that scheme, a broad range of metal–silane adducts and other metal–silyl complexes were investigated by the computation of metal–silyl interaction energies to outline the established tools that rationalize the bonding relationship that exists between the metal center and a SiR_3 moiety. Also, this research revealed a clear separation between cases in which the Z character of the silyl moiety is the best description, and cases that belong to "classical" situations in which the X character dominates. Moreover, we postulated that for metal–silane adducts that possess a low intrinsic silylicity, a high "silylicity" can be triggered by ligand replacement or by changing in the charge of the complex. While working on this topic, we discovered that in the presence of tetrahydrofuran (THF), $[(Ir-H) \rightarrow SiRH_2]^+$ adducts readily convert by H_2 gas elimination at sub-ambient temperature into new THF-stabilized metallacyclic Ir(III)-"silylene" complexes. The emergence of metal silylene complexes via sequential H-Si activations followed by the spontaneous release of H_2 featured in this thesis is unique. The primary goal of this thesis finally was to fully characterize those elusive complexes by NMR spectroscopy analyses and X-ray diffraction analysis. Furthermore, theoretical investigations (static DFT-D reaction-energy profiling, ETS-NOCV) and NMR kinetic studies were utilized to demonstrate the role of THF which facilitated H_2 elimination. Coupled with silylene metal complex chemistry mentioned above, cationic iridacycle **1b** is of interesting catalytic reactivity toward nitro arenes, which can perform the nitro reduction in arenes to give aniline type products. In crafting a new development of this chemistry, it is safe to hypothesize that cationic hydrido-Ir(III)-silylium species, whose catalytic reactivity is of significant correlation with the extend of polarization of the molecule can enhance in the key intermediates the molecule polarization, and therefore increase its catalytic reactivity. Such polarization that occurs already in the Ir-silane adduct stems from the electropositivity of Si centre. Keeping the main ligand backbone constant, introduction of a fluoro substituent can improve the polarization of the same molecule and by way of consequence increase its catalytic reactivity. As expected, F-**1a** also displays remarkable catalytic reactivity toward a benchmark test reaction that can be followed by piezometry, i.e. the O-dehydrosilylation of alcohols at room temperature with Et_3SiH. A hydrido-Ir(III)-silylium intermediate crystal was trapped as well following on a reaction with Et_2SiH.

In conclusion, based on the discovery of hydrido-Ir(III)-silylium intermediates associated with a comprehensive study of their reactivity and catalytic performance, this thesis has taken steps to advance knowledge of Ir-silicon complexes by synthesis and the full structural characterization of notoriously elusive metal silylene complexes. Also, sophisticated computational methods have been employed to shed light on the mechanism of conversion of Ir-silane adducts into silylenes of which a great number were trapped by reactive recrystallization and subsequently characterized by X-ray diffraction analysis.

Résumé en français

Cette thèse englobe les avancées les plus récentes dans l'étude des liaisons chimiques des complexes iridium-silicium, dans lesquelles un groupe silyle lié à un métal se comporte comme un ligand Z qui maintient une liaison dative avec le centre du métal. Ceci contraste grandement avec le cas où ce groupe se comporte comme un ligand X, c'est-à-dire où ce groupe silyl se lie à Ir par une liaison covalente. Enfin, il est intéressant de noter que les ligands de silylène devraient en principe établir une double liaison avec le centre de l'Ir. L'idée d'évaluer et d'ajuster le caractère électrophile du fragment silyl et de sa ''silylicité'' a été explorée de manière expérimentale et théorique. Pour mener à bien cette étude, une large gamme d'adduits métal – silane et d'autres complexes métal – silyl ont été étudiés par calcul des énergies d'interaction métal – silyl afin de définir la relation de liaison existant entre le centre métallique et une entité SiR_3. En outre, cette recherche a révélé une séparation nette entre les cas dans lesquels le caractère Z du fragment silyl est la meilleure description, et les cas appartenant à des situations "classiques" dans lesquelles le caractère X domine. De plus, nous avons postulé que pour les adduits métal – silane qui possèdent une faible silylicité intrinsèque, une "silylicité" élevée peut être déclenchée par le remplacement du ligand ou par une modification de la charge du complexe. Tout en travaillant sur ce sujet, nous avons découvert qu'en présence de tétrahydrofurane (THF), les adduits $[(Ir-H)\rightarrow SiRH_2]^+$ se convertissent facilement par élimination de H_2 à une température sub-ambiante en un nouvel au complexe métallacyclique de ''silylene''stabilisé par une molécule de THF. L'émergence de complexes silylène-métal via des activations séquentielles de liaison H-Si, suivies de la libération spontanée de H_2 décrite dans cette thèse de doctorat, est unique. L'objectif principal de cette thèse était enfin de caractériser complètement ces complexes a priori insaisissables par des analyses par spectroscopie RMN et par analyse par diffraction des rayons X. De plus, des études théoriques (profil statique énergétique réactionnel déterminé DFT-D, ETS-NOCV) et des études cinétiques de RMN ont été utilisées pour démontrer le rôle du THF dans l'élimination de H_2. Couplé à la chimie des complexes silylène métalliques mentionnés ci-dessus, l'iridacycle cationique **1b** présente une réactivité catalytique intéressante vis-à-vis des nitro-arènes, qui peuvent effectuer la réduction du groupe nitro pour donner des produits dérivés de l'aniline.Il est raisonnable de supposer que la réactivité catalytique des espèces cationiques d'hydrido-Ir(III)-silylium, est en corrélation significative avec l'étendue de la polarisation de la molécule. Une telle polarisation qui se produit déjà dans le produit d'addition Ir-silan l'électropositivité du centre Si. En maintenant l'ossature du ligand principal constante, l'introduction d'un substituant fluoré augmente la polarisation de la même molécule et, par voie de conséquence, impacte sa réactivité catalytique. Comme on pouvait s'y attendre, F-**1a** présente également une réactivité catalytique remarquable vis-à-vis d'une réaction de test de référence pouvant être suivie par piézométrie, c'est-à-dire la O-déshydrosilylation d'alcools à la température ambiante avec Et_3SiH. Un cristal de l'intermédiaire hydrido-Ir(III)-silylium a également été piégé à la suite d'une réaction avec Et_2SiH.

Mots clés : silylène-métal, silylium, silylène métalliques, l'iridacycle cationique, ligand X, ligand Z, DFT-D, ETS-NOCV, silylicité